THE UNIVERSITY OF ASTON IN BIRMINGHAM

THE EFFECT OF ELEVATED TEMPERATURES ON THE WEAR OF MEDIUM-CHROMIUM STEEL IN CARBON DIOXIDE

Thesis submitted for the degree

of

Doctor of Philosophy

by

Nicholas William Granville, M.A.

Department of Mathematics
and Physics

November
1984

SUMMARY

"The effect of elevated temperatures on the wear of medium-chromium steel in carbon dioxide"

Nicholas William Granville
Doctor of Philosophy
1984

Unidirectional and reciprocating sliding experiments were carried out at elevated temperatures on a 9% chromium steel in atmospheres of air and carbon dioxide with the aim of assessing running-in wear. It was hoped that results obtained might aid the prediction of life-times of components subject to vibration in nuclear power stations.

High speed unidirectional sliding experiments were carried out at room temperature in order to characterise the general wear behaviour of the steel. Slow speed unidirectional sliding tests were run in both atmospheres so that the effect of reduced oxygen partial pressures could be studied. An equation was developed to calculate the surface parameters (number of asperities, asperity radius, oxidation temperature and oxide thickness) from experimental data.

In an attempt to simulate the wear of the 9% chromium steel in use, slow speed reciprocating sliding experiments were carried out at elevated temperatures and in carbon dioxide environments. The contact temperatures calculated from unidirectional experiments were used in the prediction of the weight loss during running-in, assuming that the temperatures at the asperities, under a given load and sliding speed, were independent of the mode of sliding. There was good agreement between experimentally and theoretically determined weight losses.

Scanning electron microscopy and auger spectroscopy revealed that the oxide plateaux on the horizontal reciprocating sliding specimens comprised of compacted particles of debris. Diffusion-produced oxides were identified on the unidirectional sliding specimens, worn with a vertical wear scar.

For both modes of sliding, the transition to mild wear only occurred after the majority of the wear surface was covered by oxide which was supported by a work-hardened metallic layer. This metallic layer was formed almost immediately upon initiating reciprocating sliding.

Wear/Friction/Chromium steel/Oxidation/Temperature

ACKNOWLEDGMENTS

I am deeply indebted to my supervisor, J.L. Sullivan, for his guidance and encouragement during the past three years.

I must also acknowledge Dr. T.C. Chivers and Dr. J. Skinner of Berkeley Nuclear Laboratories, Gloucestershire for many helpful discussions.

Finally, I must thank A. Abbot, C.J.S. Chapman and H. Arrowsmith for the invaluable technical assistance.

CONTENTS

LIST OF TABLES

LIST OF FIGURES

NOMENCLATURE

a	asperity radius, (m)
A	real area of wear scar, (m^2)
A	cross-sectional area of the pin, (m^2)
A_L	Arrhenius constant for linear oxidation, ($kgm^{-2}s^{-1}$)
A_P	Arrhenius constant for parabolic oxidation, ($kg^2m^{-4}s^{-1}$)
A_r	real area of contact, (m^2)
B	$\frac{\pi K_o}{4\delta_{expt}K_s}$
C	$0.8605(1-\delta_{expt})-\delta_{expt}$
c_{pe}	specific heat of the environment at T_{amb}, ($Jkg^{-1}K^{-1}$)
c_{ps}	specific heat of steel, ($Jkg^{-1}K^{-1}$)
D	diameter of the pin, (m)
E	$\frac{0.1021U(1-\delta_{expt})}{2X_s}$
f	fraction of oxide film which is oxygen
F	frictional force, (N)
g	acceleration due to gravity, (ms^{-2})
G_e	width of the air gap, (m)
h	heat transfer coefficient between the cylindrical exposed surface of the pin and the environment, ($Jm^{-2}s^{-1}K^{-1}$)
H_1	heat flow rate along the pin at the interface between pin and disc, (Js^{-1})
H_2	heat flow rate entering the section of the pin where the thermocouple measuring T_A is conducting heat away, (Js^{-1})

H_3 heat flow rate leaving the section of the pin where the thermocouple measuring T_A is conducting heat away, (Js^{-1})

H_T total heat flow generated at the interface between pin and disc, (Js^{-1})

k linear oxidational rate constant, $(kgm^{-2}s^{-1})$

k^* combined linear oxidation rate for in- and out-of-contact oxidation, $(kgm^{-2}s^{-1})$

k_e thermal conductivity of environment at T_{amb}, $(Jm^{-1}s^{-1}K^{-1})$

K_{mm} wear constant for metal-metal contact

K_{mo} wear constant for metal-oxide contact

K_o thermal conductivity of oxide, $(Jm^{-1}s^{-1}K^{-1})$

K_{oo} wear constant for oxide-oxide contact

K_s thermal conductivity of steel, $(Jm^{-1}s^{-1}K^{-1})$

$k_{T_{amb}}$ linear oxidational rate constant at the ambient temperature, T_{amb}, $(kgm^{-2}s^{-1})$

k_{T_o} linear oxidational rate constant for the asperities at the oxidation temperature, T_o, $(kgm^{-2}s^{-1})$

L dimensionless sliding parameter

L_1 length of pin exposed to the environment between the holder and the disc, (m)

L_3 distance between the thermocouples recording T_A and T_B, (m)

N number of asperities

N_{Nu} Nusselt number

N_T number of cycles prior to a wear transition, (cycles)

P $(K_{mm}+K_{oo}-2K_{mo})\frac{W}{4p_m}$, (m^2)

p_m hardness of steel, (Nm^{-2})

P_{mm} probability of metal-metal contact

P_{mo} probability of metal-oxide contact

P_{oo} probability of oxide-oxide contact

Q $(K_{mm}-K_{mo})\frac{W}{p_m}$, (m^2)

Q_C heat flow due to conduction across the air gap from disc to pin, (Js^{-1})

$Q_C(max)$ the maximum heat flow due to conduction to give a valid value of the asperity radius, (Js^{-1})

$Q_C(min)$ the minimum heat flow due to conduction to give a valid value of the asperity radius, (Js^{-1})

Q_L activation energy for linear oxidation, $(Jmol^{-1})$

Q_P activation energy for parabolic oxidation, $(Jmol^{-1})$

R $K_{mm}\frac{W}{p_m}-\frac{1}{U}\left(\frac{Ak_{T_{amb}}}{\rho_o f}+\frac{Wk_{T_o}}{p_m \rho_o f}\right)$, (m^2)

R gas constant, $(JK^{-1}mol^{-1})$

R_t radius of the pin, (m)

t time, (s)

T_A temperature recorded by thermocouple at pin surface as it enters pin holder, (K)

T_{amb} ambient temperature in the environment close to the pin, (K)

T_B temperature recorded by thermocouple situated at a distance L_3 along the cylindrical surface of the pin from the thermocouple reading T_A, (K)

T_C temperature recorded by thermocouple situated on the inside surface of the copper calorimeter around the pin and insulator, (K)

T_{cd} fictitious flash temperature assuming all the heat enters the disc, (K)

T_{cp} fictitious flash temperature assuming all the heat enters the pin, (K)

T_d disc temperature, (K)

T_o temperature at the real area of contact between pin and disc, (K)

$T_o(max)$ maximum possible temperature of the real area of contact between pin and disc according to the Archard 'one-spot' calculations, (K)

T_s temperature at the surface of the pin outside the real area of contact, (K)

T_T time to reach the wear transition, (s)

U sliding speed, (ms^{-1})

V wear volume up to time t, in reciprocating sliding, (m^3)

V_T wear volume to transition, (m^3)

w instantaneous wear rate, (m^3m^{-1})

W load, (N)

y $\frac{\alpha}{T_T}$, (s^{-1})

Z $\frac{K_s}{2R_t h}$

α fraction of the wear scar covered by oxide

β temperature difference between the pin and the environment, $T_A - T_{amb}$, (K)

γ sliding constant

δ_{expt} experimentally measured division of heat at the interface between pin and disc

Δd sliding distance in time Δt, (m)

Δm mass uptake of oxygen in time Δt, (kg)

Δt a finite sliding time, (s)

ΔV total volume removed in time Δt, (m^3)

ΔV_{mm} volume removed due to metal-metal contact in time Δt, (m^3)

ΔV_{mo} volume removed due to metal-oxide contact in time Δt, (m^3)

ΔV_{oo} volume removed due to oxide-oxide contact in time Δt, (m^3)

ΔV_{ox} volume gain due to oxidation, (m^3)

θ $1/T_{amb}$, (K^{-1})

δ_d maximum excess temperature of the contact area of the disc above that of the bulk surface, assuming that all the heat flow enters the disc, (K)

δ_m maximum excess temperature of the contact area above that of the bulk surface area, (K)

δ_p maximum excess temperature of the contact area of the pin above that of the bulk surface, assuming that all the heat flow enters the pin, (K)

μ coefficient of friction

μ_e dynamic viscosity of environment at T_{amb}, $(kgm^{-1}s^{-1})$

ν kinematic viscosity of environment at T_{amb}, (m^2s^{-1})

ξ oxide thickness on the pin, (m)

ξ^* oxide thickness on the disc, (m)

ρ_e density of the environment at T_{amb}, (kgm^{-3})

ρ_o density of oxide, (kgm^{-3})

ρ_s density of steel, (kgm^{-3})

χ_o thermal diffusivity of steel, (m^2s^{-1})

χ_s thermal diffusivity of oxide, (m^2s^{-1})

W mean weight loss, (kg)

W_T mean weight loss to transition, (kg)

To my parents

CHAPTER 1
INTRODUCTION

1.1 Technological background

It was less than 40 years ago that nuclear power became a practical source of electrical energy; within that period, the commercial use of nuclear power stations increased considerably in just the last 25 years (1). In recent years, the corrosion of certain components within such power stations has been brought to the attention of the public with the result that there is now considerable debate about their safety. The nuclear accidents that have received much attention in recent years have generally been caused by the catastrophic failure of some mechanisms; for example, the most well-known and worst incident in the industry, at the Three Mile Island nuclear power station in 1979 was due to the failure of some of the water pumps used to supply the steam generator (2). At just eight seconds into the incident when the pressure was 1.6×10^7 Nm^{-2} (158 bar), the accident was immediately made worse by the failure of a safety valve and subsequently exacerbated by operator error. It is an incident like this that gives the nuclear power station a bad image.

This thesis is not concerned with the sudden failure of ancillary equipment, but more with the long-term corrosion and wear caused by vibration of components within the reactor itself. Predictions of the life-times of component parts will ensure that the large investment in building a nuclear power station will be returned by enabling operation for as long as possible and at the highest temperature possible.

Research into the corrosion of steels in nuclear applications was already under way in the 1950's when the First International Conference on the Peaceful Uses of

Atomic Energy was organised by the United Nations in 1955. One of the main areas of research at that time was corrosion by the coolant, which may have been a liquid metal. Tsuprun and Tarytina (3) studied the effect of molten lead and bismuth on an 18/8 steel. They found that the damage was caused by the metal leaching the nickel from the steel and suggested adding inhibitors to the coolant. As they found corrosion rates of 0.2 - 2.6 $mmyear^{-1}$, they concluded that for steel operating under dynamic conditions, the erosion attack of the coolant on steel could not be ignored. Hurst and Wright (4) considered the problem of corrosion by studying the reactions of the coolant rather than those of the metal under attack. The graphite-oxygen system, of great importance in gas-cooled, graphite-moderated reactors, is thermodynamically unstable under all conditions of practical interest; however, as the activation energy for oxidation is about 160 $kJmol^{-1}$, the reaction proceeds slowly in the absence of radiation at temperatures below 350°C. At these relatively low temperatures, the radiation-induced oxidation is much faster than the corresponding thermal process. However, as the reaction to produce carbon dioxide is virtually irreversible, there is a steady loss of graphite, resulting in a decrease in moderating power and reduced mechanical strength of the graphite structure.

At higher temperatures, the equilibrium between carbon, carbon dioxide and carbon monoxide (equation 1) supresses the dissociation of carbon dioxide into carbon monoxide and oxygen (equation 2):

$$C + CO_2 \rightleftharpoons 2CO \qquad (1)$$

$$CO_2 \rightleftharpoons CO + O \qquad (2)$$

The equilibrium in equation (1) is well to the left; the rate of reaction at about 450°C is only low in the absence of radiation and much faster if radiation-induced. As the position of equilibrium is temperature

dependent, the composition of the gas mixture will vary at different places in the reactor, from which one consequence could be the net movement of carbon around the coolant circuit.

By 1958, the possible importance of carbon dioxide as a coolant rather than air, steam or a molten metal was known, and more research was concentrated on the behaviour of steels heated for prolonged periods in this gas. Since that time, carbon dioxide has been used extensively in British and French gas-cooled reactors.

Recent published work (5,6) has given the results of long-term oxidation tests lasting 10,000 hours, and occasionally 20,000 hours or more. Such work often takes years to complete since there are only 8766 hours in 1 year, and so the early published work on the subject generally gave the interim results from short-term tests. Darras, Leclercq and Bunard (7) made a study of the oxidation of a low carbon steel in carbon dioxide at 350°C, a steel used in the heat exchangers and cooling circuits of nuclear reactors. They found that for the first 500 hours, the oxidation rate increased slowly, but after this period, it was linear; at 400°C, the oxidation rate was approximately parabolic, and decreased after 500 hours to become a roughly linear rate. Two oxides, Fe_2O_3 and Fe_3O_4 were observed on the surface. Only small weight increases were detected after 1300 hours at 350°C, and these corresponded to about 8 μm of metal destroyed by oxidation each year. However, the authors themselves pointed out that their experiments did not consider the possible effects of radiation or erosion due to the rapidly circulating gas. They also found that the oxide was not adherent when the specimens underwent a thermal cycle with a maximum temperature above 350°C; this was an important reason against the use of such steels in the hotter

regions of nuclear systems.

In Britain, four Magnox reactors using uranium fuel rods and a carbon dioxide coolant at about 8×10^5 Nm^{-2} (8 bar) were completed between 1956 and 1961 (8). The advanced gas-cooled reactor or A.G.R. was the logical development of the nuclear programme existing at that time, but unlike the former reactors, the A.G.R.'s were designed to supply steam at the same temperature and pressure conditions applicable to non-nuclear turbines, namely 541°C and 5×10^5 Nm^{-2} (5 bar) with one stage of reheat (9). Other important differences between the two reactor types were the increase in temperature of the fuel elements from 480°C to 1700°C while the gas temperature at the reactor outlet increased from 336°C to above 500°C and the pressure increased to 2×10^6 Nm^{-2} (20 bar). Each reactor/turbine unit was designed to have a capacity of 660 MW.

In the A.G.R.'s, a high temperature gas was used for heat transfer and temperatures of between 623°C and 660°C were adopted at the inlet to the boilers. This hot gas encountered in turn, the reheater, superheater, evaporator and economiser banks of tubing. In these boilers, an austenitic steel, AISI 316, was used for the final superheater and reheater, a mild steel for the lower section of the economiser and a 9% chromium 1% molybdenum steel, 9Cr1Mo, for the upper section of the economiser, evaporator and primary superheater tubes. The tubes were finned in some boilers, and their support members may have included 9% chromium steel components; the boilers were only removable in some reactors.

In Magnox reactors, mild steel had been used for the whole boiler and a temperature limitation of 350°C was imposed due to the oxidation of the steel in CO_2. Had gas corrosion been the only factor to consider, an

austenitic steel such as AISI 316 would have been used for all surfaces above this temperature. However, stress corrosion on the steam/water side suggested that another material would have to be used for the evaporator and primary superheater where the steam was superheated. 9Cr1Mo initially seemed a suitable material due to its lack of stress corrosion, and predictions were made saying that gas corrosion was acceptable up to 540°C (9); these predictions from the results of short-term tests initiated by the United Kingdom Atomic Energy Authority, indicated that metal losses over the 30 year life-time of a nuclear reactor at different operating temperatures would be:

350°C	0.008 mm
400°C	0.038 mm
450°C	0.102 mm
500°C	0.203 mm
520°C	0.254 mm

The boilers were built using the materials described above, while tests on the various steels were sponsored by the U.K.A.E.A. on about 1000 specimens at Atomic Power Construction, the British Nuclear Development Corporation, Babcock and Wilcox and the Reactor Engineering Mechanical Laboratories (10). These tests included accelerated tests at 550°C and above; by late 1971, it was clear that the 9Cr1Mo steels were subject to excessive oxidation in carbon dioxide containing 1% carbon monoxide and a few hundred parts per million of methane and water, at a pressure of 4.1×10^6 Nm^{-2} (41 bar)(9). It was discovered that there was slow protective oxidation until a weight gain of about 15 to 20 $mgcm^{-2}$ was reached, corresponding to a metal loss of about 0.051 mm; after this, the oxidation rate increased by 10 to 100x as the oxide became non-protective and non-adherent to the metal surface. This rapid form of oxidation producing an oxide that

does not remain on the metal is called 'breakaway oxidation.'

The rate of breakaway oxidation varied with temperature, and silicon content; specimen geometry was also important. Such oxidation was often initiated at the corners of the samples, but then spread across the flat surfaces. This made the findings all the more serious as many of the boiler tubes were finned with many sharp edges.

The U.K.A.E.A. test programme was expanded in 1972 to investigate the parameters that were thought to influence breakaway oxidation, and to collect oxidation data on a wider range of production materials (10). In addition, a joint study with the Central Electricity Research Laboratories was made on palliative treatments, initially externally applied siliceous protective coatings, and also protective films formed by the selective pre-oxidation of steels to give chromium-rich oxides. Tests on over 1000 more specimens were started.

It was found that a 12%Cr reference material had a high oxidation resistance and so there was also an expansion of research on similar materials with a view to using it as a substitute for the 9Cr steels in new or replacement boilers.

At this period in the early 1970's, there was still a small possibility that breakaway oxidation would only occur in the high temperature accelerated tests, and that below 500°C, would never occur within the 30 year design life-time of a nuclear power station. Very prolonged tests were started to investigate this while the Central Electricity Generating Board decided that it was prudent to reduce the operating temperature of the 9Cr steels wherever possible (9).

This was done in a different way on each of the four A.G.R.'s that were then being built: Heysham, Hartlepool, Hinkley Point B and Dungeness B; for example,

at Heysham, the boiler tubing had not been manufactured and it was possible to consider choosing different materials, and reducing the number of finned components, while at Dungeness B, the boiler was complete and, as replacement was not possible, the chosen course of action was to modify operating procedures in order to reduce the nominal temperature of the 9Cr1Mo finned components to about 505°C. The outcome of this represented the optimum balance between the predicted life and the achievable output.

Remedial measures considered in 1972 included changing the steel used in certain components (this could only have been done had the boilers been replaced), using coatings based on liquid silicones (surface coatings were found to be effective in the laboratory, but proved hard to apply to the plant), and changing the coolant gas. Replacing the A.G.R. gas (CO_2, 1%CO, 1000vppm CH_4, 200vppm H_2, 250wppm H_2O) with pure helium would have produced unacceptable wear on some moving parts, but an He-1%CO mixture was considered. However, a lack of data on the resultant equilibrium gas (He, 1%CO with some CO_2, CH_4, H_2O) meant that it was not possible to predict whether the breakaway oxidation would also occur in such an atmosphere, and a helium-based coolant has never been used commercially by the Central Electricity Generating Board.

In 1977, Wallace (11) started a study of the tribological and oxidational behaviour of certain austenitic steels at elevated temperatures. It was found that the oxidational behaviour of the steels was too complicated for a complete study to be made (12), and so when a similar series of experiments was planned for this thesis in 1980, it was decided to study a 9Cr1Mo steel. This has a much simpler oxidational behaviour in the temperature range of interest, having only 0.24%Ni, but, as has been shown above, is still of

importance to the nuclear power industry.

1.2 The oxidation of steels

1.2.1 Static oxidation

The behaviour of metals in gas atmospheres at high temperatures is usually very complicated. The metal may have oxygen, hydrogen, nitrogen, carbon or sulphur as impurities, as well as other metals present in small quantities. The gas atmosphere may also consist of several components, of which in air, the most important is oxygen, but the presence of nitrogen, hydrogen, carbon dioxide and water vapour cannot be ignored.

One of the earliest simple studies of a gas-metal reaction was that of the oxidation of copper in atmospheric air at 1050°C (13). The layer of copper I oxide formed was free from visible pores and so separated the copper from the atmospheric oxygen; however, the reaction continued and after a few hours, a layer 1 mm thick had formed. The only means by which the reaction could have proceeded was if one or more of the reactants was able to diffuse across the oxide layer.

Gulbransen (14) gave a good general view of the classification of gas-metal reactions and assigned the various phenomena into one of five regions of activity: metal, metal-oxide interface, oxide, oxide-gas interface and gas. Figure 1.1 shows the possible chemical activity in each zone of a general metal in an oxidising environment at high temperature.

The rate of oxide growth is a very important means for determining the reaction mechanism. There are several ways in which the rate of reaction can vary with time, but of the ideal rate laws listed below, only the first two are important (the real rate laws tend to be more complicated)(15):-

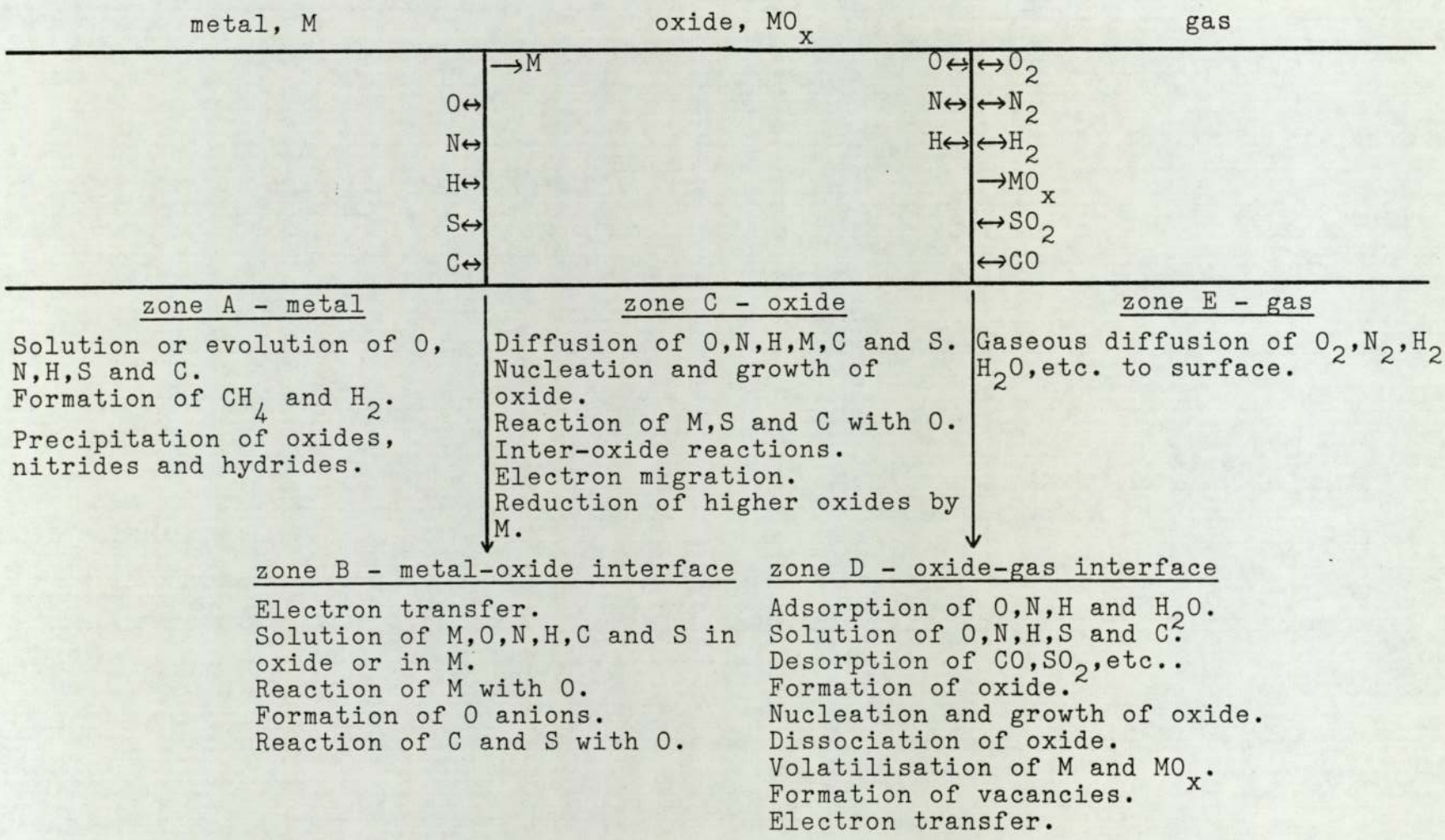

Figure 1.1 The possible chemical activity of a metal in an oxidising atmosphere at high temperature, showing oxide-type reactions (ref 14)

i) linear $\xi = k_l t$

ii) parabolic $\xi^2 = k_p t$

iii) cubic $\xi^3 = k_c t$

iv) logarithmic $\xi = k_e \log(at + t_0)$

v) inverse logarithmic $1/\xi = A - k_i \log t$

The oxidation of iron in air to form wustite, FeO, was studied at 600°C and above; the thickness of the oxide layer varied linearly with time at 600°C, but at 700°C or 800°C, there was a parabolic rate of reaction (16). The reaction kinetics were an indication of the rate-determining step of the oxidation process; for example, had the adsorption of the gas on the metal surface been the slowest reaction, then the rate of reaction would have been proportional to the area available for adsorption, and would not have varied with time; alternatively, on a metal with a thick oxide layer formed at the metal-oxide interface, diffusion of the oxygen atoms through the oxide might have been the rate-determining step, and a parabolic rate observed.

As parabolic rates of reaction are common, for example on iron or copper at high temperatures, and on uranium or molybdenum at low temperatures (15), considerable effort has been made towards understanding the diffusion process more fully. Adolf Fick's First and Second Laws of Diffusion first derived theoretically in 1855 (17) are still the basis of present day diffusion theories, although now quantitive experimental work can be performed (13).

The oxidation of pure iron in air was one of the first systems to be studied (16,18). Stanley et al. studied oxidation from 500°C to 900°C and found a parabolic rate (equation (ii) above) and a temperature dependence of the rate constant, k_p, given by:

$$k_p = 37\ e^{-140000/RT} \quad kg^2m^{-4}s^{-1} \qquad (1.1)$$

where R is the gas constant, and T is the absolute

temperature. At 500°C, only one oxide, magnetite or Fe_3O_4, was formed, but at temperatures between 600°C and 900°C, two other oxides, wustite or FeO and haematite or α-Fe_2O_3 were also observed. At 600°C, FeO is adjacent to the metallic iron with Fe_3O_4 next and α-Fe_2O_3 as a very thin layer at the surface. As the oxidation temperature increased, the percentage of the oxide layer that was FeO increased; after 2 hours at 800°C, wustite comprised about 95% of the total oxide. At 900°C, heavy loose scale was observed; however, as no experiments ever lasted for more than 2 hours, no conclusions were made as to the effect of the oxide becoming non-adherent. This work was among the first to show that two or more oxides could be formed at one time, and as a result, more was learned about the mechanism of oxidation.

Paidassi (18) carried out a similar series of experiments in a higher temperature range. He found that the scale comprised of three continuous and compact layers of the iron oxides up to his highest studied temperature of 1250°C. FeO was about 95% of the scale with Fe_3O_4 4% and α-Fe_2O_3 1%; the temperature dependence was not great (FeO formed 94.5% of the oxide at 700°C, 95.2% at 900°C (the maximum) and 93.8% at 1250°C). It was possible that the small amounts of Fe_3O_4 and α-Fe_2O_3 were due to reactions of the FeO upon being cooled to room temperature, but Paidassi did not refer to any observed changes in oxide. The oxide growth law was parabolic and the activation energy was 170 $kJmol^{-1}$. In a few experiments, a discontinuity was observed at the metal-oxide interface and this had the effect of considerably altering the composition of the scale, but no observations were made about an increased rate of reaction.

At temperatures below 570°C, the oxidation rate was found to be dependent upon the growth of Fe_3O_4 (1) and not FeO as found at high temperatures. The growth

mechanism was:

Iron	Wustite	Magnetite	Haematite	Oxygen
Fe	FeO	Fe_3O_4	α-Fe_2O_3	O_2
	Fe^{2+} $\longrightarrow$	Fe^{2+} $\xrightarrow[20\%]{}$ O^{2-} $\xleftarrow[80\%]{}$	O^{2-} $\longleftarrow$	

Wustite is a metal-deficient oxide with cation vacancies and so it is possible for Fe^{2+} ions to migrate through it whereas magnetite is a metal-excess oxide with anion vacancies which enable O^{2-} migration. The oxygen ions are more mobile.

Many elements are added to pure iron in order to improve its strength or oxidation resistance. Table 1.1 gives the effect of some elements frequently added singly or in combination to form steels; table 1.2 presents the oxidational behaviour of certain steels often considered for use in nuclear applications. In recent work on 9% chromium steels in carbon dioxide (19), a weight gain of 20 $mgcm^{-2}$ has been taken as an indication that breakaway oxidation has occurred; such weight gains are found after just 1000 hours at 927°C on steels AISI 310 or 321. Long-term tests may show similar excessive weight gains at lower temperatures.

Much work has been carried out on the behaviour of Fe-Cr alloys and stainless steels in air (20, 21, 22, 23). Rickett and Wood (21) found a spinel, $FeCr_2O_4$, with Cr_2O_3 on the inside and α-Fe_2O_3 on the outside of scale found on Fe 12-28%Cr alloys oxidised in oxygen at 980°C or 1090°C; McCullough et al. (22) found that at 980°C, the spinel was formed adjacent to the metal but that the majority oxide in the scale was α-Fe_2O_3; Caplan and Cohen (23) found both the spinel and Cr_2O_3, but no pure iron oxides on Fe 11-26%Cr alloys.

Wretblad (24) showed that Fe_2O_3 and Cr_2O_3 formed a continuous series of solid solutions. Caplan and Cohen (23) also found evidence of Fe_2O_3 dissolved in

Element	Effect on oxidation
Carbon	None up to 700°C; deleterious above 700°C
Silicon	None up to 700°C; beneficial above 700°C
Molybdenum	Beneficial up to at least 2% addition
Nickel	None in the range of alloying
Aluminium	Beneficial
Sulphur	None in small quantities
Phosphorus	Deleterious
Chromium	Beneficial

Table 1.1 The effect of adding different elements upon the oxidation of iron (ref 1)

Steel AISI number	Nominal analysis	Temperature /°C	Weight change in 1000 hours /mgcm^{-2}	Maximum temperature without excessive scaling /°C
304	18Cr 8Ni	816	1.9	899
		927	31	
		1093	930	
310	25Cr 20Ni	871	3.9	1093
		982	10	
		1093	15.5	
316	18Cr 8Ni Mo			899
321	18Cr 8Ni Ti	816	2.3	899
		927	23	
		1093	110	

Table 1.2 The oxidational behaviour of some steels often considered for use as nuclear power station components (ref 1)

Cr_2O_3-type scale. The spinel $FeCr_2O_4$ is not necessarily stoichiometric, but forms a series of solid solutions with magnetite (25).

Seybolt (20) observed that Fe-Cr alloys with less than 13% Cr were in equilibrium with the spinel, and that oxidation occurred internally at temperatures above 1000°C. Alloys with a higher chromium content exhibited very different behaviour; the equilibrium oxide was Cr_2O_3, and this was produced almost entirely by Cr^{3+} diffusion through the scale for oxidation to proceed at the oxide-gas interface. He suggested that the initial oxidation resistance of stainless steels might be increased by pre-oxidation to produce a highly defective Cr_2O_3 structure which would then protectively oxidise further.

Having described the results of diffusion on the oxidation of various alloys and stainless steels, it is now possible to consider the mechanisms of diffusion. Wagner (13) gave a general account and reviewed diffusion in several different systems: oxide with excess metal, oxide with a metal deficit, oxide with excess oxygen and oxide with an oxygen deficit. Carter and Richardson (26) measured the diffusion of iron in wustite and found oxide of the composition $Fe_{0.92}O$ after 48 hours at 1000°C. Lattice diffusion was the primary means of cation migration because the excess metal atom concentration was proportional to the square of the distance from the metal; had the mechanism been grain-boundary diffusion, there would have been a linear relationship between concentration and distance.

Several workers (27, 28, 29, 30) have attempted to form a model describing atom diffusion in oxidation. Wagner (27) described the oxidation of binary alloys of a noble metal (gold or platinum) with an oxidisable metal (eg nickel). The oxidation rate was found to be dependent upon the nickel migration to the alloy-NiO

interface whenever nickel was the minority metal. In a later very mathematical paper (28), he considered the distribution of lattice defects as well as their movement in binary alloys of two oxidisable components. When such an alloy oxidised, the ratio of the metals in the scale was usually different from the ratio in the alloy. There were two different diffusion rates, and in general, the more reactive metal entered the scale preferentially. In Ni-Cr alloys, the scale was a solid solution of NiO and Cr_2O_3, with the cation vacancy concentration dependent upon the Cr_2O_3 content; internal oxidation also occurred to produce $NiCr_2O_4$. The concentration of the Cr_2O_3 in the oxide scale was found to vary with distance from the surface; as chromium was the more reactive metal, the concentration was greatest at the air-oxide interface. When this occurred, the protective Cr_2O_3 film had the effect of increasing the NiO content in the bulk of the scale and, since most metal atom migration was due to the cation vacancies in the Cr_2O_3, the oxidation rate decreased.

Wagner's model assumed a parabolic oxidation rate, independence of the different self-diffusion coefficients and thermodynamic ideality. Using Fe-Cr alloys with greater than 23% Cr which oxidise exclusively to Cr_2O_3 (20), weight gain measurements were made on samples which were heated to 1250°C for up to 100 hours (29). It was found that iron entered the scale during the initial stages of oxidation only and that its concentration was greatest at the oxide-alloy interface, but decreased with time. The weight gain was found to increase less steadily than the theory predicted. This may have been due to the decreasing iron content; just 4% Fe_2O_3 added to Cr_2O_3 increased the electrical resistance and so reduced the diffusion rate (31). Voids at the oxide-alloy interface would have the opposite effect and increase diffusion.

Cox et al. (30) oxidised iron-chromium alloys with less than 20% chromium in a carbon dioxide based gas and found a duplex oxide of which the outer layer contained very little chromium (figure 1.2); this was due to the difficulty of the chromium atoms migrating through the inner layer, a spinel.

Linear oxidation was observed initially and was followed by a parabolic oxidation rate, indicating a diffusion-controlled process. As markings initially on the metal surface were found at the oxide-oxide interface, the outer layer must have grown by migration of the metal atoms through the inner oxide; such migration must be easier for iron.

The spinel was considered to be a close-packed arrangement of oxygen anions, with metal ions in some of the octahedral and tetrahedral interstices. The rate of diffusion was related to the activation energy of a metal atom moving from one interstice to an adjacent vacant site. The crystal field preference energy, C.F.P.E., was zero for an iron III ion because of its 5 'd'-electrons, and maximum for a chromium III ion with 3 'd'-electrons; as Azaroff (32) found that the most favoured route was via alternate octahedral and tetrahedral sites, a low C.F.P.E. would lead to a higher diffusion rate as the metal ions would be less sensitive to their environment in the oxide lattice. By considering several first row transition elements Fe, Mn, Co, V, Ni, and Cr, Cox et al. (30) showed a correlation between parabolic oxidation rate and the C.F.P.E., assuming that oxidation proceeded via outward migration of cations through the oxide, and that it was the C.F.P.E. that caused the segregation of elements present in the alloy. However, oxidation at the metal-oxide interface would not be dependent on the C.F.P.E. of the metal ions, but on the diffusion of the oxygen ions; the resulting oxide should also have a

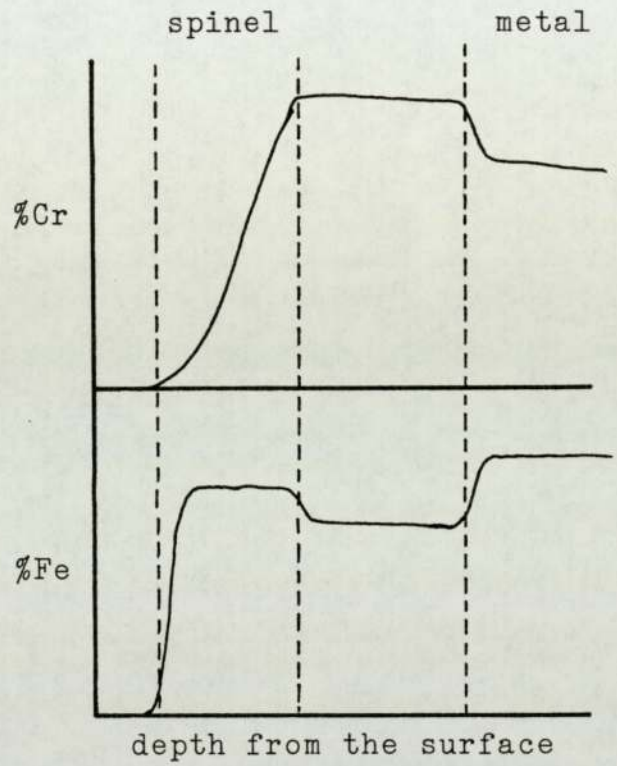

Figure 1.2 The variation in the iron and chromium concentrations in the oxides formed on an iron-chromium alloy (ref 30)

metal ratio similar to the ratio of the metals in the alloy.

1.2.2 Static oxidation of steels in carbon dioxide

The study of steels in carbon dioxide has generally been carried out in connection with a nuclear power research programme with the result that the ambient temperatures of the steels under test were usually about or just greater than the operating temperatures of the steel in the reactors. These were generally 400°C to 600°C for British or French gas-cooled reactors.

Carbon dioxide is an oxidising gas, but not to the extent of oxygen or air; as a coolant, it may contain up to 2% carbon monoxide plus some water vapour, methane or hydrogen. Research is often carried out in pure CO_2 for convenience or CO_2-1%CO, but proper 'A.G.R. gas', which has the approximate composition of CO_2-1%CO plus 1000vppm CH_4, 200vppm H_2 and 250wppm H_2O, is also frequently used. Since the late 1970's, the volume of methane present in the coolant gas has been reduced to about 250-300vppm.

Table 1.3 presents a summary of the behaviour of some steels in various carbon dioxide-based atmospheres.

The oxide formed on carbon and low alloy steels in CO_2 is mainly Fe_3O_4 with some α-Fe_2O_3 and with a carbide, Fe_3C, occasionally present (33). Above 600°C, the main oxide in contact with the metal is FeO, but lesser layers of Fe_3O_4 and α-Fe_2O_3 are also present (1). In the chromium alloys, a Cr-enriched spinel is the main oxide. These materials have been studied more than the mild steels due to their greater resistance to oxidation; carbon steels cannot be used at temperatures above 400°C, and even at 350°C, the penetration rate into the metal is 8μm per year (7).

Among the low alloy Cr-Mo steels to have been studied, the Fe2¼CrMo steel oxidised only slowly up to

Material	Remarks
Iron	Incompatible at 400°C in wet CO_2/0.2%CO and at 450°C in dry CO_2/5%CO
Mild steel	Compatible to 350°C, incompatible at 400°C in CO_2/CO/500ppmH_2O
Rimming steel	Incompatible at 400°C in CO_2/CO/ 500ppmH_2O and at 450°C in dry CO_2/CO
Stainless steel	Compatible to 500°C
Stainless steel AISI 304(18Cr 8Ni)	25.4μm local penetration after 16000 hours at 650°C
Stainless steel AISI 321(18Cr 8Ni Ti)	Compatible at 500-600°C in dry CO_2
Stainless steel AISI 310(25Cr 20Ni)	Compatible to 650°C in dry CO_2, some scale flaking at 750°C

Table 1.3 The compatibility of some stainless steels with carbon dioxide (ref 1)

500-525°C in dry CO_2 and up to 425-450°C in moist CO_2; however at 550°C, breakaway oxidation occurred in wet gas after about 750 hours (34,35).

More water vapour or carbon monoxide in the coolant caused increased post-breakaway oxidation rates and a shorter period to reach such oxidation on low alloy steels (36); an increase in the gas pressure also reduced the time to reach breakaway. The post-breakaway rates were again dependent upon the moisture content (37). Addition of elements to reduce iron carbide formation such as niobium and titanium as well as other elements like silicon or tin increased the time required to reach breakaway oxidation (38). A 3% Nb mild steel did not reach breakaway in 38000 hours at 500°C in moist CO_2.

A possible mechanism of breakaway oxidation, suggested by Price and Whittle (39), was that carbon deposits trapped in the growing oxide layer later reacted to form carbon monoxide, which caused a disturbance and eventual breakaway in the oxide. Addition of elements with more stable carbides than that of iron, such as manganese, chromium or molybdenum decrease this reaction. The presence of water vapour may also have increased the rate of CO formation at the metal-oxide interface.

$$3Fe + 2CO_2 \longrightarrow Fe_3O_4 + 2C \qquad (3)$$

$$3Fe + 4CO \longrightarrow Fe_3O_4 + 4C \qquad (4)$$

$$2CO \rightleftharpoons CO_2 + C \qquad (5)$$

$$H_2O + C \rightleftharpoons H_2 + CO \qquad (6)$$

Price was also able to suggest why an increase in gas pressure decreased the time to reach breakaway. Reactions (3) and (4) proceeded faster at high pressures and so the volume of carbon deposited also increased; it was thought that water vapour was also more easily absorbed by the oxide at these pressures. Thus the equilibrium of equation (6), considered to be one of the

essential reactions, moved to the right and more gas was liberated within the oxide. Figure 1.3 gives a schematic diagram showing how the protective oxide was imagined to be disturbed (39).

The effect of varying the CO content has not been extensively studied but has been found to have an effect on the extent of carburisation. With a CO_2-5%CO mixture, 'carbon soot' was deposited (40). The CO was necessary to reduce the oxidising potential of the coolant.

$$CO_2 + C \longrightarrow 2CO \qquad (7)$$

$$CO_2 \rightleftharpoons CO + O \qquad (8)$$

$$CO_2 \rightsquigarrow CO + O \qquad (9)$$

The result of the near-irreversible reaction (7) was to remove carbon from the moderators in the reactor, and thus reduce their effectiveness; in a non-flowing CO_2 coolant, this reaction also proceeded using the carbon in the stainless steel (40, 41). The equilibrium in equation (8) shifted to reduce the amount of free oxygen present when the carbon monoxide content increased. Unfortunately, this reaction was also radiation induced (40).

Price and Whittle (39) found that pure iron and rimming steel were particularly subject to breakaway, but that medium and high alloy steels were much less susceptible. The majority of recent research has been carried out on Fe-Cr alloys with about 9% Cr (10, 19, 42, 43, 44) or on austenitic steels, e.g. 18Cr8Ni (5, 11, 33, 45).

Brierley (10) classified the oxidation that had been observed on 9Cr steels into four types:

a) growth of regular stacked duplex oxides resulting in the formation of a thick uniform oxide.
b) sustained growth of complex oxides in the form of mounds or larger areas of raised oxide.
c) rapid, non-protective oxidation with a rate of

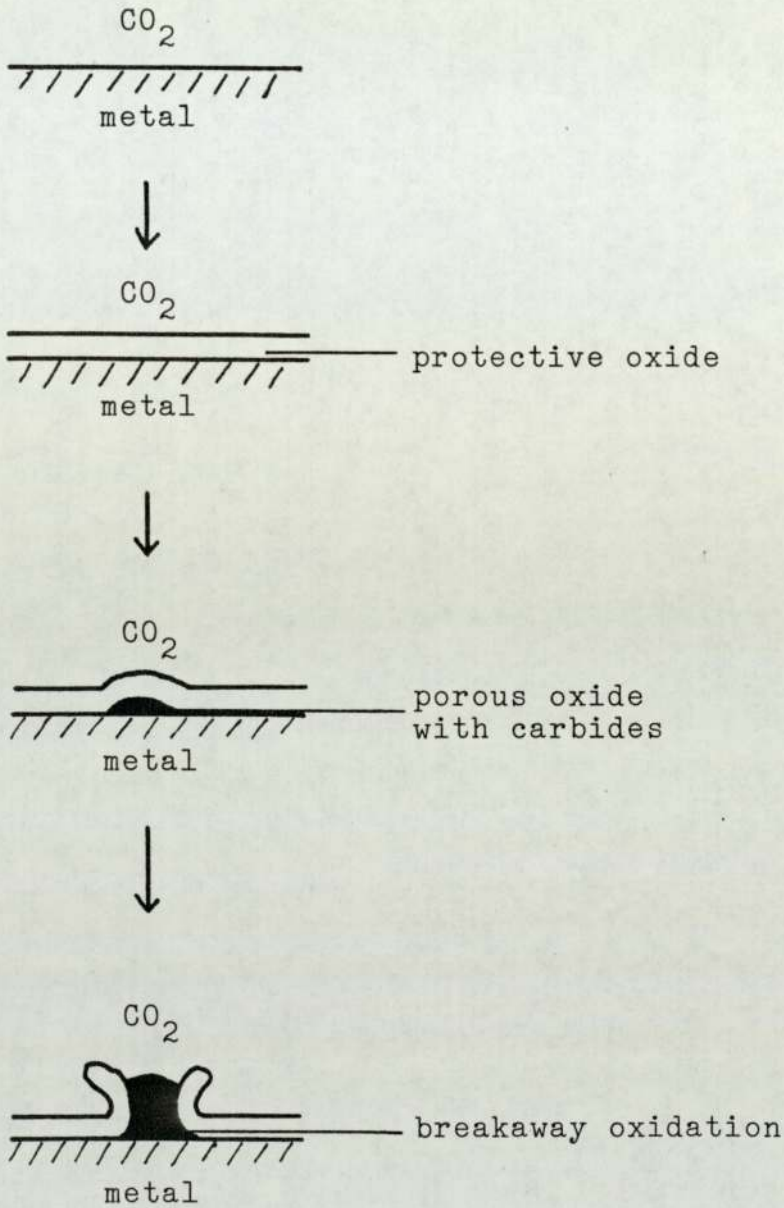

Figure 1.3 A schematic diagram of a suggested mechanism to reach breakaway oxidation (ref 39)

progress along the original metal-oxide interface which is greater than that of the breakaway oxidation front in the metal or its component parallel to the interface. This causes a peeling back of the oxide layer.

d) rapid, non-protective oxidation where the rate of progress along the existing metal-oxide interface is equal to or less than that of the breakaway oxide front in the metal.

The kinetics of protective oxidation can be given by:

$$w = at^b \qquad (1.2)$$

where w is the weight gain, a and b are constants and t is the time. b is generally between 0.3 and 0.5 and so the oxidation is between parabolic and cubic kinetics. The post-breakaway rates can be given by:

$$w = rt \qquad (1.3)$$

where r is a constant and dependent upon temperature, gas composition, the steel silicon content and specimen size (42).

The rate of oxidation of types (c) or (d) was very high and the area subject to breakaway oxidation could be measured by direct observation; the post-breakaway rates were 1000 $mgcm^{-2}hr^{-1}$ at 650°C and 100 $mgcm^{-2}hr^{-1}$ at 600°C (10). In an attempt to measure the rate from 450°C to 550°C, specimens undergoing breakaway oxidation at 650°C were cooled and the new oxidation rate measured; these were found to be very high and a continuing programme of accelerated tests is going on test specimens from reactor production batches of 9Cr steel. However, the reliability of the post-breakaway data is not known for the accelerated tests.

Three components were observed in the scale on Fe9Cr1Mo steels, two oxides and an internal oxidation zone (42). The outer oxide was almost pure magnetite,

whereas the inner oxide was a spinel enriched in chromium; this layer also had a high carbon content and thus supported the theory of breakaway oxidation proposed by Price and Whittle (39). Oxidation of the outer layer occurred at the oxide-gas interface and of the inner layer at the oxide-metal interface although some oxidation may have occurred within this oxide.

Hampton et al. (43) have found supporting evidence that the diffusion is a two way process, by metal diffusion to form Fe_3O_4 at the oxide-gas interface, and by gas diffusion to form an iron-chromium spinel at the metal-oxide interface. Sufficient pores were observed in the outer oxide layer to indicate that the diffusion rate of the CO_2 through the outer layer was high enough not to be the rate-determining step. This agreed with Rowlands (42) who prepared taper sections in which the outer oxide was removed and then found that this did not significantly alter the oxidation rate. The oxidation rate was found to be proportional to $pO_2^{\frac{1}{4}}$ at high pressure and $pO_2^{-\frac{1}{3}}$ at low pressure (where pO_2 is the partial pressure of oxygen); this suggested two different diffusion mechanisms, via ion vacancies at high pressure and by iron diffusion at low pressure (43). Hampton (43) also made the tentative suggestion that the walls of the pores did not oxidise until the pores were blocked because the adsorbed gas on the walls may have had a different composition from the gas in the pores.

Rowlands and Whitlow (19) have carried out long-term tests of about 10000 hours duration on 9Cr1Mo steels and been able to estimate the life-times of components in normal use. Assuming an operating temperature of 450°C, life-times in excess of the design life-time of the reactor were predicted. Mortimer (44) has studied the oxidation of Fe-Cr alloys at higher temperatures and found that the addition of chromium was only beneficial when more than 8.5% was present in the alloy. Breakaway

oxidation was observed at 650°C and found to be independent of chromium content. However, the protective spinel occurring at 450°C was independent of both gas composition and pressure.

The final group of steels to consider are the austenitic steels of which the simplest example is 18Cr8Ni or AISI 304. Early work (45) found that 20Cr25Ni or Fe40Al steels were better than 18Cr8Ni as cladding materials. It was discovered that 25Cr20Ni steels oxidised to form Cr_2O_3 adjacent to the metal and chromium depleted spinels and M_2O_3-type oxides further from the metal (46, 47).

McCoy (48) oxidised AISI 304 in carbon dioxide and found very complex kinetics (approximately parabolic oxidation with some initial periods of linear kinetics); α-Fe_2O_3 was formed at the gas-oxide interface and a spinel at the metal-oxide interface. Carburisation was found to be very pressure dependent.

Wallace (11) and Smith (5) have carried out recent studies of 18/8, 18/10 and 18/12 austenitic steels in carbon dioxide. The oxidation of the 18Cr12Ni steel to form a Cr-rich M_2O_3-type oxide followed parabolic kinetics (11), whereas the 18Cr8Ni steel had logarithmic oxidation. This was shown to be due to the replacement of the oxide with an iron-rich nodular oxide which consisted of two layers , α-Fe_2O_3 on a complex Fe-Cr-Ni spinel. Smith (5) also observed a duplex oxide on 18Cr8Ni in which the outer oxide was mainly heavily grained magnetite with some added Ni and about 1-2.5% Cr, while the inner oxide was an almost featureless spinel, often with as much as 46% Cr (equivalent to $FeCr_2O_4$) at 650°C. The chromium percentage decreased as the temperature was lowered to 550°C, but was always highest at the metal-oxide interface. A complicated series of spinels was formed. $NiFe_2O_4$ was an inverse spinel which allowed replacement of all the Fe^{3+} ions in the octahedral sites by Cr^{3+} ions

while still maintaining the inverse structure (49).

After the discussion about the behaviour of so many steels, a short summary is in order emphasising the oxidational behaviour of the 9Cr1Mo steels of most relevance to this thesis. Oxidation at 450°C produces magnetite on a Fe-Cr spinel with the oxides being formed at the gas-oxide and oxide-metal interfaces respectively. The outer oxide is iron-rich due to the very slow diffusion rate of chromium through the spinel, but as it is also porous, the inward diffusion of the carbon dioxide is rapid and not the rate-determining step for spinel oxidation. Breakaway oxidation has been observed at higher temperatures and in accelerated tests.

1.3 Mechanisms and classifications of friction and wear

1.3.1 Introduction

Several attempts have been made to classify wear as no one method can be considered perfect because many sliding systems exhibit features comprising of a combination of two or more types of wear.

Archard and Hurst (49) devised one of the earliest and simplest classifications. They studied the wear rates of metal pins wearing on steel rings and found that although there was a wide range of wear rates (the volume removed per unit sliding distance), the debris was one of only two types, either metallic or oxidised. Severe wear was characterised by a high wear rate with granular metallic debris; mild wear was indicated by a much lower wear rate (often 1000 times less) with debris comprising of powdered oxide.

This classification was criticised for being over simplistic, but did have the advantage that as the debris was easy to characterise, any system could be quickly assigned to one class of wear. However, the more recent work of Welsh (50, 51) has identified wear

in which oxidation was not necessary to produce a mild wear rate; he attributed this to excessive phase hardening reducing the wear rate to values associated with oxidational mild wear. This would conflict with Archard and Hurst's simple approach.

Another classification was devised by Kragelskii (52); he suggested that wear could be catagorised by considering the manner in which the frictional bonds were broken at or near the sliding surfaces, i.e. by:

a) elastic displacement
b) plastic displacement or repeated deformation
c) cutting of the material
d) destruction of the surface film
e) destruction of the bulk material.

Unfortunately, a disadvantage of this type of classification is that it is usually very difficult to determine the mechanisms.

The classification that has been most widely accepted was devised by Burwell and Strang (53, 54) in 1952: four main types of wear were identified:

a) adhesive or galling wear. This is equivalent to the severe wear of Archard and Hurst.
b) abrasive or cutting wear. This is generally caused by the presence of a third body.
c) corrosive wear. This is oxidational or mild wear if air is the medium.
d) surface fatigue. This generally only occurs in systems with very low wear rates.
e) minor types of wear. These include erosion or abrasion by high velocity fluids and also impact wear in which the two surfaces come together at an angle before starting to slide against each other. Fretting is also a minor type of wear that often occurs when the removed debris is trapped and abrasion follows. Due to its

relevance to this thesis, it will be treated in as much detail as the other four main types of wear in the ensuing sections.

1.3.2 Adhesive wear

Galling, scuffing and scoring are other terms used by some workers when referring to particular types of adhesion.

Adhesive wear occurs when two smooth surfaces slide over each other (55) and small areas of each surface adhere together; both Rabinowicz (56) and Kragelskii (52) consider that cold welding of the asperities is the mechanism of bond formation. As sliding continues, these bonds must be broken and should the break not occur at the point at which it was formed, the result is a fragment from one body being transferred to the surface of the other body. In later passes, these fragments may be retransferred or else removed completely to form separate particles of wear debris.

As matter is normally transferred between the two sliding bodies, studies of metallic transfer have been made. Bowden and Tabor (57) considered that the shearing process could occur in four ways. If the junction is weaker than the bonds within each body, then fracture will occur at the same spot and so both transfer and wear will be minimal; alternatively, if the junction is stronger than the bonds in only one metal, then shearing may occur within the softer metal. Transfer will take place from the softer to the harder metal and wear will be higher even though the friction may not be much different from the previous example. When the bonds within both bodies are weaker than the junction, transfer occurs in both direction, but preferentially towards the harder body.

Finally, an example of relevance to the work in this thesis is that of a metal sliding upon itself. The

process of deformation and welding will work harden both surfaces and increase their shear strength; as a result, shearing will rarely take place at the interface, and so transfer, surface damage and the wear rate will all be high. The net transfer will be towards the specimen that work hardened more quickly.

The above four examples indicate that there is no direct relationship between the coefficient of friction and the wear rate (57). Rabinowicz and Tabor (56) also found that metallic transfer was more sensitive to changes in the surface conditions than to the coefficient of friction.

1.3.3 Abrasive wear

There are two kinds of abrasive wear. Two-body abrasive wear occurs when a soft body is worn against a harder rough surface. Avient et al. (58) found a linear relationship between volume removed and coefficient of friction once the softer surface had reached its equilibrium roughness.

Three-body abrasive wear occurs in systems in which hard abrasive particles are trapped between two softer sliding surfaces. Rabinowicz et al. (59) found that three-body abrasive wear rates were in general about a factor of ten less than two-body abrasive wear rates. This was attributed to the fact that the loose abrasive particles spent most of their time rolling and only about 10% of their time abrading.

Three-body wear can also occur when the oxidised wear debris from a metallic system, which is much harder than the metallic surfaces, is trapped between those surfaces. This is more likely to occur in systems with horizontal sliding surfaces; the iron oxide, Fe_2O_3, has been used to polish metals (54). Abrasive wear can therefore follow from corrosive wear.

A special type of wear called fretting is the result

of abrasive wear caused by trapped oxide particles produced by reciprocating sliding. These examples show that it is often very difficult to classify different types of wear.

1.3.4 Corrosive wear

For corrosive wear to occur, both corrosion and sliding are necessary. The corrosive environment may be a liquid metal, e.g. sodium used in some nuclear power stations, or a much less hostile environment such as the atmosphere or impure carbon dioxide used in some other nuclear power stations.

The effect of a lubricant may be to protect the surfaces and thus reduce corrosion, or to react with the surface to produce an alternative form of wear (54, 60). It is possible that addition of a lubricant may produce adverse wear. However, unlubricated metal sliding in air or carbon dioxide-based environments giving corrosive or oxidational wear is of most relevance to this thesis.

Research has already identified several different metal oxides on the surface of steels undergoing equilibrium corrosive wear (61, 62). Quinn studied the oxidised wear debris in an attempt to estimate the temperature at which the oxidation had occurred (61, 63). Tao (62), in his model explaining the corrosive wear caused by atmospheric oxygen, concluded that the wear rate was more dependent upon oxidation than the rate of debris removal.

Corrosive wear will often change into abrasive or adhesive wear. If the surface is removed too rapidly for an equilibrium oxidised layer to form, adhesive or severe wear will generally result; abrasive wear can occur when the oxidised debris is trapped.

1.3.5 Surface fatigue wear

This type of wear mainly occurs between surfaces in

rolling as well as sliding contact. The wear rates in such systems are small, and so the surfaces fatigue rather than wear due to the repeated loading and unloading; once the surface has become fatigued, pitting or flaking occurs and pits of up to 1 mm in diameter are formed after the debris has been removed (55). Pitting occurs in the presence of a lubricant when the wear is negligible.

The wear characteristics are also very different from those of other forms of wear already described; a surface in rolling contact can often operate normally up to the time at which it starts pitting, but after this, the surface is damaged too much to be of any practical use (54). Because of this, the life-time of components subject to rolling contact surface fatigue wear is measured, rather than the wear rate.

Miki and Kobayashi (64) suggested that the process of pit formation occurred in four steps: 1) wear, 2) plastic flow, 3) fatigue, 4) work hardening. Hardened surfaces increased the time to pitting due to decreased strain hardening (65).

Experiments have also been carried out in which the ratio of sliding to rolling varied; in such cases, the fatigue life is related more to the coefficient of friction than the ratio of sliding to rolling (66). However, some sliding is essential to cause the friction.

1.3.6 Fretting wear

Although both Burwell (54) and Rabinowicz (55) only considered fretting to be a minor type of wear, an increasing amount of research is carried out on this form of wear. The work is frequently carried out in connection with a nuclear power programme (11, 67, 68).

Fretting wear occurs when two contacting surfaces undergo reciprocating motion of small amplitude. Rabinowicz (55) stated that the debris was oxidised after

removal from the surface due to adhesive wear.

Halliday and Hirst (69) referred to such wear as fretting corrosion after studying mild steels sliding with amplitudes between 2 μm and 420 μm. The friction and wear were greater at the larger amplitudes studied; the friction was also much greater immediately after any loose debris had been manually removed. The term fretting corrosion was not completely correct as other workers have found fretting in the absence of oxidation (67, 70). Godfrey and Bailey (70) found that fretting started with severe adhesion or cold welding; plowing was caused by surface asperities or protruding transferred material. Oxides were observed on iron after 50 cycles of fretting and could be seen on mild steel after just half a cycle.

Wright (71) suggested that the oxidation of the finely divided newly formed debris was immediate due to the increased chemical reactivity of the surfaces and that as a result, normal oxidation products may not be formed.

More recent work has been carried out, particularly on steels at elevated temperatures (67, 68, 72, 73), and a more detailed account will be given later.

1.3.7 Theories and mechanisms of wear

Many studies of wear have been made, and a recent review of metallic wear has been given by Childs (74). Archard (75) was amongst the earliest workers in this field and formulated the wear law that is now associated with his name. A great number of theories have since been proposed of which in recent years, two of the most important have been the oxidational wear theory proposed by Quinn (76, 77, 78) and the delamination wear theory suggested by Suh (79, 80).

Archard was not alone in dividing wear into just two catagories, namely severe and mild; several other workers including Hirst, Kerridge, Lancaster and Welsh

made similar observations (49, 50, 51, 81, 82). However, Archard provided one of the earliest attempts to understand wear in terms of the processes occurring at the wearing surfaces. He considered the height variation on a nominally flat surface in order to estimate the distribution of contacts between two such surfaces (75) and then measured the contact area from the electrical resistance to find that the size and number of contacts increased with the load, in addition to the wear rate being proportional to the load. The wear process itself was explained by assuming that lumps of material were removed at points of contact by plastic deformation.

Kerridge and Lancaster (81) studied the mechanism of removal on a pin-on-ring system more closely and suggested that transfer of material from one sliding member to the other occurred before the debris was formed. The wear particles were larger than the transferred fragments which were identified by using radioactive tracers. In later work, Lancaster (82) considered the transition between severe and mild wear and found that mild wear of brass resulted from three causes: intermittant metal-to-metal contact, abrasion by oxide particles and flaking of the oxide layers from the surface.

More recently, both Suh and Quinn have proposed wear theories. Suh et al. (79, 80) formulated the delamination theory which was applicable to the conditions of dry wear that produce metallic debris with surface smoothing, but without transfer. Quinn's work referred to systems which produced oxidised debris (76, 77, 78).

The delamination theory of wear was first proposed in 1973 (79) and based on the following premises:-

1) during wear, material at the surface was cold-worked much less than that in the sub-surface layer. This was due to the elimination of dislocations by migration to the surface.
2) the dislocation density increased during wear in

this sub-surface layer and eventually voids formed.

3) with continued sliding, the voids joined together to produce a crack parallel to the surface, and once the crack had reached a critical length, the material between the crack and the surface sheared to produce a plate-like wear particle.

Much supporting evidence for this theory has been found, not only by Suh, but also by Rigney and his co-workers (83, 84, 85). Hirth and Rigney (83) considered how the mechanism of delamination wear was dependent upon crystal plasticity and the stacking fault energy. In some hexagonal close-packed (h.c.p.) metals, the closeness of the ratio of the lattice parameters to the ratio expected in a theoretically perfect array of metal atoms was found to be related to the wear. Metals such as magnesium, cobalt or rhenium, with ideal $^{c}/_{a}$ ratios (the lattice parameters are identified in figure 1.4) have low wear rates and the basal plane is usually normal to the wear surface; this plane has a low stacking fault energy and after slipping, cross-slip of prismatic or pyramidal planes is prevented. Thus, faults parallel to the surface are preferred and delamination wear is possible. In a later paper (84), it was stated that low stacking fault energies encouraged the formation of cells in the microstructure (due to a higher fault density at the surface); in addition, it was suggested that if the wear particles separated from the bulk material at the boundary of the cellular and non-cellular regions, then the particle thickness could be related to the stacking energy. Hsu et al. (85) noted that the friction and wear behaviour of austenitic steels depended upon their stability with respect to martensitic transformations to the ϵ(h.c.p.) and α'(b.c.c.) phases. This was in support of Rigney's original paper (83) which concentrated on h.c.p. metals, but said that factors which encourage coplanar or single slip in other crystal structures, such as body-centred cubic, would also

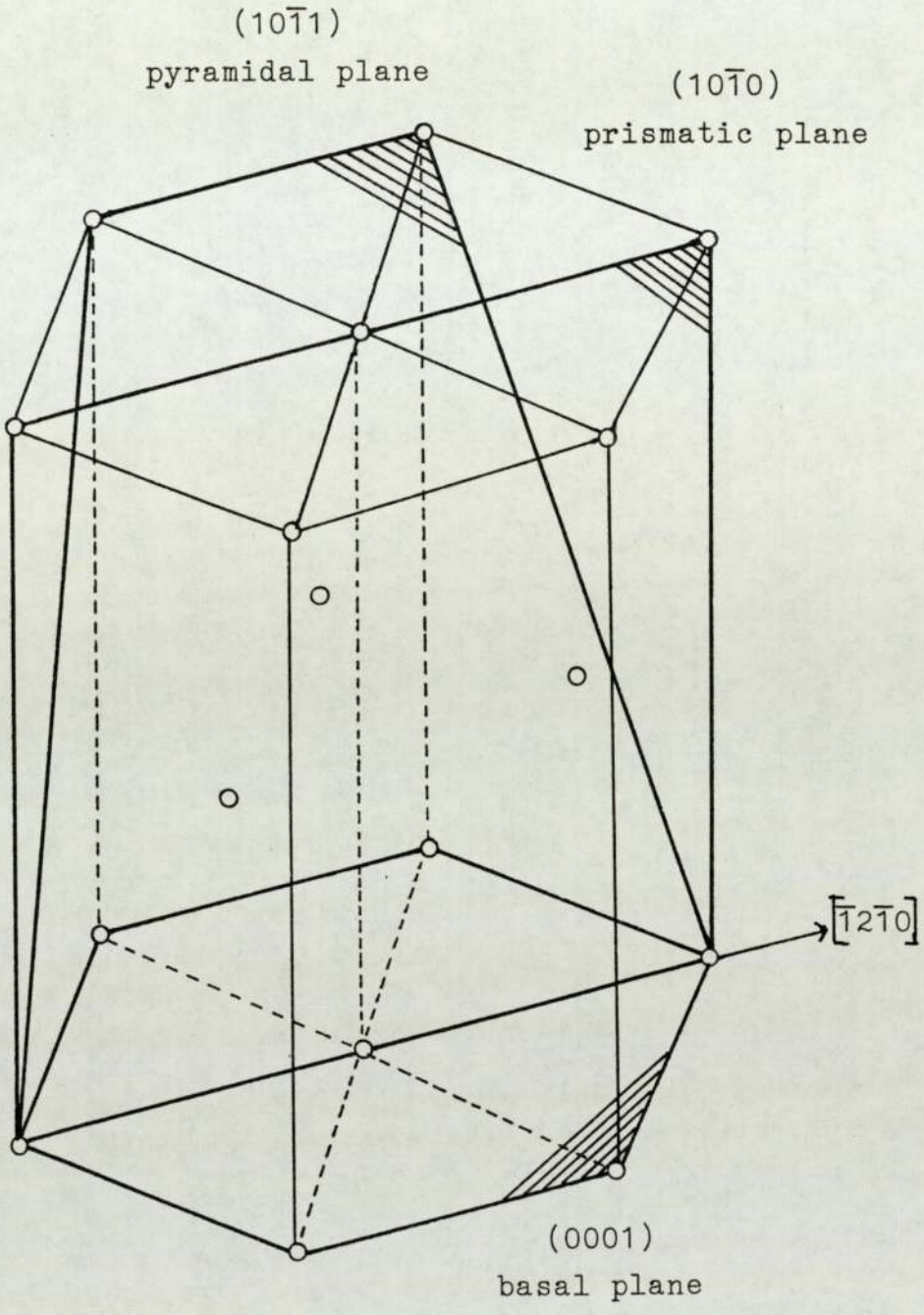

Figure 1.4 Planes in a hexagonal lattice with a common [$\bar{1}$2$\bar{1}$0] direction (86)

influence their wear properties as well.

Most of the experimental work carried out by Suh, Rigney and their co-workers employed low loads and speeds so that the wear was always below the T_1 transition described by Welsh (50). Theories of oxidational wear are generally more applicable to systems with larger loads and higher sliding speeds with the result that the increased oxidation and greater wear rates made metal fatigue a much less likely mechanism of material removal.

Several wear theories which also concern oxidation have been proposed; Tao (62), Quinn (76, 77, 78), Yoshimoto and Tsukizoe (87) and Tenwick and Earles (88) have all made contributions.

Tao (62) considered that two extreme models for corrosive wear were possible. In his model 1, the oxide layer was presumed to grow gradually, and then be removed instantaneously by the rubbing action once a critical thickness, ΔS, had been reached; model 2 presumed the opposite situation in which oxidation to the critical thickness was instantaneous and its removal by wear was a gradual process. Figure 1.5 shows how, in these two extreme cases, the oxide thickness varied with time. By separately considering these two situations, Tao showed that the rate of oxide build-up was more controlling than the rate of oxide removal. The model also predicted a higher rate constant and lower activation energy in a tribological situation than for static oxidation at a similar temperature. Tao showed that the wear rate decreased as the load got smaller, even assuming a constant critical oxide thickness, by considering the hot-spot temperature calculated in the manner proposed by Archard (89).

Yoshimoto and Tsukizoe (87) derived an oxidational wear theory from the distribution of the real area of contact. The number and size of the metal areas of contact were derived theoretically by considering the

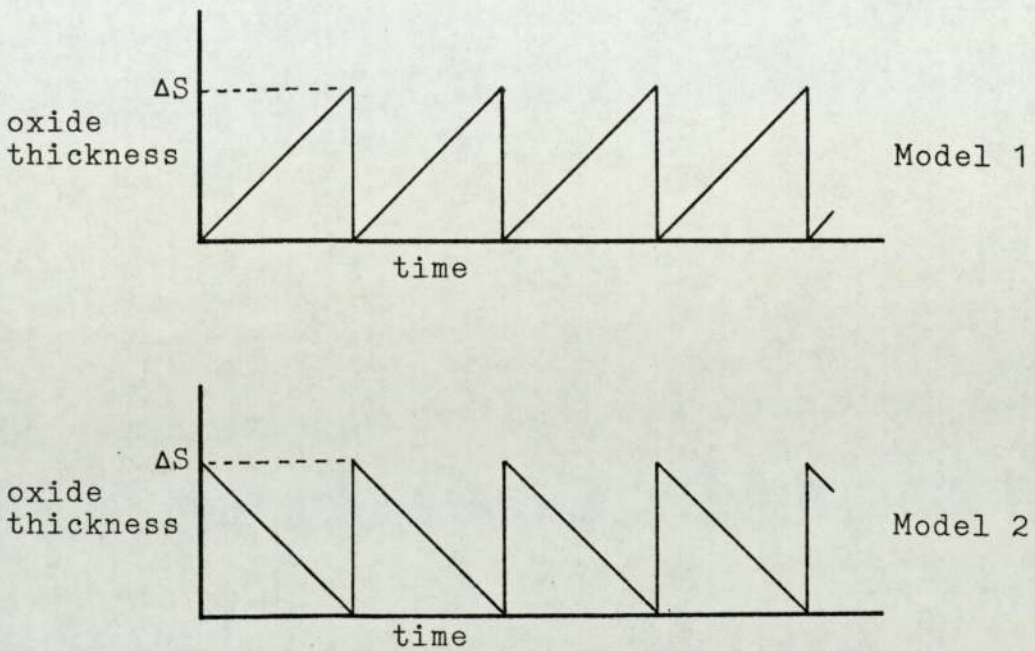

Figure 1.5 The two extreme models for corrosive wear of Tao (ref 62)

surface profiles. Three wear regimes were classified - mechanical or metal-metal contact wear, Fe_2O_3 film wear and Fe_3O_4 film wear. They assumed linear oxidation and that each contact produced a wear particle; although linear oxidation is quite possible in thin films, it is very unlikely that a new wear particle will be produced each time a contact is made. They concluded that the wear rate was proportional to the square root of the load, was approximately proportional to the contact area and inversely proportional to the sliding velocity. The first conclusion is not supported by the results from other laboratories; the second agrees with the Archard wear equation (75). Not much work has been carried out at different velocities, but with a constant load; however, there is some evidence that the wear rate decreases as the velocity increases (77).

Tenwick and Earles (88) developed an oxidational wear theory which assumed linear oxidation at the bulk surface temperature of the pin. This does not seem likely as one consequence of the majority of oxidation occurring at the surface temperature would be that the oxide thickness on in- and out-of-contact areas would be approximately the same; this would imply that when the former areas had reached the critical oxide thickness and wear particles had separated, the new load-bearing areas would already have a thick oxide layer and would soon produce wear debris. Their theory would also imply that the rate of static oxidation at the bulk temperature would be roughly equal to that for tribo-oxidation. However, Tenwick and Earles suggest that the cyclic loading and unloading of the contact areas would increase the probability of oxide cracking, which would then make linear oxidation more likely as oxygen could diffuse towards the substrate metal more easily, whereas the undisturbed areas are more likely to oxidise parabolically. It is also probable that frequently disturbed metal is

more reactive.

Parabolic oxidation was assumed to take place on the asperities in the model of oxidational wear proposed by Quinn (76). Initially, this theory assumed that all oxidation took place at the asperities, but more recent developments (90) have attempted to consider out-of-contact oxidation as well; this is especially important when the theory is applied to wear at elevated temperatures. Quinn assumed, as did Tenwick and Earles (88) that a critical oxide thickness was necessary for a particle of wear debris to be produced. Quinn used the Archard wear equation (91) as his starting point:

$$w = K A_r \qquad (1.4)$$

where w is the wear rate, A_r is the real area of contact and K is the wear constant. In assuming that K was the probability of a wear particle being produced at one particular contact, Quinn equated $^1/_K$ to the average number of contacts between two particles of wear debris separating from the same asperity. The critical oxide thickness was estimated from scanning electron microscopy observations (92); the oxidation time was dependent upon the time of contact at the asperities, i.e. the sliding speed and the asperity diameter.

An expression was therefore obtained for the wear constant of K-factor (78). An interesting aspect of Quinn's work was his attempt to determine the oxidation temperature from the proportion of the different iron oxides and pure iron in the wear debris (93). The spinel, Fe_3O_4, was the majority oxide above about 290°C; thus, if a pin-on-disc experiment run at room temperature produced more spinel oxide than rhombohedral oxide, α-Fe_2O_3, then the oxidation temperature must have been above 290°C.

Each of the oxidational and delamination wear theories is only applicable to a small range of loads and sliding

speeds. The difficulties in obtaining accurate values of the Arrhenius constant for different oxides, as well as in measuring the actual temperature of oxidation introduce inaccuracies into the oxidational wear theories of Tenwick and Earles, and Quinn; Suh, on the other hand, has restricted the majority of his work to low wear situations in which metal fatigue is more likely. Suh has also observed delamination wear at high sliding speeds (94) when the debris was plate-like, but as the surface was roughened by sliding, and there was large scale plastic flow, it seems unlikely that cracks parallel to the surface could form. The oxidational wear theories have the advantage of not stating a mechanism of particle removal.

The above workers have attempted to establish the principles of adhesive or corrosive wear. Work on abrasive wear has also been in progress. Khruschov (95) devised fourteen basic principles of 'abrasive wear during friction against fixed abrasive grains'; he did, therefore, restrict his work to two-body abrasion. He established that the wear rate was proportional to the stress, but independent of friction at low sliding velocities and in the absence of external heating. Wear was related to the grain size up to some maximum above which there was little dependence. The relative hardnesses of the abrasive and the abraded metal were also important.

Spurr (96) has carried out more recent work on the abrasive wear of metals; he found that the wear rate was proportional to the load and the contribution of the friction due to ploughing. Wear decreased as the hardness of the metal increased. The ploughing contribution was found to be dependent upon the shape of the abrasive grains; such particles form a prow ahead of a groove, and built-up edges on either side. Wear particles are produced when the tensile stresses are exceeded.

The importance of grain shape may explain the

difference between two- and three-body abrasive wear rates; Rabinowicz et al. (59) attributed this to the fact that loose grains spent the majority of their time rolling and not abrading. It is possible that after some abrasion, some particles have a decreased ability to abrade and cause less ploughing; such a change may result in a smaller coefficient of friction, but neither Khruschov (83) nor Spurr (84) commented on any decrease in friction with time.

1.3.8 Theories of friction

The study of friction has been made for over five hundred years with Leonardo da Vinci, Amontons and Coulomb each making contributions between the 15^{th} and 18^{th} centuries (97). In 1781, Coulomb made a suggestion that is still considered to be partly true today, that friction results from surface roughness and the interlocking of asperities (98, 99). The most recent review of friction theories and mechanism is that due to Madakson (100).

There are more ideas concerning friction than there are about wear because both the wear rate and debris can be studied, whereas only the coefficient of friction can be measured and no direct observations can be made on the force between two contacting asperities. However, theories of friction are simpler than those of wear in one significant way; it is assumed that every asperity contributes to the total friction, whereas only a small proportion produce wear particles. The estimation of this fraction, often necessary when formulating a wear theory, introduces further error. While considering the friction due to individual contacts, Williams (98) suggested that if asperities were assumed to be conical in shape, then the apical angle could range from 0° to 180°; Koura (99) concluded that asperities could not be conical, but noted that the assumption that they were cylindrical or hemispherical only gave qualitive

predictions of the coefficient of friction.

Bowden and Tabor (57, 101) suggested that the frictional force was due to the shearing of the minute welds formed at points of contact between the two rubbing bodies, and the plowing of the hard asperities over a hard surface. Rabinowicz (55, 102) considered that the surface energy made a major contribution to the friction. Rigney and Hirth (103) and Walton (104, 105) proposed that the plastic work done in the sub-surface regions caused the frictional force.

Rubenstein (106) produced a general theory of friction based upon adhesion theory in which the contacting asperities deformed according to the relation, stress α (strain)^{x}, and showed that the friction force was dependent upon the applied load, the surface roughness, area of contact and the physical properties of the sliding material. In the theory presented by Suh and Sin (107), the friction force resulted from the deformation of the asperities and adhesion at regions within the area of contact.

The above discussion has shown the importance of the real area of contact. Bowden and Tabor (57) considered how this area changed with load. They imagined a load, W, on a hemispherical slider resting on a metal; the softer metal deformed until the area of contact, A, was sufficient to support the load. This occurred when:

$$A = \frac{W}{p_m} \qquad (1.5)$$

and p_m was the hardness of the metal.

Archard (91) carried out a more thorough analysis. Initially, he considered the simplified example of a single spherical asperity deformed elastically and found that:

$$A \propto W^{\frac{2}{3}} \qquad (1.6)$$

and therefore:

$$A \propto W^{-\frac{1}{3}} \qquad (1.7)$$

He then calculated how the area of contact would vary if more realistic conditions of multiple contact were assumed, and found that the area was very nearly proportional to the load with the result that the coefficient of friction was independent of load. He suggested that as elastic deformation was a much more frequent occurrence than welding, it was the former process which largely determined the magnitude of the friction.

Friction has also been found to be dependent upon material properties such as hardness, surface energy, strain, density, shear strength and surface roughness as well as the sliding velocity. At low velocities, friction increases with velocity and at high velocities, friction decreases with velocity (108, 109). Whitehead (110) and Archard (111) found that surface roughness had greatest effect at low load. Harder surfaces had lower friction (57, 101) and consideration of the thermodynamics and deformation energy has shown that the frictional force also depends upon density and temperature (52, 108).

The effect of sliding distance on friction has also been studied; the variation in friction is due to the extent of the initial deformation of the surface which is in turn due to the physical properties of the sliding surfaces, load, velocity and environment. Suh and Sin (107) devised a friction space diagram in which the coefficient of friction could be plotted against an adhesion function and the asperity diameter. During sliding, the friction may pass through up to three distinct stages; an initial stage dependent upon the surface finish and the nature and breakdown of the oxide film; this can be followed by plastic deformation and work hardening of the sub-surface layers, and finally an equilibrium is reached in the micro-structure due to the balance between oxide formation and removal (100). Rigney and Hirth (103) suggested that this final stage was due to the micro-structure achieving a steady state,

while Blau (112) considered that it was due to a reorientation of the sub-surface micro-structure.

Running-in friction has also been studied by Suh and Sin (107) and Blau (112), who found that it was generally low for steels, but dependent upon the load, velocity and environment. At larger loads or velocities, the initial friction is high (113, 114, 115).

This thesis is primarily concerned with the friction and wear that occur in carbon dioxide-based atmospheres; such environments have the effect of reducing the oxygen partial pressure. This can also be caused by carrying out wear experiments under vacuum or near-vacuum conditions. Barnes et al. (116) have studied the frictional behaviour of iron and iron-chromium alloys under pressures as low as 10^{-8} Pa (10^{-13} bar) and Iwabuchi et al. (117) have studied fretting under pressure in the range 10^{5} Pa to 10^{-3} Pa (1 bar to 10^{-8} bar).

Barnes (116) carried out experiments at one pressure, but increased the temperature of the iron-chromium alloys during the test which was stopped once seizure occurred; this was defined as having occurred once the coefficient of friction was above 25. Seizure occurred between 500°C and 600°C for alloys with a chromium content of between 0% and 27.8%; however, an Fe-40.6%Cr alloy did not seize even at above 800°C. Rabinowicz (102) suggested that a decrease in hardness of a material increased the friction, whereas Tabor (118) commented that the hardness of a metal had little direct effect on the frictional behaviour since a decrease in hardness was usually accompanied by a decrease in shear strength. Barnes (116) measured the hardness of the alloys under investigation and found that they softened at between 350°C and 420°C, always at least 50°C below the seizure temperature. He also found that admitting oxygen to a pressure of 10^{-5} Pa did not prevent seizure, but a pressure of 10^{-4} Pa prevented seizure, even at 750°C.

Bowden and Young (119) also found that admitting 10^{-4} mmHg or 1.3×10^{-2} Pa oxygen into the environment of sliding metals reduced the coefficient of friction from well above 10 to about 2.5.

Barnes et al. (120) also compared the behaviour of these alloys under unidirectional and reciprocating sliding at reduced pressures. He found lower wear rates with reciprocating motion which were attributed to the wear debris remaining within the wear track and encouraging the nucleation of protective layers. Ward (121) carried out a similar study and found opposing results; he attributed the higher reciprocating wear rate to greater abrasion by the debris. However, as he carried out his tests at atmospheric pressure, oxidation would have been much greater. It is quite possible, under conditions that only just support mild wear, that trapped debris encourage nucleation and further oxidation but an excess of debris increases abrasion in a high partial pressure of oxygen.

Iwabuchi et al. (117) found that a 0.45%C steel had frictional behaviour that was dependent upon gas pressure. The coefficient of friction increased with a decrease in pressure below 1 Pa and was insensitive to pressure above 1 Pa. Oxidative wear was significant above 0.1 Pa and adhesive wear below 0.1 Pa; this critical pressure is evidence that both Barnes (120) and Ward (121) may be correct in their observations.

In summary, friction is higher at very low pressures, but the presence of 10^{-4} Pa of oxygen reduces the coefficient to the values obtained at atmospheric pressure. Friction is caused by a combination of the adhesion between asperities and the plastic deformation of the surface layers; the presence of impurities, such as oxygen, decreases the adhesive force.

1.4 The wear of metals

1.4.1 Unidirectional wear

Many studies have been made on unlubricated metallic wear, of which that by Archard and Hirst (49) was amongst the first. This paper included the results from experiments carried out using a wide range of loads and sliding speeds on several different alloys and steels. They confirmed that the equilibrium wear rate was independent of the apparent area of contact, and determined values of K, the wear coefficient, for several materials; they found that the coefficient ranged from 7×10^{-3} to 1×10^{-7}, and concluded that the absence of an explanation for the value of K in any one system was a major unsolved problem.

A recent review by Eyre (122) considered wear from an industrial viewpoint and estimated that abrasive metallic wear accounted for about 50% of wear in industry. The effect of alloying elements on the microstructure and wear resistance of different steels was also described. Austenitic manganese steel, one of the softer steels, had even worse mechanical properties if cementite, an iron carbide, was allowed to form at the austenitic grain boundaries while a low-carbon chromium molybdenum steel had its abrasion resistance caused by its fully martensitic structure. Eyre also considered that choosing a costly harder-wearing steel initially might be better economically in the long term.

Welsh (50, 51) made an important contribution to the early studies of metallic wear. Using pin-on-disc apparatus, he found and characterised three wear transitions as the load increased with all other experimental conditions held constant. There was mild wear at low loads, which changed to severe wear at a transition, T_1; he considered that this occurred at the load for which the combined rates of oxidation and strain-hardening that caused the mild wear, were no longer

able to withstand the increasing disturbance due to the severe wear. The T_2 transition was marked by the change back to mild wear, and was found to be due to a phase change brought on by frictional heating, but oxidation was still necessary to sustain mild wear. The ratio between the rates of severe and mild wear at the T_1 or T_2 transitions was about 1000:1. Finally, there was a much smaller change in wear rate at a transition, T_3, which marked the load at which the pin and disc started having different wear rates; this was because the mild wear was sustained by excessive phase hardening, with the result that oxygen was no longer necessary for mild wear.

In addition to many wear tests, Welsh also measured the hardness of several specimens and was able to estimate the hardness necessary to support an oxide film. His work on the running-in behaviour before reaching mild wear, and the associated formation of a hardened surface layer, has also been continued by several other workers (112, 123, 124). It is also of special relevance to the work described in this thesis as the majority of experiments were concerned with the running-in time before the onset of mild wear.

Farrell and Eyre (123) studied the relationship between load and sliding distance, at constant speed, on two steels. A 0.3%C - 3%Cr steel needed much greater running-in distances than a 0.3%C steel; for both materials, the variation with load was of the form:

$$\log(\text{load}) = K - m(\text{distance}) \qquad (1.8)$$

where K and m are different constants for each material.

The running-in distance was less sensitive to load on the chromium steel. This research, carried out to study the scuffing tendency of steels, suggested that determination of running-in coefficients (m in the above equation) might provide a quick test of the readiness of a metal to scuffing. The experiments were carried out

using pin-on-disc apparatus and are, therefore, comparable with the work described in this thesis.

Farrell and Eyre carried out a superficial examination of the specimens. Eyre continued this investigation with Baxter (124) in order to study what surface changes were necessary in the specimens to support mild wear. A 'hard' or 'white layer', so-called due to its resistance to etching, was found at the surface. Such layers were found under many sliding conditions; in 1941, Trent (125) reported finding them on steel ropes subject to repeated sliding, and described them as martensitic. He estimated that the temperature gradient at the surface of a sliding rope was about 150°C per inch (5.9 $^{\circ}C\mu m^{-1}$). Archard (89) and Quinn (61) also considered that the temperatures at the asperities were sufficient to cause the steel to change structure and harden. Unfortunately, little has been done to investigate the microstructure of this layer. Nakajima and Mizutani (126) found a network of cells approximately 0.5 μm to 1.0 μm in diameter, but were not certain that they were studying a white layer.

Blau (112) studied the running-in behaviour of experiments carried out by several other workers and cited many examples of sliding metal couples, assigning each system into one of the eight different ways in which friction could vary with time. His examples (b), (f) and (h), reproduced in figure 1.6, are of most relevance to the work described in this thesis. He did not claim that there were just eight different mechanisms, but merely adopted an empirical approach and attempted to classify the results of other workers into one of eight frictional variations. Figures 1.6 (i) and (ii) are similar in that the frictional steady state value is approached from a higher value. Recent work using Brico 65 on 21/4N, or EN8 or EN31 sliding on themselves using pin-on-disc apparatus (127, 129), or a Ni-Cr alloy sliding on itself using a flat-on-flat system (128) has

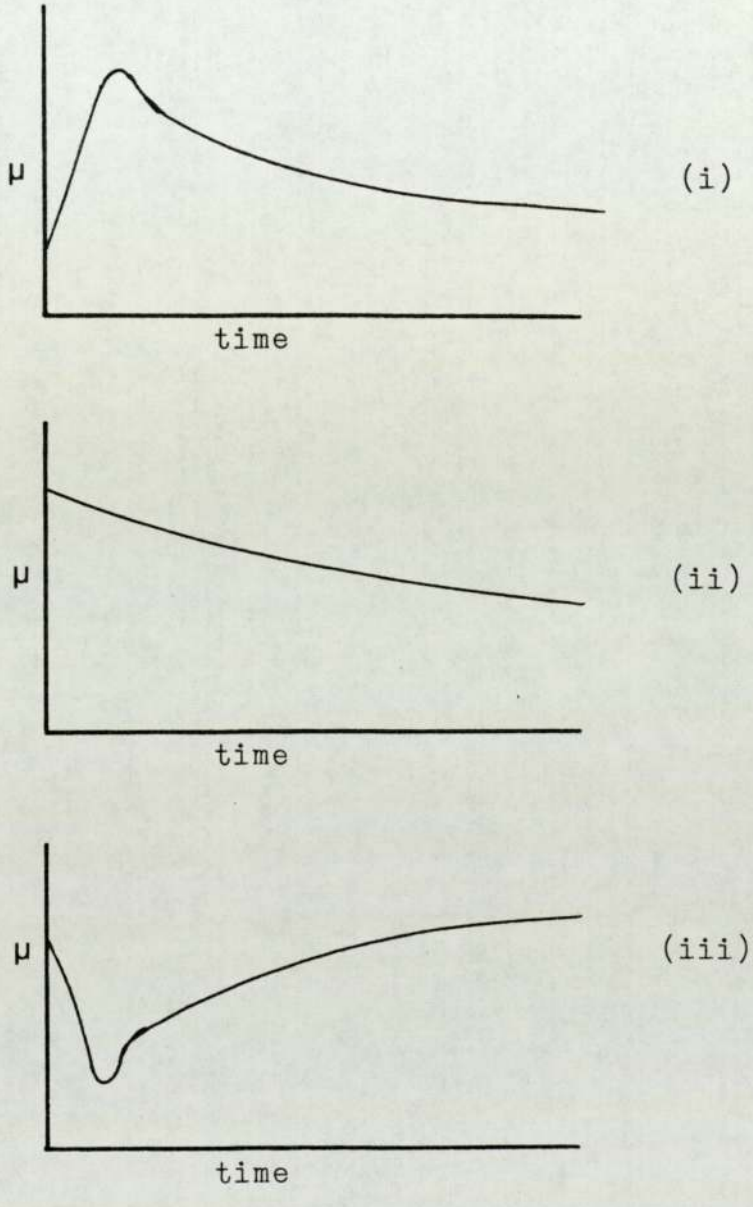

Figure 1.6 Typical variations of friction with time in different sliding systems (ref 112)

produced type (ii) variations. A type (i) curve might have resulted when the initial contact was not the equilibrium contact (e.g. had the two flat specimens not been perfectly aligned, the initial contact might have been edge-on-flat). Type (iii) curves have been observed with Al_2O_3 or MgO sliding on a Ni-Cr alloy (128) or AISI 316 sliding on itself (pin-on-flat) (67, 130). Specimen geometry seemed to affect the friction variation; Blau found that most flat-on-flat systems produced type (ii) or (iii) curves, while pin-on-disc or flat-on-roller systems frequently produced type (i) curves.

1.4.2 Fretting wear

Hurricks studied the fretting of mild steel from room temperature to 500°C (72, 73) and also wrote reviews of the mechanism of fretting (131) and the influence of temperature (132, 133) in which he considered that there were three stages of wear. In the initial stage, the two unworn surfaces were only protected by a thin surface oxide layer; the normal process of wear soon removed this at a rate determined by the oxide, the metal hardnesses and the degree of adhesion. The outcome was a combination of metal transfer and plastic deformation which affected subsequent wear damage. Hurricks considered that the second stage could be identified by studying the debris, as initially this was expected to be metallic, but also to contain adsorbed oxygen at the free surfaces and internal disturbed regions; in practice, the final debris was oxidised due to the increased reactivity of the disturbed metal during removal. The formation of a layer of oxide then reduced metallic contact and adhesion. During the final stage, in the steady state, there was a gradual breakdown of the zones formed during the running-in wear, and the surface became more uniform due to the unremoved debris being a mixture of oxide and metal. The oxide layer reduced adhesion and Hurricks suggested that

abrasive wear was not significant, and that fatigue wear was the primary cause of damage. Abrasion was not considered important because the oxide particles were much smaller than the initial metallic debris, and work hardening of the metal may have made it as hard as the oxide (72).

Hurricks (72) found that for a constant number of cycles, the fretting wear of mild steel decreased at temperatures above 150°C; this decrease was associated with the absence of oxidised debris; a similar transition was observed for carbon steels at about 200°C. The transition temperature was dependent upon the oxide thickness which was, in turn, dependent upon the oxidation characteristics of the steel.

An important mechanism of oxidation is tribo-oxidation, described by Waterhouse and Wharton (134), as the result of plastic deformation of the surface during sliding in an oxidising environment followed by a reaction. Tribo-oxidation does not proceed via metal removal and subsequent oxidation of the particles, but by oxidation at metal zones within the oxide film; layers produced by such a process may be thicker than the oxide layers formed by other means, e.g. by a diffusion mechanism. Krause (135) reported finding layers that were not homogeneous up to 7 μm thick. Both Kostetskii and Filipchuck (136) and Toth (137) described the surface layer as a solid solution of oxygen in metal as well as oxides.

It was stated in section 1.3.7 that delamination wear proceeded via crack propagation parallel to the surface and so it would be expected that the amplitude of motion in fretting experiments would affect the wear rate. It was anticipated that the wear rate would drop once the amplitude had fallen below a critical distance which was dependent upon the surface topography as well as the structure of the sub-surface layer. The delamination wear theory proposed just one mechanism for three

'different' types of wear, adhesive, fretting and fatigue wear. Unfortunately, the experimental results of several workers conflicted; Halliday and Hirst (69) found a decrease in wear rate at low amplitude, while Stowers and Rabinowicz (138) cited both their own results along with those of others in which no decrease in wear rate was observed.

More work done on fretting by Waterhouse and Taylor (139) suggested that as fretting corrosion was dependent upon the environment, it was unlikely to have a delamination mechanism unless the nature of the environment altered the surface layer. Studies of some titanium alloys in air and 1% sodium chloride solution found little variation in the fatigue strength (143), while studies of a stainless steel in air or nitrogen (144) showed that wear was significantly less in air. It is therefore probable that the delamination wear theory is not applicable to all fretting systems.

Kayaba and Iwabuchi (68) and Taylor et al. (145) have each carried out studies of fretting at higher temperatures than those of Hurricks. Kayaba found that fretting decreased with increasing temperature and that there was a transition temperature above which the coefficient of friction was less and the wear mechanism different. Below the transition, which occurred at 200°C on a 0.45%C steel and at 300°C on an 18Cr8Ni austenitic steel, flake-like particles of oxide debris were formed and removed from the sliding interface. Above the transition temperature, the debris was transferred from the flat to the ring and accumulated; pit-like damage then occurred on the flat. Stott et al. (146), studying nickel-based alloys, also observed a transition temperature above which the friction reduced, but attributed the reduction to the formation of an oxide 'glaze' on the surface. Waterhouse (147), considering that a glaze was essential for low wear fretting at high temperatures, proposed that compaction of the surface oxide to form a smooth

surface, supported by a creep-resistant substrate, was necessary to sustain low wear.

Kayaba and Iwabuchi (148) have studied the effect of hardness on fretting at different amplitudes; several specimens were heat-treated in different ways and then worn, at room temperature only, with a slip amplitude of 45 μm or 260 μm. They discovered that hardness only had a minor influence upon the fretting wear rate; the effect of the oxide debris was greater. Black and brown oxides were observed, but electron diffraction revealed that both were α-Fe_2O_3. The black oxide acted as an abrasive, but protected the surface on which it was produced; the red oxide was formed on the wear track, and was easily removed as wear debris. Oxidative mild wear was the predominant mechanism, but damage caused by delamination was also observed. Wear at the two amplitudes was similar; this disagreed with the work of Ohmae and Tsukizoe (149) who found that oxidation was significant at amplitudes of less than 70 μm, and abrasion was important at larger amplitudes. Three-body abrasive wear is likely to be smaller at low amplitudes because the wear particles move less; therefore oxidation may be the predominant influence on the wear rate. As neither Kayaba (148) nor Ohmae (149) commented on any experiments in which oxidation was not observed, it is likely that few experiments were carried out near a severe/mild wear transition and therefore it is probable that trapped debris particles which encourage nucleation and further oxidation were not essential to the mild wear that they observed.

Fretting wear has also been studied in carbon dioxide by Taylor et al. (145), Waterhouse (147) and Skinner (67, 130). Taylor (145) investigated the wear of an 18Cr8Ni austenitic steel, AISI 321, at 650°C; examination after the wear test showed accumulations of debris at the edge of the contact zone. Small patches

within this zone had been disturbed and the surface material removed, but areas surrounding these patches had a relatively undisturbed oxide covering. Energy dispersive analysis by X-rays, E.D.A.X., revealed chromium depletion within these patches, which extended approximately 1 μm into the metal; this was caused by selective oxidation to form Cr_2O_3 on the surface. Iron-rich oxides, e.g. a spinel, could form on the metal exposed after removal of the Cr_2O_3 (150). Killeen et al. (150) also found that the rate of oxidation was dependent upon the chromium diffusion.

Fretting usually refers to high frequency, low amplitude sliding; for example, Taylor used a fretting amplitude of 75 μm and a frequency of 100 Hz. Skinner (67) has also studied a 321 austenitic steel in carbon dioxide. He used a 9 mm stroke and a much lower frequency, typically 1 - 6 Hz; this is more usually referred to as reciprocating sliding. Skinner was more interested in running-in wear and the sliding distance prior to the onset of mild wear; he found that the running-in distance increased with sliding speed or load, but decreased with temperature. There was also some evidence to suggest that mild wear did not occur above a certain sliding speed.

It was concluded that the sub-surface layer properties determined the friction and wear behaviour during running-in, and the point at which mild wear commenced; these properties were the outcome of the disturbed layer due to sliding, but also dependent upon the degree to which the oxide had become incorporated into it. The transition to mild wear was explained by a change from plastic to elastic contact mechanisms. On specimens within the mild wear regime, there was an iron-rich oxide at the surface, but the overall appearance of the specimens was still that due to the disturbance that occurred during the severe wear running-in period; this remained

so even after many hours of mild wear. While running-in, large chunks of oxidised debris were produced that did not suggest a delamination mechanism of removal.

In summary, fretting at high temperatures tends to produce surface layers that are a combination of oxide and a solid solution of metal and oxygen. The surface oxide is usually iron-rich on austenitic steels.

1.5 Programme of research

The nuclear power industry has been concerned with the long-term wear of certain components within reactors for many years; such components often have to operate at high temperatures and in hostile environments for as long as 30 years. Under circumstances that make replacement of these parts costly and very difficult, it is essential that not only mild wear is the equilibrium wear regime, but also that the period of severe wear before the transition to equilibrium wear is not overlong.

The University of Aston Tribology Group has long studied a range of steels wearing by unidirectional sliding at high speed, both at room temperature and elevated temperature. Berkeley Nuclear Laboratories, B.N.L., have studied the running-in behaviour of steels under reciprocating sliding at slow speed, elevated temperatures and in carbon dioxide.

The aim of this study is to carry out three series of experiments in an attempt to bridge the differences between the techniques of the two research groups, with the main emphasis being on the running-in reciprocating wear of a 9% chromium steel of interest to B.N.L..

The steel was first studied under sliding conditions familiar to the Aston Tribology Group in order to determine the general wear behaviour of the material. Unidirectional experiments were then carried out with the sliding speed, load, ambient temperature and atmosphere that were to be used for the reciprocating

sliding tests with the aim of making a comparison between the two forms of sliding.

The emphasis of this study was on the last series of experiments. The running-in behaviour and equilibrium wear of the 9% chromium steel was investigated under reciprocating sliding at slow speed, elevated temperatures and in carbon dioxide. The running-in times or periods of severe wear were of special importance and the variation in the total wear volume during these periods with sliding speed and temperature was studied; a very low mild wear rate was of no use to the nuclear power industry if there was excessive severe wear preceding it.

A different pin was used in each experiment, and the debris was collected from all runs. A variety of analytical techinques were used. Selected samples of debris were analysed by X-ray diffraction; several pins were chosen for examination by scanning electron microscopy and measurement of their surface hardness. Taper sections were prepared so that analysis of the surface layer could also be carried out.

CHAPTER 2
EXPERIMENTAL DETAILS

2.1 Introduction

The unlubricated wear of a 9% chromium steel was studied under both reciprocating and unidirectional sliding. The experimental work was divided into three main parts:

a) the unidirectional wear at room temperature in air at high sliding speeds
b) the unidirectional wear at elevated temperatures in carbon dioxide or air at slow sliding speeds
c) the reciprocating wear at elevated temperatures in carbon dioxide at slow sliding speeds.

2.2 The unidirectional wear test machines and ancillary equipment

2.2.1 Introduction

Two unidirectional wear machines were used in this study. Initial experiments were carried out at sliding speeds of 0.5 ms^{-1} and 2.0 ms^{-1} at room temperature so that the behaviour of this material could be compared with other steels. It was intended in this work to compare unidirectional and reciprocating sliding and in order to achieve as close a comparison as possible, it was decided to modify an existing wear machine to operate at the sliding speeds and temperatures of the reciprocating wear test apparatus. The wear machine used for the above unidirectional experiments was not suitable for alteration and so a different machine was modified to slide at speeds between 0.01 ms^{-1} and 0.2 ms^{-1}; this was then used for all the slow speed sliding experiments at elevated temperatures.

The means of applying the load, and of measuring wear and friction were the same for both machines and

so will only be described in detail for the slow speed unidirectional sliding experiments.

2.2.2 The slow speed unidirectional wear test machine

The wear machine (figure 2.1) was of pin-on-disc geometry and is more fully described elsewhere (140). The disc (C in figure 2.3) was screwed onto the main shaft of the machine (F). A heater (B) could be bolted to the non-wearing side of the disc and could raise the disc temperature up to about 600°C, receiving power from a variac via carbon brushes running on copper slip rings (figure 2.2). The chrome-aluminium thermocouple wire which was used to measure the disc temperature was also the input to a temperature controller which regulated the variac output. This maintained the disc temperature constant to within two degrees. The disc was separated from the main shaft by a 30 mm thick asbestos block (D) and the shaft was water-cooled to prevent the bearings overheating. The power was provided by a 3-phase, 0.25 h.p. electric motor via a variable speed gearbox which could give sliding speeds between 0 mms^{-1} and 500 mms^{-1}. The number of revolutions of the disc was counted with an optical switch so that the mean sliding speed could be calculated.

The pin (J) was mounted in a sindanyo insulator held in a copper calorimeter which was bolted onto the loading shaft (K). This shaft was mounted on both rotary and linear bearings; the linear bearings allowed the pin to remain in contact with the disc as each was worn away, whereas the rotary bearings were present to allow the frictional force to be measured. Thermocouples measured the temperatures of the calorimeter and at two positions along the pin.

Figure 2.1 The slow speed unidirectional wear test machine.

Figure 2.2 Detail of the heating assembly and the specimens.

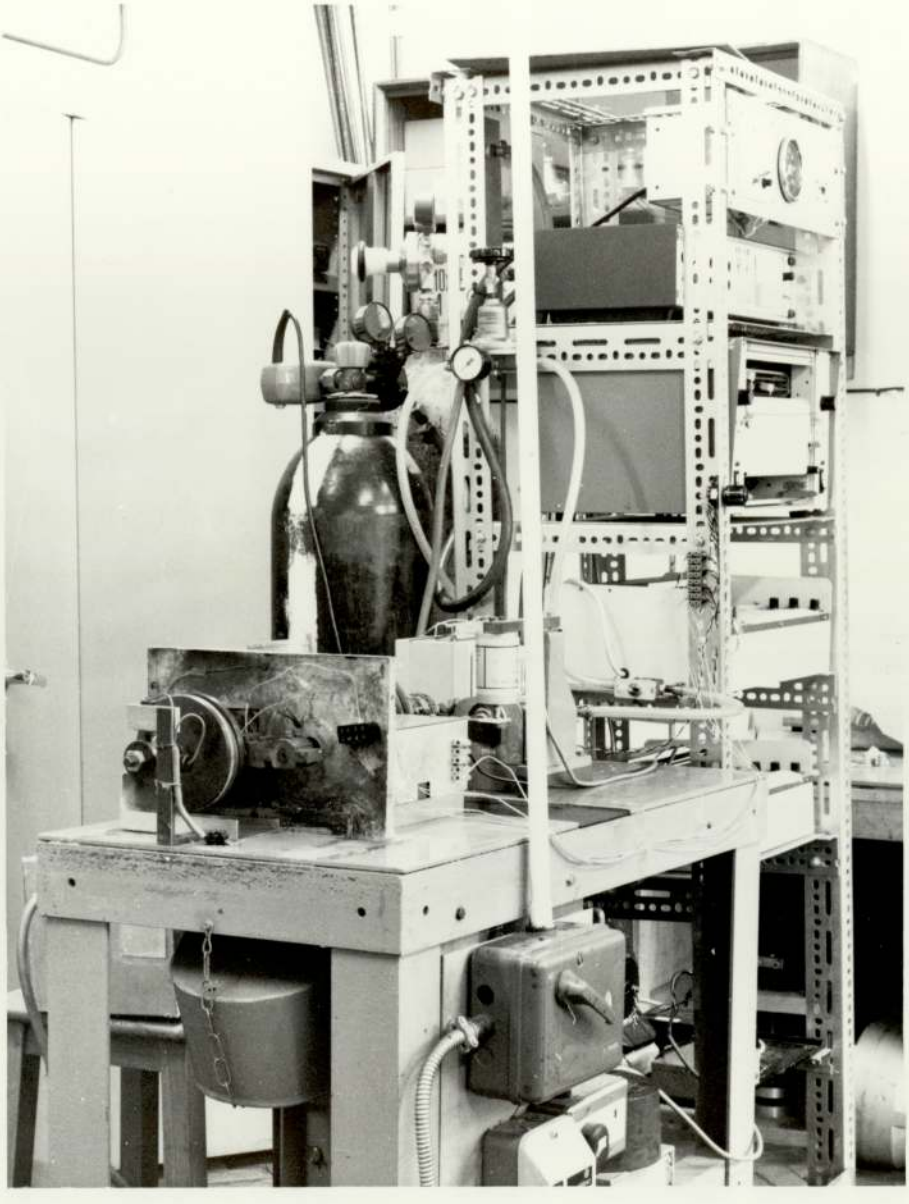

Figure 2.1

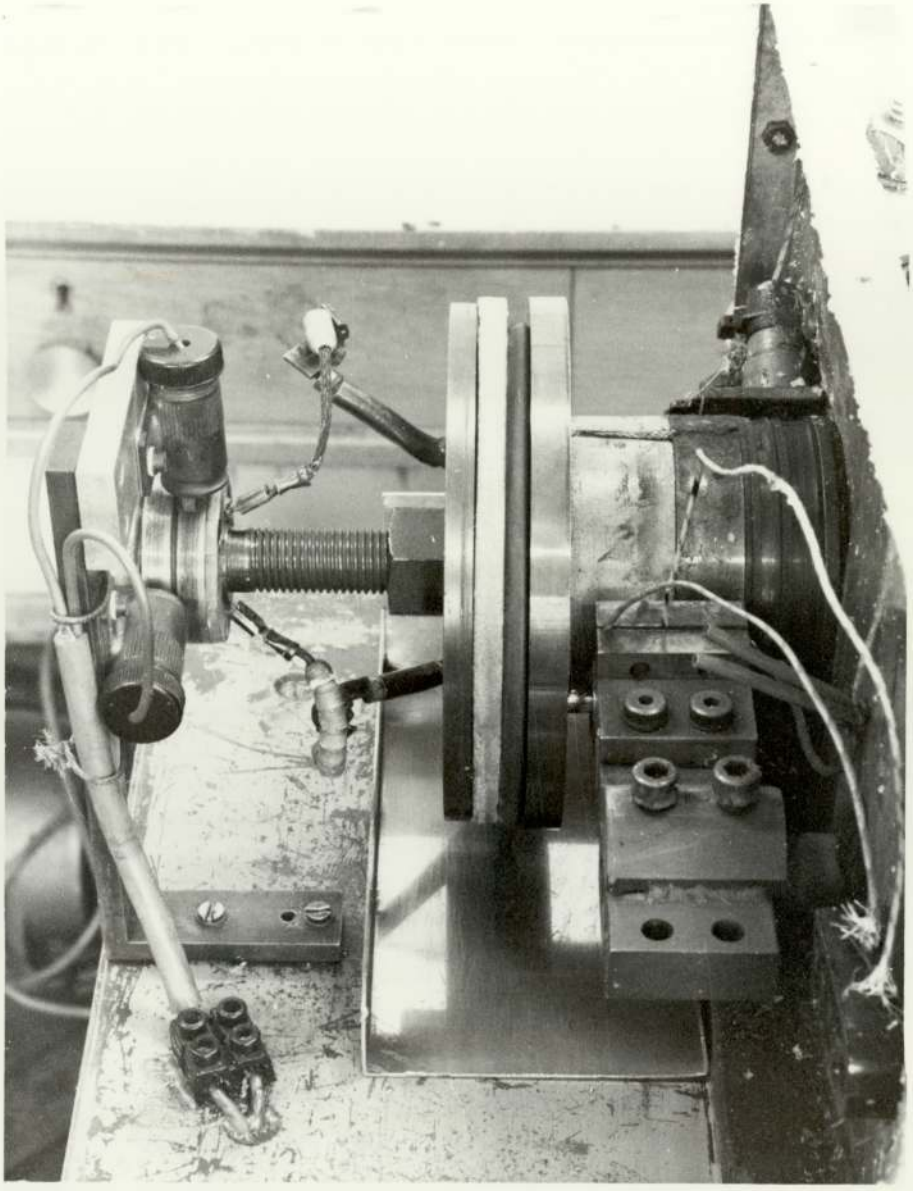

Figure 2.2

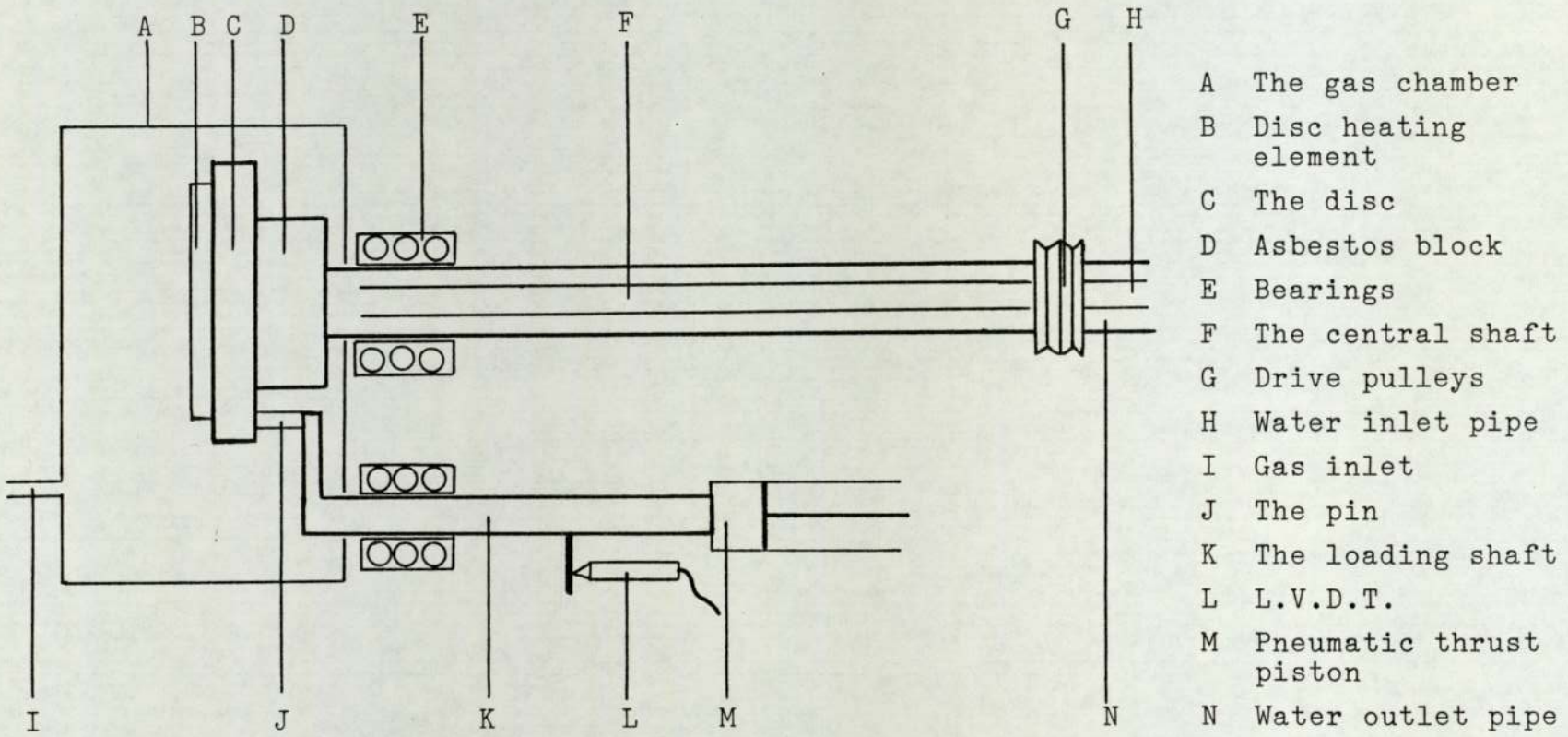

Figure 2.3 A schematic diagram of the slow speed unidirectional wear test machine

2.2.3 Preparation of the specimens and the carbon dioxide atmosphere

The pins were produced from 9% chromium steel cut from a 6.35 mm diameter rod into 31.75 mm lengths. The discs were made of the same material and were 127 mm in diameter and about 15 mm thick. Both specimens were degreased in petroleum ether, washed in acetone and finally dried before attachment to the wear machines.

The original test machine was not designed to run in a controlled environment. A stainless steel box (A) was placed over the test specimens and firmly held in place by screws. Large cracks between the machine and the box were filled with plasticine and all small cracks including the screw holes were blocked with a silicon rubber. This hardened in a few hours, but always remained pliable; as a result, after a liberal application of the rubber, all accessible crevices were sealed. However, there was a large gap around the bearings which could not be closed, and because of this, it was not possible to evacuate the specimen chamber; therefore, the carbon dioxide environment was obtained by passing gas from a cylinder through the chamber and out past the bearing for several hours. The flow rate was set at about 0.0005 $m^3 min^{-1}$ for a minimum of one hour, and reduced to about 0.0001 $m^3 min^{-1}$ for a further twelve hours (overnight). In this way, about 0.1 m^3 of gas was passed through the chamber, of which the volume was about 0.011 m^3, before the experiment was started. The flow rate was maintained at about 0.0001 $m^3 min^{-1}$ for the duration of the wear test.

During early experiments in carbon dioxide, samples of the outflowing gas were analysed by a Perkin Elmer gas chromatograph and found to contain about 0.1% oxygen. This oxygen concentration was small enough to produce significantly different wear behaviour from experiments run in air, but an even smaller concentration would have

been desirable in order to match A.G.R. conditions as closely as possible.

2.2.4 Load, friction and wear measurements

The load was applied pneumatically by air from a cylinder, and this provided a maximum load of about 150 N; small loads were best applied using a system of weights, but this was not necessary in this investigation. The air pressure gauge was calibrated against the load and the results presented in figure 2.4.

The friction was measured by a strain gauge dynamometer; this detected the torque exerted on the loading shaft by the frictional force. The output from the dynamometer was continuously displayed on a pen chart recorder. It was determined that the calibration factor was 3.23 mVN^{-1}.

Wear was measured by a linear voltage displacement transducer (L.V.D.T.) which detected the forward movement of the loading shaft. The output was also continuously displayed on the same recorder. It was found that the calibration factor was 825 $mVmm^{-1}$.

2.2.5 The high speed unidirectional wear test machine

Many austenitic and mild steels have been studied under unidirectional or reciprocating sliding conditions, but relatively little work has been done on 9% chromium steel. It was therefore necessary to carry out a series of reference experiments at high speeds and at room temperature so that the behaviour of this steel could be compared with that of other steels.

This wear machine (63) had a pin-on-disc geometry and was similar in many ways to the slow speed wear machine described above. The main differences were as follows. The shaft was not water-cooled and there was no heater on the back of the disc; thus the pin could

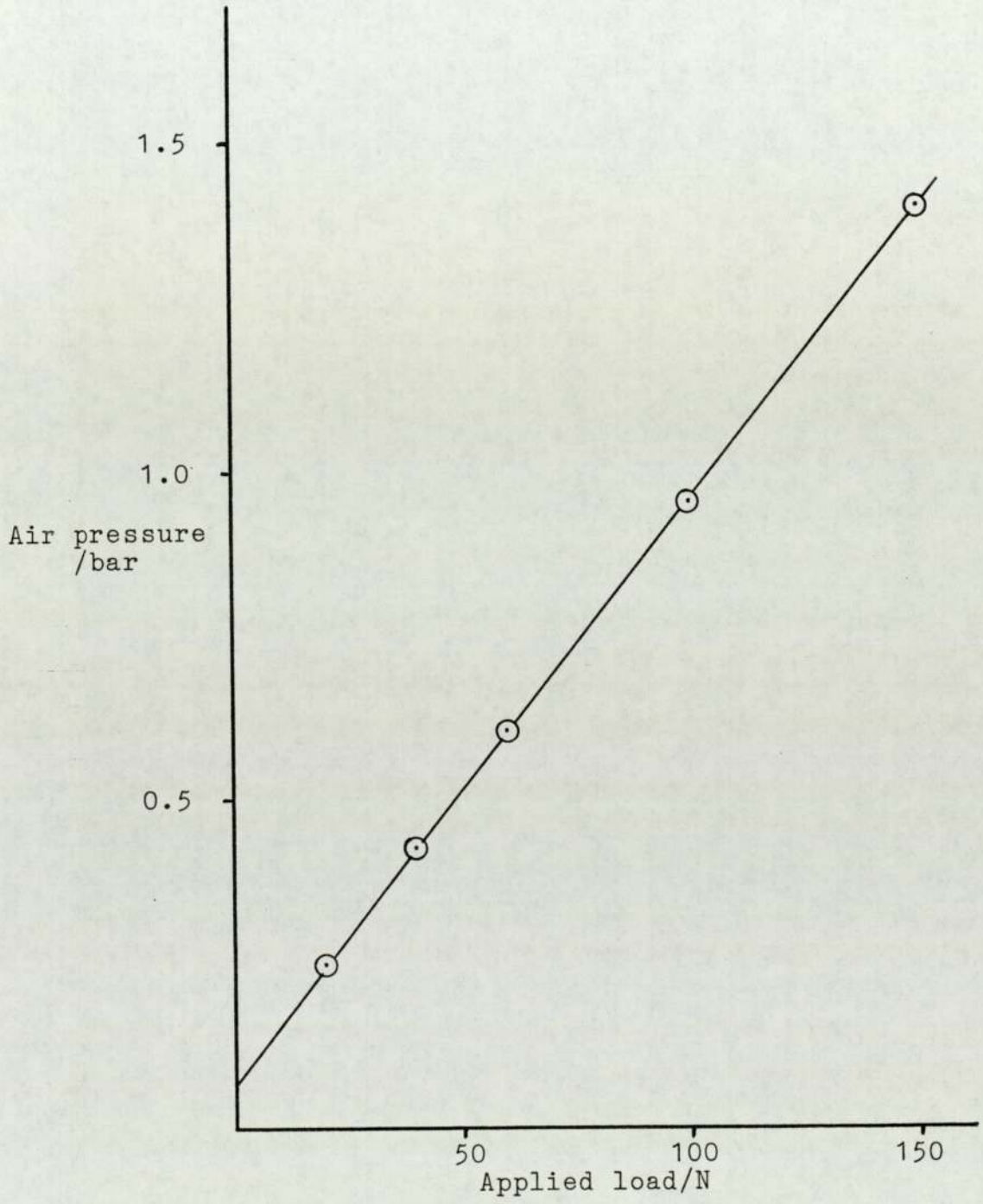

Figure 2.4 The variation of the applied load with the air pressure

wear against this face of the disc (figure 2.5) and the whole assembly could be much more open (figure 2.6). There was also no asbestos block adjacent to the disc and this meant that the disc was bolted directly onto a considerable bulk of metal. This had the effect of reducing the temperature to which the disc would rise through frictional heating. The temperatures of the copper calorimeter and of the pin itself were also generally lower. This was not due to the absence of the asbestos, but to the more open pin assembly as the pin was worn against the side of the disc away from the wear machine.

The pins were 6.35 mm in diameter and 31.75 mm long; the discs were 127 mm in diameter and about 15 mm thick. The motor was a 3-phase, 5 h.p. electric motor with a variable speed gearbox. The sliding speed range was 0.5 ms^{-1} to 8.5 ms^{-1} with a maximum load of 60 N; this was applied pneumatically and calibration of the air pressure control showed that 1 bar was equivalent to a load of 28.9 N.

The wear was measured using as L.V.D.T. and continuously recorded on a pen chart recorder. The calibration of the transducer was found to be 850 $mVmm^{-1}$. The friction was measured using a strain gauge dynamometer and was also continuously recorded on the same recorder; the calibration factor was determined to be 3.39 mVN^{-1}.

2.2.6 Heat flow analysis

The pin was held in a copper calorimeter and its temperature was determined at three points (figure 2.7); at the point where the pin was first insulated by the sindanyo, T_A, at some point further along the pin, T_B, and at the end where the pin was in contact with the copper calorimeter, T_C. The distances from the worn surface of the pin to the point at which the first thermocouple wire was spot-welded to the pin, L_1, and

Figure 2.5 Detail of the pin assembly on the high speed unidirectional wear test machine.

Figure 2.6 The high speed wear test machine.

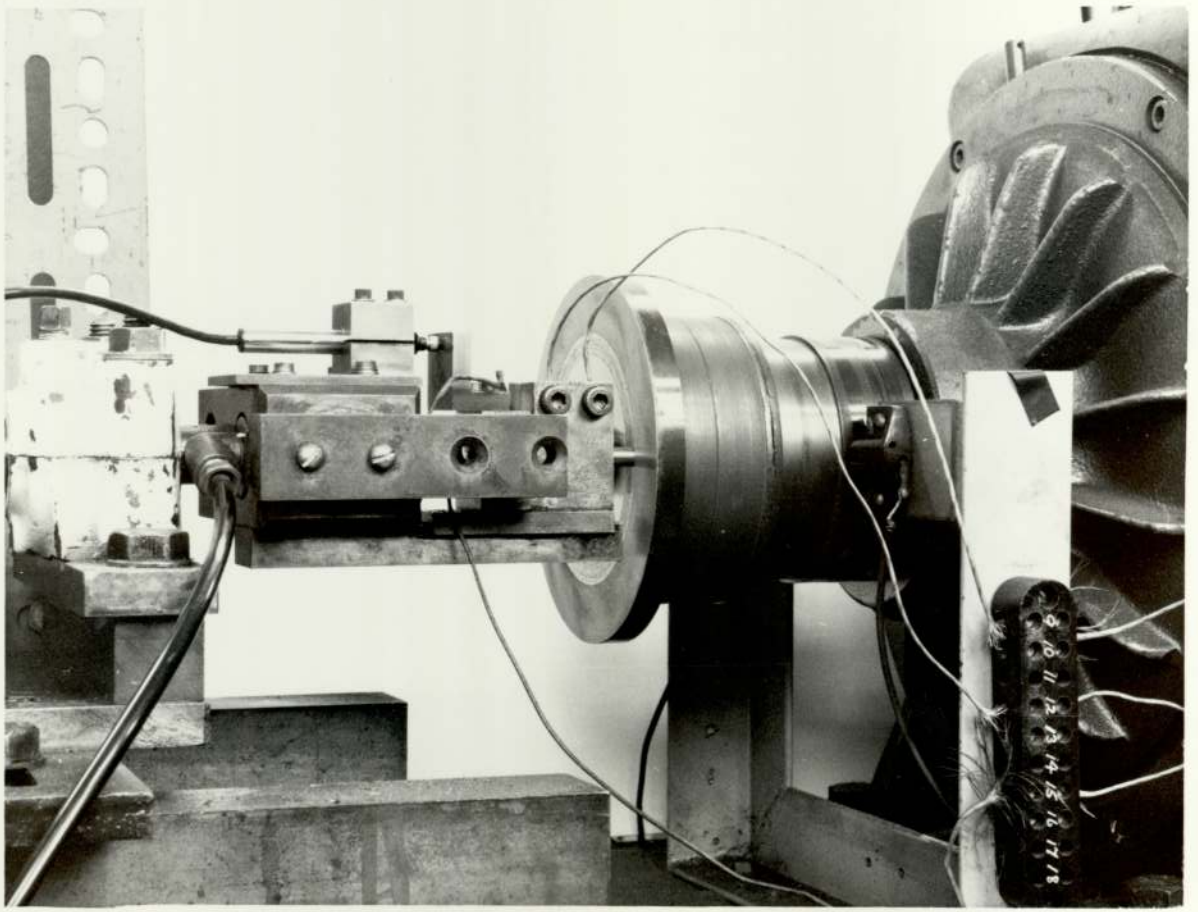

Figure 2.5

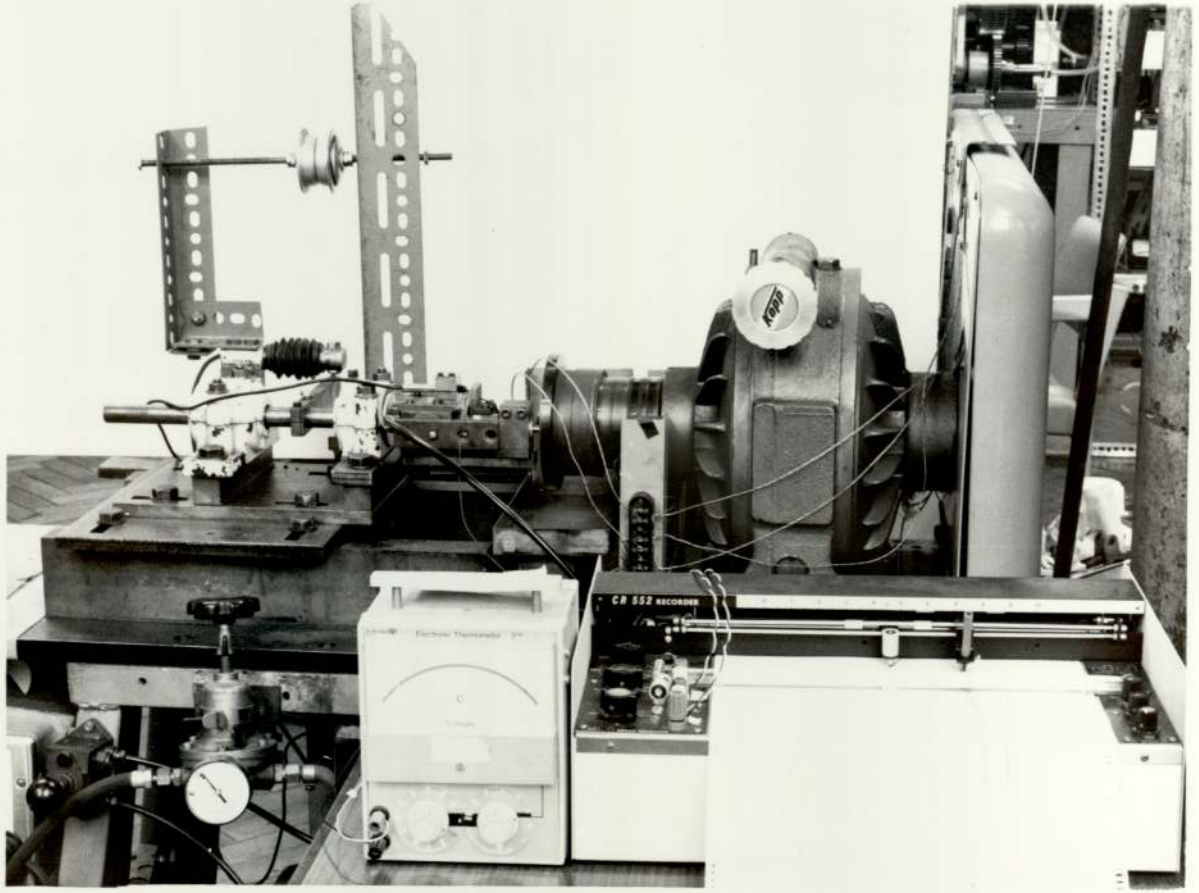

Figure 2.6

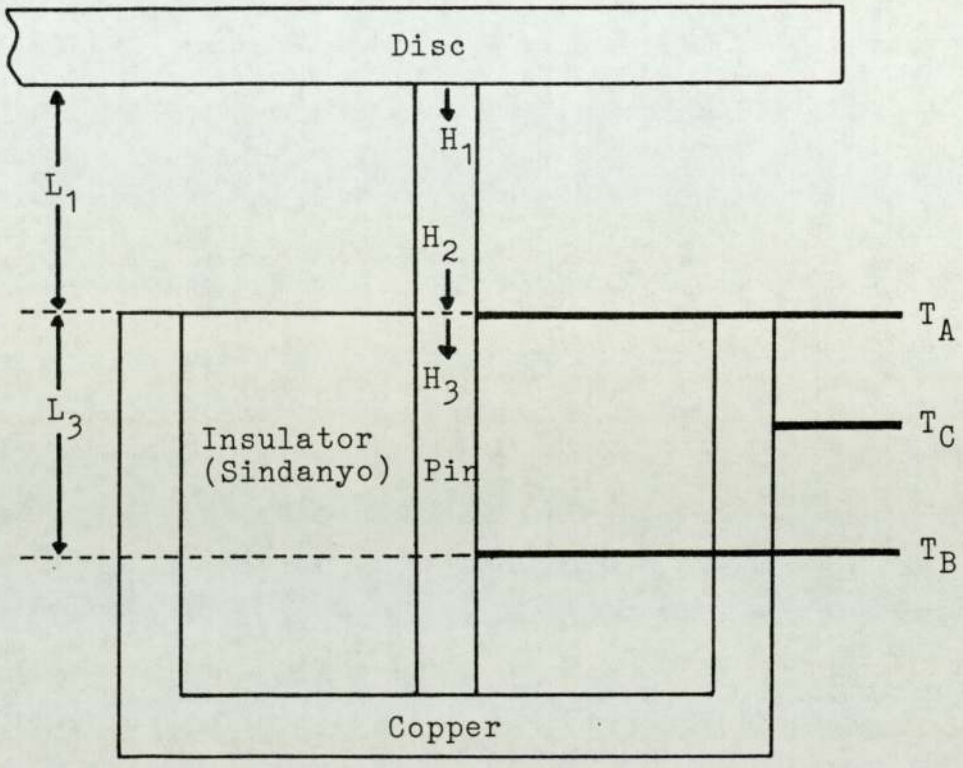

Figure 2.7 A diagram of the heat flow in the pin holder

between the first and second thermocouples, L_3, were also measured.

A detailed account of the heat flow analysis has been given by Rowson and Quinn (141). Using standard heat flow equations, the temperature at the surface of the pin, T_s, and the heat flow down the pin from this point, H_1, could be calculated using the above measurements. It was found that:

$$T_s = (T_A - T_C)\,\mathrm{Cosh}\left[\frac{L_1}{ZR_t}\right] + \frac{ZH_2}{K_s R_t}\mathrm{Sinh}\left[\frac{L_1}{ZR_t}\right] + T_C$$

$$H_1 = \frac{K_s R_t}{Z}(T_A - T_C)\mathrm{Sinh}\left[\frac{L_1}{ZR_t}\right] + H_2\mathrm{Cosh}\left[\frac{L_1}{ZR_t}\right]$$

where $Z = \dfrac{K_s}{2R_t h}$

and R_t = radius of the pin

K_s = thermal conductivity of steel

h = heat transfer coefficient between the cylindrical exposed surface of the pin and air

H_2 = heat flow into the point at which thermocouple T_A takes some heat from the pin.

Modifications were made to the heat flow analysis for the slow speed experiments as the heat transfer coefficient was very different at such speeds; in addition, the high ambient temperature of the pin was taken into account for experiments run in carbon dioxide. These will be described in Chapter 4.

2.3 The reciprocating wear test machine and ancillary equipment

2.3.1 The wear test machine

The wear test machine used for all reciprocating sliding experiments was designed and built by Berkeley Nuclear Laboratories.

The apparatus, drawn schematically in figure 2.8, was very versatile because both the amplitude and

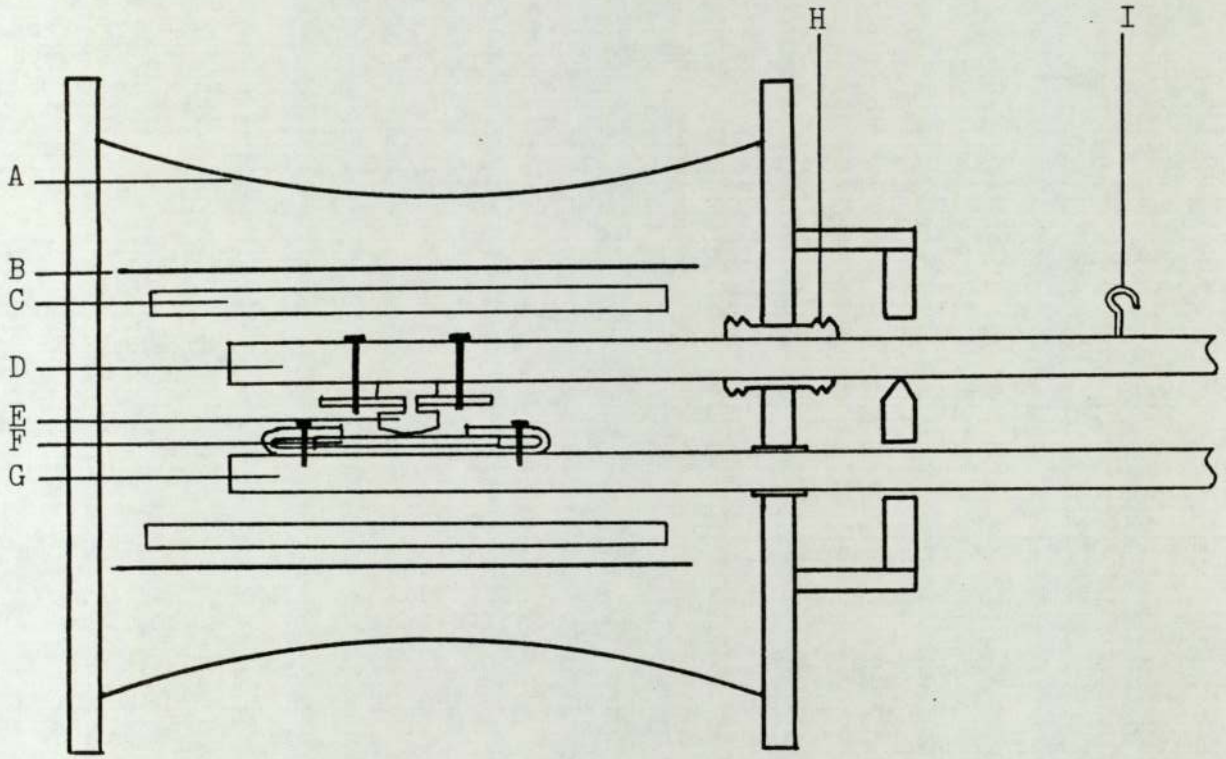

A The air-tight specimen chamber

B The metal heat shield

C One of the ten 300W heaters

D The upper or loading beam

E The pin specimen

F The flat specimen

G The lower or sliding beam

H The bellows allowing vertical movement of the loading beam

I The point at which the load was applied

Figure 2.8 A schematic diagram of the reciprocating wear test machine

Figure 2.9 The reciprocating sliding wear test machine.

Figure 2.10 Detail of the pin and flat specimens in position.

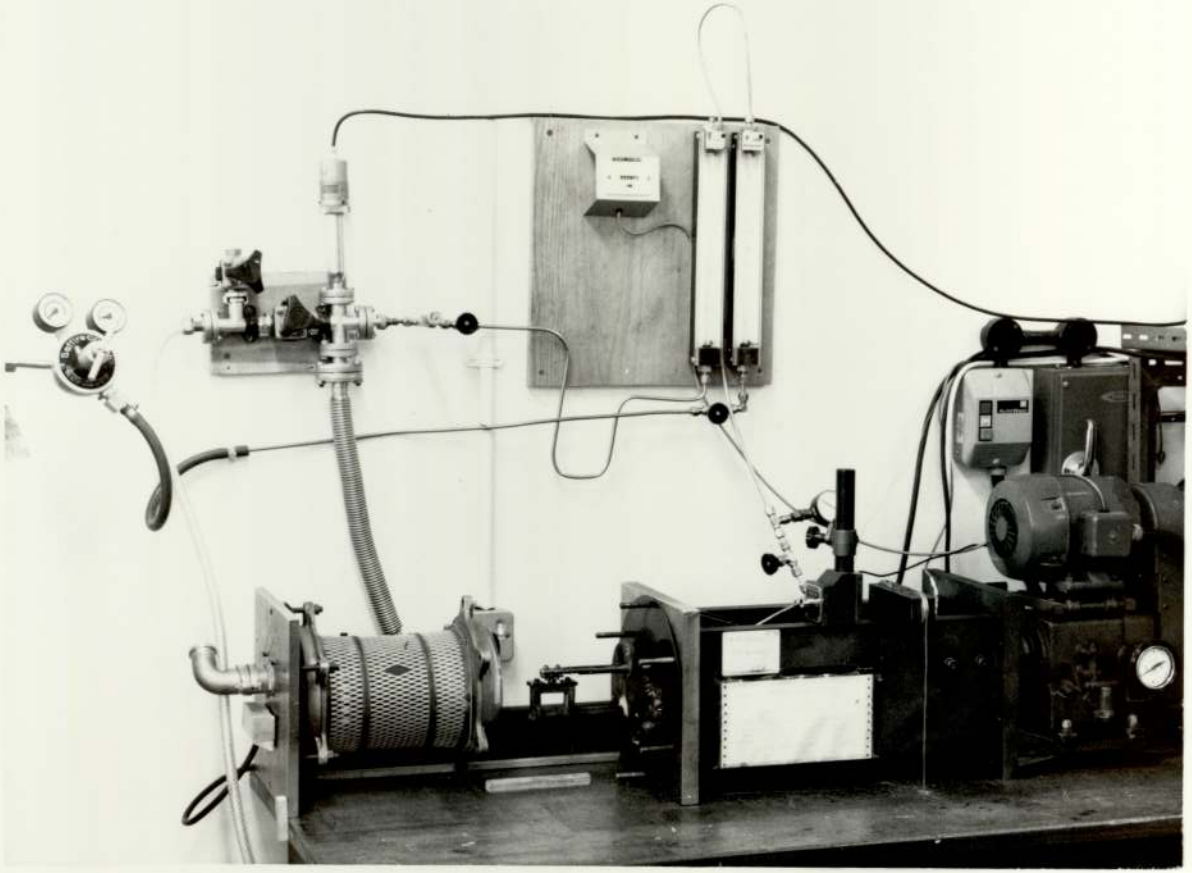

Figure 2.9

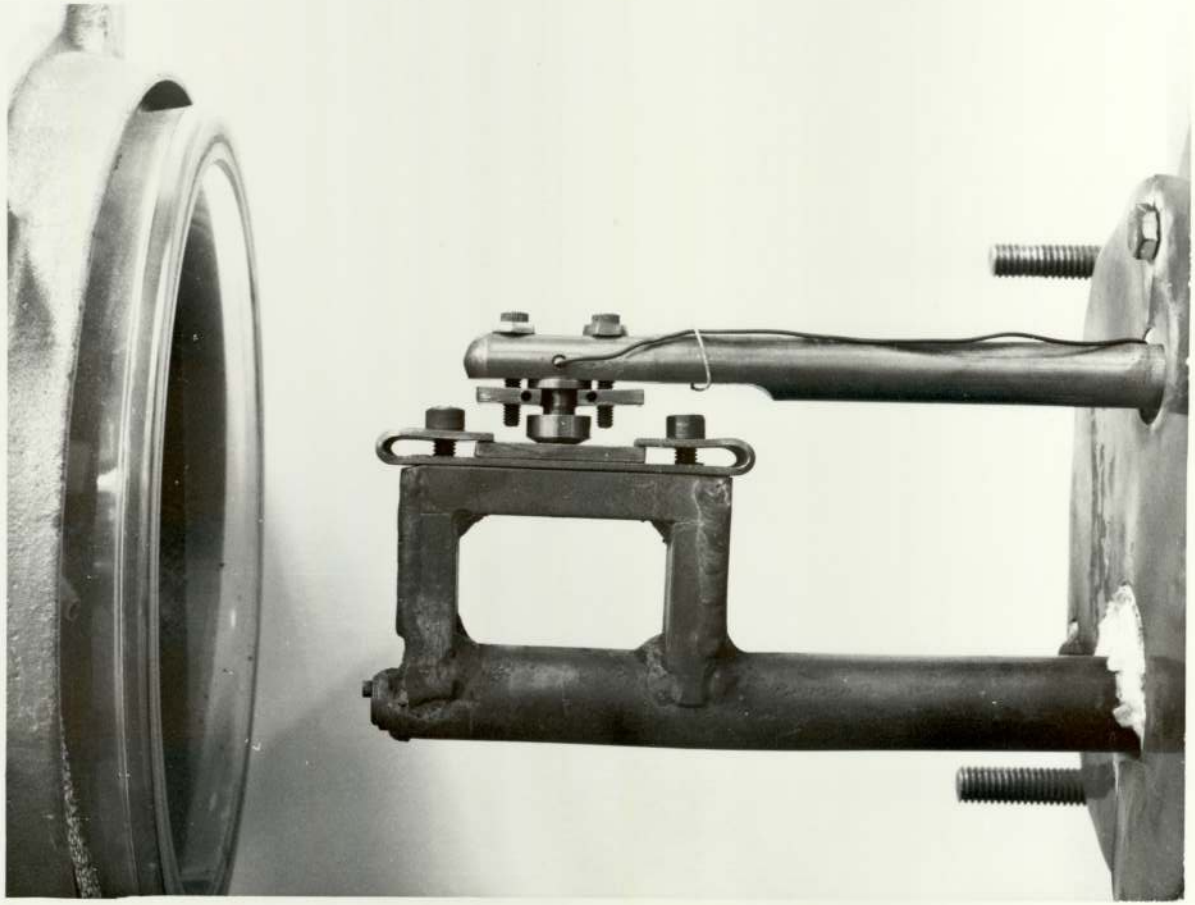

Figure 2.10

frequency of the reciprocating motion as well as the load could be varied; in addition, the ambient temperature and surrounding atmosphere were able to be controlled.

A flat specimen, 32 mm x 13 mm x 3 mm, (F) was held in place by means of two clamps on the lower or sliding beam (G). The reciprocating motion of the beam was due to a crank which was firmly attached to a wheel driven by a motor. The motor had a variable speed gearbox for altering the sliding speed. The amplitude of the stroke was changed by moving the position at which the crank was fixed to the drive wheel. A pin specimen, 12 mm in diameter and 13 mm long with a slightly domed end (E), was held under the upper loading beam (D) by a bracket screwed to the beam itself. In this way, both the flat and pin specimens could be clamped in position without any screw holes having to be made in the actual specimens. This was important because the specimens could then be more thoroughly cleaned since there was no possibility that any swarf, that may have been produced while drilling the fixing holes, remaining; clean specimens were essential for accurate weight loss measurements.

The specimens were surrounded by ten 300 W heaters (C), arranged so that there were two sets of five in parallel. This was so that should a heater element burnt out during an experiment, the remaining five heaters would maintain the same ambient temperature. The heaters were within an outer metal shield (B), and the whole assembly was inside an airtight chamber (A). There was a bearing on the sliding beam at its point of entry into the chamber; the loading beam had a bellows arrangement which permitted limited vertical movement of the beam. The fulcrum about which the load was applied was just outside the specimen chamber. The load was applied using dead weights that hung under the test machine, and via two pulleys, pulled the loading beam upwards, thus pressing the pin specimen down onto the

flat specimen.

The amplitude of the stroke could be set to between 0 mm and 10 mm. The machine was not designed for small strokes, and amplitudes of 1 mm or less could not be reliably maintained. In addition, the stroke was difficult to alter quickly and so for this work, the effect of changing stroke was not studied. It was set to 9.20 mm for the first 55 experiments; after this time, it was found that a bearing on the crank had seriously worn, producing an irregular sliding speed. The crank was replaced and the stroke was subsequently reset to 9.26 mm.

The frequency could be varied from 0.3 Hz to 10 Hz. At the minimum sliding speed, the drive belt between the motor and the drive pulley had a tendency to stick; at the maximum sliding speed, the wear machine was subject to excessive vibration and, at these speeds, the effect of such vibration might have altered the results in some way. For this work, frequencies between 1 Hz and 9 Hz were used.

The load could be altered from zero to above 60 N. The effect of varying load was not extensively investigated in this work, and the load was always set to either 22 N or 41 N. The temperature could be set to within one degree between room temperature and 600°C. There was a thermocouple embedded in the loading beam immediately above the pin specimen. The heater elements were controlled by a variac of which the output voltage was set according th the temperature required. This was because it had been found that had the heater been run directly from the mains, the action of the thermocouple would have caused small fluctuations in the temperature of the specimen chamber. The temperature range studied in this investigation was between 200°C and 550°C, with most work being carried out at about 300°C.

2.3.2 Preparation of the carbon dioxide environment

The specimens were washed in petroleum ether and acetone before being dried and weighed. They were then clamped in position and the specimen chamber was carefully placed in position and bolted firmly to the rest of the test machine. The chamber, labelled A in figure 2.8, was then evacuated by the rotary vacuum pump for several hours. A diagram of the vacuum system is shown in figure 2.11. The best obtainable vacuum was about 5×10^{-1} torr or 70 Pa. A better vacuum was not possible due to the two beams, both of which needed to move, and the bellows and bearing around them.

The specimen chamber was then filled with carbon dioxide from a cylinder to a pressure of 2 atmospheres; using the pressure relief valve, this was reduced to about 1.1 atmospheres and more carbon dioxide was admitted to increase the pressure again. This process was repeated about eight times before the gas flow rate was reduced to about 0.0001 $m^3 min^{-1}$ and the pressure was allowed to equilibrate at about 1.5 atmospheres. There was always a positive pressure with respect to the outside environment so that any gas leak at the bearing was out of the specimen chamber. The gas was left to flow through the chamber overnight, and the experiment was generally started on the following day.

2.3.3 Load, friction and wear measurements

The load was applied by means of weights hung under the wear test machine, which forced the loading beam (D) towards the sliding beam (G). As the fulcrum was not precisely half-way between the point at which the weights were attached to the loading beam, and the pin specimen, the load needed to be calibrated. There was also an adjustment needed due to the bellows (H) around the beam at the point at which the beam entered the specimen chamber. The net result of these two effects was to

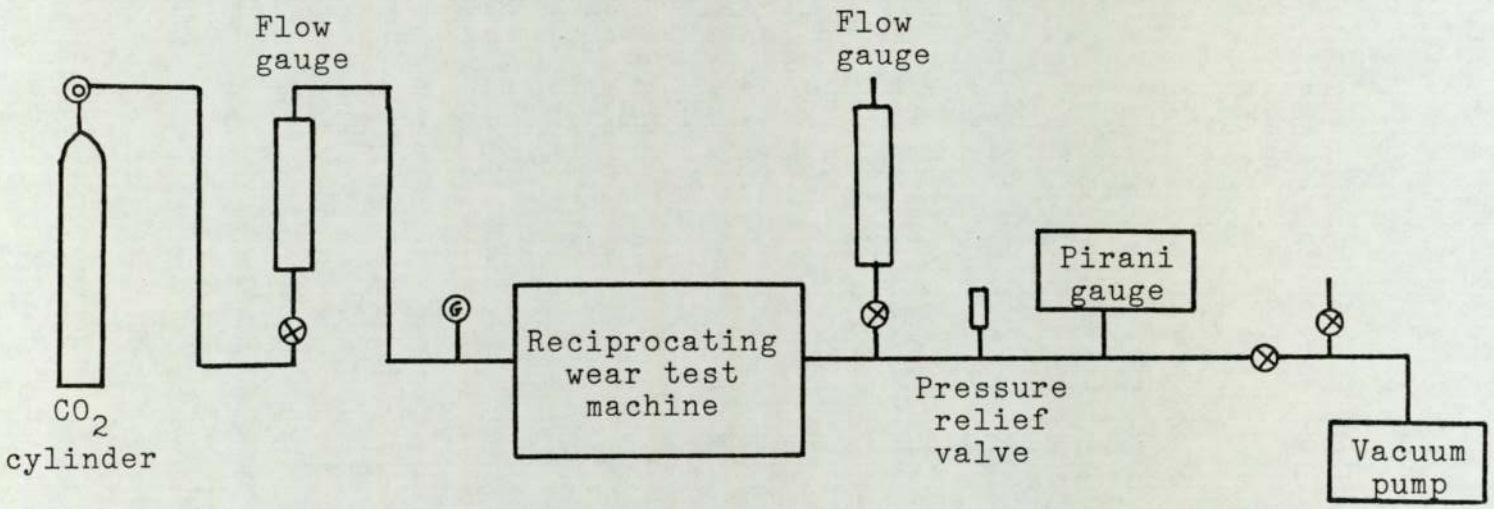

Figure 2.11 The vacuum system of the wear test machine

increase the real load by about 3 N and reduce it by a factor of 1.3 (figure 2.12).

The real load in nearly all experiments in this investigation was either 21.6 N or 40.7 N.

The friction was measured by a strain gauge dynamometer situated at the end of the loading beam. The output from this was amplified and displayed on a voltmeter and could be recorded on an ultra-violet chart recorder. This was calibrated against the frictional force by applying a force pulling the loading beam away from the dynamometer and measuring the displacement of the light beam. Recalibration was carried out each time that an experiment was done using a different load from that used in the previous test. A typical calibration of the light beam deflection against frictional force is shown in figure 2.13.

There were two general forms of the friction trace; that due to severe wear shown in figure 2.14 had a much greater variation within each reciprocating cycle than the mild wear trace shown in figure 2.15. The maximum and minimum friction values were measured and the mean coefficient of friction was calculated. The ratio of the maximum to the average coefficient was also determined, and although this reduced at the wear transition, it did not increase significantly afterwards, unlike the actual value of the coefficient of friction.

The wear rate was determined by weight loss. The specimens were first degreased in petroleum ether, then ultrasonically cleaned in acetone, and finally dried. Each pin and flat specimen was weighed three times on a balance sensitive to 0.01 mg, and an average of the three readings taken. A similar procedure was followed after each wear test, except that the specimens were not degreased. Weight losses of the pin and flat, as well as the average weight loss of the two specimens were then recorded.

A disadvantage of this method of measuring the

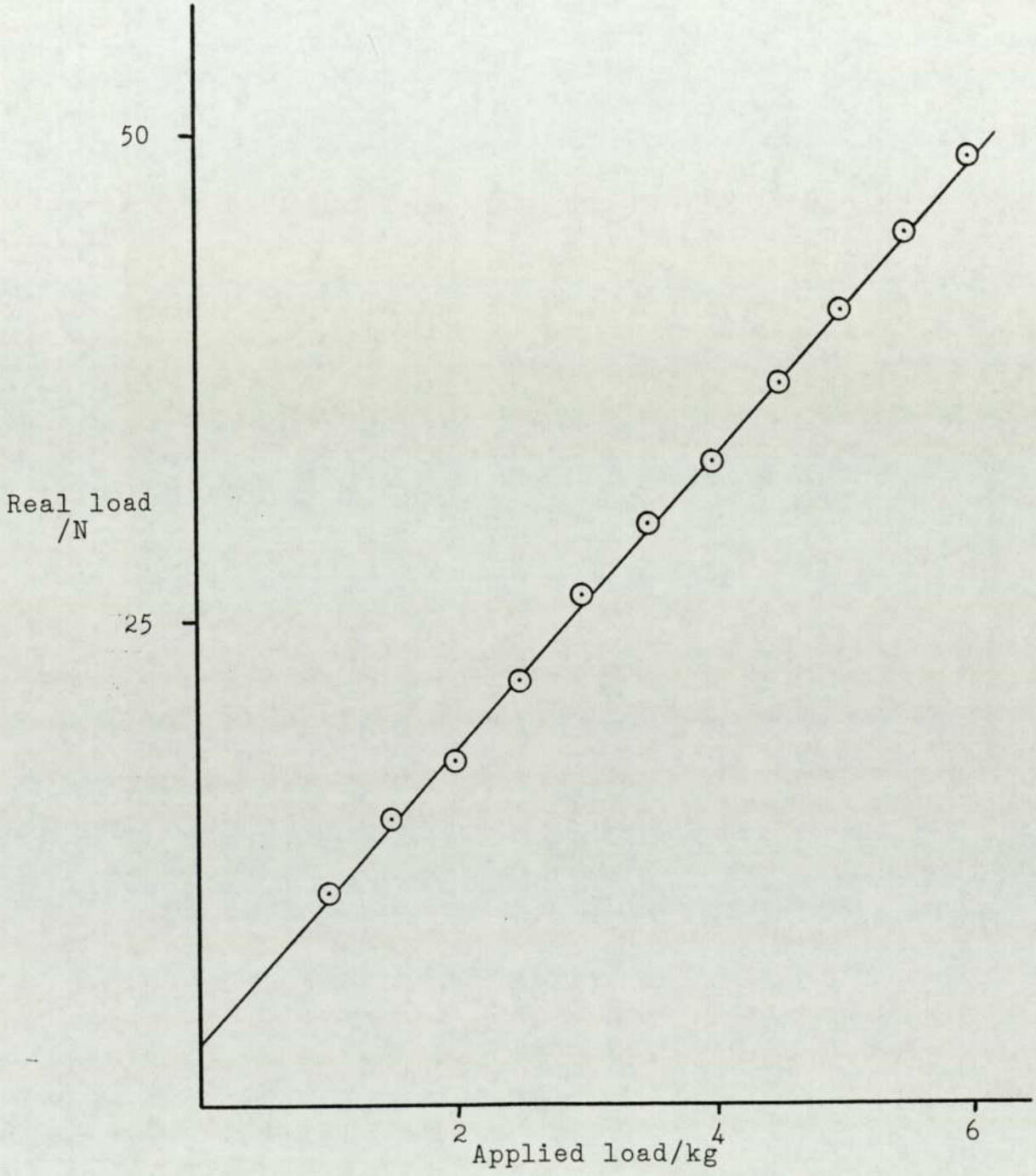

Figure 2.12 The variation of the real load with the applied load

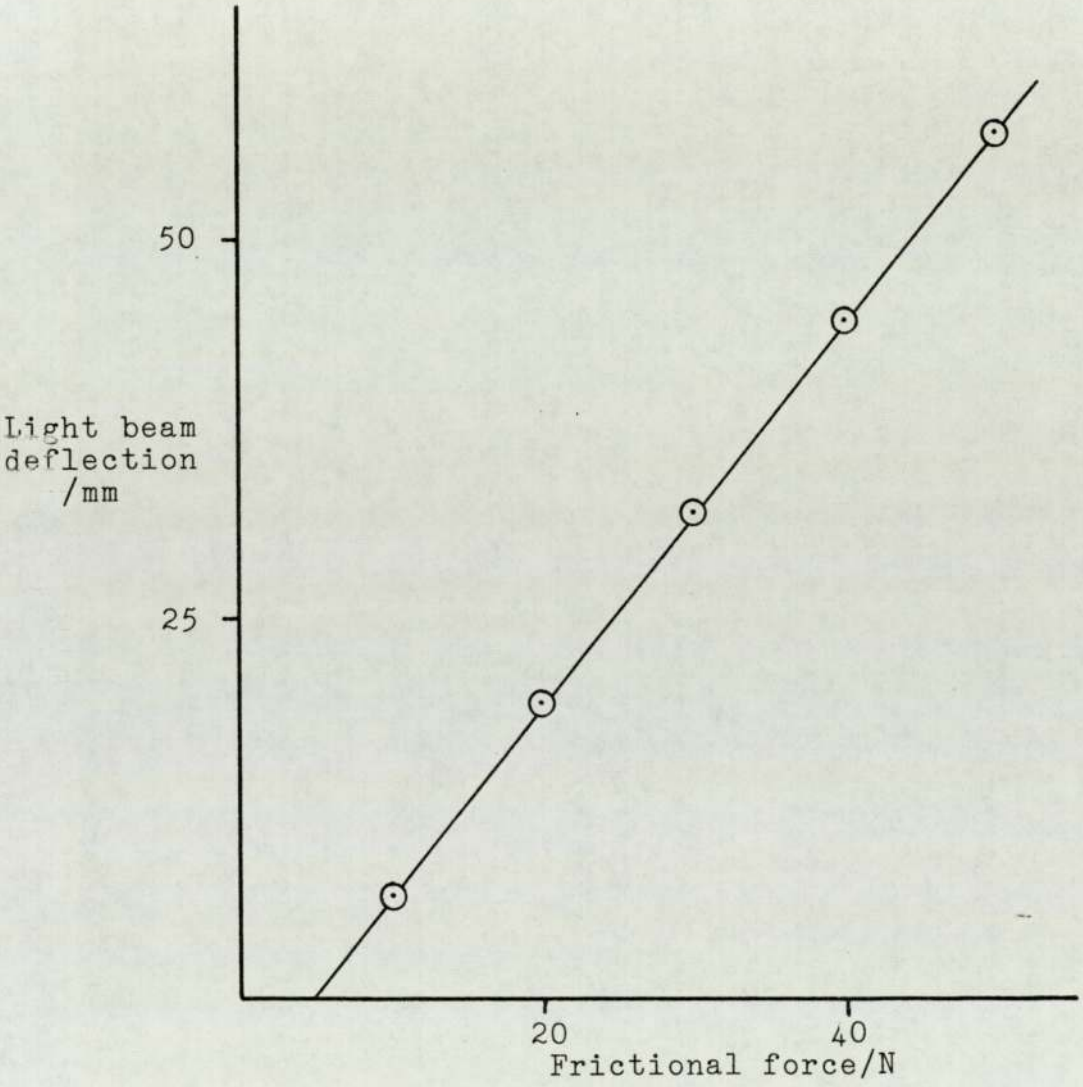

Figure 2.13 The typical variation of the light beam deflection with the frictional force

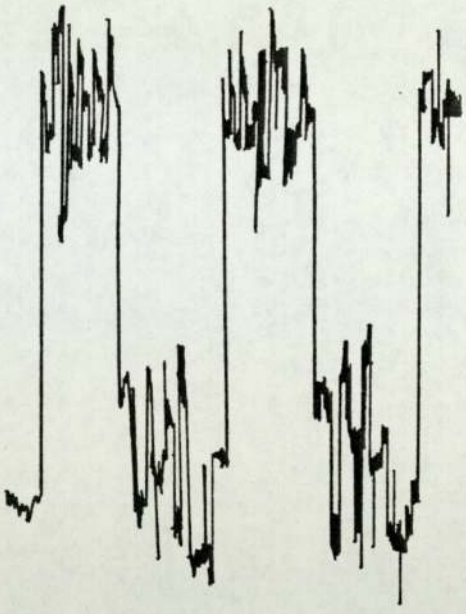

Figure 2.14 The variation of the coefficient of friction during a cycle of severe wear
(after approximately 180 cycles)

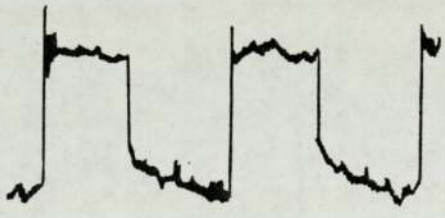

Figure 2.15 The variation of the coefficient of friction during a cycle of mild wear
(after approximately 7200 cycles)

The experimental conditions for both traces were:-

sliding speed	37 mms^{-1}
load	22 N
temperature	450 ^{o}C

wear rate was that it was not sensitive enough for short wear tests when the weight loss was less than 1 mg; in addition, only the overall wear rate was determined and not the instantaneous wear. This was of particular importance as there was often a transition from severe to mild wear. The wear rates of these two wear regimes differed by a factor of about 100. It was important, therefore, to try and determine the instantaneous wear rate within each period of wear. In an attempt to achieve this, an L.V.D.T. was added to the wear test machine, pointing down onto the upper loading beam; as the pin specimen was worn away, the loading beam moved about the fulcrum and this movement was measured by the L.V.D.T.. Unfortunately, little useful wear data were collected from this because the differential linear displacement of the pin specimen due to wear was very small compared to the vibration of the wear machine. However, after the transition to mild wear, the vibration was much less, and the L.V.D.T. gave some data about the mild wear rate. There was no practical way that the transducer could be placed closer to the pin, nor could it be set inside the specimen chamber due to the heating elements all around the specimens.

2.3.4 Wear test procedure

All experiments in this investigation were carried out at elevated temperatures between 200°C and 550°C.

Once sufficient carbon dioxide had passed through the specimen chamber, the heater was switched on and its power supply adjusted so that the thermocouple did not cause any variation in the ambient temperature as the power was switched on and off. This took about 20 to 30 minutes. The ultra-violet chart recorder was switched on, and once the experiment was ready to proceed, the recorder and a clock were started simultaneously with the drive motor on the wear machine. The domed end

of the pin specimen allowed the friction to be measured from the first reciprocating cycle without the possibility of an edge of the pin gouging into the flat specimen. Friction was measured continuously for the first 15 seconds, and then every 15 seconds for the next 2 minutes, roughly every 2 minutes for the following 8 minutes, and thereafter every 5 minutes, but less frequently as the experiment progressed. After several hours, the friction was measured at most once per hour. Because the frequency of the reciprocating motion was known, each frictional measurement was related to the friction after a known number of cycles.

It was found that the friction decreased rapidly during the first hundred cycles, but less quickly as the experiment progressed. As a result, friction measurements were taken less frequently. It was impossible to record the friction continuously for long periods because the minimum paper speed on the u.v. recorder was not slow enough. So when an experiment had to be run overnight, the friction was measured as late as possible one day, and as early as convenient on the following day. The continuous wear measurements using the L.V.D.T. were very useful for such tests. The pen chart recorder could be set to record continuously at the slowest speed overnight, and so the time at which any wear transition occurred could be noted.

Figure 2.16 shows a typical friction variation during a test. The experimental conditions were 4 Hz, 9.20 mm stroke with a load of 22 N and at 450^{o}C in carbon dioxide. It was observed that the friction decreased after 6.9 $\pm$ 0.5 x 10^3 cycles, and the experiment was stopped after 14.4 x 10^3 cycles. Reasons for this behaviour of the friction are given in a later chapter.

After the wear test was completed, carbon dioxide was still passed through the specimen chamber while the

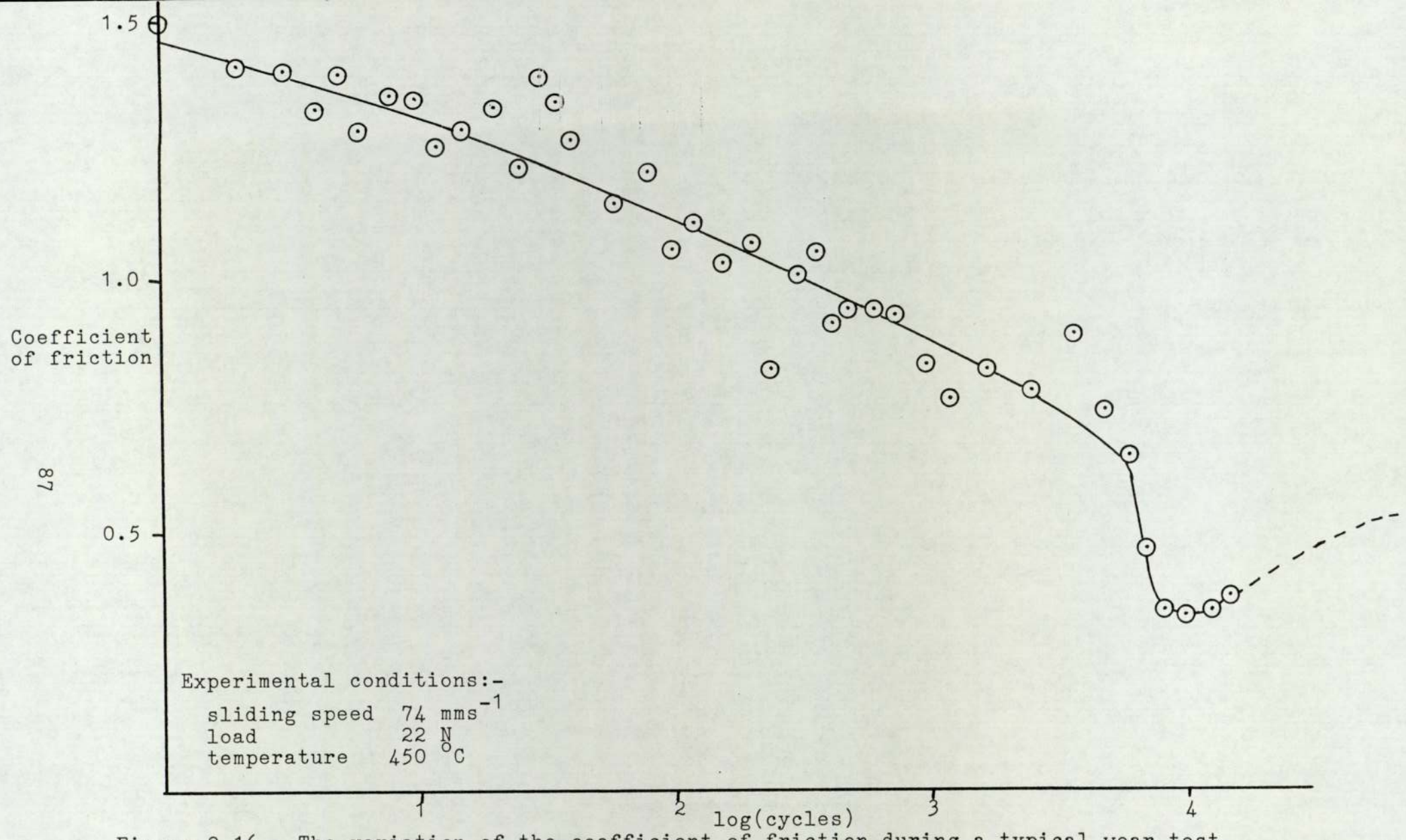

Figure 2.16 The variation of the coefficient of friction during a typical wear test

specimens cooled down to room temperature in order to minimise any air oxidation. The weight loss of each specimen was measured and the overall wear rate calculated.

2.4 Material specification

The pin and flat specimens for the reciprocating experiments and the pins and flats for the unidirectional sliding tests were all provided by Berkeley Nuclear Laboratories. The analysis gave:

	C	Mn	Si	S	P	Cr	Mo	Ni	Fe
Weight%	0.11	0.42	0.66	0.010	0.005	8.89	1.00	0.24	remainder
Atomic%	0.50	0.42	1.30	0.02	0.01	9.42	0.57	0.23	remainder

2.5 The experimental range of wear tests

Reference wear tests were carried out on the high speed unidirectional wear test machine at two speeds, 0.5 ms^{-1} and 2.0 ms^{-1}. All tests were done at room temperature in air and with loads of up to 60 N. These tests were carried out so that the behaviour of the 9% chromium steel could be compared with that of other steels already studied in this laboratory. A different pin specimen was used for each experiment; this was worn against a disc that had been reground and cleaned.

Tests were also carried out on the slow speed unidirectional wear test machine with speeds between 18 mms^{-1} and 110 mms^{-1}. These tests were at temperatures between 25°C and 300°C and with loads of up to 41 N.

Similar slow speed tests were done in a carbon dioxide atmosphere. The range of sliding speeds was from 18 mms^{-1} to 147 mms^{-1}, and the temperature from 200°C to 350°C. The load was maintained at 22 N for all experiments.

The conditions of the unidirectional sliding experiments in carbon dioxide were chosen to be as

similar as possible to the conditions that could be obtained using the reciprocating sliding test machine. The reciprocating frequency was varied from 1 Hz to 9 Hz; this was equivalent to mean sliding speeds of 18 mms^{-1} to 167 mms^{-1}. The amplitude was kept constant at 9.2 mm for all experiments, and the load was either 22 N or 41 N. A different pair of pin and flat specimens was used in each test.

Five series of reciprocating experiments were carried out. The wear at different temperatures between 200°C and 550°C was studied, with all other experimental conditions constant (sliding speed 37 mms^{-1}, load 22 N). In the remaining four series of experiments, all conditions were held constant except the sliding speed which was varied between 18 mms^{-1} and 167 mms^{-1}. Each series of tests was carried out with one load and at a particular temperature:

1) temperature 450°C, load 22 N
2) temperature 300°C, load 22 N
3) temperature 290°C, load 22 N
4) temperature 300°C, load 41 N

The running-in times of unidirectional sliding experiments were not normally recorded. However, they were measured for the slow speed sliding experiments in this work so that a comparison could be made between these tests and those on reciprocating sliding.

In addition to the above series of experiments, several experiments were carried out to investigate the effect of dwell periods on the running-in times. A dwell period was a length of time during which the specimens did not move, but the other experimental conditions (atmosphere, ambient temperature and load) were maintained in the states reached during sliding. Experiments were run for a short period, typically about 15 minutes and then the specimens were left at the

elevated temperature for 24 or 96 hours before being run again. Three reciprocating and one unidirectional dwell tests were made.

2.6 The physical methods of analysis

2.6.1 Surface profilimetry

Surface profiles were made using a Taylor-Hobson talysurf of discs worn at slow speeds. No quantitive calculations were possible because the wear tracks were too rough for the centre line average (c.l.a.) to be calculated. Qualitive graphical measurements were made.

2.6.2 Microhardness tests

Microhardness measurements were made on many specimens using a Leitz microhardness tester. The load was 50 g. The flat specimens and the pin specimens from the unidirectional tests were mainly those studied, although the hardnesses of some discs were also measured. No significant difference was found between the surface hardnesses of the pin and the disc from any one experiment. About twelve measurements were taken per specimen and the average was calculated.

Sections were made of unidirectional pins and reciprocating sliding flat specimens so that the sub-surface microhardness could also be measured.

2.6.3 Metallographic taper sections

Sections were made on several specimens in order to study the surface and sub-surface changes. A few sections were made normal to the specimen surface; these were prepared using a diamond cutting wheel. However, any changes were so near the surface as to be not easily observable and so most analysis was carried out on taper sections.

A flat specimen or a pin specimen from a unidirectional wear test was mounted upside down in a

conductive bakelite mould. The surface to be examined was totally embedded in the bakelite at this point. Using an abrasive belt, the mould was ground away at an angle of nominally 11° until the specimen surface was encountered. Subsequent grinding was carried out using several grades of emery paper, ending with polishing on a 6μ and then a 1μ diamond wheel. This procedure was followed so that no damage could occur to the specimen surface while the taper was prepared.

The angle of the taper was then measured accurately. Knowing this, a distance from the edge of the polished specimen could be related to the depth into the specimen from the surface. An 11° taper gave magnification by a factor of about five. Microhardness tests were made at various depths into the specimen until the hardness values obtained were equal to the hardness of the bulk material.

Some sections were etched using Vilella's reagent (5 ml HCl, 1 gm picric acid, 100 ml 95% ethanol) and subsequently examined by scanning electron microscopy.

2.6.4 X-ray diffraction

Powder X-ray diffraction of the wear debris and glancing angle X-ray diffraction of flat specimens was carried out.

A Debye-Scherrer camera was used with the wear debris held in a 0.5 mm diameter capillary tube; the sample was irradiated with cobalt K_α radiation for about one hour at a voltage of 40 kV and a current of 30 mA.

Glancing angle X-ray diffraction was carried out on a few flat specimens (142). Each section was cut using a diamond cutting wheel and mounted in plasticine such that one edge of the specimen blocked about half of the X-ray beam, with the worn surface of the specimen at an angle of about 30° to the beam. Irradiation was for about 40 minutes and the film was then developed in

the usual way.

This method of analysis was used on the reciprocating specimens because the wear debris was predominately obtained during the severe wear regime. Separate collection of the severe and mild wear debris was not possible due to the sealed specimen chamber.

2.6.5 Scanning electron microscopy

Scanning electron microscopy, s.e.m. was carried out on a wide selection of normal and tapered specimens. Energy dispersive analysis by X-rays, E.D.A.X. was also carried out on many specimens, but this technique was mainly used upon tapered sections in attempts to show how the constituent elements varied in concentration near the surface.

E.D.A.X. was capable of three kinds of output. It was possible to determine the distribution of one element over the sample surface, and produce an elemental map. A second form of output showed graphically how the concentration of one element varied across a particular cross-section of the surface; this was called making an elemental profile. Both of these measurements were displayed on the s.e.m. monitor and could be photographed.

The final type of output could not be photographed; instead, a microcomputer gave a print out of the results. It was possible to analyse a spot or an area on the specimen, and the computer linked to the system calculated the percentage of each element in the sample. In practice, as the user informed the computer which elements were present, the technique was better at giving the ratio between the two or more elements for which it was analysing. Unfortunately, with the crystals available, this E.D.A.X. could not analyse for oxygen or other light elements.

Oxide thicknesses were measured by increasing the tilt of the specimens to 50°, and then correcting for

this. The edges of any oxide plateaux could be clearly seen, and measurements of their thicknesses made.

2.6.6 Auger spectroscopy

Auger spectroscopy was used to give more information about the variation in iron, chromium and oxygen concentrations near the surface. The technique was no more accurate than E.D.A.X., but was able to measure the oxygen content.

Using an argon ion gun, the surface was etched away and the variation in concentration with depth was studied without having to prepare tapered sections. This technique was also able to produce elemental maps.

CHAPTER 3
EXPERIMENTAL RESULTS

3.1 Introduction

The unidirectional sliding experiments were carried out first; the results of the high speed reference tests, carried out at room temperature are presented, followed by the results of the elevated temperature tests in air or in carbon dioxide. Finally, the reciprocating sliding results are presented.

The various analytical techniques used in this work are considered individually. The two most informative methods were scanning electron microscopy and microhardness testing.

3.2 High speed unidirectional wear tests at room temperature

3.2.1 Wear

The wear was investigated at sliding speeds of 0.5 ms^{-1} and 2.0 ms^{-1} using loads of up to 59 N.

At 0.5 ms^{-1}, there was severe wear for all loads in the range studied. Wear rates were directly proportional to the load (figure 3.1) and the specific wear rate was 2.67×10^{-12} $m^3N^{-1}m^{-1}$. The debris was metallic; equilibrium wear was generally obtained after five minutes, but tests were run for about one hour or more to confirm that there was no transition to mild wear during that time.

At 2.0 ms^{-1}, both severe and mild wear occurred in the range of loads studied. There was a Welsh T_2 type transition (50, 51) at 26 N. At loads less than this, the severe wear was proportional to the load (figure 3.2) and the specific wear rate was 8.19×10^{-13} $m^3N^{-1}m^{-1}$. At loads above 26 N, there was mild wear of which the rate was almost independent of the load. The mean wear

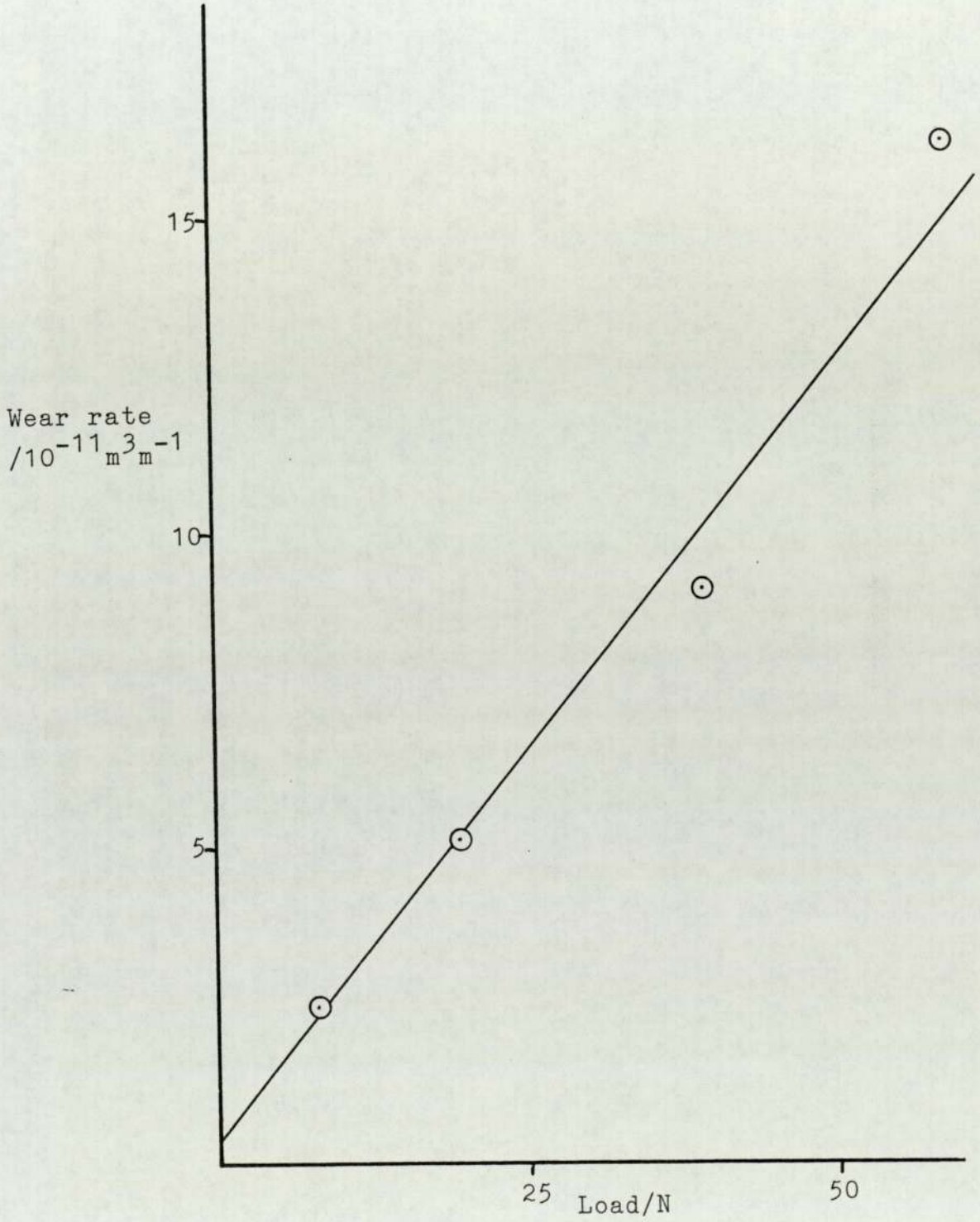

Figure 3.1 The variation of the wear rate with the load, at 0.5 ms^{-1}

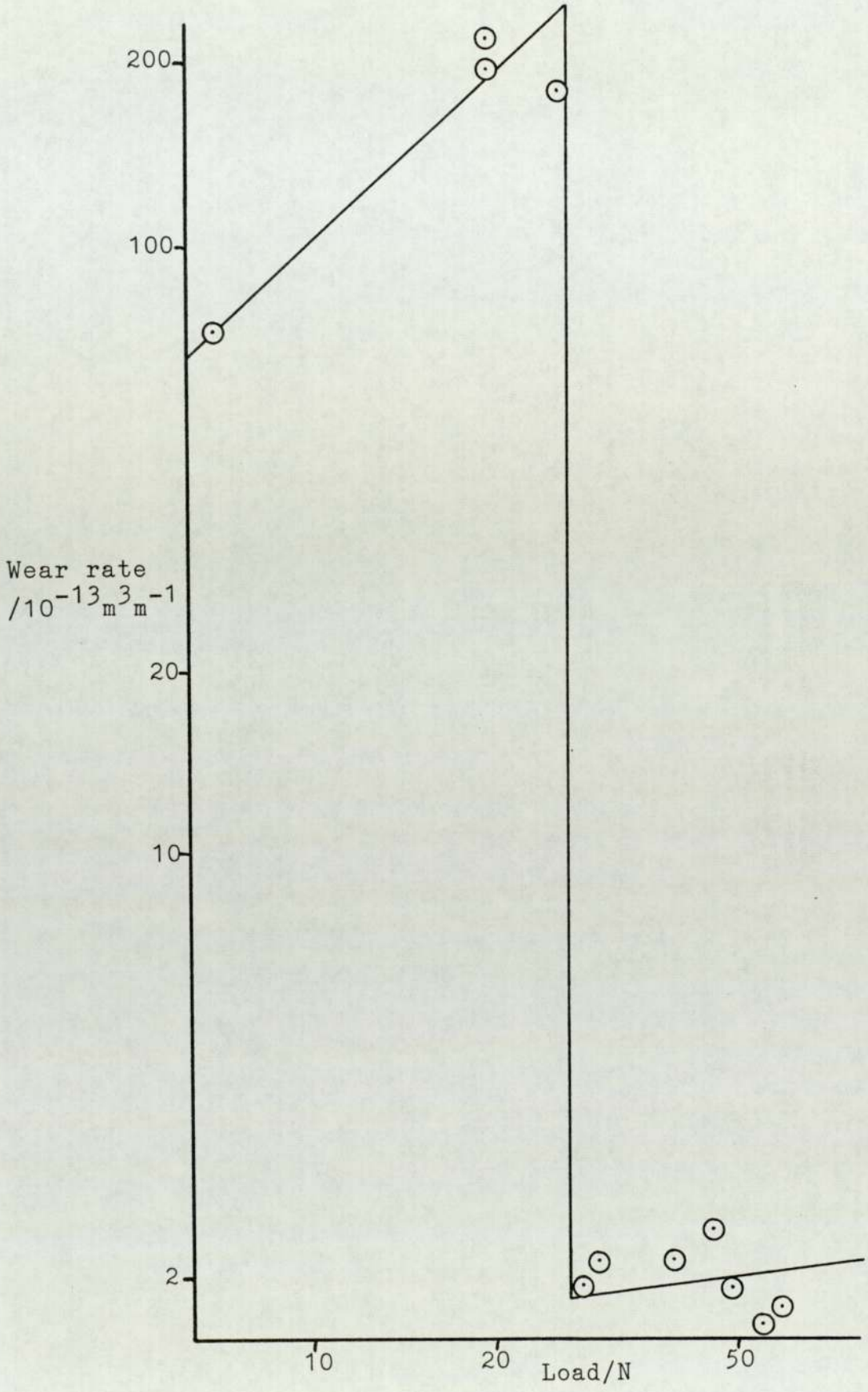

Figure 3.2 The variation of the wear rate with the load, at 2.0 ms^{-1}

rate varied from 1.7×10^{-13} $m^3 m^{-1}$ to 2.4×10^{-13} $m^3 m^{-1}$. Mild wear running-in times decreased from 25 minutes to 5 minutes as the load increased. The equilibrium mild wear debris was a black powder.

3.2.2 Friction

Friction was measured continuously, and its value was recorded once equilibrium wear was established. Running-in was indicated by larger frictional values; once equilibrium was attained, both the magnitude and fluctuation of the friction reduced.

At both sliding speeds, there was a gradual decrease in the coefficient of friction as the load increased. At 0.5 ms^{-1}, the reduction was about 10% of the average value (figure 3.3), and so may not have been significant. At the higher sliding speed, 2.0 ms^{-1}, the coefficient decreased with increasing load in the mild wear region, except at very small loads; other workers have reported an increase in friction at small loads followed by a subsequent decrease (129).

3.2.3 Heat flow

The heat flow calculations were different for the slow and high sliding speeds. For the high speed sliding, it was assumed that it was forced convection that cooled the exposed part of the pin. Due to the air disturbance caused by the rapidly rotating disc, the speed of the air past the pin was assumed to equal the sliding speed of the pin on the disc.

At these high speeds, the frictional heating was the only source of the heat that flowed down the pin, and the results in this section showed that the heat flow equations produced valid answers from these experiments.

The temperatures at certain points on the pin were measured in order to calculate the temperature on the

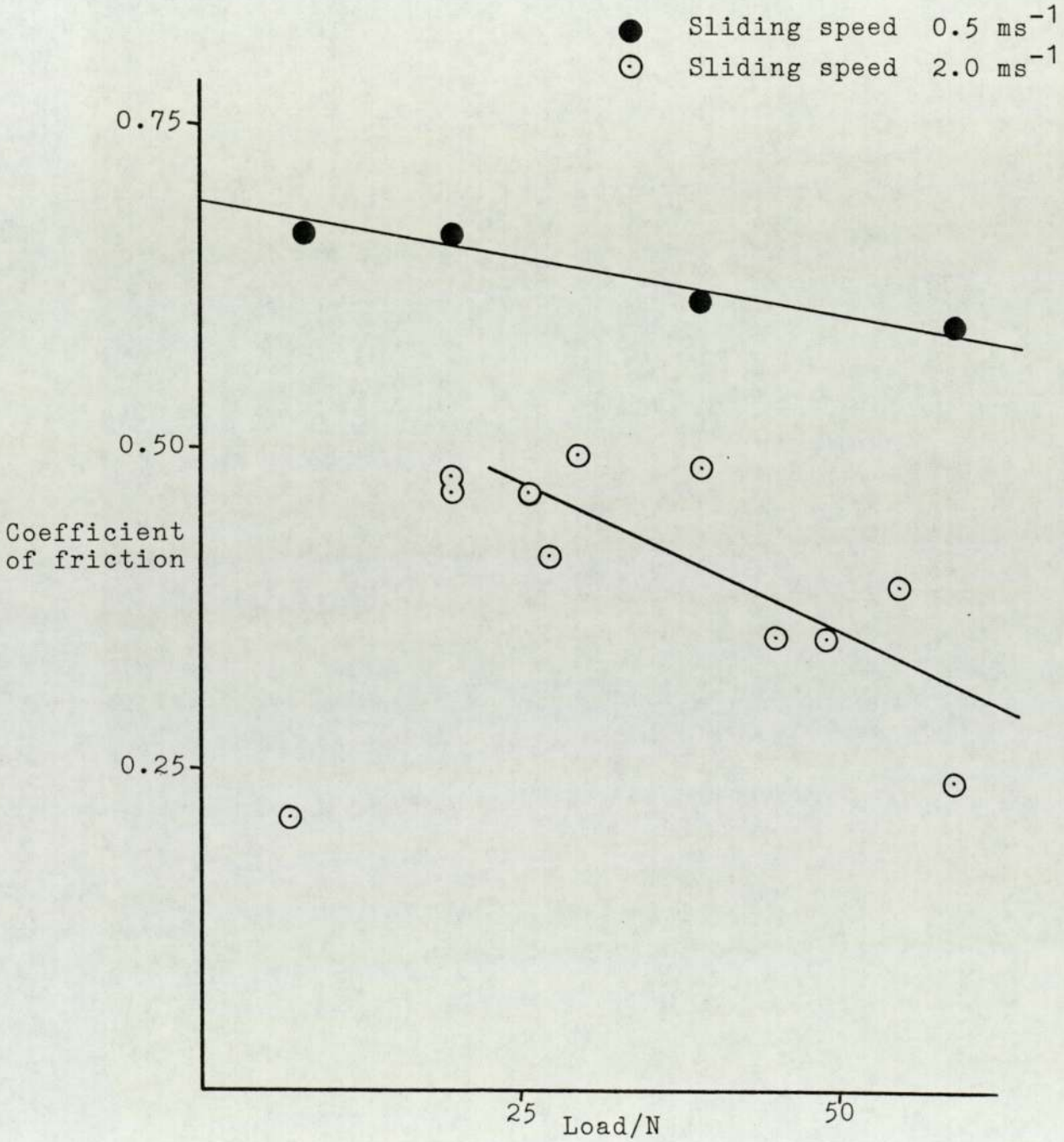

Figure 3.3 The variation of the coefficient of friction with the load

surface of the pin, T_s, and the heat flowing into the pin from this point, H_1. The total heat generated, H_T, was the product of the sliding speed, U, and the frictional force, F. The experimental division of heat, δ_{expt}, was the fraction of the total heat to enter the pin, and was defined by:

$$\delta_{expt} = \frac{H_1}{H_T}$$

These parameters were important when applying the oxidational wear theory (141).

The measured temperatures and values calculated from the heat flow considerations are presented in tables 3.1 and 3.2. The variation of the surface temperature with the load is shown in figure 3.4. In the severe wear regions, there was a steady increase in the temperature with increasing load, but in the mild wear regime at 2 ms^{-1}, above the wear transition at 26 N, the surface temperatures were not only much less, but also less load dependent. This was due to the surface oxide layer having a smaller thermal conductivity than the metal.

3.3 Slow speed unidirectional wear tests at elevated temperatures

3.3.1 In air

Twenty-six experiments were carried out in air at speeds between 17 mms^{-1} and 110 mms^{-1} (reciprocating sliding tests at 1 Hz and 6 Hz respectively gave similar sliding speeds), and at temperatures between 25°C and 300°C. The load was normally 22 N, but a few experiments were carried out with loads up to 41 N. Table 3.3 presents the experimental conditions, the specific wear rate and the frictional force; table 3.4 gives the data and results of the heat flow analysis.

The heat flow analysis was much more complicated for the elevated temperature experiments than for the

load /N	T_A /°C	T_B /°C	T_C /°C	T_s /°C	H_1 /W	H_T /W	δ_{expt} /%
7.9	35	31	29	38	0.37	2.58	14.4
19.7	54	41	36	63	1.17	6.45	18.2
39.3	66	47	35	85	2.00	12.9	15.5
59.0	88	57	42	112	3.06	17.4	17.6

Table 3.1 The heat flow analysis at 0.5 ms^{-1}

load /N	T_A /°C	T_B /°C	T_C /°C	T_s /°C	H_1 /W	H_T /W	δ_{expt} /%
6.9	44	36	32	53	0.94	2.88	32.5
19.7	92	60	42	99	2.88	18.2	15.8
19.7	95	57	42	119	3.87	18.2	21.3
25.6	116	67	47	156	5.11	23.4	21.9
27.5	60	48	41	73	0.91	22.4	4.0
29.5	55	43	36	69	0.93	28.8	3.2
39.3	56	45	36	68	0.86	37.5	2.3
45.2	63	47	38	80	1.20	31.9	3.8
49.2	72	52	41	94	1.56	34.9	4.5
55.0	82	55	42	102	1.91	42.5	4.5
59.0	76	52	39	92	1.68	28.8	5.8

Table 3.2 The heat flow analysis at 2.0 ms^{-1}

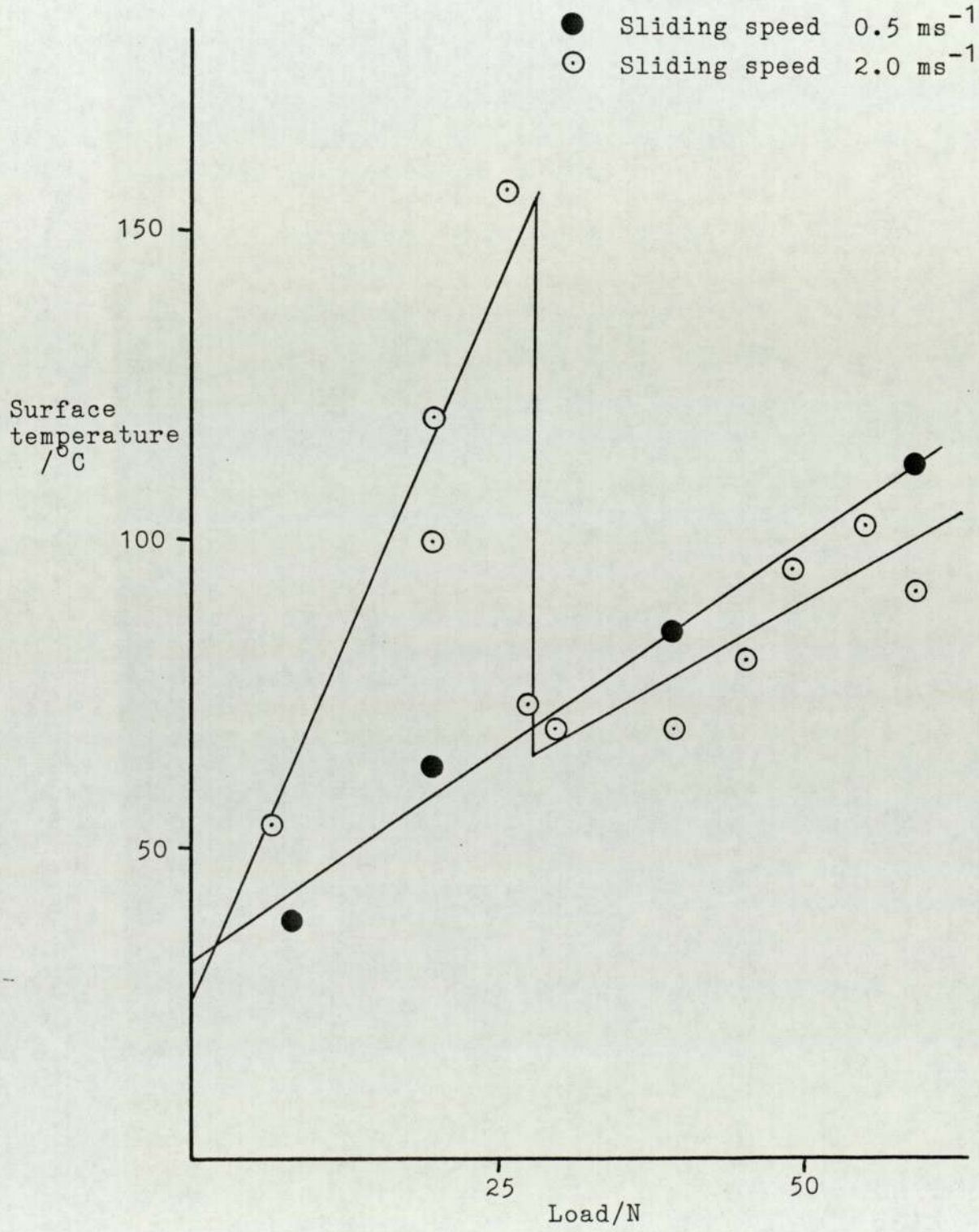

Figure 3.4 The variation of the surface temperature with the load

Test Number	Temperature /°C	Sliding Speed /mms^{-1}	Load /N	Specific Wear Rate /m^{3}N^{-1}m^{-1}	Frictional Force /N
1	25	36.8	22	4.44×10^{-12}	29.1
2	100	17.8	22	7.76×10^{-13}	29.0
3	100	37.5	22	1.41×10^{-13}	23.1
4	100	55.3	22	2.17×10^{-13}	24.0
5	100	72.3	22	1.84×10^{-12}	23.2
6	100	91.2	22	1.73×10^{-12}	24.9
7	100	108.7	22	2.13×10^{-12}	24.9
8	100	18.0	26	6.65×10^{-13}	31.5
9	100	36.8	26	1.67×10^{-14}	29.0
10	100	55.4	26	2.33×10^{-12}	25.7
11	100	18.6	31	6.09×10^{-13}	32.3
12	100	36.8	31	1.19×10^{-12}	34.8
13	100	36.8	31	1.15×10^{-12}	29.9
14	100	36.8	41	1.74×10^{-12}	42.3
15	200	18.9	22	6.31×10^{-14}	24.9
16	200	37.7	22	3.13×10^{-14}	24.9
17	200	73.6	22	3.36×10^{-14}	23.2
18	200	109.4	22	4.25×10^{-14}	21.6
19	200	22.6	41	9.50×10^{-14}	37.2
20	200	18.3	41	8.12×10^{-14}	41.5
21	200	37.9	41	4.56×10^{-14}	39.0
22	300	17.7	22	5.65×10^{-14}	19.9
23	300	36.8	22	6.65×10^{-14}	21.6
24	300	39.5	22	9.97×10^{-14}	21.6
25	300	17.5	41	2.62×10^{-14}	35.7
26	300	38.7	41	7.39×10^{-14}	33.9

Table 3.3 The conditions and measured wear parameters for experiments carried out in air

test number	temper -ature /°C	T_A /°C	T_B /°C	T_C /°C	T_s /°C	H_1 /W	H_T /W	δ_{expt}	running-in time /min
1	25	28.8	27.5	25.6	29.1	.08	1.07	0.07	
2	100	68	50	44	76	1.04	0.52	0.06	80
3	100	71	48	41	81	1.32	0.86	0.36	132
4	100	70	56	44	74	0.85	1.33		692
5	100	80	55	47	88	1.37	1.68		
6	100	80	54	46	89	1.43	2.27		
7	100	87	61	49	90	1.42	2.70		
8	100	73	49	45	83	1.37	0.57	0.63	80
9	100	77	59	44	84	1.13	1.07	0.11	748
10	100	79	57	43	82	0.98	1.42		
11	100	76	50	41	87	1.48	0.60	0.79	140
12	100	77	52	43	86	1.32	1.28		
13	100	74	55	47	79	0.66	1.10		
14	100	77	53	44	85	1.22	1.56		
15	200	124	77	59	147	2.84	0.47		16
16	200	135	74	49	162	3.66	0.94		36
17	200	105	81	65	117	1.53	1.71	0.30	26
18	200	128	90	66	147	2.36	2.36	0.57	14
19	200	120	75	56	139	2.64	0.84		86
20	200	119	97	63	130	1.60	0.76	0.78	47
21	200	127	86	65	146	2.46	1.48	0.99	38
22	300	173	101	81	210	4.26	0.35		14
23	300	209	139	99	247	4.39	0.40		6
24	300	155	94	77	184	3.60	0.85		4
25	300	171	100	84	207	4.17	0.62		12
26	300	162	114	89	186	2.98	1.31		10

Table 3.4 The heat flow analysis for experiments carried out in air
(The absence of a running-in time indicates that equilibrium wear was severe.)

room temperature experiments because the heat flow from the disc to the pin was due primarily to the heated disc and conduction from the disc to the pin, rather than the frictional heating. This led to several modifications in the calculation of the surface temperature of the pin, T_s, which was then used when applying the oxidational wear theory. In addition, the heat flow equations themselves had to be changed because, due to the much slower sliding speed, forced convection around the exposed part of the pin caused by the rotating disc could no longer be assumed. The equations were altered to allow for free convection from the pin; modifications were also made to allow for the slightly raised ambient temperatures near the pin, due to the hot disc.

All these modifications are discussed in more detail in Chapter 4.

The values of H_1, shown in table 3.4, were those calculated before the conduction from the disc to the pin had been estimated. The division of heat was only calculated when H_1 less conduction had a value compatible with H_T; this had to be positive but less than H_T. The wide range of values of δ_{expt} was due to the difficulty in estimating the conduction across the air gap between the heated disc and the pin; the surface temperature, T_s, was not affected by the conduction.

The method by which these estimates were made, and the experiments upon which they were based is also described in Chapter 4.

3.3.2 In carbon dioxide

Twenty-nine experiments were carried out in carbon dioxide at speeds between 18 mms^{-1} and 148 mms^{-1} (equivalent to reciprocating sliding frequencies of 1 Hz and 8 Hz), and at temperatures between 200°C and 350°C. The load was always 22 N. Table 3.5 presents the experimental conditions, the specific wear rate and the

Test Number	Temperature /°C	Sliding Speed /mms^{-1}	Load /N	Specific Wear Rate /m^{3}N^{-1}m^{-1}	Frictional Force /N
1	200	36.8	22	2.20×10^{-12}	27.4
2	200	37.4	22	2.24×10^{-12}	28.2
3	200	105.8	22	1.36×10^{-12}	24.9
4	210	38.9	22	1.35×10^{-12}	24.0
5	215	90.4	22	1.49×10^{-12}	27.4
6	250	36.8	22	2.37×10^{-13}	24.9
7	250	70.2	22	2.70×10^{-13}	23.2
8	250	106.9	22	2.23×10^{-13}	24.9
9	257	112.1	22	4.89×10^{-13}	17.5
10	261	19.1	22	1.38×10^{-12}	24.9
11	261	57.4	22	4.01×10^{-13}	29.9
12	261	112.9	22	2.50×10^{-13}	19.1
13	266	19.4	22	3.47×10^{-13}	26.5
14	266	55.7	22	4.95×10^{-13}	27.4
15	266	110.6	22	1.09×10^{-13}	21.6
16	266	119.0	22	1.16×10^{-13}	14.9
17 dwell test	266	118.5	22	(2.35×10^{-14})	24.0
18	266	140.3	22	1.64×10^{-13}	17.4
19	266	140.1	22	6.55×10^{-14}	21.6
20	266	150.4	22	1.31×10^{-13}	24.0
21	266	157.1	22	1.26×10^{-13}	12.4
22	270	105.8	22	1.61×10^{-13}	20.7
23	273	19.7	22	1.68×10^{-13}	24.0
24	273	56.7	22	1.96×10^{-13}	25.7
25	273	111.3	22	6.09×10^{-14}	23.2
26	280	38.1	22	8.45×10^{-14}	25.7
27	285	105.8	22	3.44×10^{-14}	13.3
28	300	38.8	22	7.02×10^{-14}	19.1
29	350	36.8	22	2.72×10^{-14}	11.6

Table 3.5 The conditions and measured wear parameters for experiments carried out in carbon dioxide

test number	temper -ature /°C	T_A /°C	T_B /°C	T_C /°C	T_s /°C	H_1 /W	H_T /W	expt	running-in time /min
1	200	149	108	95	165	1.63	1.01		
2	200	146	104	90	164	1.60	1.05		
3	200	137	110	97	141		2.63		
4	210	163	112	101	171	1.95	0.94		
5	215	151	112	96	160	0.72	2.47	0.29	
6	250	158	115	91	178	0.46	0.92		
7	250	172	127	100	190	1.03	1.63		
8	250	183	132	107	200	1.68	2.67		
9	257	151	112	94	166		1.97		
10	261	155	114	95	174	2.44	0.48		540
11	261	183	127	104	208	3.34	1.71		192
12	261	176	127	104	195	2.92	2.15	0.76	750
13	266	159	122	99	178	2.29	0.51		57
14	266	191	136	109	215	3.34	1.52		140
15	266	181	130	110	200	2.95	2.38	0.70	530
16	266	170	123	105	191	2.80	1.78	0.85	338
17 (dwell)	266	157	117	101	175	2.37	2.85	0.38	(47)
18	266	164	125	101	181	2.38	2.44	0.44	98
19	266	183	122	108	202	3.31	3.02	0.67	245
20	266	178	131	106	197	2.82	3.62	0.42	108
21	266	186	133	108	207	3.14	1.95	0.94	225
22	270	165	128	107	179	2.21	2.19	0.42	780
23	273	184	128	104	209	3.27	0.47		42
24	273	178	123	105	202	3.19	1.46		168
25	273	186	136	108	207	2.98	2.58	0.65	272
26	280	190	134	112	210	3.22	0.98		160
27	285	175	135	112	193	2.42	1.40	0.81	185
28	300	186	139	118	209	2.78	0.74		54
29	350	208	166	133	230	2.68	0.43		25

Table 3.6 The heat flow analysis for experiments carried out in carbon dioxide
(The absence of a running-in time indicates that equilibrium wear was severe.)

frictional force; table 3.6 gives the data and results of the heat flow analysis which were calculated in a manner similar to the method used on the slow speeds tests run in air and described in Chapter 4.

One dwell experiment was carried out. In this experiment, heat flow measurements were made in the absence of sliding. An estimate was made of the heat flow due solely to the conduction of the heat from the disc to the pin in the absence of frictional heating and thus the width of the air gap was calculated. Unfortunately, the air gap was less during the dwell periods when there was no vibration than during the sliding periods with the result that the calculated heat flow was greater than that which would be expected to be due to conduction during sliding. As a result, no estimate of the conduction could be made and values were restricted to those derived from calculations fully described in a later chapter.

Estimates were again made of the carbon dioxide temperature around the exposed portion of the pin. These were much higher than for the experiments run in air because the enclosed specimen chamber reduced gas convection.

In table 3.6, the division of heat was calculated only when the value of H_1 less that due to conduction was compatible with the total heat generated. Chapter 4 gives a detailed account of these calculations.

3.3.3 Dwell tests and running-in times

One dwell test was carried out; this is discussed with the reciprocating sliding dwell tests in section 3.4.7.

Running-in times of unidirectional and reciprocating sliding experiments are compared in section 3.4.6.

3.4 Reciprocating wear tests

3.4.1 Introduction

Ninety-five reciprocating wear tests were carried out. Not all experiments were included in the series of tests detailed in section 2.5. The experiments described below are those tests which were carried out to study the variation in friction and to determine the overall wear rate. Experiments carried out to study the sub-surface changes are described in section 3.7.

Appendix 1 presents, in chronological order, the conditions and results for all experiments. It also includes references to any unusual features of the tests and a discussion on the accuracy of the measurements.

3.4.2 Friction

A typical experiment was described in section 2.3.4 and figure 2.16 showed how the coefficient of friction could vary during a wear test.

The initial coefficient of friction was about 1.6 for tests with a 22 N load, but this was already reduced to 1.4 after about 10 to 20 reciprocating cycles; there was a further steady decrease to about 0.8 after 1000 cycles and the friction stayed at about that value (0.7 to 0.8) until a wear transition occurred. For tests carried out with a 41 N load, the initial friction coefficient was about 1.8 and decreased to about 0.7 to 0.9 after a few thousand cycles or a sliding distance of about 50 to 60 m.

The wear transition marked the change from severe running-in wear to equilibrium mild wear and was associated with a sudden decrease in the coefficient of friction from about 0.8 to 0.3 over approximately 100 cycles or 2 m. Once in the mild wear mode, there was a very gradual increase in the friction; after 1000 cycles, it was 0.4 and after about 100000 cycles or 2000 m of mild wear, an equilibrium friction coefficient

of about 0.6 was reached. This increase in friction was not observed in all tests because only a few experiments were run for more than 5000 cycles in the mild wear mode. The mild wear frictional behaviour was independent of load.

If no transition occurred, the coefficient of friction remained fairly constant at about 0.75.

The different ways in which the friction can vary during the course of an experiment are shown in figure 3.5.

3.4.3 The transition point

The previous section described a gradual decrease in the coefficient of friction as an experiment in the severe wear mode proceeded; this could be followed by a transition to mild wear. When such a transition occurred, the time, T_T, was recorded, and knowing the frequency of the reciprocating movement, the number of cycles required to reach the wear transition, N_T, was calculated. The time, T_T, was only considered to be important for experiments carried out at 450°C and above. At this temperature, it was found that N_T was proportional to the frequency and so the time needed to reach the wear transition was constant. This was because the high ambient temperature caused more oxidation than the frictional heating.

One series of experiments was carried out to investigate how N_T varied with temperature under a standard set of sliding conditions. The results are shown in figure 3.6; the specific wear rates and test conditions are given in table 3.7. The wear rates did not change significantly over the temperature range; the values at 200°C and 275°C were less than the remaining values, but this was not due to the lower temperatures. It will be shown in the next section that the severe wear rate decreased as the experiment pregressed. For the tests

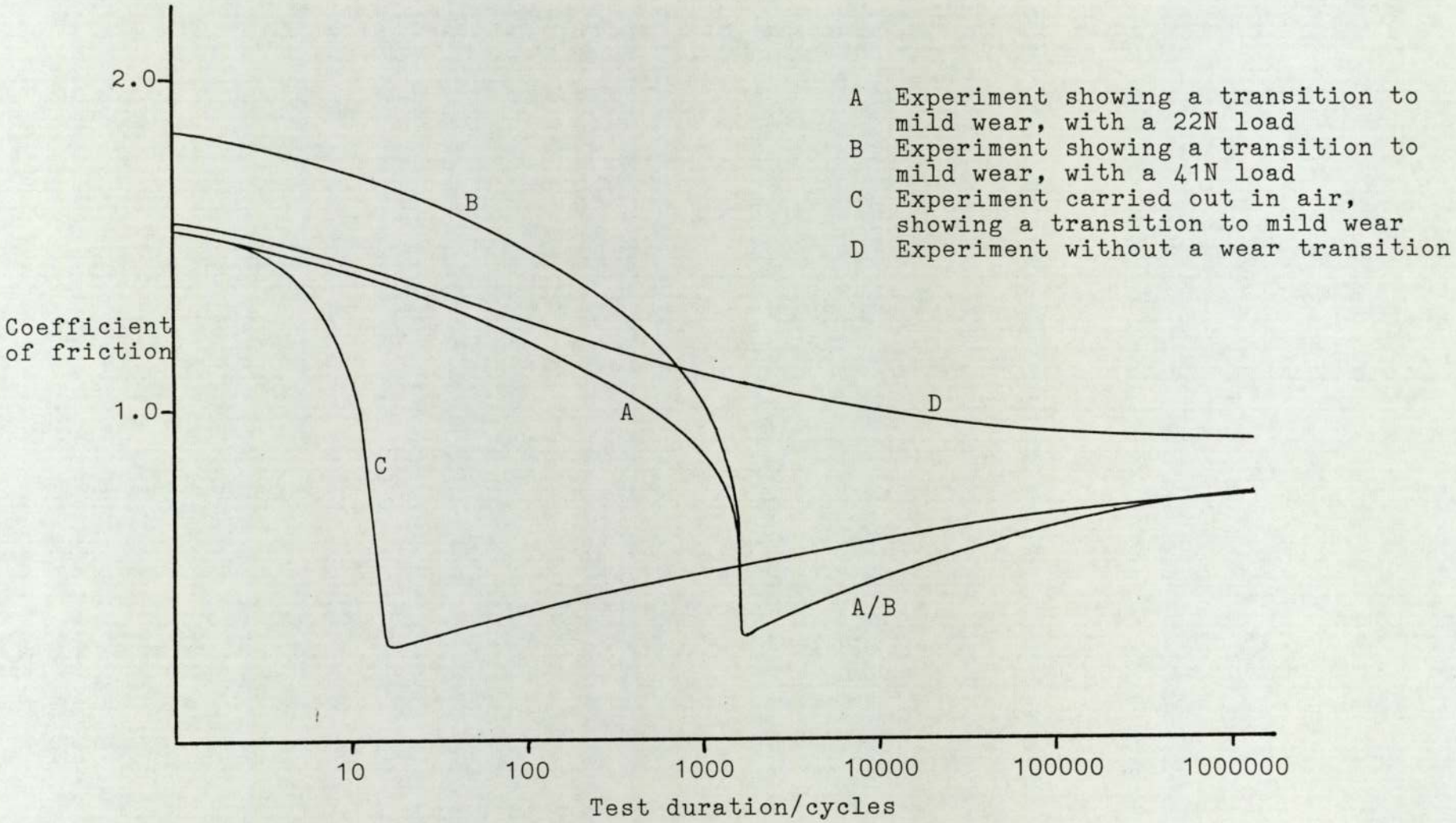

Figure 3.5 The variation of the coefficient of friction during typical reciprocating wear tests

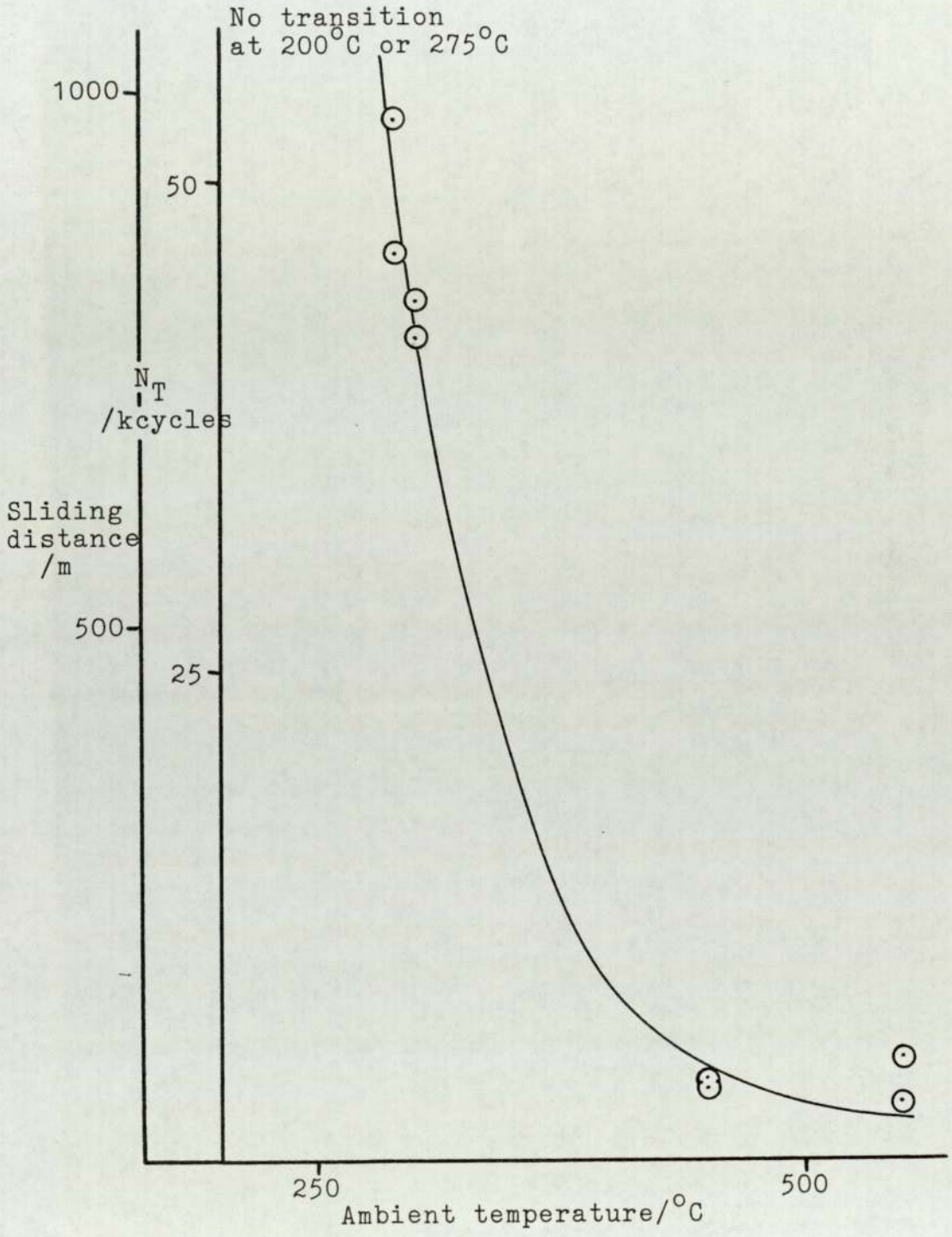

Figure 3.6 The variation of N_T with the ambient temperature

Temperature /°C	N_T /kcycles	K_T /$m^3N^{-1}m^{-1}$	Test duration, N /kcycles
200	No transition	3.51×10^{-13}	179.4
275	No transition	1.76×10^{-13}	709.8
290	46.0±2	8.97×10^{-13}	
290	52.7±1	Not measured	
300	41.7±2	6.70×10^{-13}	
300	43.9±1	9.55×10^{-13}	
450	3.6±0.25	3.63×10^{-13}	
450	4.0±0.25	9.89×10^{-13}	
550	5.0±0.25	6.04×10^{-13}	
550	2.8±0.25	5.43×10^{-13}	

Table 3.7 The variation of N_T and the wear rate with the ambient temperature

The standard conditions were:

stroke	9.2 mm
frequency	2 Hz
load	22 N

in which a transition occurred, there was a sudden decrease in the instantaneous specific wear rate at the transition; in these tests, the average specific wear rate was calculated by assuming that all the weight loss occurred during the severe wear. There was no equilibrium wear in these experiments before the transition to mild wear occurred because the friction never reached the value associated with equilibrium severe wear. As a result, the average wear rate was related to the sliding distance needed to reach the transition. However, for tests without a transition, the wear rate decreased until an equilibrium severe wear rate was obtained; this wear rate was always less than the running-in wear rate.

Results showing the variation of N_T with sliding speed at 450°C, in figure 3.7, show that there was a linear relationship between N_T and sliding speed. The straight line on the graph went through the origin and so represented a line of equal time to reach the wear transition, as shown by the values of T_T in table 3.8.

The results of a similar set of experiments carried out at 300°C are presented in figure 3.8. The results show that there was probably a levelling off or even a decrease in N_T as the sliding speed increased above 110 mms^{-1}; however, the results could have been similar to those obtained at 450°C, but with much more scatter.

A third series of tests was carried out at 290°C with a load of 22 N. This temperature was chosen because although transitions occurred at 300°C, no transition was observed at 275°C; therefore the wear behaviour of the chromium steel must change considerably over this small temperature range. The results, presented in figure 3.9, show that there was markedly different behaviour at this temperature in comparison to the results obtained at 450°C. There was a steady increase in N_T with the sliding speed up to 100 mms^{-1}, but at 110 mms^{-1},

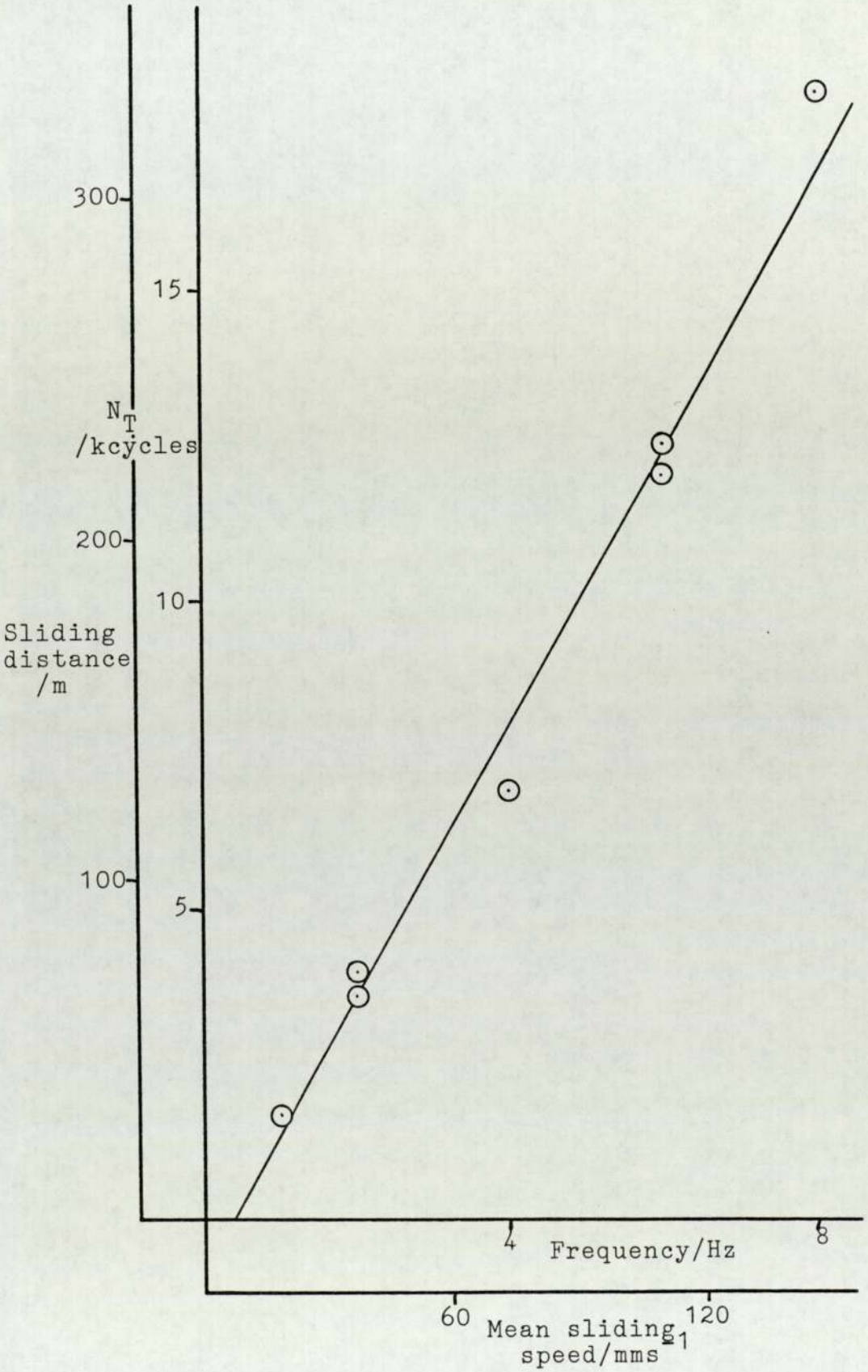

Figure 3.7 The variation of N_T with the sliding speed at 450°C (with a 22N load)

Reciprocating Frequency /Hz	Mean Sliding Speed /mms^{-1}	N_T /kcycles	K_T /$m^3N^{-1}m^{-1}$	T_T /minutes
1	18.4	1.7±0.1	21.1×10^{-13}	28
2	36.8	3.6±0.25	3.63×10^{-13}	30
2	36.8	4.0±0.25	9.89×10^{-13}	33
4	73.6	6.9±0.5	5.73×10^{-13}	29
6	110.4	12.0±0.5	7.83×10^{-13}	33
6	111.1	12.5±0.25	5.97×10^{-13}	35
8	148.2	18.2±0.2	3.78×10^{-13}	38

Table 3.8 The variation of N_T and T_T with the sliding speed at 450°C

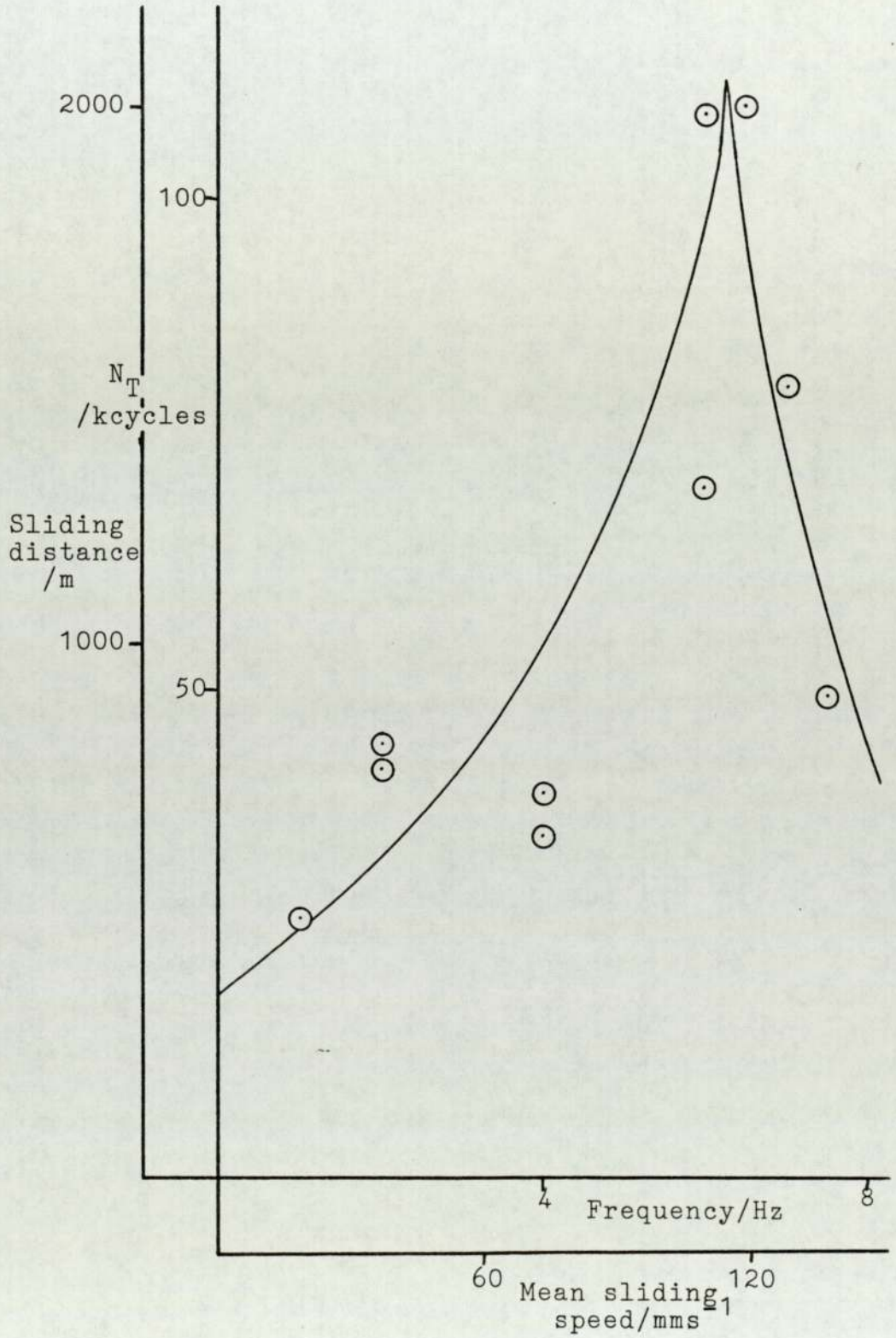

Figure 3.8 The variation of N_T with the sliding speed at 300°C (with a 22N load)

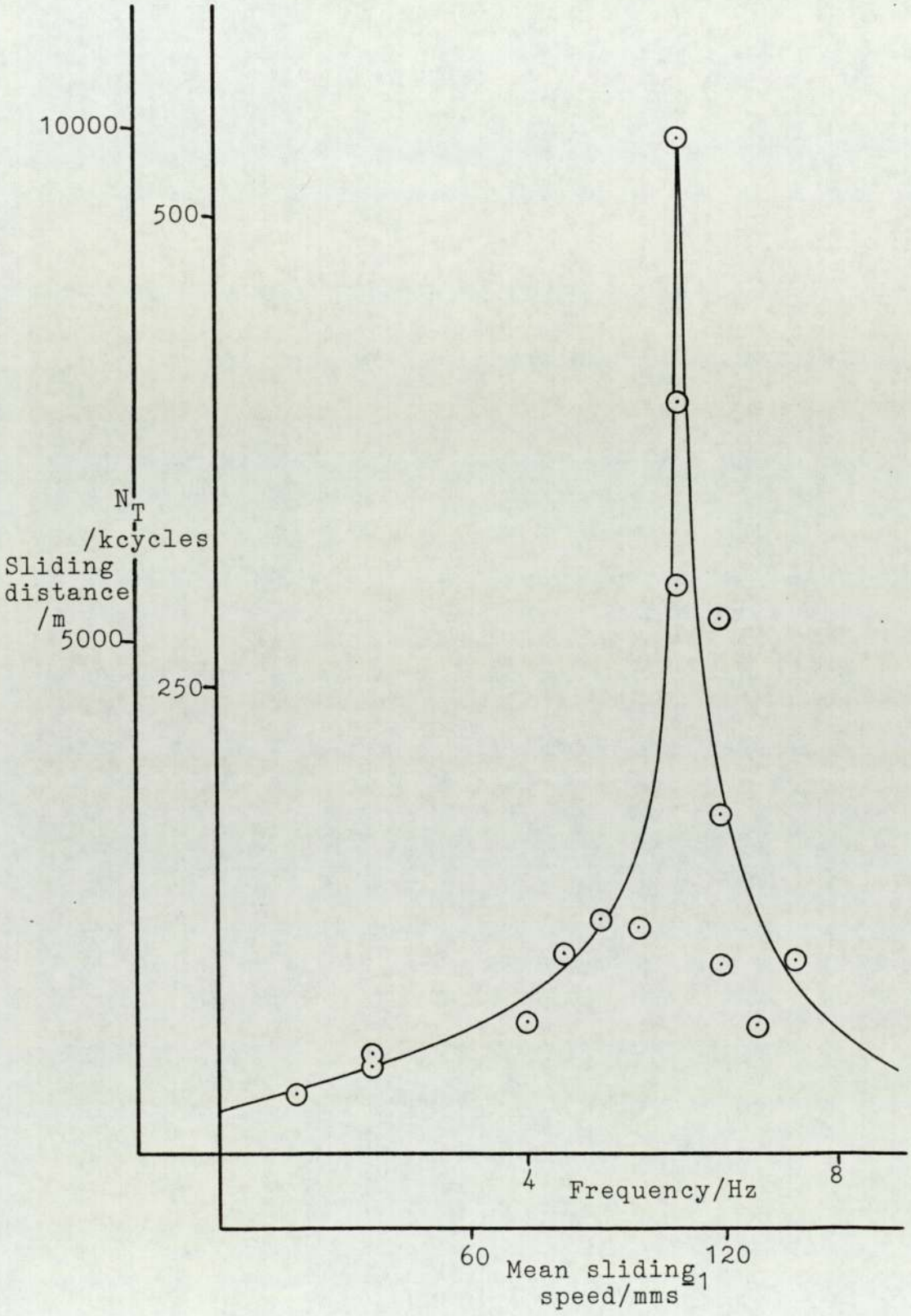

Figure 3.9 The variation of N_T with the sliding speed at 290°C (with a 22N load)

it took a much longer time to reach the wear transition; in one experiment, the transition occurred after about 25 hours of sliding. As the sliding speed increased above 110 mms^{-1}, N_T decreased.

As the wear rate would increase in the set of experiments carried out with a load of approximately double that used in all the previously described reciprocating wear tests, the ambient temperature was increased slightly to increase oxidation. The results at 300°C, but with a load of 41 N, given in figure 3.10, were very similar to those obtained at 290°C with the lower load, but with the peak value of N_T greater (850 kcycles or after roughly 36 hours), and at a higher sliding speed (120 mms^{-1}). It always took longer to obtain a wear transition under a load of 41 N than under 22 N, even when all other experimental conditions were the same.

3.4.4 Severe wear

The specific wear rates for all the experiments so far described are included in table 3.9. In general, the wear rates were higher at slower sliding speeds. However, closer examination of the results showed that the wear rate was more related to N_T than to the sliding speed (figure 3.11). Two experiments carried out with a load of 22 N did not have a wear transition; there results were included because the severe wear rate could still be calculated. The wear was averaged over the length of the test, N cycles, and not the number of cycles to any transition, N_T; it was the former value that was used in figure 3.11. A similar variation in the wear rate with N_T was observed in the tests run with a 41 N load (figure 3.12) even though it usually took many more cycles to reach the wear transition.

In the series of experiments carried out to investigate the variation in the severe wear rate during

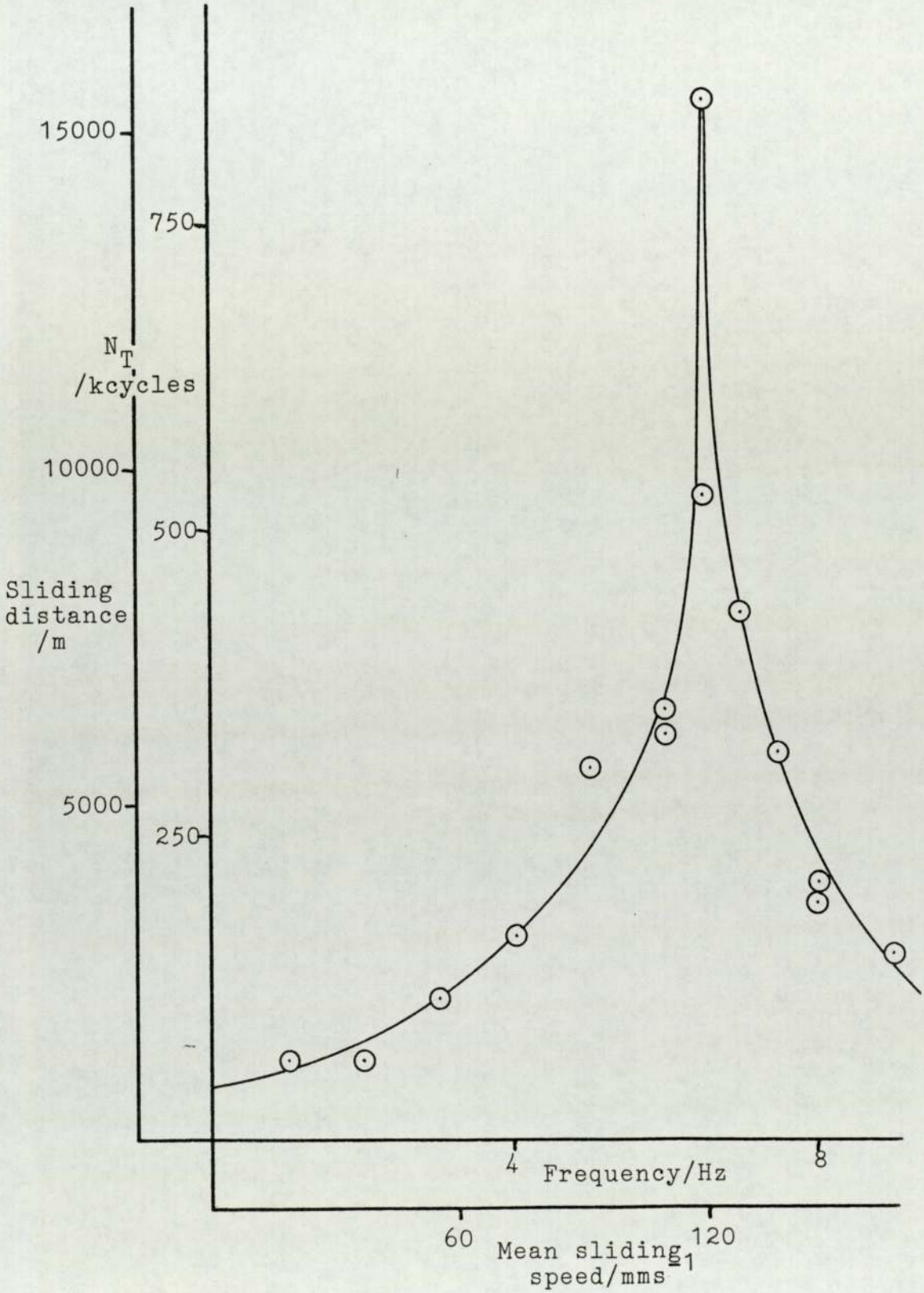

Figure 3.10 The variation of N_T with the sliding speed at 300°C (with a 41N load)

Frequency /Hz	Temperature /°C	Specific Wear Rate /$m^3N^{-1}m^{-1}$
1	290	8.89×10^{-13}
1	300	13.6×10^{-13}
1	300	9.83×10^{-13}
1	450	21.1×10^{-13}
2	290	8.97×10^{-13}
2	300	6.70×10^{-13}
2	300	9.55×10^{-13}
2	300	8.20×10^{-13}
2	450	3.63×10^{-13}
2	450	9.89×10^{-13}
3	300	6.48×10^{-13}
4	290	3.92×10^{-13}
4	300	7.05×10^{-13}
4	300	7.39×10^{-13}
4	300	6.68×10^{-13}
4	450	5.73×10^{-13}
4.5	290	3.13×10^{-13}
5	290	2.49×10^{-13}
5	300	4.49×10^{-13}
5.5	290	2.52×10^{-13}
6	290	1.96×10^{-13}
6	290	1.20×10^{-13}
6	290	2.12×10^{-13}
6	300	7.70×10^{-13}
6	300	3.26×10^{-13}
6	300	5.53×10^{-13}
6	300	4.70×10^{-13}
6	450	7.83×10^{-13}
6	450	5.97×10^{-13}
6.5	290	3.76×10^{-13}
6.5	290	1.40×10^{-13}
6.5	290	1.13×10^{-13}
6.5	300	4.65×10^{-13}
6.5	300	3.26×10^{-13}
6.5	300	3.48×10^{-13}
7	290	4.18×10^{-13}
7	300	4.27×10^{-13}
7	300	3.77×10^{-13}
7.5	290	3.74×10^{-13}
7.5	300	4.48×10^{-13}
7.5	300	3.88×10^{-13}
8	300	4.23×10^{-13}
8	300	5.96×10^{-13}
8	450	3.78×10^{-13}
9	300	4.91×10^{-13}

Table 3.9 The variation of the specific wear rate with the frequency

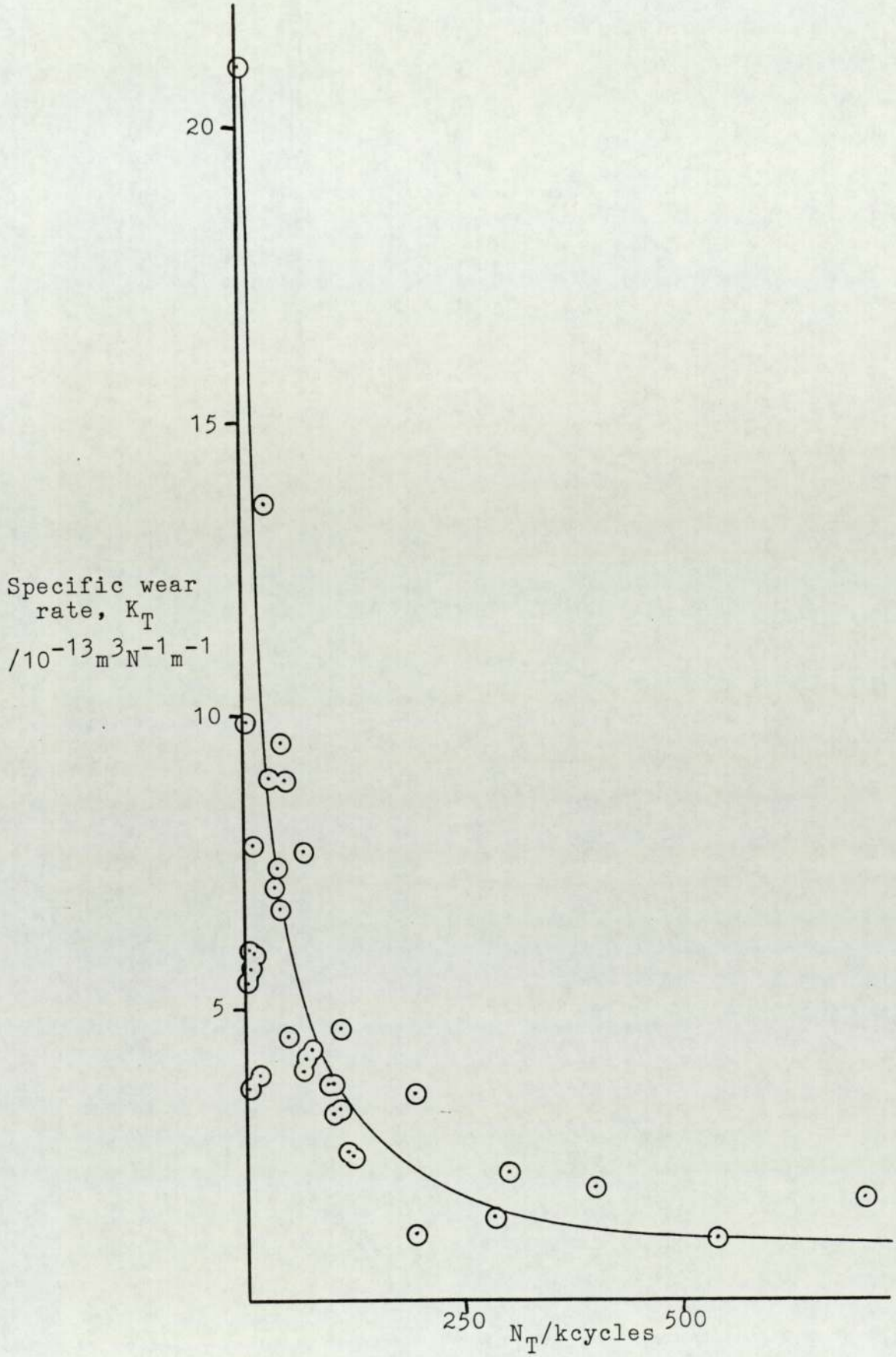

Figure 3.11 The variation of the specific wear rate with N_T (with a 22N load)

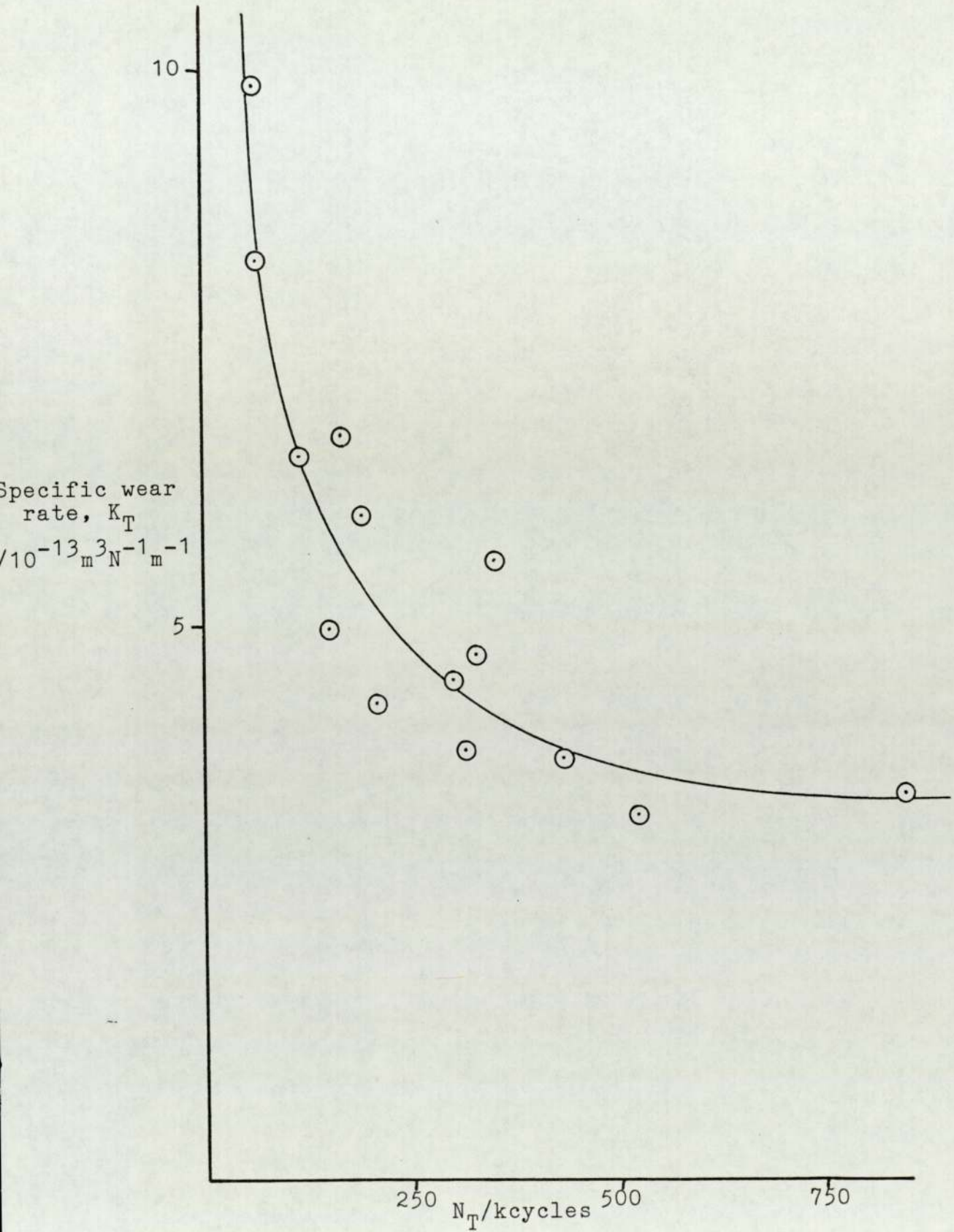

Figure 3.12 The variation of the specific wear rate with N_T (with a 41N load)

a test, the conditions in each experiment were: stroke 9.26 mm, frequency 2 Hz, load 22 N, temperature 290°C. Different tests were stopped after various periods of sliding, and the wear rate determined as usual by weight loss. The results, in table 3.10, showed that the initial wear rate was over ten times greater than the equilibrium severe wear rate.

The weight loss of each specimen, shown in figure 3.13, increased less rapidly as the experiment progressed while the wear rates, in figure 3.14, calculated using the average weight loss of the two specimens, decreased. The flat specimens had a larger weight loss than the pin specimens and, in general, the proportion of the weight loss due to the flat specimens was greater in the shorter tests. This was evidence that material transfer took place from the flat to the pin. In support of this, of the 57 experiments of which the results have been given above, the flat had a greater weight loss in 42 tests, the pin greater weight loss in 14, and the two weight losses were equal in just 1. In 11 of the tests where the pin weight loss exceeded that of the flat, more than 150 kcycles of sliding had been completed. This suggested that transfer took place preferentially from the flat to the pin during the initial running-in period; after this, wear was approximately the same on each specimen and so the volume transferred gradually became an insignificant percentage of the total volume removed.

3.4.5 Mild wear

It was difficult to measure mild wear rates because wear rate was determined by weight loss; most of this was due to the severe running-in period. If it was assumed that the mild wear rate was 100 times less than the severe wear rate, and that it took 5 hours to reach the transition point, then it would have taken 500 hours or about 3 weeks to obtain an equivalent amount of mild

Test duration /kcycles	N_T /kcycles	Weight Losses Pin /mg	Flat /mg	Mean Severe Wear Rate $/m^3N^{-1}m^{-1}$
75.6	46.0	119.62	135.92	8.97×10^{-13}
45.0		138.51	159.75	10.6×10^{-13}
30.0		83.42	99.75	9.79×10^{-13}
30.0		63.11	60.47	6.65×10^{-13}
15.0		47.43	54.04	10.9×10^{-13}
5.0		17.17	24.55	13.4×10^{-13}
1.0		7.14	7.80	24.0×10^{-13}
0.1		0.84	2.91	60.3×10^{-13}

Table 3.10 The weight losses and mean severe wear rate of standard experiments with different test durations

The standard conditions were:

stroke	9.2mm
frequency	2Hz
load	22N
temperature	290°C

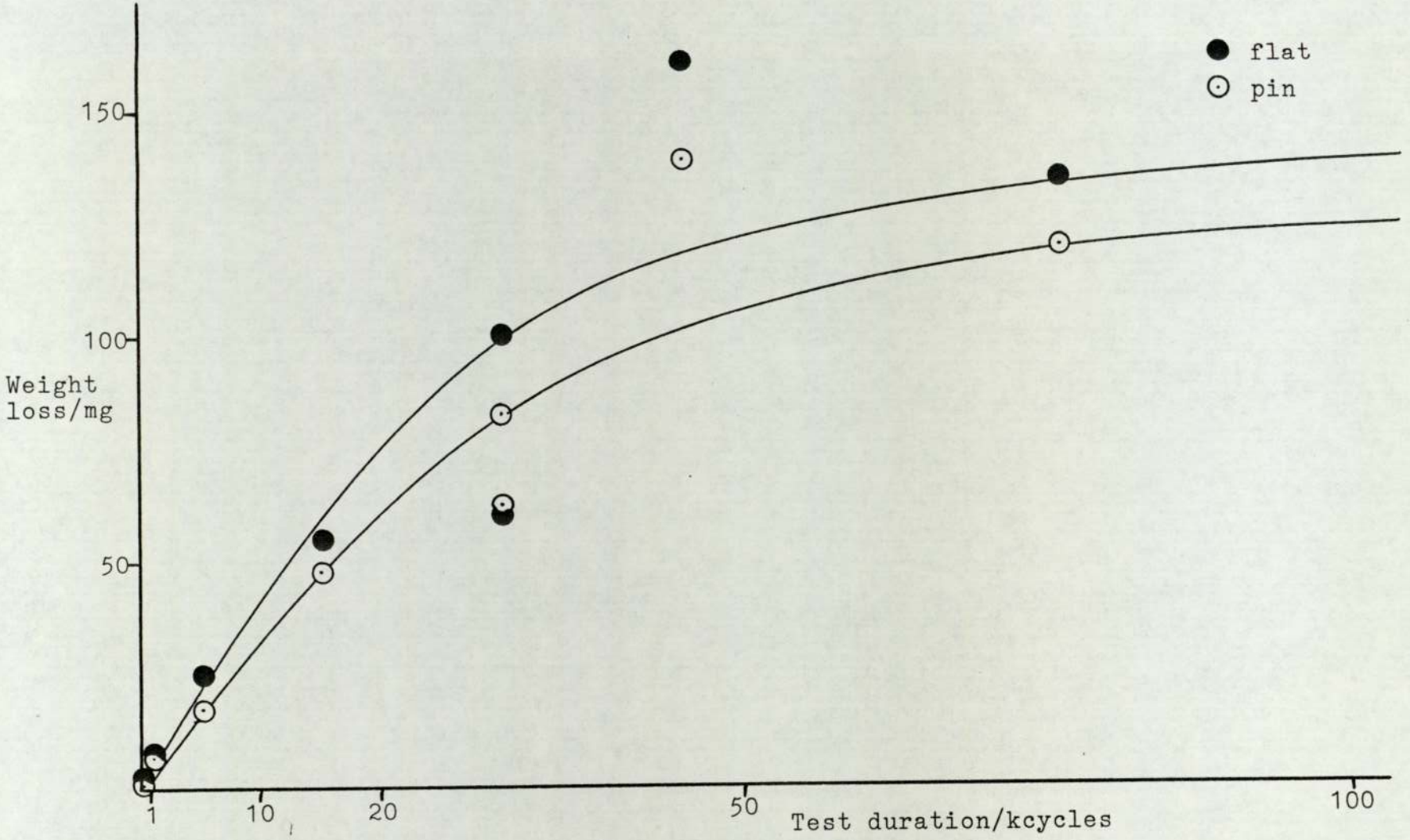

Figure 3.13 The increase in weight loss as an experiment progressed

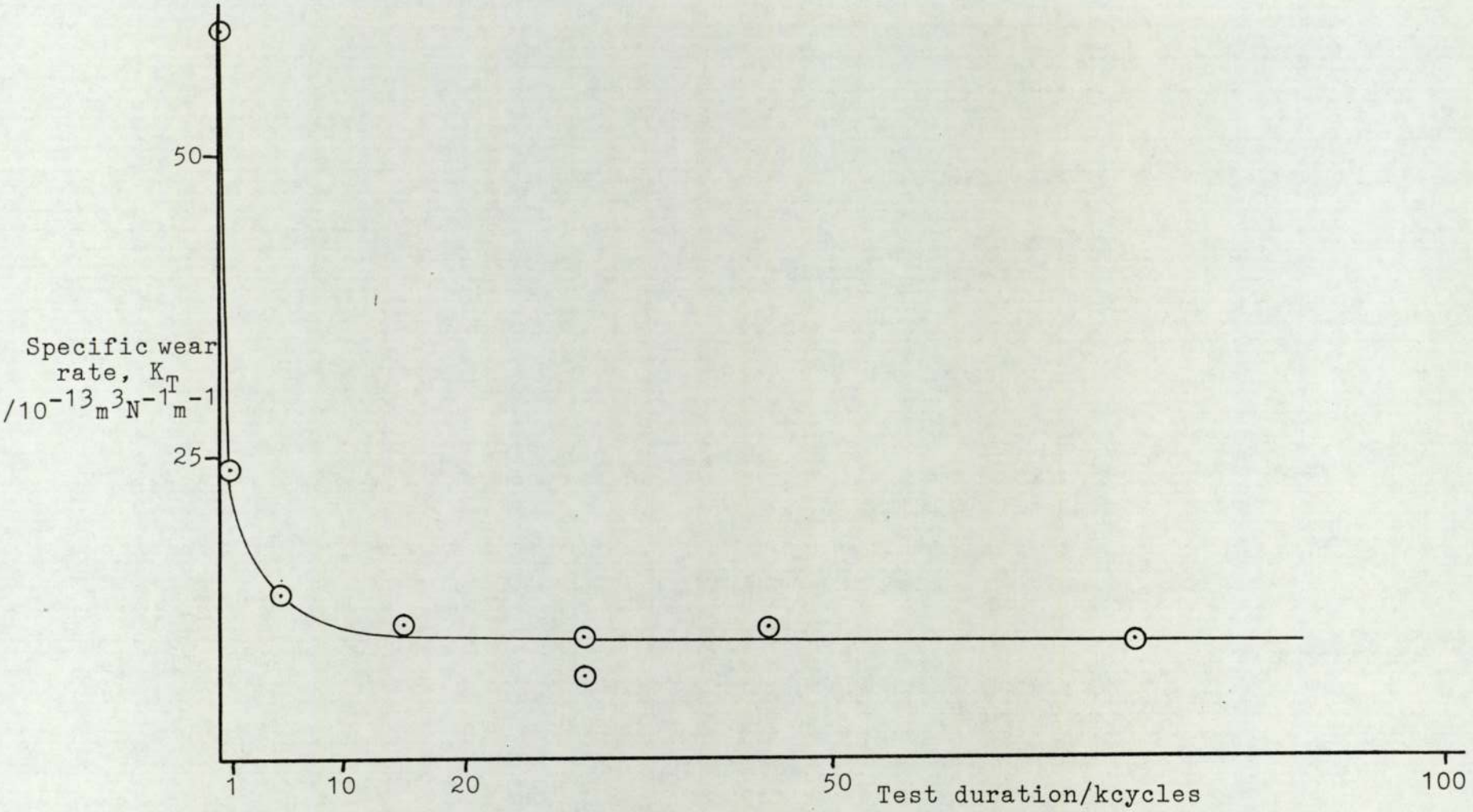

Figure 3.14 The decrease in mean specific wear rate as an experiment progressed

wear debris. Even after this length of time, the effects of the severe running-in wear could not be ignored when considering the much longer mild wear period.

Two attempts were made to calculate the mild wear rate. The first used the results from two experiments, run under similar conditions (sliding speed 37 mms^{-1}, load 22 N, temperature 300°C):-

		test 1	test 2
length of test, N	(kcycles)	64.2	2764.8
N_T	(kcycles)	41.7	47.0
mean weight loss	(mg)	86.56	128.41
period of severe wear	(kcycles)	41.7	47.0
period of mild wear	(kcycles)	22.5	2717.8

The mean weight loss was assumed to be due to two components, one for each wear regime. A pair of simultaneous equations was solved and gave the following average wear rates:-

severe wear rate	$6.68 \times 10^{-13}\ m^3N^{-1}m^{-1}$
mild wear rate	$3.70 \times 10^{-15}\ m^3N^{-1}m^{-1}$

The mild wear rate was also calculated from another experiment that had two separate periods of sliding. The conditions were: sliding speed 37 mms^{-1}, load 22 N, temperature 290°C. The experimental procedure was slightly different from that given in sections 2.3.2 and 2.3.4.

The specimens were prepared in the usual manner and worn for 150 kcycles. After the transition to mild wear occurred at 52.7 kcycles, the specimens were weighed and the test continued for a further 4650 kcycles of sliding; this took about 27 days. Finally, the specimens were weighed, again without cleaning.

As the wear transition occurred in the first run, there was only mild wear during the second sliding period. The weight loss was over 100 mg and therefore could be measured accurately; an error was introduced by not

weighing cleaned specimens, but this could not be done between the first and second runs because it was felt that had the specimens been cleaned, there may have been some severe wear at the start of the second run. Great care was also exercised at the start of the second run to ensure that the wear tracks on the specimens from the first run were parallel. The aim of this experiment was to have a long period of mild wear in the absence of any severe wear.

The mild wear rate calculated from this test was 1.27×10^{-14} $m^3N^{-1}m^{-1}$. This value was likely to be higher than the true mild wear rate because any disturbance of the specimens was likely to initiate a short running-in period. A second estimate of the wear rate was made using the L.V.D.T. monitoring the movement of the loading beam during the mild wear; this gave a mild wear rate of 4.87×10^{-15} $m^3N^{-1}m^{-1}$.

In conclusion, the mild wear rate was about 5×10^{-15} $m^3N^{-1}m^{-1}$; this compared with an equilibrium severe wear rate of 200×10^{-15} $m^3N^{-1}m^{-1}$ and an initial severe wear rate of 6000×10^{-15} $m^3N^{-1}m^{-1}$. Due to the difficulties in calculating the mild wear rates, this result only implied that the wear rate was between 10^{-16} and 10^{-15} $m^3N^{-1}m^{-1}$. Calculations concerning the severe wear rates were more accurate due to the larger weight losses and the fact that the specimens need not be disturbed during each experiment; the errors were about $\pm 10\%$.

3.4.6 Running-in times

The variation in the number of cycles required to reach the wear transition, N_T, has already been described in section 3.4.3. It was stated that the running-in time or time to reach the wear transition, T_T, was not of importance except for the experiments carried out at 450°C (table 3.8).

However, the running-in times were a convenient way of comparing the results of the two types of sliding. In unidirectional sliding experiments, the pin slid 317 mm for each revolution of the disc; this was equivalent to about 17 reciprocating cycles. Table 3.11 presents the running-in times of three series of experiments. In all cases, the running-in times were longest at sliding speeds of about 110 mms^{-1}. The times were shorter for the unidirectional sliding experiments because the carbon dioxide atmosphere contained a greater percentage of oxygen. The variation in running-in periods for the reciprocating tests at 290°C between 250 minutes and 1500 minutes contrasted very strongly with the near-constant times obtained from experiments carried out at 450°C (table 3.8).

3.4.7 Dwell tests

Seven dwell tests were carried out. Six of these experiments were on reciprocating sliding; only one was carried out using the unidirectional wear test machine because the carbon dioxide atmosphere was not as pure and could not be guaranteed to be of the purity necessary for an experiment of several days. Four tests were of a standard form in which specimens were worn for about 20 minutes and then left stationary for several days before being worn again. The conditions and results are given below along with the results obtained from normal experiments carried out without dwell:-

test 1)	experimental conditions:	reciprocating sliding	
		sliding speed	110 mms^{-1}
		load	22 N
		temperature	290 °C
	dwell conditions:	run period	4 kcycles
		dwell period	24 hours
	result:	no transition in 80 kcycles	
	result expected without dwell:	N_T	about 450 kcycles

Approximate Sliding Speed	Unidirectional Sliding	Reciprocating Sliding	
	22N / 266°C	22N / 290°C	41N / 300°C
	Running-in time	Running-in time	Running-in time
/mms^{-1}	/minutes	/minutes	/minutes
18.5	57	517	1042
36.9		383/439	551
55.4	140		639
73.8		238	692
83.1		384	
92.3		417	1007
101.5		364	
110.8	530/338	1111/1500/833	972/917
120.0		256/731/462	1346/2179
129.2	98/245	167	1024
138.5		229	700
147.7	108/225		438/396
166.1			280

Table 3.11 The running-in times of some unidirectional and reciprocating sliding experiments

test 2)	experimental conditions:	as test 1	
	dwell conditions:	run period	10 kcycles
		dwell period	96 hours
	result:	N_T	31 ± 1 kcycles
	result expected without dwell:	N_T	about 450 kcycles
test 3)	experimental conditions:	reciprocating sliding	
		sliding speed	120 mms^{-1}
		load	41 N
		temperature	300 °C
	dwell conditions:	run period	10 kcycles
		dwell period	96 hours
	result:	N_T	50 kcycles
	result expected without dwell:	N_T	about 700 kcycles
test 4)	experimental conditions:	unidirectional sliding	
		sliding speed	118.5 mms^{-1}
		load	22 N
		temperature	266 °C
	dwell conditions:	run period	584 disc revolutions (equivalent to 10 kcycles of reciprocating sliding
		dwell period	96 hours
	result:	running-in period	47 minutes (of sliding)
		running-in period	about 400 minutes

Tests 2, 3 and 4 show that introducing dwell reduced the running-in time by a factor of about 10 or more. The static oxidation which took place during each dwell period must have been important; however, the result of test 1 suggested that the ratio of sliding distance to dwell time was also important if the effect of static oxidation was to be significant.

Three other reciprocating dwell tests were carried out to study the weight losses and gains during some of

the sliding or dwell periods, and to investigate the effect of a prolonged dwell period before any sliding. The experimental conditions and results are given below:-

test 2) in the 5th dwell period, the weight increases for each specimen were:-

flat	0.07 mg
pin	0.19 mg

in the 6th run period, the weight losses were:-

flat	0.83 mg
pin	0.76 mg

test 5) experimental conditions: as test 3

dwell conditions: run period 10 kcycles
dwell period 96 hours

in the 1st run period, the weight losses were:-

flat	57.47 mg
pin	54.76 mg

in the 1st dwell period, the weight gains were:-

flat	0.04 mg
pin	0.08 mg

test 6) experimental conditions: as test 1

dwell conditions: 750 hours before a normal experiment

result: N_T 300 kcycles
result expected without dwell: N_T about 450 kcycles

test 7) experimental conditions: reciprocating sliding

sliding speed	110 mms^{-1}
load	22 N
temperature	450 ^{o}C

dwell conditions: the initial run period was 2 kcycles, followed by a 4 hour dwell period. The test was then run to completion.

result: N_T 12.5 kcycles
result expected without dwell: N_T about 12.0 kcycles

The weight change data produced from tests 2 and 5 showed that even in mild wear, more material was lost during 25 minutes of wear than was gained during 4 days of static oxidation. This implied that dwell must affect parts of the specimen not worn away; it was thought that dwell periods increased the oxide thickness on the non-load-bearing areas so that by the time that they became load-bearing asperities, the oxide thickness was greater, and mild wear more likely. In this way, although the oxidation weight gain was only 0.06 mg, and over 50 mg of material was lost in the first sliding period, the remaining oxidised asperities could still assist the onset of mild wear.

Test 6 showed that dwell periods in the absence of sliding had very little effect upon N_T. This was due to the oxidation taking place only upon the surfaces of an unworn specimen; these surfaces were greatly disturbed and worn away almost immediately once the sliding started, and so the increased surface oxide due to the dwell period was quickly removed.

Finally, test 7 was carried out at 450°C, a temperature at which the time to transition was fairly constant. The test showed that introducing dwell did not reduce the sliding distance prior to the transition in tests run at temperatures when the experimental conditions did not affect T_T.

The full significance of the results from these seven tests will be more apparent in Chapter 4.

3.5 X-ray diffraction

3.5.1 Introduction

The debris from selected slow speed experiments was analysed by X-ray diffraction. When trying to determine the composition of the mild wear debris from experiments run in carbon dioxide, there was so much severe wear debris present that it was often not possible to identify

any oxide. Glancing angle X-ray diffraction was carried out on a few mild wear specimens to identify the oxide present on the worn surfaces. Unfortunately, the oxide layer on the flat specimens after reciprocating mild wear was not uniform and so it was still only possible to identify the majority oxide. A thorough analysis of the mild wear debris was only possible for the experiment in which the test was stopped after the wear transition and a separate collection made of the mild wear debris. In this test, the onset of mild wear was at 52.7 kcycles, and the debris was collected after 150 kcycles; the conditions were: sliding speed 37 mms^{-1}, load 22 N, temperature 290°C. A more thorough examination could not be made to investigate whether the oxides occurring in the mild wear debris varied with the experimental conditions.

The X-ray diffraction lines were assigned using the A.S.T.M. index (151, 152). The rhombohedral oxide is a solid solution of α-Fe_2O_3 and Cr_2O_3, and is designated $(Fe,Cr)_2O_3$. The two oxides are completely soluble within each other. The other oxide identified in this work was the spinel and this also can have variable composition; its formula is $FeFe_{(2-x)}Cr_xO_4$ where x is between 0 and 2.

Wustite or FeO was not discovered in any debris.

3.5.2 Unidirectional wear

Tables 3.12 and 3.13 show the composition of the debris obtained from two experiments, one run in air and the other in carbon dioxide. The test carried out in air lasted 1415 minutes; there was severe running-in wear for the first 36 minutes. The debris analysed was collected over several hours towards the end of the experiment. Both ferrite and the rhombohedral oxide were present at a time when mild wear was well established; this was a a feature of all the slow speed experiments run in either atmosphere.

Intensity	2θ	d_{hkl} / Å	Possible Identification	
faint	28.0	3.669		α-$(Fe,Cr)_2O_3$
**	39.75	2.699		α-$(Fe,Cr)_2O_3$
*	42.75	2.513		α-$(Fe,Cr)_2O_3$
	49.5	2.2015		α-$(Fe,Cr)_2O_3$
***	53.5	2.024	α-Fe	
v. faint	59.5	1.840		α-$(Fe,Cr)_2O_3$
	65.5	1.696		α-$(Fe,Cr)_2O_3$
v. faint	75.5	1.488		α-$(Fe,Cr)_2O_3$
v. faint	77.5	1.454	α-Fe	α-$(Fe,Cr)_2O_3$
	101.5	1.173	α-Fe	

Table 3.12 Powder diffraction pattern of the debris from a unidirectional sliding experiment run in air at 200°C (Test 16 in table 3.3)

Intensity	2θ	d_{hkl} / Å	Possible Identification
**	52.5	2.024	α-Fe
faint	77.5	1.435	α-Fe
*	99.75	1.173	α-Fe
faint	124.0	1.015	α-Fe

Table 3.13 Powder diffraction pattern of the debris from a unidirectional sliding experiment run in carbon dioxide at 250°C (Test 8 in table 3.5)

There was severe wear for all 2468 minutes of the experiment run in carbon dioxide. Similar X-ray diffraction photographs were obtained from mild wear experiments run in the same atmosphere. This was because the severe wear rate was about 50 times greater than the mild wear rate, and as it was not possible to carry out experiments for longer than about 2500 minutes due to the crude assembly of the specimen chamber, when the running-in times were greater than 250 minutes, the debris produced during this period always exceeded the amount of mild wear debris produced during the remainder of the experiment.

3.5.3 Reciprocating wear

X-ray diffraction photographs were taken of several samples of debris from different reciprocating experiments. In all cases, only lines that were due to metallic debris were observed; this was because of the much higher severe wear rate.

The debris in one sample came from an experiment run for 126 kcycles when the transition to mild wear occurred after just 80 kcycles; the average wear rate for the test was 2.71×10^{-13} $m^3N^{-1}m^{-1}$. Using the mild wear rate calculated in section 3.4.5 (5×10^{-15} $m^3N^{-1}m^{-1}$), the ratio of severe to mild wear was about 54:1, while the ratio of severe to mild sliding distance was 80:46. From this, it was calculated that 99% of the debris was due to running-in and just 1% to mild wear. It is recognised that X-ray diffraction does not generally detect compounds that form less than a few per cent of the total sample (153).

Glancing angle X-ray diffraction was carried out to try and obviate this problem. Unfortunately, as the surfaces of the flat specimens were disturbed a great deal during running-in, the oxide layer necessary for mild wear was not sufficiently uniform to produce very

informative X-ray photographs. On several photographs, all the strong lines were due to the ferrite, while just one faint line due to the rhombohedral oxide was observed.

In one experiment, carried out to determine the mild wear rate, described in section 3.4.5, the mild wear debris was collected separately and so was able to be analysed in the absence of the metallic debris produced during running-in. X-ray diffraction was carried out on both the running-in and mild wear debris, and the results presented in tables 3.14 and 3.15. It was found that the mild wear debris consisted mainly of the rhombohedral oxide, but that some of the spinel oxide was also present. For once, the ferrite line at 52.5° was not the strongest line present. Had ferrite been produced during mild wear, it was possible that a significant proportion of it may have oxidised during the 27 day test.

The technique of X-ray diffraction has shown that the mild wear debris was mainly the rhombohedral oxide, α-$(Fe,Cr)_2O_3$, with small amounts of the spinel oxide, $FeFe_{(2-x)}Cr_xO_4$; some ferrite, α-Fe, was also present. Debris of similar composition could have been caused by the metallic debris oxidising to the rhombohedral oxide during the test; however, this would not explain the oxide observed on the worn surfaces from glancing angle X-ray diffraction photographs.

3.6 Surface profilimetry

The initial roughness of the discs used in this work was about 0.32 μm centre line average (c.l.a.); the reciprocating flat specimens had a roughness of about 0.17 μm c.l.a..

This technique was not very informative about worn specimen surfaces. It was not possible to measure the roughness of the pins or flat specimens due to their geometry. Analysis was, therefore, restricted to the

Intensity	2θ	d_{hkl} / Å	Possible Identification
***	54.5	2.024	α-Fe
*	79.0	1.435	α-Fe
**	101.5	1.173	α-Fe
*	125.0	1.015	α-Fe

Table 3.14 Powder diffraction pattern of the running-in debris from a reciprocating sliding experiment run at 37 mms^{-1} and 290°C

Intensity	2θ	d_{hkl} / Å	Possible Identification	
*	28.5	3.669	α-$(Fe,Cr)_2O_3$	
faint	35.25	2.956		$FeFe_{(2-x)}Cr_xO_4$
***	38.75	2.699	α-$(Fe,Cr)_2O_3$	
***	41.75	2.513	α-$(Fe,Cr)_2O_3$	$FeFe_{(2-x)}Cr_xO_4$
*	48.0	2.2015	α-$(Fe,Cr)_2O_3$	
faint	50.5	2.089		$FeFe_{(2-x)}Cr_xO_4$
*	52.5	2.024	α-Fe	
*	58.25	1.840	α-$(Fe,Cr)_2O_3$	
**	64.0	1.696	α-$(Fe,Cr)_2O_3$	$FeFe_{(2-x)}Cr_xO_4$
v. faint	67.5	1.601	α-$(Fe,Cr)_2O_3$	$FeFe_{(2-x)}Cr_xO_4$
*	74.25	1.488	α-$(Fe,Cr)_2O_3$	$FeFe_{(2-x)}Cr_xO_4$
*	76.25	1.454	α-Fe α-$(Fe,Cr)_2O_3$	
faint	84.25	1.351	α-$(Fe,Cr)_2O_3$	
v. faint	91.0	1.258	α-$(Fe,Cr)_2O_3$	
faint	99.5	1.173	α-Fe	
v. faint	104.0	1.142	α-$(Fe,Cr)_2O_3$	
v. faint	108.5	1.103	α-$(Fe,Cr)_2O_3$	
v. faint	116.0	1.056	α-$(Fe,Cr)_2O_3$	

Table 3.15 Powder diffraction pattern of the mild wear debris from a reciprocating sliding experiment run at 37 mms^{-1} and 290°C

discs. All discs were too rough for the talysurf to measure the c.l.a. quantitively and the majority of discs were also too rough for the stylus to produce a graphical output that remained on the chart recorder, even at the lowest magnification. From these limits, the centre line average was greater than 5 μm, and the peak-to-trough distance on the wear track was greater than 5×10^{-5} m.

Graphical output was restricted to the mild wear specimens with short running-in periods; two such traces are included (figures 3.15 and 3.16).

3.7 Microhardness measurements

3.7.1 Surface measurements

Microhardness measurements were made on many reciprocating and unidirectional specimens. The surface hardness of each specimen fell into one of four ranges of values:

1) The hardness of an unworn unidirectional pin was 250 ± 8 VPN (2.7 GPa) and of an unworn flat specimen was 279 ± 10 VPN (2.9 GPa). These values were based upon approximately twenty measurements made on five different specimens. The two types of specimen used on each of the wear test machines had the same composition; any small variation in the microhardness was due to the machining necessary to produce the specimens.

2) The hardness of a surface in the severe wear regime sliding at 2.0 ms^{-1} was 467 ± 72 VPN (4.9 GPa). This was based upon more than twenty readings made on three specimens.

Severe wear specimens worn at the slow speed had a mean microhardness of 593 ± 117 VPN (6.2 PGa). The standard deviation was greater because the surfaces were much rougher, and it was harder to make accurate hardness measurements. It was likely that the surface was not significantly harder than the severe wear surfaces obtained

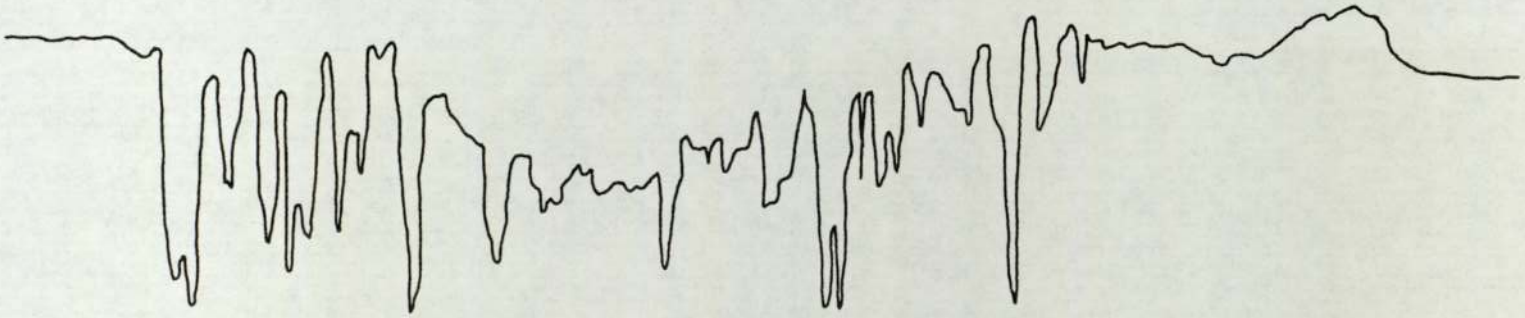

Experimental conditions:

unidirectional sliding	
sliding speed	17.8mms^{-1}
load	22 N
temperature	100 ^{o}C

10^{-3}m

10^{-5}m

Figure 3.15 The surface profile of a mild wear specimen worn in air

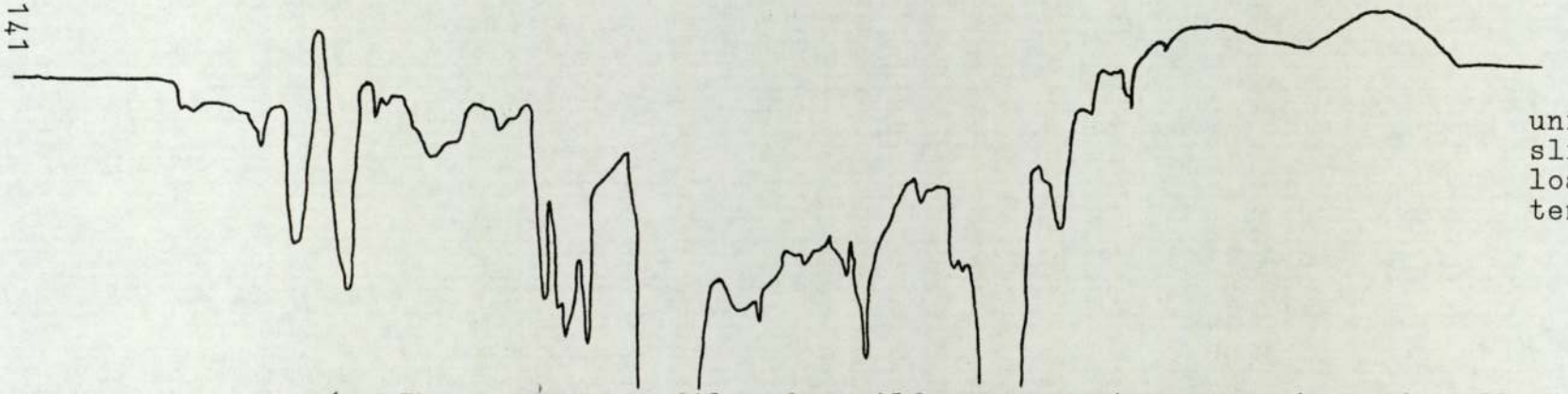

unidirectional sliding	
sliding speed	19.7mms^{-1}
load	22 N
temperature	273 ^{o}C

Figure 3.16 The surface profile of a mild wear specimen worn in carbon dioxide

from the high speed sliding experiments.

3) The hardness of surfaces subject to mild wear at low or high speeds was 769±101 VPN (8.1 GPa). This was based on about forty measurements on five specimens. The microhardness of a reciprocating specimen that did not undergo a wear transition was 753±52 VPN (7.9 GPa). It was probable that although the two surfaces had similar hardness values, the nature of each surface was different because the unidirectional specimens had an oxide layer whereas the reciprocating specimens had a hardened metallic layer only.

4) The average surface microhardness of mild wear reciprocating flat specimens was 1189±162 VPN (12.1 GPa). This was calculated from over forty measurements on nine specimens. These values were hard to obtain because the surfaces were very dark and consequently the indentation could not be measured accurately.

3.7.2 Measurements from taper sections

Two series of taper sections were made. The first was prepared from the set of specimens worn to investigate the variation in severe wear rate during an experiment (table 3.10). Taper sections were made as described in section 2.6.3.

The microhardness was measured at several depths. Typical variations of hardness with depth are shown in figure 3.17. The maximum hardness on different specimens varied from 332 VPN to 898 VPN (3.5 GPa to 9.5 GPa); this variation was due to the differing nature of the surface at the point from which the microhardness measurements were made. The higher values were due to an oxide, but the lower values did not imply a total absence of oxide, but that its thickness was not sufficient for the hardness to be measured on the taper

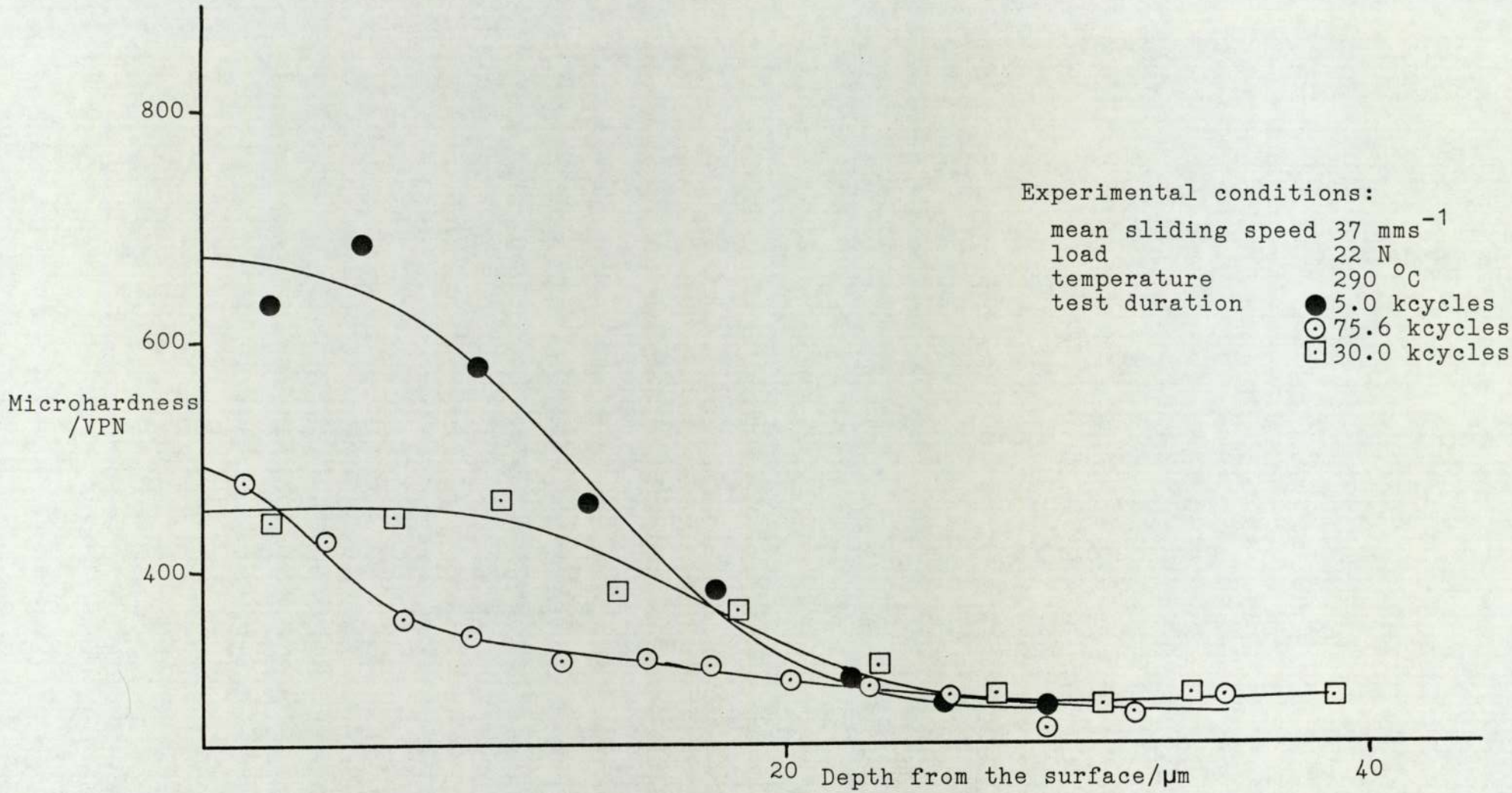

Figure 3.17 The variation of the microhardness with depth on reciprocating flat specimens

section; surface hardnesses were easier to determine on specimens that had not been sectioned.

The depth of the hardened layer did not vary significantly as the test duration or sliding distance increased (figure 3.18), with the average depth about 35 ± 15 μm. The hardened layer was already this deep after 1000 cycles of sliding; it was also probable that this layer was formed within 100 cycles, but the wear scar after such a brief test was very small, and accurate microhardness values were difficult to obtain.

Figure 3.19 presents the results from a similar series of tests, carried out with a larger load, which showed very different behaviour from those obtained with a 22 N load. The depth of the hardened layer increased gradually over the first 500 kcycles to about 75 μm, but was still this depth after 1667.3 kcycles. The maximum values of the hardness (1320 VPN or 14.1 GPa) were also considerably higher than similar measurements obtained from the low load specimens. The hardness values of 1000 VPN (10.6 GPa) and above were due to the presence of oxide at the point on the surface from which distances were measured into the taper section; the absence of this oxide did not appear to affect the depth of the hardened layer. There was never sufficient oxide, however, to produce mild wear.

3.8 Scanning electron microscopy

3.8.1 Reciprocating sliding specimens

Scanning electron microscopy was carried out on many flat specimens. Loose surface debris was removed before examination as the specimens were cleaned due to the wear rate being determined by weight loss.

General features of the surfaces are shown in figure 3.20. The severe and mild wear specimens were worn under similar sliding conditions. Figure 3.20(a) showed the surface of a specimen with mild wear which had

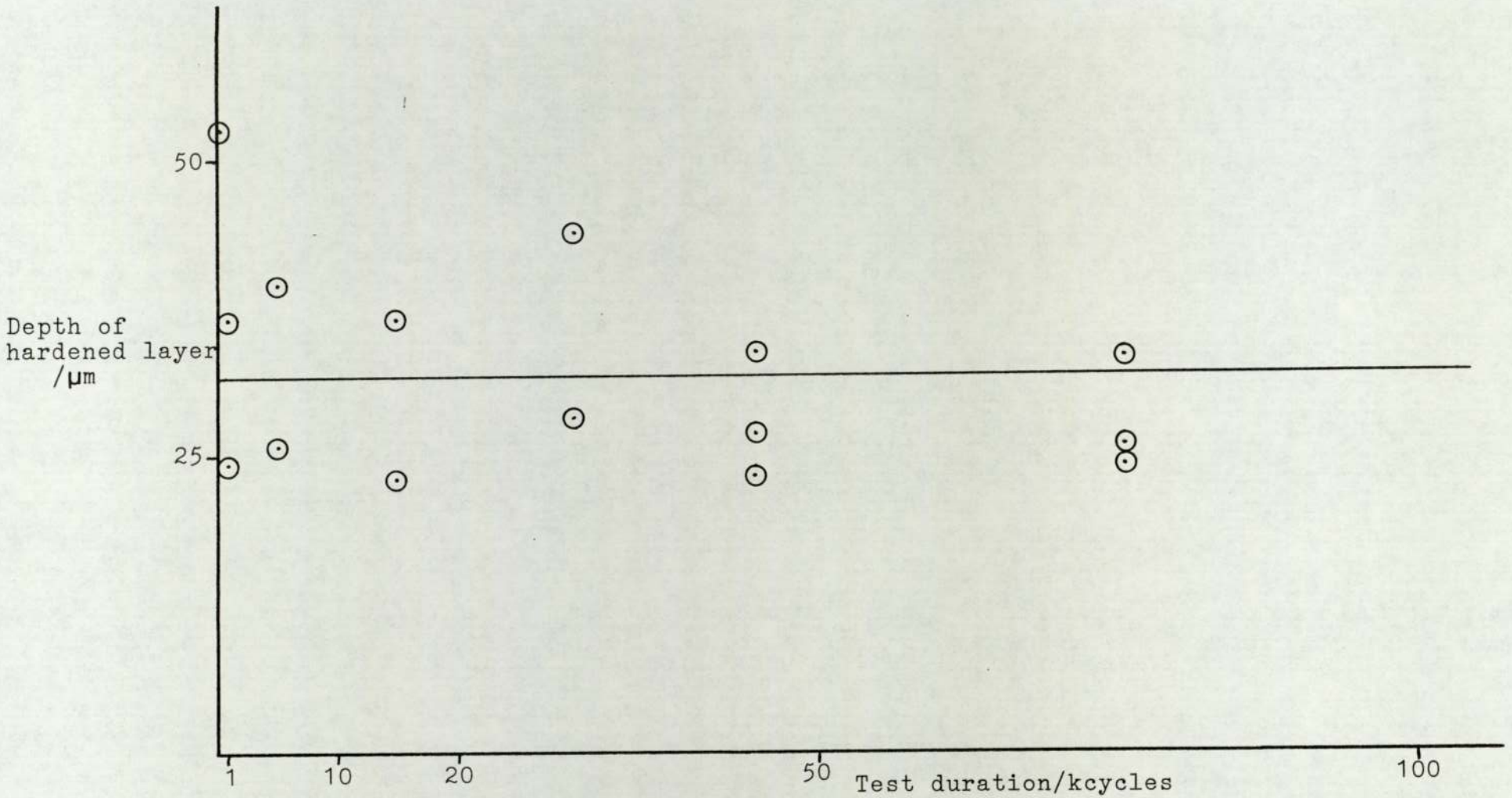

Figure 3.18 The variation of the depth of the hardened layer with sliding distance (with a 22N load)

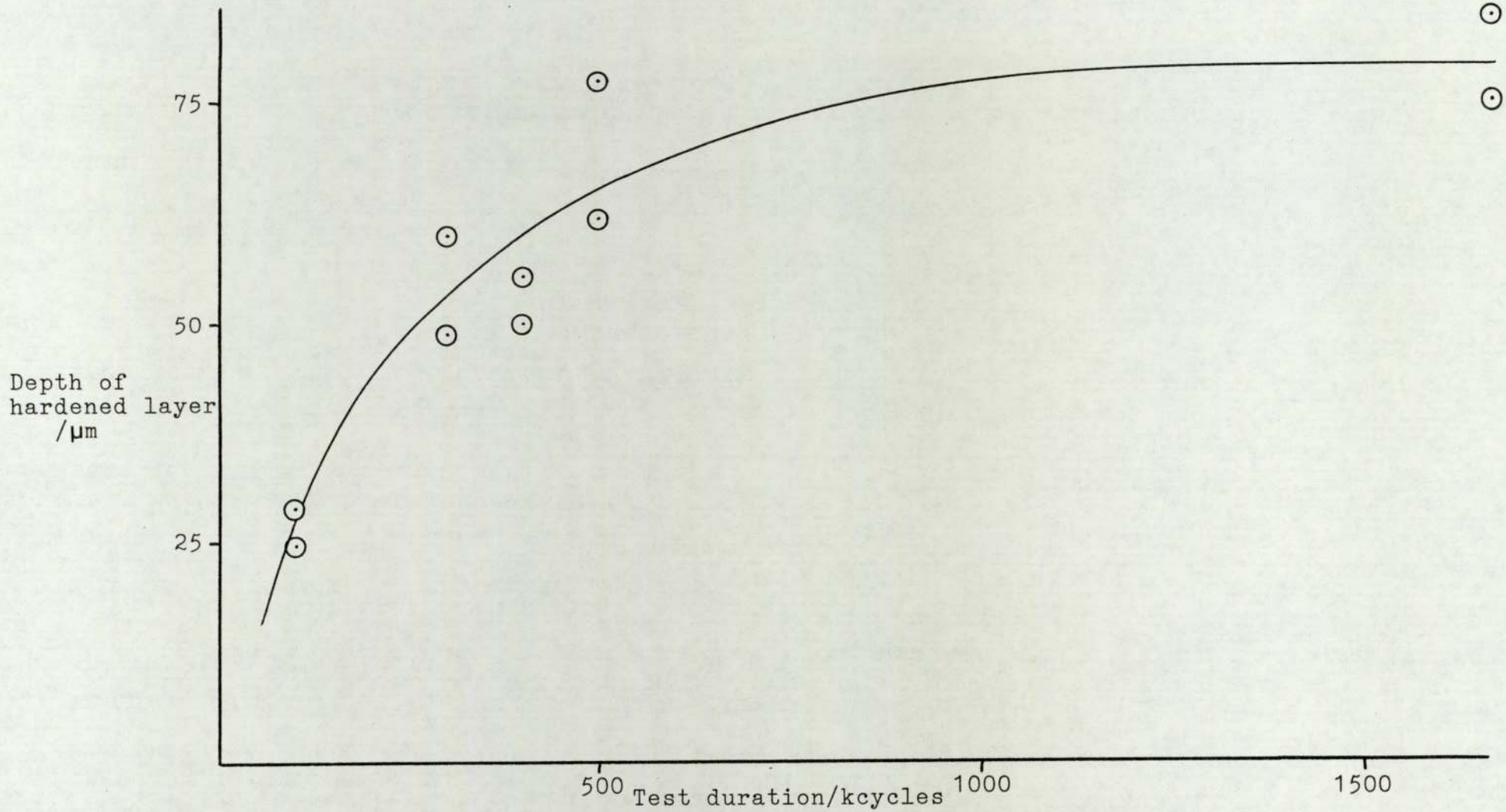

Figure 3.19 The variation of the depth of the hardened layer with sliding distance (with a 41N load)

Figure 3.20 Scanning electron micrographs of flat specimens

a) mild wear, experimental conditions: sliding speed 36.8 mms^{-1}, load 22 N, temperature 290°C, test duration 75.6 kcycles;
b) severe wear, experimental conditions: as (a), test duration 15.0 kcycles.

Figure 3.21 Scanning electron micrographs of debris

a) removed debris;
b) the edge of a particle of removed debris;
c) surface debris.

Figure 3.22 Scanning electron micrographs of oxide plateaux

a) experimental conditions: sliding speed 120.4 mms^{-1}, load 41 N, temperature 300°C;
b) experimental conditions: sliding speed 36.8 mms^{-1}, load 22 N, temperature 300°C.

Figure 3.23 Scanning electron micrographs of flat specimens

Experimental conditions: sliding speed 120.4 mms^{-1}, load 41 N, temperature 300°C.
a) smeared out transferred particle;
b) oxide plateau;
c) detail of oxide edge in centre of (b).

Figure 3.24 Scanning electron micrographs of an oxide plateau on a flat specimen

Experimental conditions: sliding speed 18.4 mms^{-1}, load 22 N, temperature 290°C,
a) the specimen surface;
b) chromium distribution in (a);
c) iron distribution in (a).

Figure 3.25 Scanning electron micrographs of a flat taper section

Experimental conditions: sliding speed 18.4 mms^{-1}, load 22 N, temperature 290°C,
a) the taper section surface;
b) chromium distribution in (a);
c) iron distribution in (a).

Figures 3.20 to 3.25 Reciprocating sliding flat specimens

a

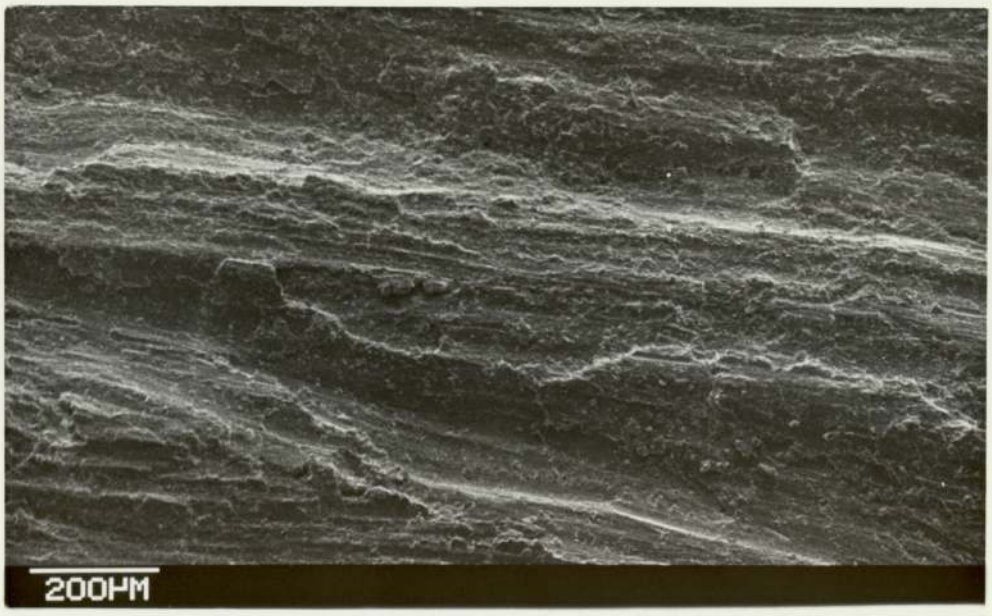

b

Figure 3.20

a

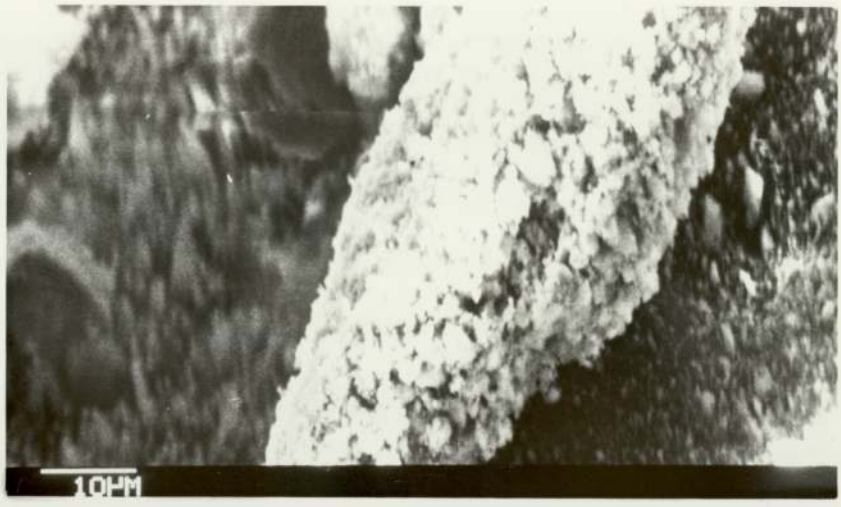

b

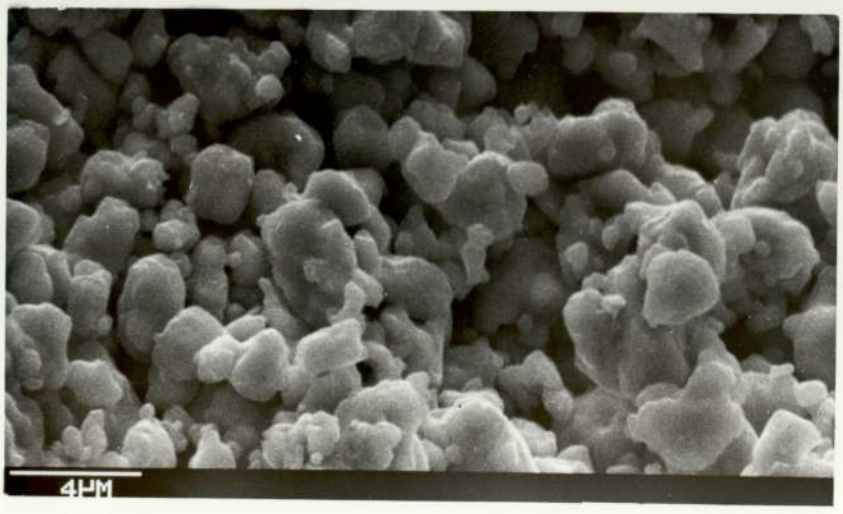

c

Figure 3.21

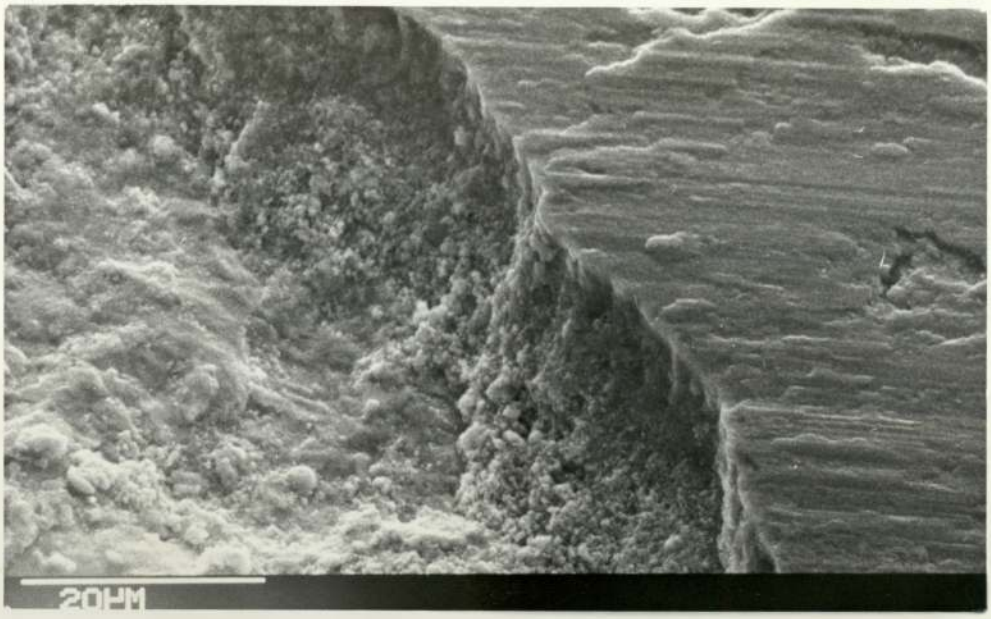

a

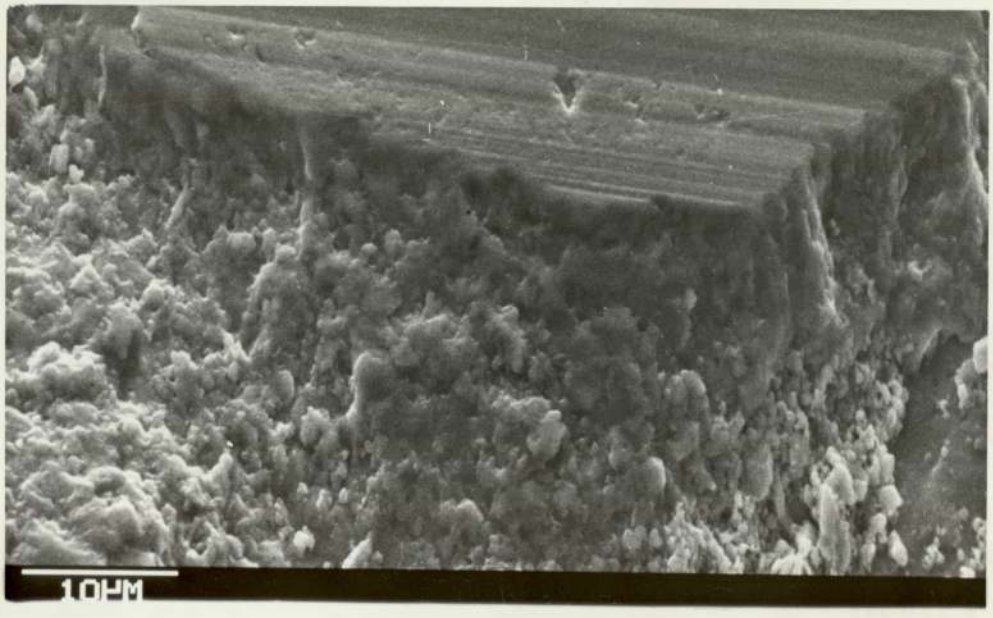

b

Figure 3.22

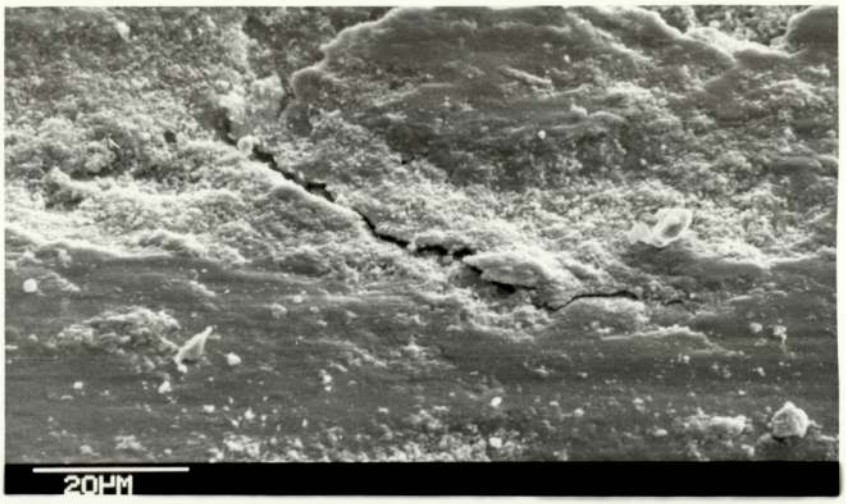

a

b

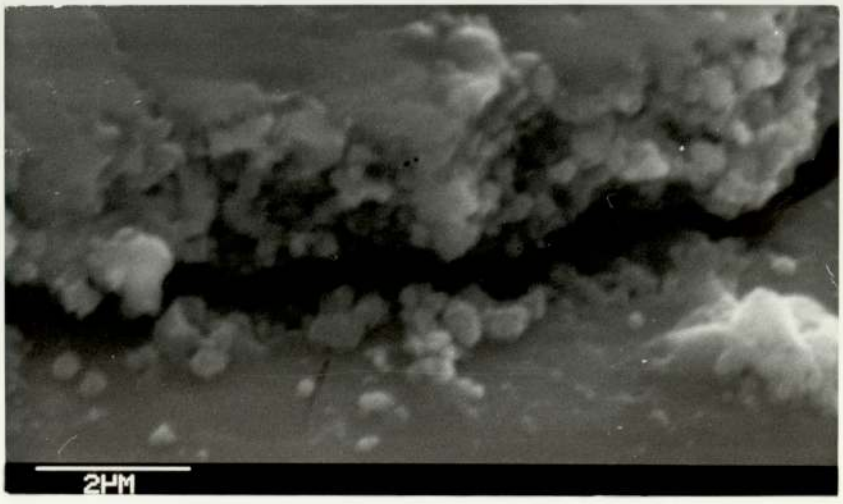

c

Figure 3.23

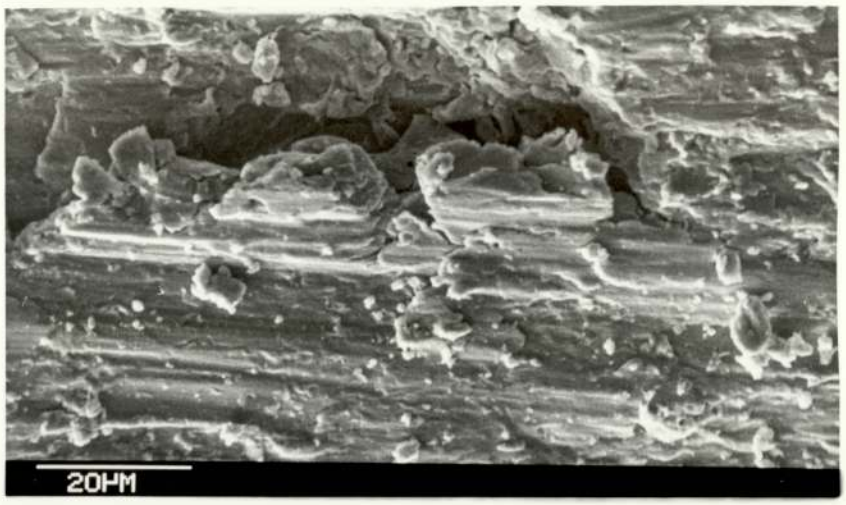

a

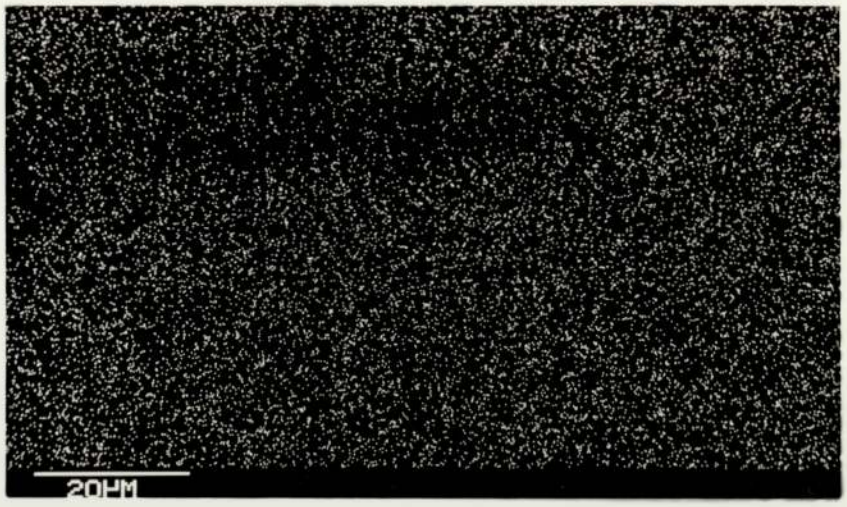

b

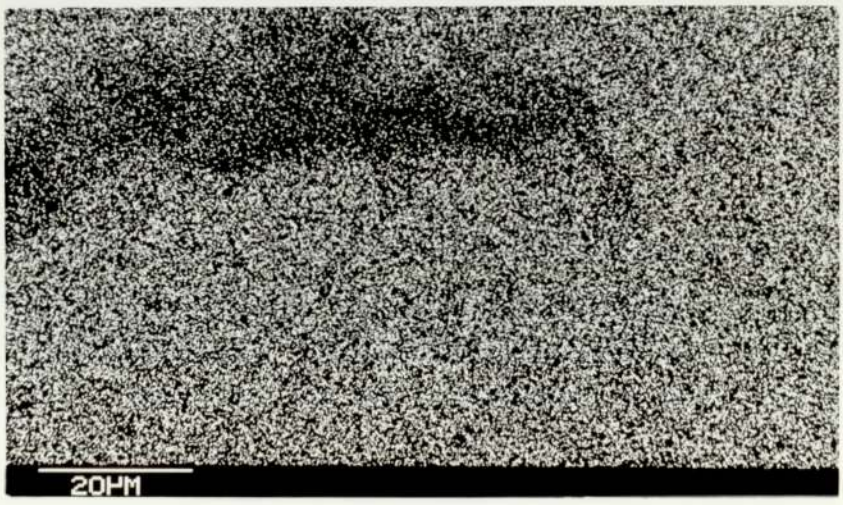

c

Figure 3.24

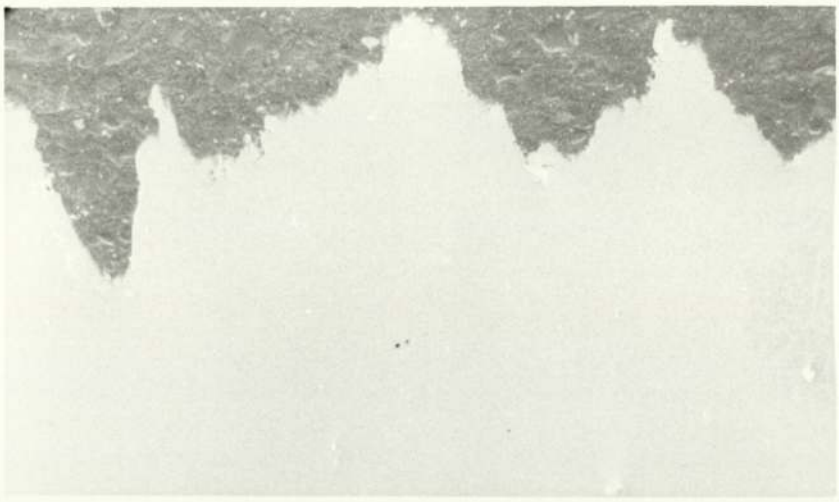

a

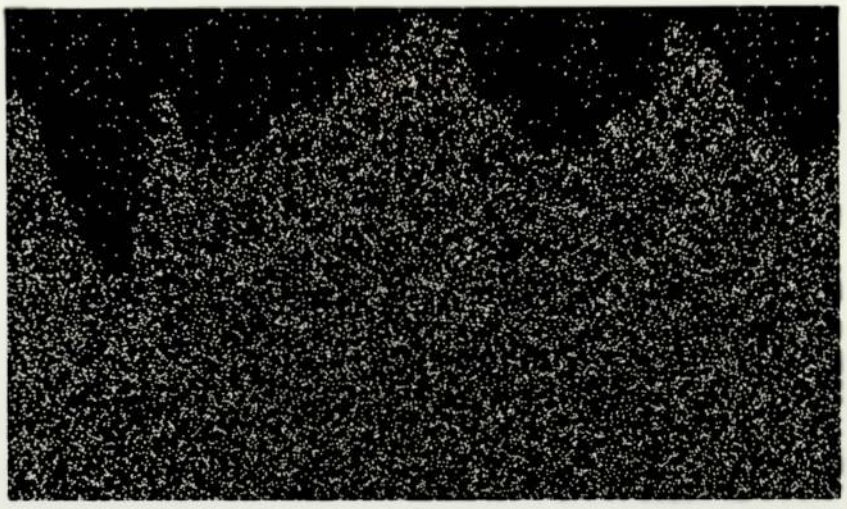

b

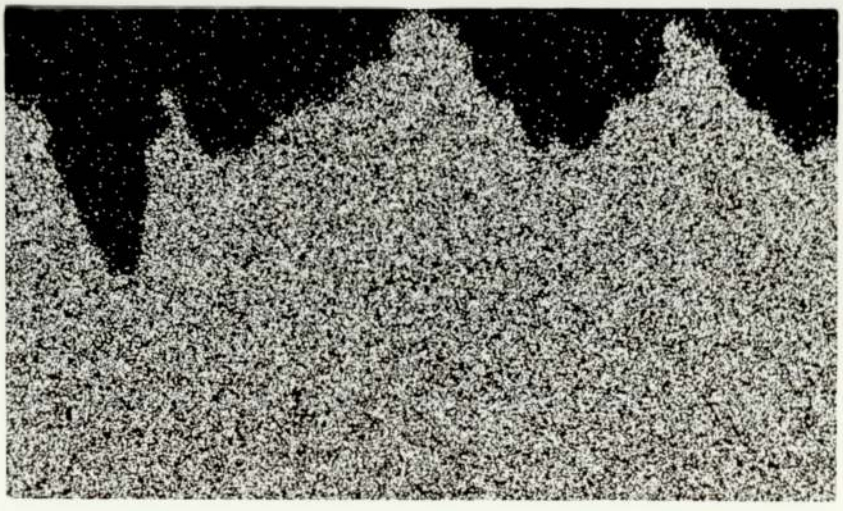

c

Figure 3.25

a wear transition after 46 kcycles of severe wear; the experiment was stopped after a further 30 kcycles of mild wear. The severe wear specimen, in figure 3.20(b), which was run for just 15.0 kcycles, had a metallic surface with no oxide plateaux. On the mild wear specimen, the plateaux were about 20 μm to 40 μm in width and generally showed the direction of sliding by small grooves on the plateau surface. Mild wear specimens worn under the larger load normally had larger plateaux, frequently well over 100 μm long; part of such a plateau is shown in figure 3.23(b).

The debris collected from a reciprocating sliding test is shown in figures 3.21(a) and (b), while figure 3.21(c) shows the debris that was often found on the surface of flat specimens, even after cleaning in an ultrasonic bath. This latter form of debris was made up of roughly spherical particles, 2 μm to 4 μm in diameter, whereas the debris shown in the other photographs consisted of plate-like fragments generally over 20 μm in length and were similar in appearance to the debris particles reported by other workers (68, 154). The edges of the plate-like particles, shown in figure 3.21(b), were observed to consist of smaller debris particles compacted together. The surface debris was generally found 'in the shadow' of steep-sided oxide plateaux.

All the surface debris and some of the removed debris consisted of oxide, or oxide-coated metallic particles because the photographs showed that the particles were charging up (this occurred when the specimens were poor conductors of electricity, like all iron-chromium oxides). It was possible that the thicker oxide layers observed in the reciprocating sliding tests were due to agglomerations of oxide particles rather than surface oxide growth. Energy dispersive analysis by X-rays, E.D.A.X., showed that there was little or no difference in composition between the plateaux and the

surface debris. It was found that some of the removed debris was metallic (the darker fragments not charging up in figure 3.21(b)); this was because the majority of the removed debris was formed during the severe wear period before the wear transition.

Figure 3.22 shows two oxide plateaux. The specimen tilt was increased to 50° so that the thickness of the plateaux could be measured. Both of these examples were about 10 μm, but thicknesses between 5 μm and 20 μm were observed, with the mean about 10 μm. The oxides were generally slightly thicker on the specimens worn under a 41 N load, but this might have been due more to the increased number of plateau edges available for measurement than to any significant increase in oxide thickness. Grooves on the plateau surfaces were observed, indicating the direction of sliding. No systemic variation in the oxide thickness was found on specimens worn at different sliding speeds. In previous work (77, 155), any such variation has always been load dependent; no study of the effect of changing load was made in this work.

Other general features of the worn surface are shown in figure 3.23. Figure 3.23(a) is a photograph of a smeared out particle that was probably transferred from the pin specimen. The oxide often cracked only part of the way through the total thickness and the crack in figure 3.23(b) is shown enlarged in figure 3.23(c). The edge, shown to be jagged, implied that the oxide layer could have been made up of compacted debris. The form of the oxide edge was different in figure 3.23(c) from the steeper and cleaner edges in figures 3.22(a) or (b).

Figure 3.24 shows a plateau and the chromium and iron distribution on the surface around it, obtained using E.D.A.X.. It was often observed that the chromium and iron concentrations were less on the plateaux; this was due to the presence of oxygen which could not be

measured by E.D.A.X.. In the taper section shown in figure 3.25, the chromium and iron are shown to be fairly evenly distributed over the surface of the section.

More details of the results obtained using energy dispersive analysis by X-rays are given in section 3.8.3.

3.8.2 Unidirectional sliding specimens

Many unidirectional sliding specimens were studied using scanning electron microscopy. A selection of photographs is included.

The general appearance of the pin specimens was very like that observed on the flat specimens; flat plateaux were seen on the mild wear specimens and severe wear was indicated by a more disturbed, metallic, and less flat surface. Figures 3.26 and 3.29(a) show parts of four plateaux and their edges; in general, the oxide thickness was much lower than on the reciprocating sliding specimens. Thicknesses of about 5 μm and 2 μm were observed on the slow speed specimens shown in figures 3.26(a) and (b), but the high speed specimen in figure 3.26(c) did not have a significantly thicker oxide. This difference in oxide thickness between forms, but not speeds, of sliding, might have been due to the specimen geometry. The wear surfaces on the pin-on-disc unidirectional sliding machines were vertical and so most debris fell away from the disc due to gravity. On the reciprocating sliding test machine, the surfaces were horizontal and so the debris was not always removed; as a result, it could have compacted to form thicker oxide layers than were formed due to sliding alone.

The oxide surface was also more prone to exhibiting cracks, as shown in figure 3.27. This was again probably due to the specimen geometry. Loosely held oxide flakes were less likely to be removed in the sliding was always in one direction; the surfaces were always disturbed more on the reciprocating specimens due to the backwards and

Figure 3.26 Scanning electron micrographs of oxide plateaux

a) experimental conditions: sliding speed 18.3 mms^{-1}, load 41 N, temperature 200°C, in air;
b) experimental conditions: as (a);
c) experimental conditions: sliding speed 2 ms^{-1}, load 59 N, room temperature, in air.

Figure 3.27 Scanning electron micrographs of the oxide cracking on pin specimens

a) experimental conditions: sliding speed 2 ms^{-1}, load 35 N, room temperature, in air;
b) experimental conditions: sliding speed 36.8 mms^{-1}, load 22 N, temperature 325°C. in CO_2.

Figure 3.28 Scanning electron micrographs of pin taper sections

a) experimental conditions: sliding speed 38.8 mms^{-1}, load 22 N, temperature 300°C, in CO_2;
b) experimental conditions: sliding speed 39.5 mms^{-1}, load 22 N, temperature 300°C, in air.

Figure 3.29 Scanning electron micrographs of an oxide plateau on a pin specimen

Experimental conditions: sliding speed 150.4 mms^{-1}, load 22 N, temperature 266°C, in CO_2,
a) the oxide surface:
b) chromium profile up the centre of (a);
c) iron profile up the centre of (a).

Figure 3.30 Scanning electron micrographs of a pin taper section

Experimental conditions: sliding speed 39.5 mms^{-1}, load 22 N, temperature 300°C, in air,
a) the taper section surface;
b) chromium distribution in (a);
c) iron distribution in (a).

Figure 3.26 to 3.30 Unidirectional sliding pin specimens

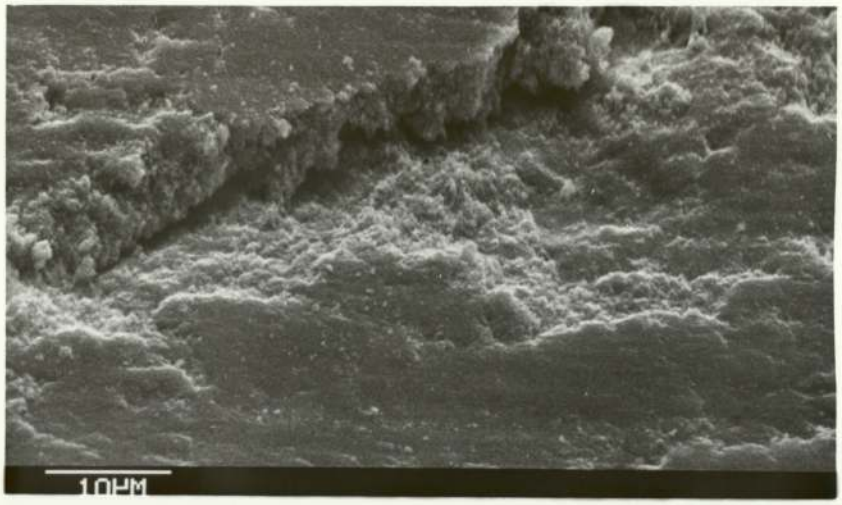

a

b

c

Figure 3.26

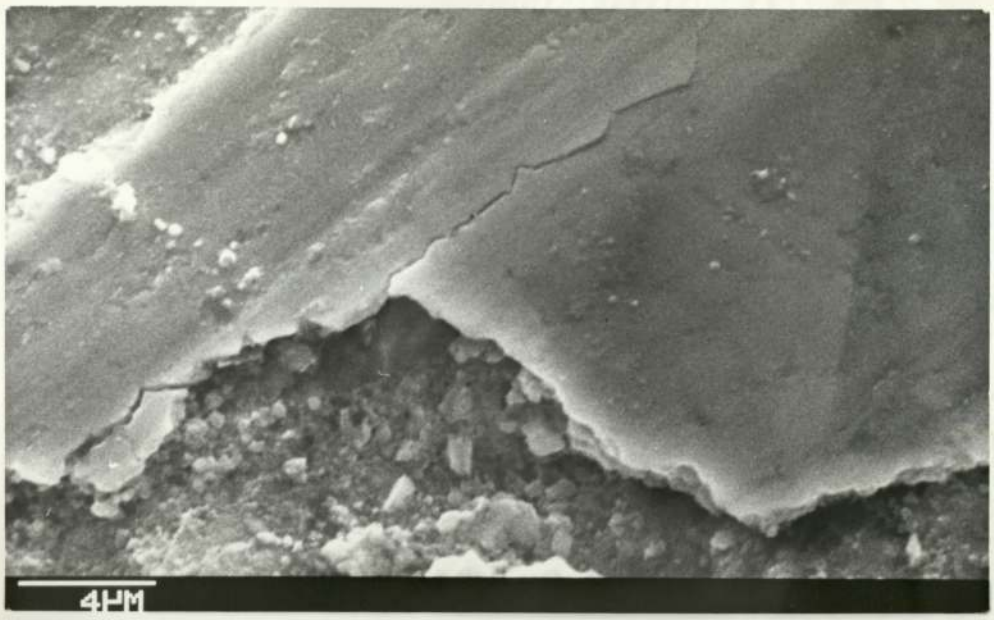

a

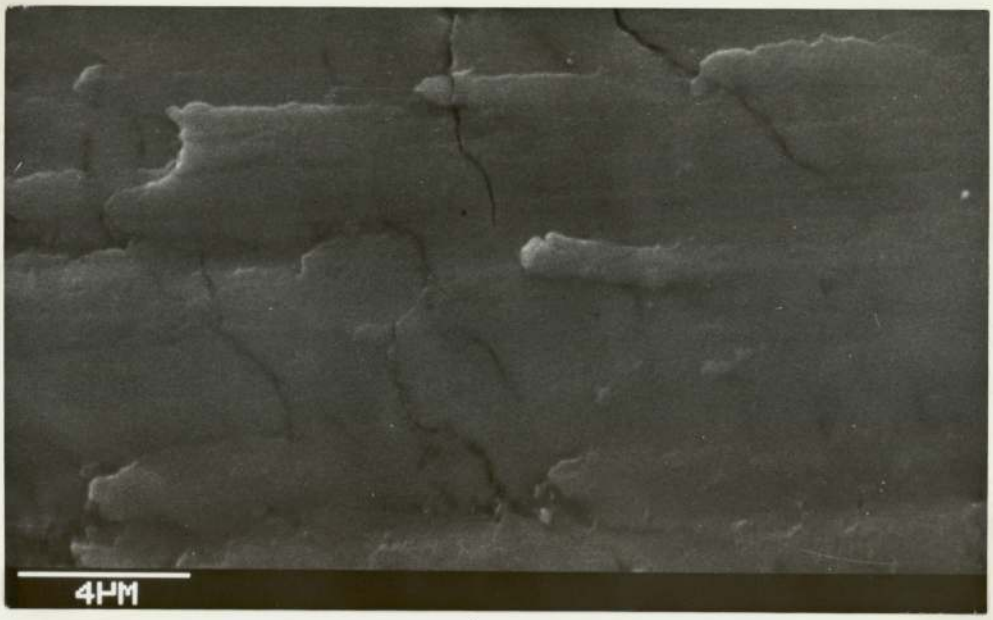

b

Figure 3.27

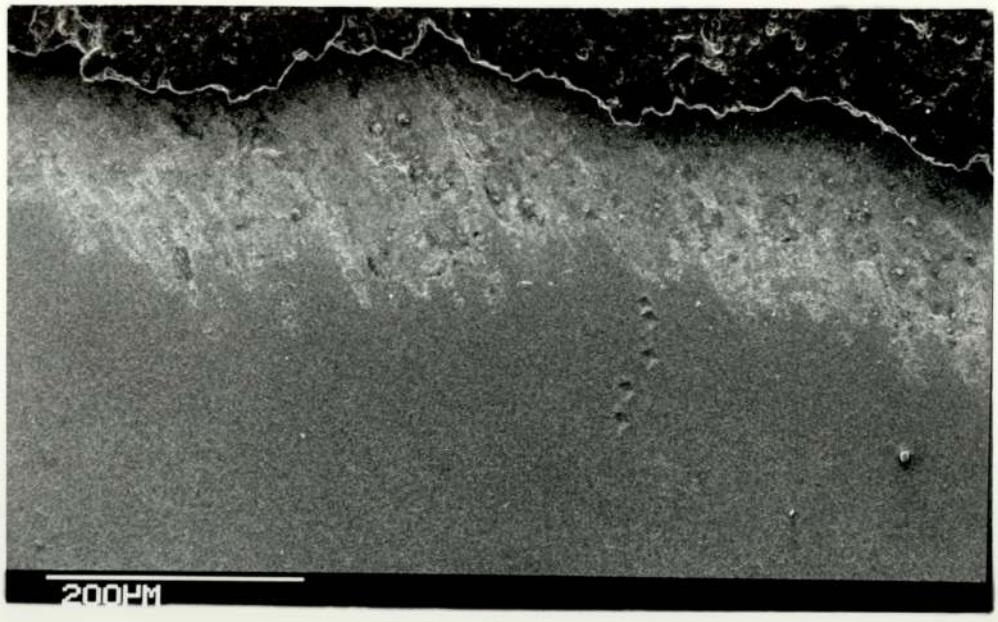

a

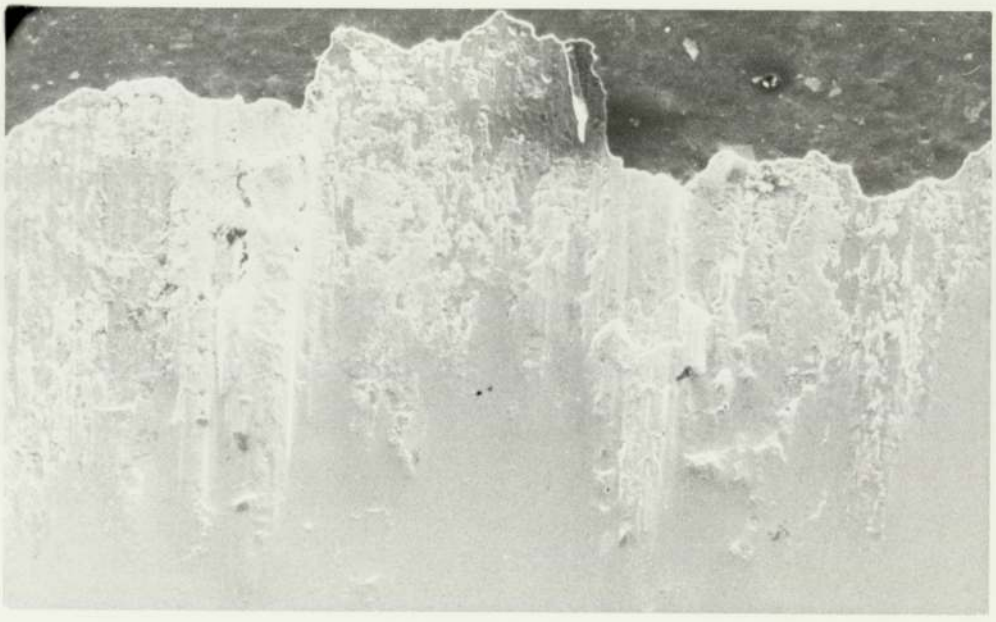

b

Figure 3.28

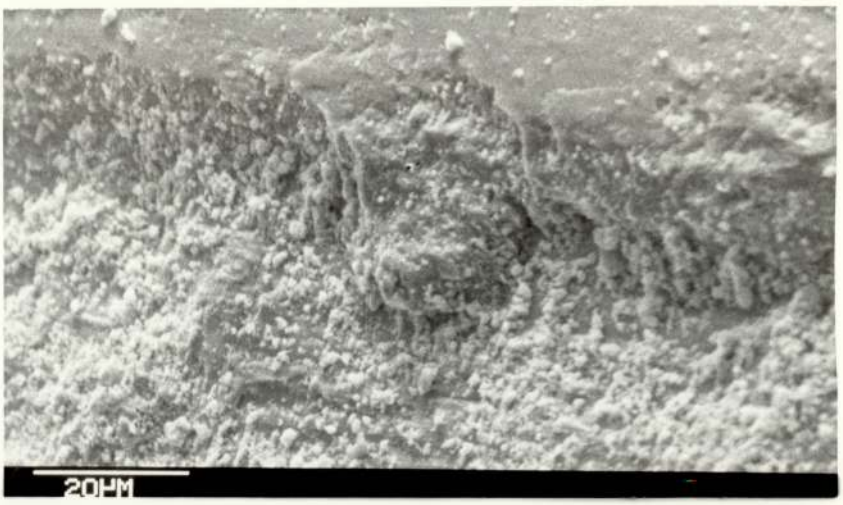

a

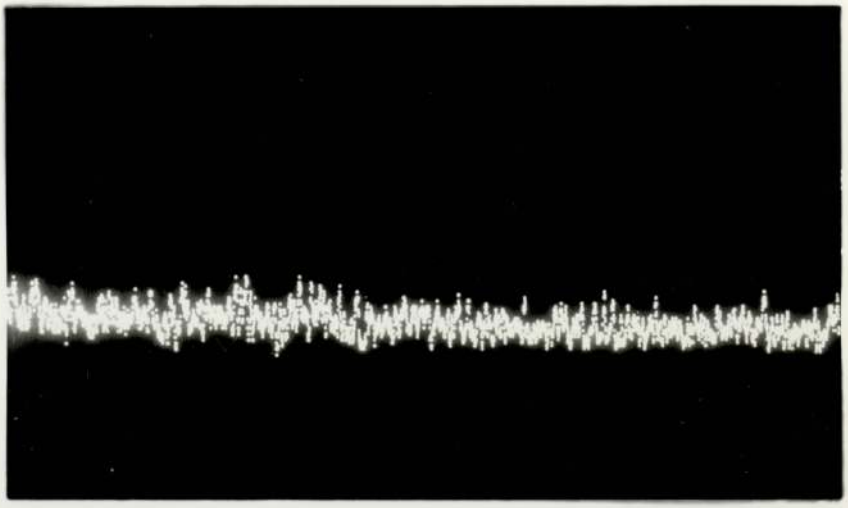

b

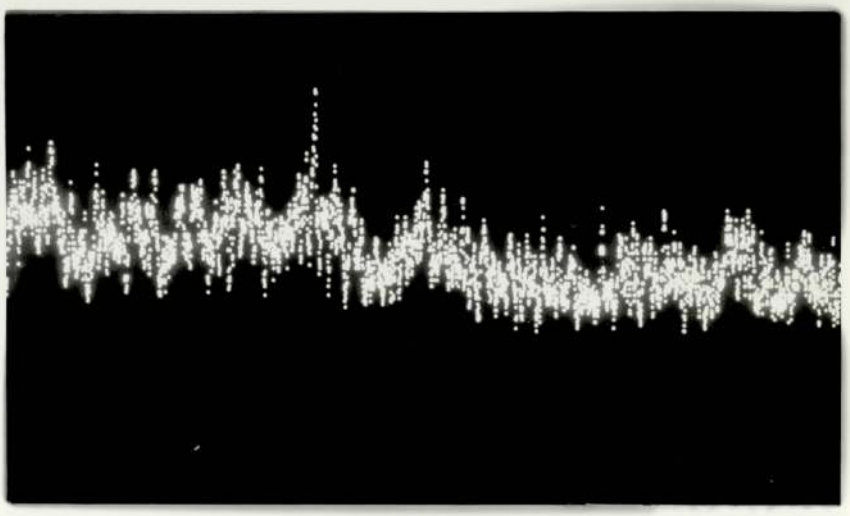

c

Figure 3.29

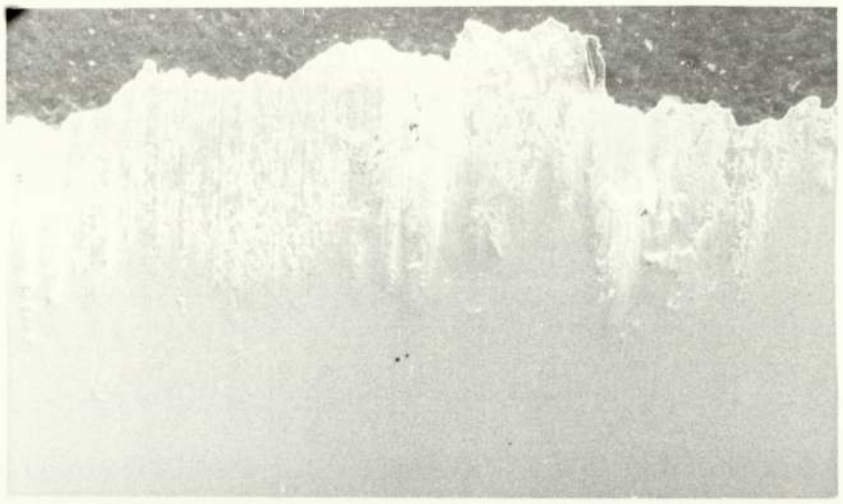

a

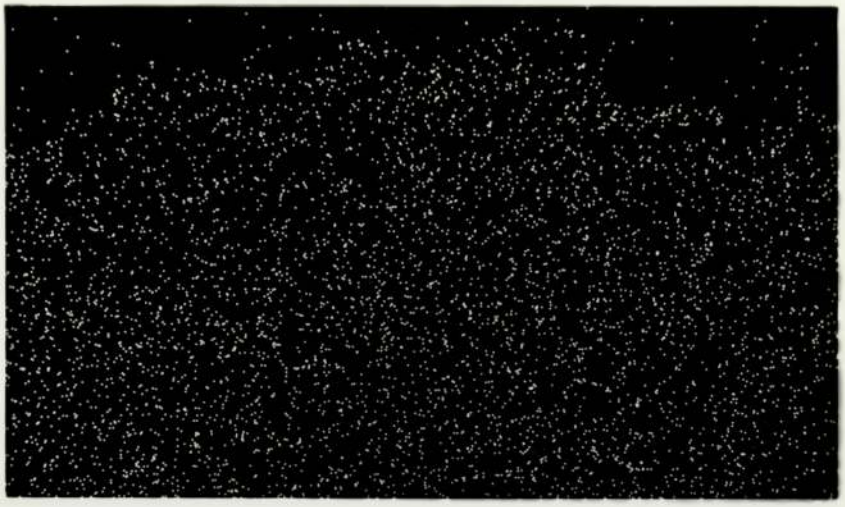

b

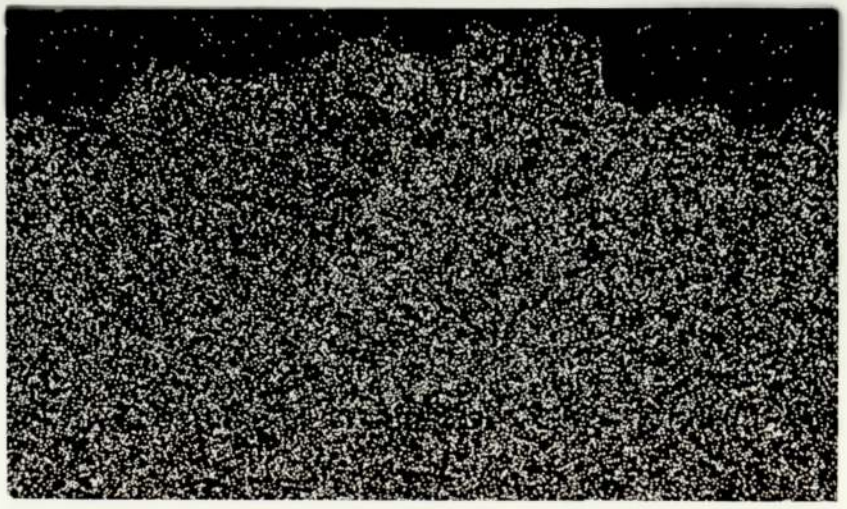

c

Figure 3.30

forwards motion.

Figure 3.28 shows two taper sections in which the surface layers can be identified, of which the depth, as observed in the photographs, was dependent not only upon the real thickness on the specimen, but also on the taper angle. The worn surface was often observed in similar photographs and it was frequently very difficult to decide where the surface ended, and where the taper section started entering the specimen. The surface was smoother on the specimen worn in carbon dioxide because the running-in period was longer (54 minutes in carbon dioxide, 6 minutes in air). The transition to mild wear occurred in air before the pin and disc were fully in contact with each other; had the experiment been stopped after about 10 minutes, it would have been found that parts of the disc were completely unworn, while other parts of the wear track exhibited mild wear. In carbon dioxide, a normal complete wear track was made before the transition to mild wear; as a result, wear across all the pin was more even at the instant of the wear transition. The pin cross-section due to severe wear always remained for a long time after the wear transition because the mild wear rate was much less.

3.8.3 Energy dispersive analysis by X-rays

E.D.A.X. was used to produce elemental maps and profiles of sections as well as analyses of spots on the specimen surfaces. Figure 3.24 shows that the oxide which was part of the plateau contained less chromium and iron than the surrounding surface; this was due to the presence of oxygen in the plateau. The X-ray maps did not reveal any detail about the ratio of the iron to chromium concentrations. Similar information was shown by the elemental profiles in figure 3.29, which were taken at some point up the centre of figure 3.29(a). The metal concentrations were less on the plateau.

Neither the reciprocating nor unidirectional sliding taper sections in figures 3.25 and 3.30 showed any variation in the chromium or iron concentrations with depth.

Spot analyses were found to give the most useful results, and are shown in table 3.16. Analyses were carried out on the plateau and non-plateau regions of specimen surfaces as well as on taper sections at varying distances from the specimen surface. These distances were converted into depths from the surface when the taper angle was measured.

All sets of results except one showed that there was chromium enrichment in the oxide layer compared to the non-oxide regions of the surface, and in the surface layer compared to the bulk material. However, as the accuracy of these results was very low, it was quite likely that the specimen in which chromium depletion was measured near the surface was subject to larger errors than normal because there was nothing unusual about the experimental conditions. This result was included in table 3.16 in order to give an indication about the accuracy of the results. Another measure of the errors was shown by the spread in iron to chromium ratios; the ranges varied from 7.45 to 8.32 for the plateaux and 8.25 to 8.83 for the non-plateau regions. Care was exercised when comparing the ratios measured on different occasions as it was necessary to recalibrate the X-ray analyser every time that it was used. Each set of results in table 3.16 was obtained on the same occasion; it would be incorrect to compare elemental ratios in the range 8.25 to 8.32 if the plateau and non-plateau measurements were made at different times.

Auger spectroscopy provided a technique to compliment that of energy dispersive analysis by X-rays.

Experimental Conditions		Area under analysis	Iron:Chromium ratio(standard deviation)	Conclusion
mean sliding speed	$18.4 mms^{-1}$	plateau	7.47(0.59)	Cr enrichment at surface
load	22 N	non-plateau	8.25(0.45)	
temperature	290°C			
mean sliding speed	$148.2 mms^{-1}$	plateau	8.04(0.15)	Cr enrichment at surface
load	41 N	non-plateau	8.55(0.17)	
temperature	300°C			
mean sliding speed	$110.4 mms^{-1}$	plateau	8.23(0.46)	Cr enrichment at surface
load	22 N	non-plateau	8.83(0.25)	
temperature	290°C			
mean sliding speed	$120.4 mms^{-1}$	plateau	7.53(0.05)	Cr enrichment at surface
load	41 N	non-plateau	8.32	
temperature	300°C			
sliding speed	$150.4 mms^{-1}$	plateau	8.95(0.05)	Cr depletion at surface
load	22 N	non-plateau	8.65(0.25)	
temperature	266°C			
atmosphere	CO_2			
sliding speed	$110.6 mms^{-1}$	plateau	8.32(0.22)	Cr enrichment at surface
load	22 N	non-plateau	8.65(0.05)	
temperature	266°C			
atmosphere	CO_2			
sliding speed	$39.5 mms^{-1}$	spot 20μm deep	7.45(0.45)	Cr enrichment in surface layer
load	22 N	spot 330μm deep	8.55(0.25)	
temperature	300°C			
atmosphere	air			
sliding speed	$38.8 mms^{-1}$	spot 20μm deep	8.32	Cr enrichment in surface layer
load	22 N	spot 360μm deep	8.49	
temperature	300°C			
atmosphere	CO_2			

Table 3.16 Results of EDAX spot analyses on reciprocating and unidirectional sliding specimens

3.9 Auger spectroscopy

One reciprocating flat specimen and one pin specimen from a unidirectional sliding experiment were analysed using auger spectroscopy. Unavailability of the spectrometer and lack of time prevented a more thorough comparison of the two sliding regimes.

The flat specimen selected for examination was the one worn in the long experiment run in order to determine the mild wear rate. This was chosen because it was thought that any subsurface changes in a specimen would be most likely to be observed in one that had been heavily worn.

Auger analysis was carried out on the surface, and the percentages of oxygen, iron and chromium present were calculated from the peak-to-peak heights of their major auger peaks and the application of corresponding inverse sensitivity factors (156). The specimen was then etched by bombardment with argon ions and a repeat analysis was completed. The surface was etched at the very approximate rate of 10 pmmin^{-1} for a total of 2265 minutes. Auger analyses were carried out every 60 minutes to 120 minutes.

The results, in figure 3.31, show that the oxygen percentage was constant at about 45% during the first 750 minutes of etching but decreased to under 15% after 2250 minutes. The iron percentage remained at 50% for 750 minutes, but then increased to about 80% as the etching continued. The chromium percentage was about 4% at low depths, and about 7% towards the end of the etching period.

Analysis was carried out in a similar manner on the pin specimen; the results are shown in figure 3.32. The pin selected for analysis was one worn at 300^{o}C in carbon dioxide. A high temperature specimen was chosen because it was hoped that any oxide layer would be more easily observed. Figure 3.32 shows that the percentages of

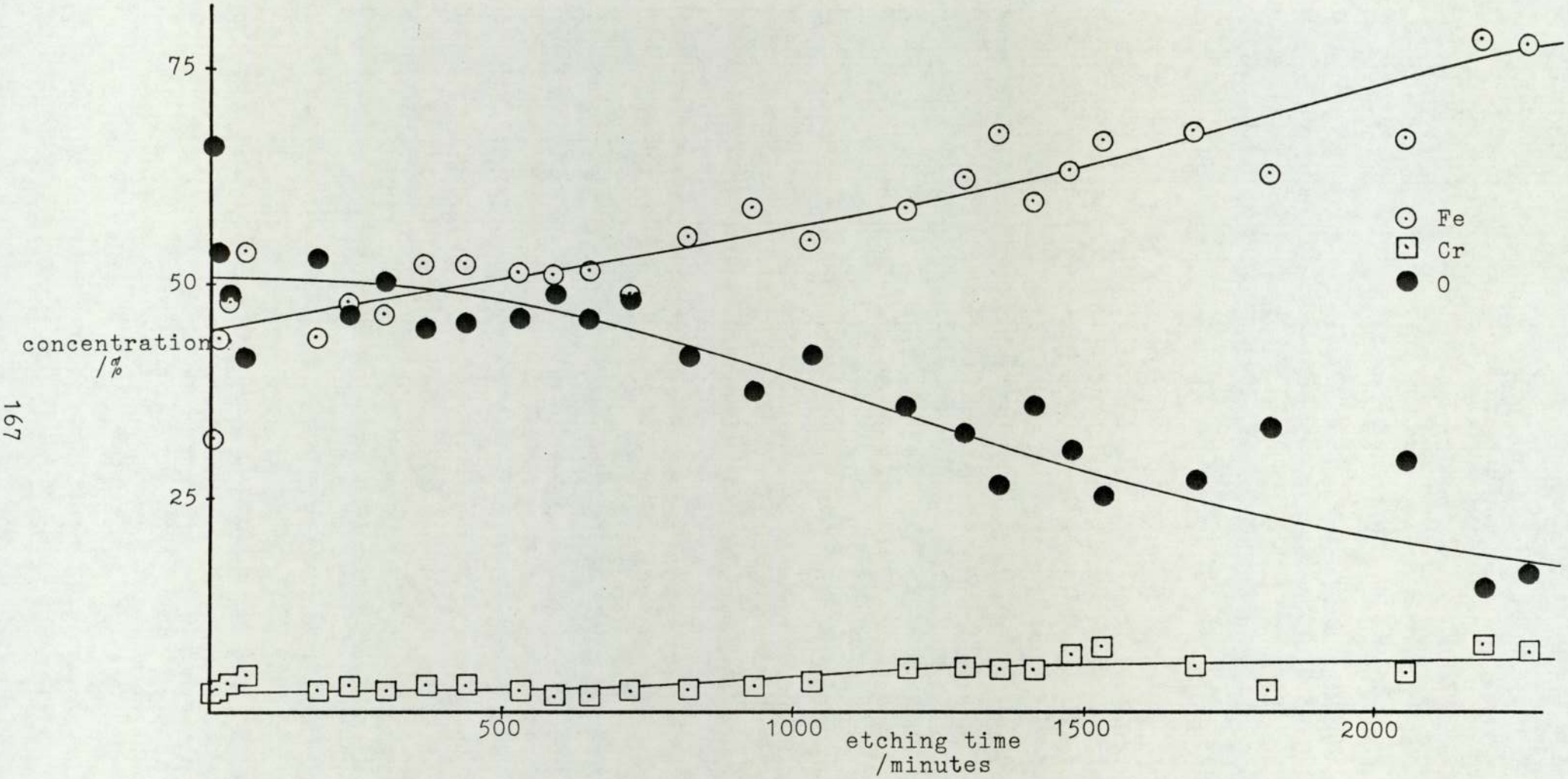

Figure 3.31 The variation in iron, chromium and oxygen concentration with etching time on a reciprocating flat specimen

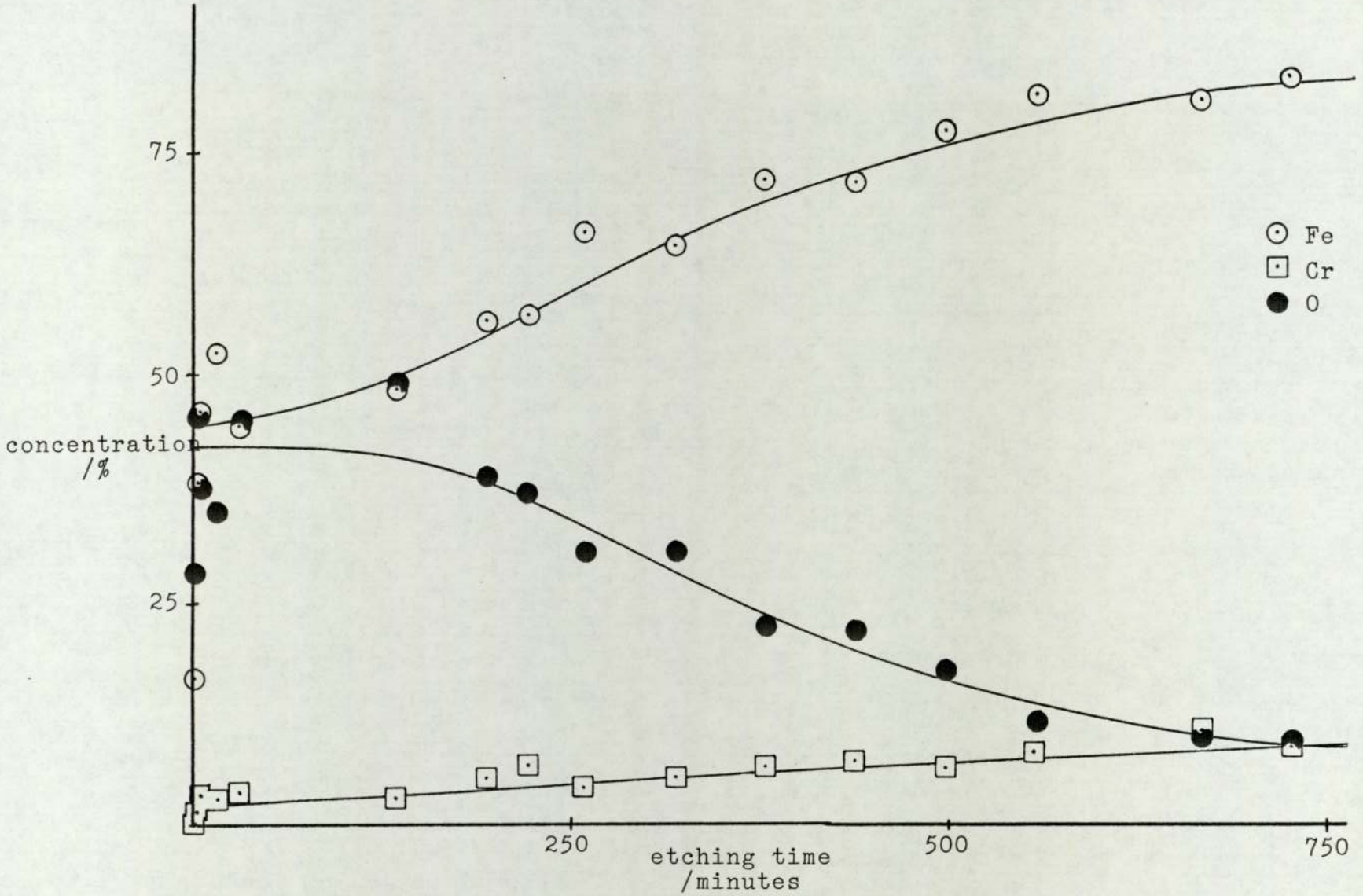

Figure 3.32 The variation in iron, chromium and oxygen concentration with etching time on a unidirectional pin specimen

iron and oxygen were each about 45% at the surface, but changed to 80% and 10% respectively after about 600 minutes of etching; this etching time was much less than the corresponding time required to reach the depth on the reciprocating specimen which had the elemental composition of the bulk material.

A small increase in the chromium content with increasing depth was again observed. However, as auger analysis is not accurate when measuring small elemental percentages, it was not possible to state whether there was any significant change in the iron to chromium ratio near the surface.

These observations were not unexpected after having carried out the s.e.m. studies; diffusion-produced oxides have a much slower rate of formation than surface layers caused by agglomeration. Diffusion-produced oxides would also have a fairly well defined boundary between the oxide and metal; figures 3.31 and 3.32 confirm that the oxygen content dropped from its maximum at the surface to the bulk value over 1500 minutes on the reciprocating specimen, but over only 550 minutes of etching on the pin.

It was possible that this change was due more to the different thickness of each surface layer than to the differing mechanisms of formation. As it was also possible that the wear test duration (about 4 weeks for the reciprocating specimen, but only 5 hours for the pin) was responsible for the very different oxide thicknesses, it was unfortunate that a more extensive analysis by auger spectroscopy could not be made.

CHAPTER 4
THEORETICAL MODIFICATIONS

4.1 Unidirectional wear

Previous workers in this laboratory have used a computer program which implemented an iterative technique used in the estimation of the asperity diameter, a, and the subsequent calculation of the number of asperities, N, the oxide thickness, ξ, and the oxidation temperature, T_o (77); however, such calculations have been carried out on data relating to low alloy steels with sliding speeds generally greater than 1 ms^{-1}.

The computer program, listed in the appendix of reference 77 was divided into two main parts of which the first was concerned with heat flow down the pin caused by the frictional heating and the subsequent calculation of the surface temperature of the pin (141). The heat flow was also considered in two stages, down the insulated portion of the pin, and in the exposed part close to the disc. It was assumed that the speed of the air flowing past the pin was equal to the sliding speed of the pin on the disc (155) and that forced convection was the result.

While this assumption may have been true at sliding speeds of 2 ms^{-1} and above (equivalent to about 10 disc revolutions per second), it was definitely invalid at sliding speeds of 20 mms^{-1} to 150 mms^{-1} (15 to 2 seconds per revolution). The part of the program relating to the calculation of the surface temperature was, therefore, rewritten to allow for free convection. It was also necessary to take two additional temperature measurements because the ambient temperature of the pin was slightly higher than the mean laboratory temperature for experiments carried out in air, and much higher for tests carried out in carbon dioxide. The disc temperature was

measured by a thermocouple situated between the disc and the asbestos block (figure 2.3); the ambient temperature was monitored using a Comark electronic thermometer for air tests, but could only be estimated for experiments run in carbon dioxide since these were carried out in an enclosed chamber.

Alterations have also been made to the program since it was first published in 1980 (77). In the original program, it was assumed that all oxidation occurred on the pin and took place at the contact temperature. Later examination of the disc surface revealed that the surface had oxidised; in addition, significant oxidation occurred at the bulk surface temperature when the wear test was carried out with a heated disc. Athwal (129) considered the oxidation that took place on both the pin and disc and calculated the contact temperature on each specimen using Archard's approach (89). By equating these temperatures (which should be equal during contact), and assuming the oxide thickness to be the same on each specimen, he obtained an expression for the contact radius from which other relevant values could be calculated. This program, listed in appendix 1 of reference 129, was used to calculate the oxide thickness and other parameters from the room temperature high speed experiments. The following equations were used:

$$a = \frac{-(B-G) \pm ((B-G)^2 - 4EJ)^{\frac{1}{2}}}{2E} \qquad (4.1)$$

$$T_o = \frac{\delta_{expt} H_T}{4aK_s N} + \frac{\delta_{expt} H_T}{a^2 K_o N} \qquad (4.2)$$

$$\xi = Ca(X-Ya) \qquad (4.3)$$

given:

$$B = \frac{H_1 p_m}{K_s W} \qquad (4.4)$$

$$G = \frac{0.8605 p_m (H_T - H_1)}{K_s W} - \frac{0.1021 p_m U (H_T - H_1) \xi}{2X_o K_o W} \qquad (4.5)$$

$$E = \frac{0.1021 p_m U (H_T - H_1)}{2 \chi_o K_s W} \qquad (4.6)$$

$$J = T_s - T_d + \frac{H_1 p_m \xi}{K_o W} - \frac{0.8605 p_m \xi^* (H_T - H_1)}{K_o W} \qquad (4.7)$$

$$C = \frac{\pi K_o}{4 \delta_{expt} K_s} \qquad (4.8)$$

$$X = 0.8605(1-\delta_{expt}) - \delta_{expt} \qquad (4.9)$$

$$Y = \frac{0.1021 U (1-\delta_{expt})}{2 \chi_s} \qquad (4.10)$$

$$N = \frac{W}{\pi a^2 p_m} \qquad (4.11)$$

where:

a = asperity radius, (m)
T_o = oxidation temperature, (K)
ξ = oxide thickness, (m)
δ_{expt} = the fraction of the heat generated at the sliding interface to enter the pin
H_T = total heat generated at the sliding interface, (Js^{-1})
K_s = thermal conductivity of steel, ($Jm^{-1}s^{-1}K^{-1}$)
N = number of asperities
K_o = thermal conductivity of oxide, ($Jm^{-1}s^{-1}K^{-1}$)
H_1 = heat flow entering the pin, (Js^{-1})
p_m = hardness of steel, (Nm^{-2})
W = load, (N)
U = sliding speed, (ms^{-1})
χ_o = thermal diffusivity of the oxide, (m^2s^{-1})
T_s = bulk surface temperature, (K)
T_d = disc temperature, (K)

The input data were the load, speed and disc temperature (in these experiments, room temperature or 20°C) along with heat flow into the pin, the total heat flow and the bulk surface temperature calculated from an earlier program (77). The output comprised of the

number and radius of the asperities with the oxide thickness and the oxidation temperature. Table 4.1 presents these values, and figures 4.1 and 4.2 show the variation of N, T_o and T_s with load.

The modifications necessary for the calculation of the surface parameters relevant to the slow speed experiments were extensive and are explained in detail below. The complete program is listed in Appendix 2.

The calculation of the heat transfer coefficient allowing for free convection, listed in lines 1830 to 2320 of the program, is now described. Firstly, the density of air, ρ_e, at the ambient temperature, T_{amb}, was calculated by (156):

$$\rho_e = \frac{1.293}{(1+0.00367T_{amb})} \qquad (4.12)$$

The dynamic viscosity, specific heat and thermal conductivity at the ambient temperature were interpolated from data in Weast (156), Hsu (157) and Rogers and Mayhew (158) respectively.

The Nusselt number, N_{Nu}, for free convection around a horizontal pin was then calculated at the desired ambient temperature (157):

$$N_{Nu} = 0.554 \frac{(g\beta D^2\delta)}{\nu_e^2} \frac{(c_{pe}\mu_e)}{k_e}^{\frac{1}{4}} \qquad (4.13)$$

where:

g = acceleration due to gravity, (9.81 ms^{-1})
β = temperature difference between the pin and the environment, $T_A - T_{amb}$, (K)
D = diameter of the pin, (m)
δ = $1/T_{amb}$, (K^{-1})
ν_e = kinematic viscosity at T_{amb}, (m^2s^{-1})
c_{pe} = specific heat at T_{amb}, ($Jkg^{-1}K^{-1}$)
μ_e = dynamic viscosity at T_{amb}, ($kgm^{-1}s^{-1}$)
k_e = thermal conductivity at T_{amb}, ($Jm^{-1}s^{-1}K^{-1}$)

load /N	T_s /^oC	a /μm	ξ /μm	N	T_o /^oC
27.5	73	28	11	4	569
29.5	69	30	11.5	4	552
39.3	68	31	18	4	546
45.2	80	30	14	6	555
49.2	94	28	11	7	570
55.0	102	29	9.5	7	563
59.0	92	29	12.5	8	552

Table 4.1 Sets of values of a, ξ, N, T_o and T_s from the high speed sliding experiments

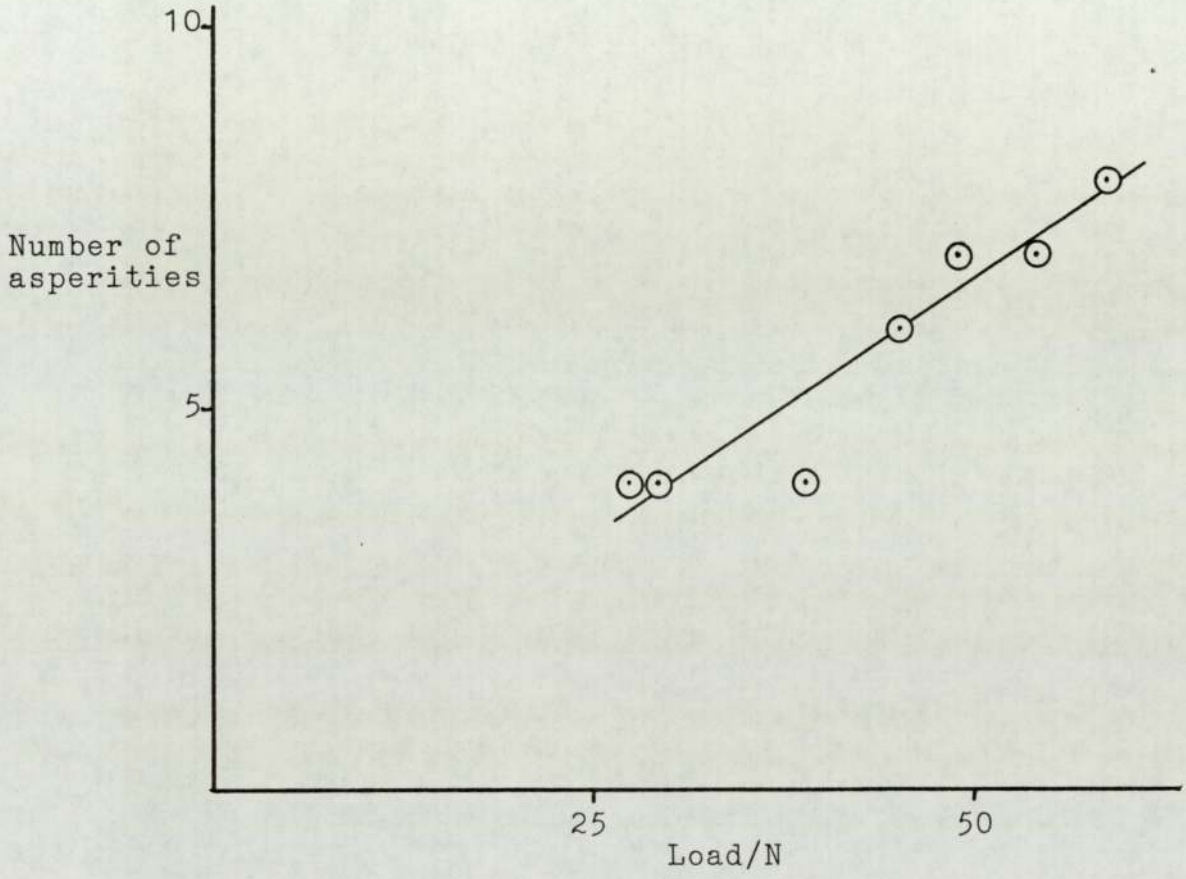

Figure 4.1 The variation of the number of asperities with load in the series of high speed sliding experiments

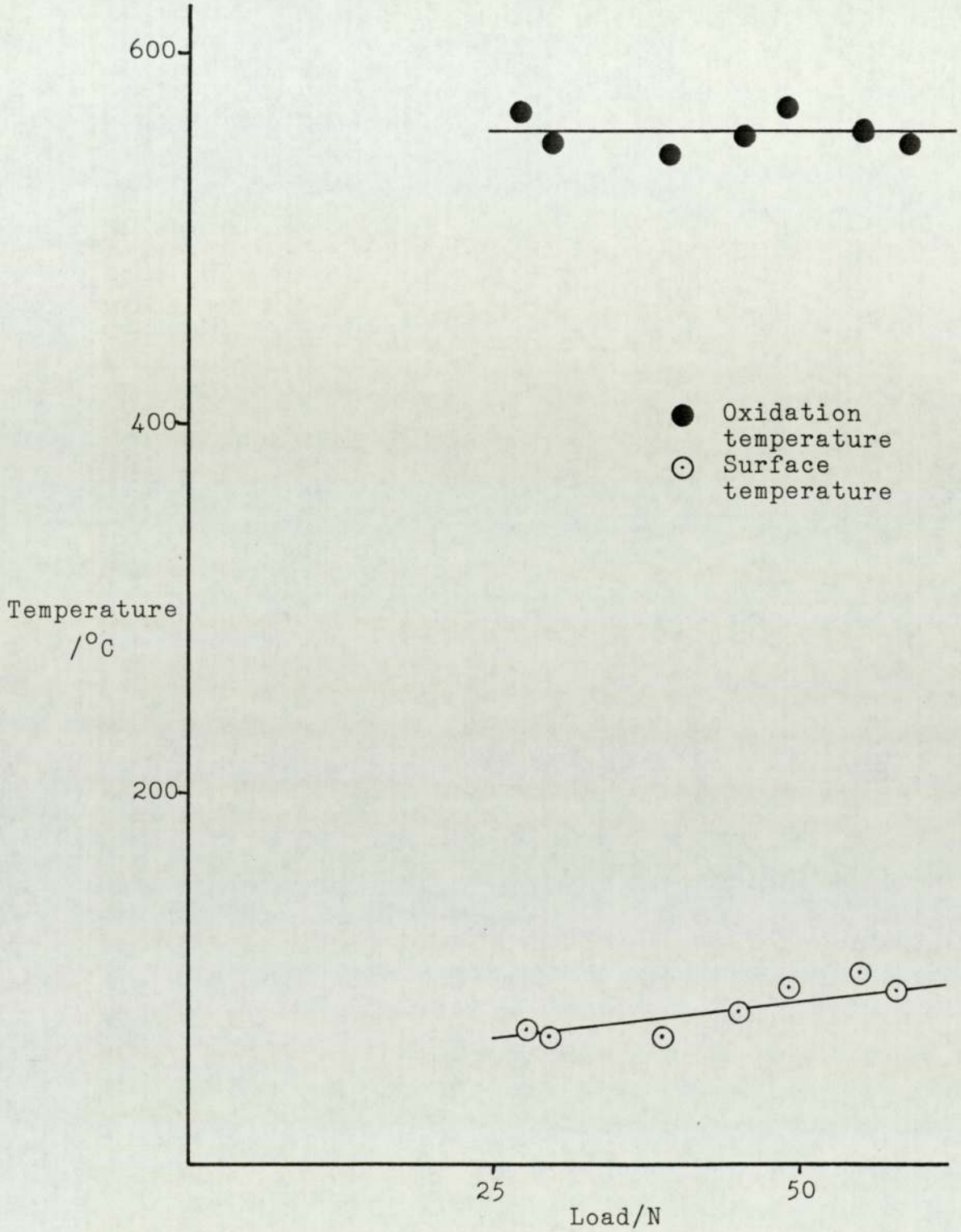

Figure 4.2 The variation of the oxidation and surface temperatures with load in the series of high speed sliding experiments

The kinematic viscosity is defined as:

$$\nu_e = \frac{\mu_e}{\rho_e} \qquad (4.14)$$

The heat transfer coefficient, h, was calculated using the Nusselt number:

$$h = \frac{N_{Nu} k_e}{D} \qquad (4.15)$$

The heat flow from the end of the pin, as shown in figure 2.7, was then determined using the original equations, described in section 2.2.6. The bulk surface temperature, T_s, and the division of heat, δ_{expt}, were also calculated.

Attempts were then made to calculate the oxidation temperature, T_o, at slow sliding speeds and high temperatures. This has already been done for high speeds at room temperature when in-contact or tribo-oxidation was generally much greater than out-of-contact oxidation.

Modifications had to be made to the method described by Quinn (76) for calculating the surface parameters in order to take into account the out-of-contact oxidation that occurred at high temperature before similar analysis could be carried out on the slow speed experiments. Equations 4.1 to 4.3 could not be altered in a simple manner to take into account the slower speed. An approach similar to that of Athwal (129) was made, but the change of speed resulted in very different final equations.

Archard (89) calculated fictitious flash temperatures by assuming that all of the heat generated at the interface went to just one sliding member; for a pin in contact with a stationary heat source, this temperature, T_{cp}, is:

$$T_{cp} = T_s + \frac{H_T}{4aK_sN} + \frac{H_T\xi}{a^2K_oN} \qquad (4.16)$$

The disc sees a moving heat source, and so a sliding constant, γ, is necessary when similar calculations are made to estimate the fictitious disc temperature, T_{cd}:

$$T_{cd} = T_d + \frac{\gamma H_T}{4aK_sN} + \frac{\gamma H_T \xi^*}{\pi a^2 K_o N} \qquad (4.17)$$

where ξ^* = oxide thickness on the disc, (m).

The sliding constant, γ, is a function of a dimensionless parameter, L, where:

$$L = \frac{Ua\rho_s c_{ps}}{2K_s} \qquad (4.18)$$

and ρ_s = density of steel, (kgm^{-3})

c_{ps} = specific heat of steel, ($Jkg^{-1}K^{-1}$).

γ was assumed to take the following values:

$L < 0.1$	$\gamma = 1$
$0.1 < L < 5$	$\gamma = 0.8605 - 0.1021L$
$5 < L$	$\gamma = 0.85L^{-\frac{1}{2}}$

Using typical values for a slow speed experiment ($U = 5 \times 10^{-2}$ ms^{-1}, $\rho_s = 7.78 \times 10^3$ kgm^{-3}, $c_{ps} = 4.95 \times 10^2$ $Jkg^{-1}K^{-1}$, $K_s = 2.72 \times 10^1$ $Jm^{-1}s^{-1}K^{-1}$) (159, 160), it was calculated that:

$$L = 3.54 \times 10^3 a$$

This showed that if, as was likely, the asperity radius, a, was less than 28 μm, the dimensionless sliding parameter, L, was under 0.1; therefore the sliding constant, γ, could be assumed to be unity, and:

$$T_{cd} = T_d + \frac{H_T}{4aK_sN} + \frac{H_T \xi^*}{\pi a^2 K_o N} \qquad (4.19)$$

The contact temperatures can be calculated knowing the division of heat. Figure 4.3 shows how the heat flow

is affected by the elevated disc temperature which causes the conduction of heat from the disc across the air gap to the pin. This will increase the temperatures as recorded by the thermocouples and therefore alter the calculated value of H_1; this calculated value will include the contribution due to conduction, Q_C, and this must be subtracted before further steps are taken to determine the oxidation temperature.

Replacing H_T with H_1 or $\delta_{expt}H_T$ in equation 4.16 gives the contact temperature of the pin assuming that all the heat flow is generated at the sliding interface. However, in high temperature, slow speed experiments, part of the heat flow down the pin is from the disc; attempts to calculate this by estimating the air gap between the pin and disc, and the temperature difference between the two specimens proved unsuccessful. Although it could only be estimated, the heat flow due to conduction across the air gap, Q_C, was not ignored, and the heat flow down the pin from which the contact temperature of the pin was calculated was considered to be H_1-Q_C. Therefore:

$$T_{cp} = T_s + \frac{H_1-Q_C}{4aK_sN} + \frac{(H_1-Q_C)\xi}{\pi a^2K_oN} \qquad (4.20)$$

Similar considerations were made concerning the disc contact temperature; H_T was replaced by $(1-\delta_{expt})H_T$ or H_T-H_1. The conduction across the air gap to the pin was assumed not to take place so the the total heat flow into the disc was $H_T+Q_C-H_1$ and:

$$T_{cd} = T_d + \frac{H_T+Q_C-H_1}{4aK_sN} + \frac{(H_T+Q_C-H_1)\xi^*}{\pi a^2K_oN} \qquad (4.21)$$

These temperatures are equal when the asperities are in contact. Evidence from scanning electron microscopy has shown that ξ and ξ^* are not significantly different.

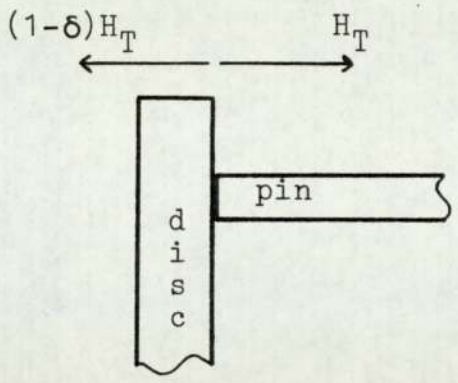

i) during a room temperature, high speed test

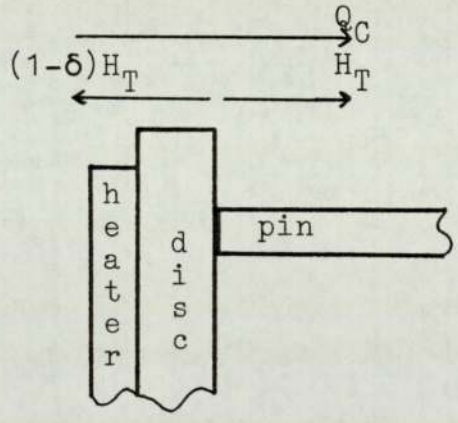

ii) during an elevated temperature, slow speed test

Figure 4.3 The heat flow at the interface between pin and disc during unidirectional sliding experiments

Therefore, assuming $\xi = \xi^*$, an expression for the contact radius involving only two other unknown quantities, ξ and Q_C, can now be obtained from equations 4.11, 4.20 and 4.21:

$$a = \frac{4K_s W}{\pi p_m} \frac{(T_s - T_d)}{(H_T + 2Q_C - 2H_1)} - \frac{4K_s \xi}{\pi K_o} \qquad (4.22)$$

ξ was estimated to average 3 μm from scanning electron microscopy measurements.

An estimate was then made of the heat flow due to conduction, Q_C. Equation 4.22 only produces valid solutions of a (i.e. when a is positive) for a small range of values of Q_C:

$$\text{Lower limit:} \quad Q_C(\min) = H_1 - \frac{H_T}{2} - \frac{K_o W}{2p_m \xi} (T_d - T_s) \qquad (4.23)$$

$$\text{Upper limit:} \quad Q_C(\max) = H_1 - \frac{H_T}{2} \qquad (4.24)$$

Q_C was increased in steps of 0.01 Js^{-1} between the two limits and sets of values of a, ξ, N, T_o and Q_C were calculated. There is no physical relationship between Q_C and a; the relationship is one of mathematical convenience only. The following equations were used to calculate the surface parameters:

$$a = \frac{4K_s W}{\pi p_m} \frac{(T_s - T_d)}{(H_T + 2Q_C - 2H_1)} - \frac{4K_s \xi}{\pi K_o} \qquad (4.22)$$

$$\xi = 3 \qquad \text{by direct observation}$$

$$N = \frac{W}{\pi a^2 p_m} \qquad (4.11)$$

$$T_o = T_s + \frac{(H_1 - Q_C) p_m}{4K_s K_o W} (\pi a K_o + 4\xi K_s) \qquad (4.25)$$

The maximum oxidation temperature was calculated using the method devised by Archard (89) in which it was assumed that there was just one contacting area. The maximum excess temperature at the contact is related to

the excess temperature of the sliding bodies by:

$$1/\delta_m = 1/\delta_p + 1/\delta_d \qquad (4.26)$$

where:

δ_m = excess temperature of the contact above that of the bulk surface area, (K)

δ_p = excess temperature of the contact area of the pin, (K)

δ_d = excess temperature of the contact area of the disc, (K)

$$\delta_p = \frac{UF}{4aK_s} \qquad (4.27)$$

where F = frictional force, (N).

As the pin and disc are made of similar material, the excess temperatures, δ_p and δ_d, are equal and therefore from equations 4.11 (assuming N=1), 4.26 and 4.27:

$$\delta_m = \frac{UF(\pi p_m)^{\frac{1}{2}}}{8K_s W^{\frac{1}{2}}} \qquad (4.28)$$

and:

$$T_{o(max)} = T_s + \frac{(\pi p_m)^{\frac{1}{2}}}{8K_s} \frac{UF}{W^{\frac{1}{2}}} \qquad (4.29)$$

Sixteen valid sets of solutions from twenty experiments which were carried out in carbon dioxide and gave mild wear, were obtained with Q_C assigned various values between 0.2 Js^{-1} and 2.4 Js^{-1}; however, most solutions were obtained when Q_C was 1.29 Js^{-1} when six experiments each produced a valid set of results; the division of heat including any contribution due to conduction varied from 1.1 to 1.7 (a value of δ_{expt} in excess of one is evidence that conduction must have occurred); after the effect of conduction had been considered, the division of heat averaged 0.74 with all

results within 15% of this figure.

Fourteen valid sets of solutions were obtained from the eighteen mild wear experiments carried out in air. The spread in the values of Q_C (from 0 Js^{-1} to 3.1 Js^{-1}) was such that no optimum value was immediately apparent. A value of 1.01 Js^{-1} was chosen for Q_C. Although just four experiments gave valid sets of solutions, no other one value of Q_C gave more.

It would be expected that the heat flow due to conduction across the air gap would be greater in carbon dioxide than in air. The attempts to calculate the heat flow used the following equation:

$$Q_C = \frac{k_e A}{G_e} (T_d - T_s) \qquad (4.30)$$

where:

k_e = thermal conductivity of the environment at $(T_d-T_s)/2$, $(Jm^{-1}s^{-1}K^{-1})$

A = cross-sectional area of the pin, (m^2)

G_e = width of the gap, (m).

The temperature was greater for experiments carried out in carbon dioxide; in addition, the thermal conductivity, at the relevant temperature, of the carbon dioxide in the gap was slightly greater than that of air.

Further supporting evidence for the relative values of Q_C came from a comparison of the division of heat data after the contribution due to conduction had been considered. The environment should not make any significant difference to the division of the heat generated by friction, but should affect the temperatures recorded by the thermocouples on the pin; it is from these measurements that the heat flow (before conduction is considered) H_1, is calculated. H_1 was generally higher for experiments run in air, but after conduction was considered, the mean division of heat was 0.744 for the air experiments and 0.740 for those run in carbon

dioxide.

The ten valid sets of solutions are presented in table 4.2.

Most of these solutions were obtained from tests with higher sliding speeds than the majority of elevated temperature experiments. This is because, at slow speeds, the frictional heating was much less than the heat flow due to conduction. For example, at 0.02 ms^{-1} and with a load of 22 N, the frictional heating was about 0.45 Js^{-1}, whereas the heat flow due to conduction for experiments run in carbon dioxide has been taken to be 1.29 Js^{-1}. Under these circumstances, it is often impossible to adjust the heat flow down the pin by the introduction of a conduction factor, Q_C, so that the oxidation temperature is less than the maximum permissible temperature while maintaining a positive value of the asperity radius.

It is possible that these inaccuracies were caused by poor calculation of the bulk surface temperature. In previous high speed experiments carried out in this laboratory (90), it has not been necessary to determine the temperature of the environment around the pin, T_{amb}. This was determined for some of the later tests carried out in air, but could not be done for any carbon dioxide experiments. Estimates were made of T_{amb} which were then used in the calculation of the oxidation temperature; these were about 35% of the disc temperature and assumed, for convenience, to be independent of sliding speed. However, it is possible that these estimates may be very inaccurate. Further errors in the determination of the bulk surface temperature arose in the calculation of the heat transfer coefficient; the forced convection around the pin assumed in previous work (90, 141) was replaced by the heat transfer coefficient for free convection. However, no quantitive adjustment could be made for the pin-on-disc assembly being enclosed in a steel box providing conditions in which the ambient temperature

test number	environment	speed /ms^{-1}	load /N	T_d /°C	T_s /°C	a /μm	ξ /μm	N	T_o /°C	$T_{o(max)}$ /°C	Q_c /Js^{-1}	δ
8	air	0.018	26	100	83	34	3	4	125	132	1.01	0.63
11	air	0.019	31	100	87	2.1	3	1080	105	135	1.01	0.79
18	air	0.109	22	200	147	35	3	3	357	366	1.01	0.57
21	air	0.038	41	200	146	7.1	3	130	201	246	1.01	0.99
12	CO_2	0.113	22	261	195	0.5	3	17500	292	395	1.29	0.76
15	CO_2	0.111	22	266	200	3.4	3	296	316	422	1.29	0.70
16	CO_2	0.119	22	266	191	0.6	3	8500	282	356	1.29	0.85
19	CO_2	0.140	22	266	202	0.2	3	67900	328	483	1.29	0.67
25	CO_2	0.111	22	273	207	7.5	3	62	348	447	1.29	0.65
27	CO_2	0.106	22	285	193	18	3	11	314	323	1.29	0.81

Table 4.2 Sets of values of a, ξ, N, T_o, T_s and data related to the division of heat from the high temperature, slow speed experiments

may have almost equalled the temperature of the calorimeter, T_c.

In most experiments, the calculated bulk surface temperature was less than the disc temperature. This was probably due to the temperature drop across the oxide layers on the pin and disc. Unfortunately, this introduced a further source of error into the calculation of T_s; the heat flow due to conduction may not have been solely due to conduction across the air gap between the pin and disc. Conduction from either side of the wear track on the disc to the side of the pin may have been significant as neither of these surfaces had an oxide layer. It may have been for this reason that the attempts to calculate the conduction across the air gap did not produce values of Q_c that were large enough. Such attempts only produced valid sets of solutions of a, ξ, N and T_o if the oxide thickness, ξ, was less than 0.5 μm. This was known to be incorrect from scanning electron microscopy observations.

In conclusion, the program developed in this section gave valid solutions to several experiments run at elevated temperatures with sliding speeds usually greater than 0.1 ms^{-1}. At lower speeds, the heat flow due to conduction, which was only estimated and not calculated, became too large in comparison to the frictional heating; as a result, just three experiments gave complete sets of results.

4.2 Reciprocating wear prior to the wear transition

The previous section has described in- and out-of-contact oxidation with reference to unidirectional sliding; similar oxidation occurs in a reciprocating sliding system.

Out-of-contact oxidation will occur at the ambient temperature, T_{amb}, over the entire wear scar, of which the

rate will be dependent upon temperature, but independent of load or sliding speed. In-contact oxidation will occur at the contact temperature, T_o, and will be higher at increased sliding speeds.

A wear transition will occur if the combined rate of oxide formation is greater than the rate of oxide removal by wear; no transition will occur if either or both of the ambient temperature or sliding speed are too low. The following theory is relevant only to those experiments in which a transition took place.

Oxide plateaux form on the wear surface and increase in both area and height during severe wear until the entire load is supported by these areas alone, and the transition to mild wear occurs. This will be at a time when a certain proportion of the wear scar is covered by oxide of thickness, ξ. On a reciprocating wear machine with horizontal sliding, the wear debris cannot easily escape and so it is likely that the plateaux grow around nucleation sites by a process comprising of diffusion-controlled oxidation and particle agglomeration. Figure 3.22b suggests that the edge of a reciprocating sliding plateau is an agglomeration of smaller particles, unlike the smoother and steeper plateau edges caused solely by oxidation in figure 3.26a.

This model also attempts to explain why the wear transition occurred quite suddenly after a period of severe wear that may have lasted for many hours. During this time, although the oxide coverage was increasing, most of the load-bearing areas were still metallic. At the wear transition, the load was able to be supported by the oxide plateaux alone and the metallic areas ceased undergoing significant wear. Out-of-contact oxidation then occurred over the non-wearing areas so that all the surface was soon oxidised. Due to the much lower mild wear rates, significant diffusion-controlled oxidation should have occurred before these areas again became

load-bearing.

It is now possible to consider wear and oxidation during initial severe wear. During a time period, Δt, then:

$$\Delta V = \Delta V_{mm} + \Delta V_{oo} + \Delta V_{mo} - \Delta V_{ox} \qquad (4.31)$$

where:

ΔV = total volume removed in time Δt, (m^3)

ΔV_{mm} = volume removed due to metal-metal contact in time Δt, (m^3)

ΔV_{oo} = volume removed due to oxide-oxide contact in time Δt, (m^3)

ΔV_{mo} = volume revoved due to metal-oxide contact in time Δt, (m^3)

ΔV_{ox} = volume gain due to oxidation in time Δt, (m^3)

If α is the fraction of the apparent contact area covered by oxide at time t, then (161):

$$P_{mm} = (1-\alpha)^2 \qquad (4.32)$$

$$P_{oo} = \alpha^2 \qquad (4.33)$$

$$P_{mo} = 2\alpha(1-\alpha) \qquad (4.34)$$

where:

P_{mm} = probability of a metal-metal contact

P_{oo} = probability of an oxide-oxide contact

P_{mo} = probability of a metal-oxide contact

The volume removed is proportional to a wear constant and the sliding distance (91):

$$V_{mm} = K_{mm} P_{mm} A_r \Delta d \qquad (4.35)$$

where:

K_{mm} = wear constant for metal-metal contact

A_r = real area of contact, (m^2)

Δd = sliding distance in time Δt, (m)

Using equation 4.32 with

$$A_r = \frac{W}{p_m} \qquad (4.36)$$

and

$$U\Delta t = \Delta d \tag{4.37}$$

then:

$$\Delta V_{mm} = K_{mm}(1-\alpha)^2 \frac{W}{p_m} U\Delta t \tag{4.38}$$

The degree of agglomeration will be proportional to the sliding time, and so it is reasonable to assume that α will increase linearly with time:

$$\alpha = yt \tag{4.39}$$

where y = a constant.

At the transition time, T_T, direct observation of the specimens showed that mild wear could be supported by a surface that was half covered with oxide. So, when $t = T_T$, $\alpha = 0.5$ and:

$$y = \frac{1}{2T_T} \tag{4.40}$$

Therefore:

$$\alpha = \frac{t}{2T_T} \tag{4.41}$$

From equations 4.38 and 4.41:

$$\Delta V_{mm} = K_{mm} \left(1-\frac{t}{2T_T}\right)^2 \frac{W}{p_m} U\Delta t \tag{4.42}$$

Similarly, it can be shown that:

$$\Delta V_{oo} = K_{oo} \left(\frac{t}{2T_T}\right)^2 \frac{W}{p_m} U\Delta t \tag{4.43}$$

$$\Delta V_{mo} = K_{mo}\, 2\left(\frac{t}{2T_T}\right) \left(1-\frac{t}{2T_T}\right) \frac{W}{p_m} U\Delta t \tag{4.44}$$

where:

K_{oo} = wear constant for oxide-oxide contact

K_{mo} = wear constant for metal-oxide contact

The continuous process of debris removal and agglomeration made the formation of thick diffusion-

produced oxide films unlikely. It was therefore probable that linear oxidation kinetics occurred. Making this assumption, then:

$$\Delta m = k\Delta t \tag{4.45}$$

and therefore:

$$\Delta V_{ox} = k \frac{A}{\rho_o f} \Delta t \tag{4.46}$$

where:

Δm = mass uptake of oxygen in time Δt, (kg)
k = linear oxidational rate constant, (kgs^{-1})
A = area of wear scar, (m^2)
ρ_o = density of oxide, (kgm^{-3})
f = fraction of oxide which is oxygen

This oxidation term comprises of two parts; in-contact oxidation takes place at the ambient temperature, T_{amb}, while tribo-oxidation takes place at the asperities only at the oxidation temperature, T_o:

$$\Delta V_{ox} = k_{T_{amb}} (\frac{A}{\rho_o f})\Delta t + k_{T_o} (\frac{A_r}{\rho_o f})\Delta t \tag{4.47}$$

where:

$k_{T_{amb}}$ = rate constant at the ambient temperature, T_{amb}, (kgs^{-1})
k_{T_o} = rate constant for the asperities at the oxidation temperature, T_o, (kgs^{-1})

Equations 4.36, 4.42, 4.43, 4.44 and 4.47 can now be substituted into equation 4.31, which after rearrangement, gives:

$$\Delta V = (P(\frac{t}{T_T})^2 - Q(\frac{t}{T_T}) + R)U\Delta t \tag{4.48}$$

where:

$$P = (K_{mm} + K_{oo} - 2K_{mo}) \frac{W}{4p_m} \tag{4.49}$$

$$Q = (K_{mm} - K_{mo}) \frac{W}{p_m} \tag{4.50}$$

$$R = K_{mm}\frac{W}{p_m} - \frac{1}{U}\left(\frac{Ak_{T_{amb}}}{\rho_o f} + \frac{Wk_{T_o}}{p_m \rho_o f}\right) \qquad (4.51)$$

As $\Delta d = U\Delta t$ (4.52)

then the instantaneous wear rate, w, is:

$$w = \frac{\Delta V}{\Delta d} = P\left(\frac{t}{T_T}\right)^2 - Q\left(\frac{t}{T_T}\right) + R \qquad (4.53)$$

In the limit as $t \rightarrow 0$, the total volume removed up to time t, V, is given by:

$$V = \int_0^t \left(P\left(\frac{t}{T_T}\right)^2 - Q\left(\frac{t}{T_T}\right) + R\right)U \, dt \qquad (4.54)$$

As $V = 0$ at $t = 0$, then:

$$V = \left(\frac{P}{3}\left(\frac{t}{T_T}\right)^2 - \frac{Q}{2}\left(\frac{t}{T_T}\right) + R\right) Ut \qquad (4.55)$$

Equations 4.53 and 4.55 are only valid for time periods less than the transition time, T_T. This is because the assumption that the fraction of oxide coverage, α, increases linearly with time can only be true in the severe wear mode. After the wear transition, the rate of increase of α may reduce as total oxide coverage is approached. No variation in the wear rate during this time should be observed; this is because the load-bearing areas are totally oxidised and further oxidation of non-contacting areas should not affect wear. The rate of agglomeration will reduce during mild wear when less debris is produced; it is therefore likely that oxidation via a diffusion mechanism may become more important. However, a change in the structure of the oxide was not observed in the one test run for many days in the mild wear regime.

4.3 Calculation of the wear volume during a reciprocating experiment

It is now possible to calculate the cumulative wear volume at any time during the running-in wear from equation 4.55. The experiment chosen for this analysis was one run at 290°C, with a mean sliding speed of 0.0368 ms^{-1} and a load of 22 N; this was the test which was repeated several times in order to investigate how the wear rate changed during the running-in period. As a result, experimentally determined wear volumes have been measured for tests stopped at six different times; the weight losses for each specimen and the decrease in specific wear rate as the experiment progressed are shown in figures 3.13 and 3.14.

If the wear is to be predicted, estimates of the wear constants K_{mm}, K_{oo} and K_{mo}, must be made. It is known that K_{mm} is much larger than K_{oo} and therefore in the severe wear mode, when metal-metal contact dominated, wear by oxide-oxide interaction was ignored. Wear from metal-oxide contact was also ignored for similar reasons; a value for K_{mo} is hard to determine, but is expected to be between K_{mm} and K_{oo}.

If figure 3.13 is redrawn on a larger scale, it is found that the average weight loss of one specimen in the first 100 seconds was about 1.25 mg. This was equivalent to a wear rate of 4.37×10^{-11} m^3m^{-1}. Using the Archard wear equation (91) and equation 4.36, the wear constant for metal-metal contact was calculated:

$$K_{mm} = 4.05 \times 10^{-3}$$

In two separate experiments, the transition occurred after 46.0 kcycles and 52.7 kcycles; the average time to transition was, therefore, 24675 seconds. The ambient temperature, T_{amb}, was 290°C or 563 K; the oxidation temperature, T_o, was estimated from the unidirectional sliding experiments. The excess

temperature, $T_o - T_s$, was about 200 K, but also slightly dependent upon the sliding speed; T_o was estimated to be 750 K.

The rate constants, $k_{T_{amb}}$ and k_{T_o}, were dependent upon the Arrhenius constant, A_L, and the activation energy, Q_L. Unfortunately, little work has been carried out to determine either value at any temperature. Most activation energies have usually been calculated from the results of static oxidation tests in which parabolic kinetics were found. However, a combined rate constant for the two types of oxidation can be calculated from the equilibrium mild wear rate. Once equilibrium was reached, the oxide thickness was constant, and assuming that all the debris was oxide, the rate of oxidation must equal the wear rate. The mild wear rate calculated in section 3.4.5 was 5×10^{-15} $m^3N^{-1}m^{-1}$ with a mean sliding speed of 3.68×10^{-2} ms^{-1} and a wear scar of 1.8×10^{-4} m^2. Therefore, the combined rate constant, k^*, was:

$$k^* = 1.18 \times 10^{-7} \text{ kgm}^{-2}\text{s}^{-1}$$

The remaining data necessary for the calculation of equation 4.55 are: $p_m = 2 \times 10^9$ Nm^{-2}; $\rho_o = 5.24 \times 10^3$ kgm^{-3} and $f = 0.3006$.

The increase in volume with time is:

$$V = 2.24 \times 10^{-22}t^3 - 3.32 \times 10^{-17}t^2 + 1.64 \times 10^{-12}t - 1.89 \times 10^{-14}t \quad (m^3) \quad (4.56)$$

or:

$$W = 1.17 \times 10^{-12}t^3 - 1.74 \times 10^{-7}t^2 + 8.48 \times 10^{-3}t \quad (mg) \quad (4.57)$$

where W = mean weight loss.

The t^3 and t^2 terms are calculated from the products involving P and Q respectively in equation 4.55. The final two quantities relate to metal-metal contact wear and combined oxidation respectively.

Equation 4.57 is plotted in figure 4.4; the

experimental points from 3.13 are also included. It can be seen that there is very good agreement between the theory and data.

However, the real test of the theory is its ability to predict the wear volumes of other experiments. Knowing the time to transition, the wear volume to transition, V_T, may be calculated from equation 4.55 when $t = T_T$; the equation simplifies to:

$$V_T = 1.203 \times 10^{-12} WUT_T - 1.89 \times 10^{-14} T_T \quad (m^3) \quad (4.58)$$

or:

$$W_T = 6.304 \times 10^{-3} WUT_T - 9.89 \times 10^{-5} T_T \quad (mg) \quad (4.59)$$

where W_T = mean weight loss to transition.

Table 4.3 presents a comparison of the actual and predicted weight losses for the first 30 experiments in Appendix 1 for which transition times were measured. The errors ranged from -61% to +146%, but for over half of the tests, were less than ±20%; the mean error was +13%. The larger errors generally occurred in tests with very long running-in periods and may have been due to the degree of oxide coverage at transition, α, being higher than normal in such tests. If experiments with the number of cycles to transition greater than 100,000 cycles were excluded (numbers 25, 27, 31, 33, 34), the mean error was +3%.

The theory did predict the weight loss in experiments with very dissimilar conditions; for example, the above equation was derived from data obtained from tests run at 36.8 mms^{-1} with a 22 N load, but was able to estimate weight losses from 73.6 mms^{-1}/41 N and 110.4 mms^{-1}/22 N experiments with errors of 20% and 3% respectively.

The main drawback of this theory is that it does not predict the duration of the running-in period.

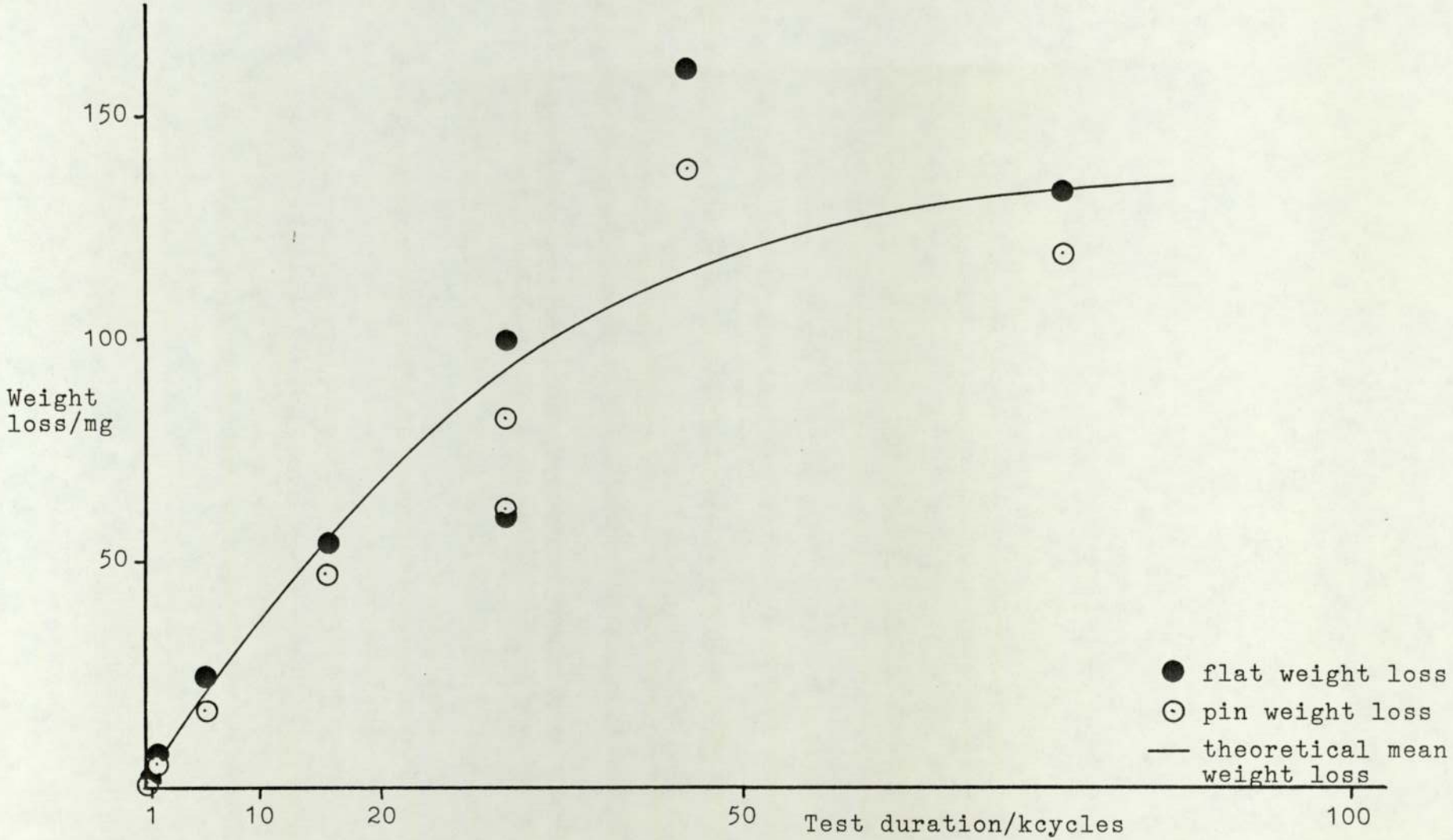

Figure 4.4 The theoretical increase in mean weight loss as an experiment progressed
(Empirical data from figure 3.13 are plotted)

test number	actual weight loss /mg	predicted weight loss /mg	error /%	test number	actual weight loss /mg	predicted weight loss /mg	error /%
1	4.50	8.83	+96	22	89.43	96.91	+ 8
2	12.25	9.82	-20	25	109.02	268.58	+146
3	80.00	65.52	-18	26	129.87	107.73	-17
4	9.43	12.27	+30	27	1129.98	1647.09	+46
6	31.78	25.70	-19	28	40.10	49.89	+24
7	5.71	4.01	-30	29	316.64	308.89	- 2
9	2.33	3.28	+41	30	358.89	288.97	-19
11	86.56	102.33	+18	31	647.99	779.83	+20
12	4.71	6.87	+46	32	341.00	447.07	+31
13	29.10	29.84	+ 3	33	906.36	1552.98	+71
14	12.25	17.10	+40	34	435.07	539.29	+24
15	10.45	4.09	-61	35	128.41	115.33	-10
16	110.59	63.24	-43	37	100.48	83.43	-17
18	75.79	86.01	+13	39	109.34	90.89	-17
21	167.44	174.58	+ 4	40	127.77	112.88	-12

Table 4.3 A comparison between the actual and predicted weight losses for several experiments

CHAPTER 5
DISCUSSION

5.1 Unidirectional wear at high speed

Two introductory series of experiments were carried out at sliding speeds of 0.5 ms^{-1} and 2.0 ms^{-1} in order to determine the general wear behaviour of the 9% chromium steel. Severe wear was the only form of wear at the slower speed but also occurred with loads less than 26 N at the higher sliding speed. At loads above this, mild or oxidational wear existed.

The specific wear rate (wear rate/load or w/W), calculated from the experiments run at different loads, was almost constant. This was because severe wear is a process that is solely dependent upon the amount of contact between specimens, and not upon any properties of or reactions involving the environment. At 0.5 ms^{-1}, the mean specific wear rate was 2.67×10^{-12} $m^3N^{-1}m^{-1}$ with a standard deviation of only 3.1×10^{-13} $m^3N^{-1}m^{-1}$ (11%). There was also high correlation between both the heat flow and bulk surface temperature, and load (figure 3.4) which implied that under conditions which did not involve reactions with the environment, the division of heat was independent of load. The heat flow down the pin is proportional to the load, which is, in turn, proportional to the real area of contact. The spread of wear rates and surface temperatures in mild wear experiments was greater because reactions with the environment were necessary. The results from slow speed experiments, and especially those carried out in impure carbon dioxide, were very dependent upon the environmental conditions.

There was a Welsh T_2 transition from severe to mild wear at 26 N with a sliding speed of 2 ms^{-1}. The average specific wear rate in the severe wear regime was

8.19×10^{-13} $m^3N^{-1}m^{-1}$ with a standard deviation of 1.54×10^{-13} $m^3N^{-1}m^{-1}$ (17%). The spread of the wear rate was much less for severe wear than for mild wear. The average specific wear rate in the mild wear regime was 4.95×10^{-15} $m^3N^{-1}m^{-1}$ with a standard deviation of 1.69×10^{-15} $m^3N^{-1}m^{-1}$ (34%). A wide range in wear rates was found by Quinn et al. (163) in their study of steels containing between 0% and 12% chromium. One steel, which contained 7.95% Cr and 0.30% C and was closest in composition to the steel used in this study (8.89% Cr, 0.11% C, 1.00% Mo), underwent a T_2-type transition at about 45 N; it has been found, however, that transition loads are dependent upon the wear test apparatus. Unlike the results described above, this 8Cr steel gave a wide range of severe wear rates averaging about 2×10^{-12} m^3m^{-1}. There may also have been a decrease in the wear rate with increasing load in the mild wear region. This dependence of specific wear rate on load was in agreement with the near-independence of the mild wear rate with load found in this work. It is possible that the variation in wear rate observed by Quinn may have been related to a change of oxide in the wear debris. More recent work in this laboratory (90, 129) has shown the existence of minor wear transitions within the mild wear regime associated with changes of oxide.

The ability of chromium steels to produce protective oxides may have caused this unusual behaviour. As the load increased within the mild wear regime, the surface temperatures increased along with the oxidation rate. It is possible then for the wear surface to be protected more at the higher loads and thus the wear rate reduce. It is known from static oxidation tests that addition of up to 8.5% chromium to iron is not beneficial and does not reduce the oxidation rate of the alloy to less than that of pure iron (44).

The idea that the protection afforded by the oxide

may increase with increasing load is supported by the microhardness measurements. The surface hardness of the severe wear specimens averaged 450 VPN (4.8 GPa); with loads in the range 29 N to 35 N, just above the wear transition, the surface hardness was about 520 VPN (5.5 GPa); hardnesses above 800 VPN (8.5 GPa) were recorded on specimens worn under loads greater than 49 N. Microhardness tests on taper sections revealed that the subsurface work-hardened layer was thicker at higher loads. This shows that stresses caused by the movement of the pin over the surface affect metal further into the pin specimen as the load on the pin increases. The subsequent formation of a modified surface layer has two effects. Equilibrium mild wear is achieved earlier at high load due to the necessary degree of work-hardening, essential for sustaining mild wear, occurring more quickly; in addition, the more highly work-hardened layers give the oxide greater stability, with the result that the lower disturbance of the surface at equilibrium results in a lower mild wear rate.

It is possible, but unlikely, that the surface and subsurface regions of specimens run at loads in the 25 N to 35 N range had not achieved the conditions normal during equilibrium mild wear. The tests were stopped about one hour after the wear rate had reached equilibrium; this occurred after about six hours if the load was 30 N, but after only 4 hours if the load was above 50 N. It was not, therefore, likely that the experimental time was responsible for the variation in surface hardness.

A summary of the wear behaviour in the mild wear regime follows. At loads just above the wear transition at 26 N, sufficient work-hardening takes place in the subsurface layers of the pin and disc to support an oxide layer. This oxide increases in thickness slowly due to the relatively low oxidation temperature at the

asperities. The modified surface layer is thin and its surface not significantly harder than that of a surface worn by severe wear. At much higher loads, about 50 N to 60 N, work-hardening occurs more quickly and the modified region goes deeper into the substrate. The oxidation temperature is higher and a thicker and more uniform oxide layer is produced. The harder surface is due to the increased work-hardening and not the presence of more oxide (oxide hardnesses were found in other experiments to exceed 1000 VPN).

The decrease in specific wear rate with increasing load is probably due to the thicker subsurface work-hardened layer allowing increased protection by the oxide.

5.2 Unidirectional wear at slow speed in air

Running-in times are not always measured in unidirectional sliding experiments because such tests are often run for the purpose of investigating equilibrium wear; this work, however, was carried out as a comparison for a series of reciprocating sliding experiments of which the running-in period was of most interest. These times, therefore, were noted in all slow speed unidirectional sliding tests and the running-in distances then calculated.

At 100°C, the distances provided an indication of the relative ease with which equilibrium mild wear was attained. Under a load of 22 N at a sliding speed of 55 mms^{-1} or 26 N at 37 mms^{-1}, the running-in distances were 2300 m (which took 692 minutes) and 1650 m (748 minutes) respectively; at a load of 31 N and a sliding speed of 19 mms^{-1}, the running-in distance was only 156 m (140 minutes). Experiments run using the same loads, but with sliding speeds that were 18 mms^{-1} greater, all produced equilibrium severe wear. The transition speeds at which equilibrium mild wear no longer occurred were estimated to be 60 mms^{-1} at 22 N, 42 mms^{-1} at 26 N and

30 mms^{-1} at 31 N. An empirical relationship between the loads and transition speeds was found:

$$U W^2 = 28.8 \qquad (5.1)$$

where U = sliding speed, (ms^{-1}).

All three series of experiments had a product of the $(load)^2$ and speed within 1.25% of this value. It is estimated from this equation that a transition would occur at 18 mms^{-1} with a load of 40 N, and at 8 mms^{-1} with 60 N. It is possible that the rate of energy input is related to the transition load. The product of load and speed is the rate of energy dissipation at the surface (having units of Js^{-1}). The equilibrium wear rate is proportional to load. Therefore the product of energy dissipation and wear rate is constant at the transition load for each sliding speed. The onset of severe wear occurs at the load for which the disturbance at the surface is great enough to prevent the formation of a stable oxide film; as the energy necessary to cause this disturbance is related to the energy dissipation, it is likely, when the rate of material removal or energy input exceeds a certain value, that severe wear results.

Welsh (50) also made a study of the variation of transition load with speed on a 0.52% C steel; he found a general decrease in the T_1 transition load as the speed increased from 0.017 ms^{-1} to 1 ms^{-1}. The product of $(load)^2$ and speed at each transition was not, however, constant. He also observed that an increase in hardness raised the transition load until, at a critical hardness, severe wear was no longer found. The T_1 transition occurs at the load at which the combined rates of oxidation and strain hardening are no longer able to outweigh the increasing disturbance of the severe wear process. Rosenberg and Jorden (164) postulated that an oxide film prevented severe wear whatever the steel hardness, but Welsh (165) observed that a lower hardness was necessary to support mild wear in air than in argon, nitrogen or hydrogen, which implied that the effect of oxidation and

work-hardening were complimentary; this was confirmed by the comparison of sliding in air and carbon dioxide carried out in this work.

The relative magnitudes of the effects of oxidation and work-hardening are dependent upon different sliding parameters; for example, oxidation at these slow speeds is dependent primarily upon the ambient temperature whereas the degree of work-hardening and wear are dependent upon the load and speed. The combined result of these influences shows that the running-in distance is dependent more upon the load and speed than upon the rate of oxidation under conditions in which the rate of work-hardening is very low.

A range of sliding speeds was also studied at 200°C. The running-in times decreased slightly with increasing speed. It is probable that all tests carried out at and above this temperature were in the mild wear regime below the T_1 transition. Experiments carried out under similar sliding conditions gave running-in times between 47 minutes and 86 minutes; it is unlikely that any variation in time is an indication of the closeness of the load or sliding speed to a transition load or speed. More highly disturbed surfaces are formed at high speeds which oxidise more easily at high temperatures; the total number of contacts during running-in wear increased with increasing speed which showed that the equilibrium between out-of-contact oxidation and wear was important and not the tribological oxidation at the asperities. Had the latter form of oxidation been the more important, the number of contacts during severe wear would have remained constant or decreased with an increase in sliding speed.

The mild wear rates were, in general, slightly higher than other unidirectional wear rates measured in this laboratory. Quinn et al. (166) recorded values between 2×10^{-13} m^3m^{-1} and 4×10^{-13} m^3m^{-1} for a B.S. EN8

steel sliding at 2 ms^{-1}. Wear per unit time, however, was about 100 times smaller for the experiments described in this thesis. This parameter is not usually considered; it is, however, relevant to sliding systems in which there can be as much as 17 seconds of static oxidation between successive contacts at one asperity on the disc. The experiments at 300°C show that significant oxidation can occur before equilibrium wear is established. At this temperature, the running-in times were all less than 15 minutes; mild wear usually occurred before the pin and disc were in full contact. The wear rate then reduced to such a value that often full contact over the wear track was never achieved during the remainder of the experiment. Thus, after many hours wear, the wear track showed both mild wear and the unworn shiny metal surface. Complete contact was rarely achieved immediately upon starting an experiment because of the difficulty in aligning the pin and disc. During experiments with longer running-in times, sufficient severe wear occurred to allow full contact between the pin and disc before the end of the running-in period. Mild wear then occurred uniformly across the wear track.

Mild wear was greatest at the lowest sliding speed, 18 mms^{-1}, at which speed there was very little variation in specific wear rate with load, and a decrease with increasing temperature. The ratio in wear rates between severe and mild wear, identified from the surface of the wear track, was about 4:1 at 100°C; this was much less than the ratio in the high speed room temperature experiments (100:1) or the reciprocating sliding tests (50:1). Another feature of the experiments carried out at 100°C was that a significant percentage of the debris was still metallic, even after several hours of mild wear. This suggests that it is not pure mild wear, but an oxidation-assisted form of severe wear. This could occur at slow speed when significant oxidation can take place

at the asperities between contacts, but insufficient oxidation is able to occur during asperity contact in order to allow 'normal' mild wear. It is, therefore, likely that for a fully protective oxide film to be formed, tribo-oxidation is essential.

These observations also suggest that the wear rate at very slow speeds may not be solely dependent upon the tribological conditions of the experiments. It is probable that the oxide is produced primarily by static or out-of-contact oxidation at the disturbed surface, rather than by tribo-oxidation at the asperities. Taper sections showed that the hardened layers were much less than the 50 μm to 70 μm layers found on high speed specimens, and therefore it is possible that the thin hardened layers were not able to support a stable oxide film alone; this statement is substantiated by the considerable proportion of ferrite found in the debris.

It is concluded that with very slow sliding speeds at 100°C, static oxidation occurs on the disturbed surface of the wear track; this has the effect of reducing the wear rate from that associated with severe wear and introducing oxide into the wear debris. A mixed mild-severe wear mode is the result.

At higher speeds, 37 mms^{-1} to 110 mms^{-1}, the wear rate increased with speed. The ratios between the wear rates at 18 mms^{-1} and 37 mms^{-1} at the three temperatures, 100°C, 200°C and 300°C, were 5, 2 and 0.5 respectively. This suggests that at 100°C there is a different mechanism at the slower speed and supports the mechanism postulated above. At the higher temperatures, however, the rate of oxidation is sufficient to support mild wear. The difference in wear behaviour at 100°C was also shown by the ratio of the wear rates at different temperatures; at 100°C, 200°C and 300°C, the ratios of the wear were 12:1:1 for 18 mms^{-1} and 5:1:2 for 37 mms^{-1} experiments. The results at the higher temperatures and higher sliding

speeds also showed a more constant specific wear rate with varying load; this is indicative that tribo-oxidation, dependent upon the contact area, which is, in turn, proportional to the load, is important.

Friction was always high at the start of an experiment, but reduced after a few minutes. Friction also dropped at the wear transition to equilibrium values between 0.8 and 1.3. These values were much higher than those measured during high speed mild wear (0.3 to 0.5). No systemic reason could be found to explain this difference; the method for determining the friction was the same for each set of experiments. The surfaces produced during the slow speed tests were very rough; quantitive talysurf measurements could not be made due to the excessive unevenness. It was this unevenness that resulted in the formation of a non-uniform oxide layer at the surface which may have been responsible for the higher friction values. Oxide layers produced by high speed sliding were always much smoother. Greenwood and Williamson (167), assuming that the real area of contact between two nominally flat metal surfaces was determined by the plastic deformation of their highest asperities, concluded that friction was related to surface topography rather than to the material properties. This idea would be supported by the experiments described above if the high friction was assumed to be caused by excessive ploughing. It has usually been found, however, that the ploughing term is small compared to the overall friction. It is probable that the high friction in these experiments is due to the mixed wear regime. These was a slight reduction in friction with increasing ambient temperature; it was also noted that the frictional values were generally slightly lower under sliding conditions which encouraged mild wear (high speeds or high disc temperatures). It would be expected that the mixed wear regime would be gradually replaced by a more usual form of mild wear as

the temperature increased.

Friction values decreased with increasing sliding speed. This may have again been due to the presence of a more uniform oxide layer.

5.3 Unidirectional wear at slow speed in carbon dioxide

The primary purpose of the reciprocating experiments was to study how the establishment of mild wear varied with the sliding conditions. In this series of unidirectional sliding experiments, particular emphasis was, therefore, placed upon discovering the temperature at which mild wear was just established using the loads and mean sliding speeds applicable to reciprocating sliding. Totally different specimen configurations were used for the two wear regimes even though the sliding parameters were similar.

No T_1 transition was found at any temperature as the speed was varied. However, as the ambient temperature was increased with the load and speed held constant, a change from severe to mild wear occurred at around 260°C. It is not possible to derive an equation similar to equation 5.1 because in any series of experiments at any one temperature, changes in the load or speed did not alter the equilibrium wear regime. This dependence upon temperature and not the sliding conditions suggests that out-of-contact oxidation is important.

The running-in times were dependent upon the sliding speed and temperature. As was found from the running-in times of the air experiments, mild wear was established more quickly as the temperature increased. Running-in times were between 3 hours and 15 hours at 261°C, but were less than 1 hour above 300°C. At temperatures at which mild wear was well established, 273°C and above, the transition to mild wear occurred after a longer time period, and a much longer sliding

distance, as the sliding speed increased from 20 mms^{-1} to 111 mms^{-1}. This shows that tribo-oxidation cannot be essential, at these temperatures, to the formation of mild wear; had this been so, the running-in times would have been almost independent of speed as both the rates of tribo-oxidation and material increase with sliding speed. A different variation with speed was observed at temperatures just above the transition temperature.

At 266°C, experiments were carried out with sliding speeds between 19 mms^{-1} and 157 mms^{-1}. Mild wear took longer to establish as the speed increased to 119 mms^{-1}, but less time when it was increased still further, showing that tribo-oxidation was becoming more important than static oxidation. The wear rates at sliding speeds above 110 mms^{-1} were all approximately 2.6×10^{-12} m^3m^{-1}, but were about three times greater at slower sliding speeds. This shows that the decrease was not due to a change in the oxide, which would have, in the event, been revealed by X-ray diffraction; this technique showed, instead, that α-$(Fe,Cr)_2O_3$ was the only oxide for all sliding conditions. In addition, there would have been a transition in the wear rate (of a factor of two or more) and the surface temperatures, as observed at transitions studied by other workers (168, 169); finally, a change in oxide would not have caused a gradual decrease in running-in time, but a sudden fall followed by an increase as the sliding speed increased still further.

The decrease in running-in time was due to more rapid oxidation at the asperities due to the higher surface and contact temperatures produced from the greater frictional heating at high sliding speeds. A similar variation was found in the reciprocating experiments carried out at 290°C and 300°C, and will be discussed in more detail later.

The equilibrium wear regime in carbon dioxide under conditions similar to those maintained during experiments run in air was severe for ambient temperatures up to 260°C; the wear rate decreased with increasing temperature. Mild wear was the equilibrium form of wear at higher temperatures and had a similar dependence on temperature. The oxidation rate would be expected to increase with temperature, and thus reduce wear. The variation of severe wear with temperature suggests that wear is dependent in some way upon oxidation; reference has been made above to an oxidation-assisted form of severe wear.

The specific wear rate in the severe wear regime of the high speed room temperature sliding experiments was almost independent of load. At the transition to mild wear, the wear rate reduced by a factor of about 100. No similar abrupt change occurred as the ambient temperature was increased in the slow speed experiments; this would suggest that the gradually increasing out-of-contact oxidation rate was as essential in determining the wear rate as was the rate of tribo-oxidation. Although other workers have carried out wear tests at widely-spaced elevated temperatures (90, 170), this is the first time that slow speed experiments have been carried out with gradually increasing ambient temperatures. These two changes would indicate the importance of out-of-contact oxidation more than any other series of tests. It is postulated from these results that significant oxidation must occur, presumeably on the disc which is open to the atmosphere for several seconds between contacts with the pin, to reduce the wear rate. Visual examination of the severe wear track revealed no oxide; X-ray analysis also failed to reveal any oxide in the debris. It was, however, possible that limited oxidation could occur on the disturbed surface and produce only a thin hardened layer; it is difficult to detect components that form less than 5% of mixtures

using X-ray diffraction (153). Similar observations were made about the wear rates when comparing the air tests run at 25°C/37 mms^{-1} and 100°C/72 mms^{-1}, 91 mms^{-1} or 109 mms^{-1}; the air test run at 25°C had the highest severe wear rate of all slow speed experiments.

The wear rate decreased slightly at any one temperature as the sliding speed increased. This was probably due to greater oxidation at the more highly disturbed surfaces; the bulk surface temperature was not significantly affected by the increase in speed.

The mild wear rate ranged from 6×10^{-13} m^3m^{-1} at the maximum ambient temperature, 350°C, up to 1×10^{-11} m^3m^{-1} just above the wear transition. All tests run at 261°C, and at 266°C with sliding speeds of 55 mms^{-1} or less, exhibited mild wear with a rate just less than that associated with severe wear. It is possible that the wear regime is a highly oxidation-assisted form of severe wear. It was often very difficult to determine whether wear was mild or severe; in general, the equilibrium regime was described as mild in tests when a wear transition was indicated by the linear voltage displacement transducer. It is somewhat of a misnomer to say that a wear transition occurs at or around 260°C because of the gradual increase in importance of out-of-contact oxidation. It is better to say that 261°C was the lowest temperature at which an oxide occurred in quantity both on the wear track and in the debris.

Tests run at 270°C and above, and the faster tests run at 266°C, had a much lower wear rate; this confirmed the theory suggested by the air experiments that mild wear and oxidised debris had two mechanisms of formation. Under these conditions, it is unlikely that out-of-contact oxidation is essential for initiating mild wear. It is likely, especially at the higher sliding speeds, that tribo-oxidation is becoming relatively more important.

A simple comparison between the wear rates in air and carbon dioxide cannot be made because there was often severe wear in one environment and mild wear in the other. This showed that the smaller oxygen partial pressure in the impure carbon dioxide (containing 0.1% oxygen) inhibited mild wear in the temperature range 100°C to 260°C. At 300°C, experiments were carried out using a 22 N load and at 37 mms^{-1} in each environment. In CO_2, the wear rate was 1.6×10^{-12} m^3m^{-1}; the experiment, carried out twice in air, gave an average wear rate of 1.8×10^{-12} m^3m^{-1}. This showed that only a small percentage of oxygen was necessary in the environment to sustain equilibrium mild wear. The running-in period, however, was about ten times as long in carbon dioxide, which indicated that more oxygen was necessary to initiate mild wear than to sustain it. It is possible that mild wear started at temperatues above 260°C may be sustained at lower temperatures; no experiments, however, were carried out to investigate this.

The dwell test carried out at 266°C supports this idea; the running-in time in this experiment was approximately one tenth of that expected in a normal continuously run test. This suggests that the presence of oxide on the specimen (formed in this example by the static oxidation during the 96 hour dwell period) can reduce the wear rate so that equilibrium mild wear is established more quickly.

The difference in running-in period but similarity of equilibrium wear rate also indicates that slow oxidation in a carbon dioxide-based environment, with little free oxygen present, can produce sliding behaviour similar to that caused by wear in air with a 20% oxygen content. The oxygen necessary to support mild wear may be in the form of O_2 molecules or O atoms. At the approximate oxidation temperature, 477°C or 750 K, only

one in 10^{16} molecules of oxygen has dissociated at equilibrium (171). It is, therefore, very unlikely that mild wear in any environment is initiated by free oxygen formed through dissociation of molecules; it is much more probable that the dissociation takes place at the metal-air interface and is assisted by the more reactive, highly disturbed metal surface. Adsorbed atoms and molecules have a different equilibrium constant from the same species in the gaseous state.

Similar calculations can be made concerning a carbon dioxide atmosphere. Having already shown that the reactive species are probably oxygen molecules (which are later adsorbed onto the metal surface), the equilibrium of most importance is:

$$CO_2 \rightleftharpoons CO + \tfrac{1}{2} O_2 \qquad (1)$$

One molecule in 10^{11} is dissociated at equilibrium at 750 K. It is again probable that dissociation occurs to a greater extent at or near the metal-gas interface. It is, however, possible that dissociation of the carbon dioxide occurs away from the metal surface, but that all the released oxygen reacts almost immediately with the metal, or is adsorbed onto it. Under these conditions, equilibrium would never be achieved and the rate of dissociation of carbon dioxide would be dependent upon the activation energy for the above reaction, and not its concentration at equilibrium.

Two further sources of oxygen must be considered. One is applicable to both air and carbon dioxide-based environments:

$$H_2O \rightleftharpoons H_2 + \tfrac{1}{2} O_2 \qquad (2)$$

One molecule of water in 10^{9} dissociates to give oxygen. This is a larger fraction than the fraction of carbon dioxide molecules that dissociated; the water vapour content was, therefore, important. Unfortunately,

this was measured neither for those experiments carried out in air, nor for those in carbon dioxide.

A final source of oxygen, not already considered but applicable to the carbon dioxide-based atmospheres only, was the oxygen impurity in the CO_2 gas. Analysis by gas chromatography indicated that the controlled atmosphere contained 0.1% of oxygen. Mention has already been made in Chapter 2 of the simple assembly of the specimen chamber, and of the cracks around the main drive bearing. As no positive pressure could be maintained inside the chamber with respect to the laboratory atmosphere, it is very likely that air diffused inwards past the bearing even though carbon dioxide was permanently being admitted to the chamber. Inward leakage could, therefore, have been the greatest source of oxygen in the carbon dioxide experiments.

The above calculations show that very little dissociation takes place independently in the gaseous state and because of this, it is very likely that the metal surface has an essential part to play in establishing mild wear.

There was little variation in friction with sliding conditions, but it was, however, slightly less in the mild wear experiments. This suggested that, within each wear regime, the real surface area, upon which friction was primarily dependent, did not vary significantly with speed. It must be noted that the real area of contact is related to the load and hardness of the specimens, and that no load variation was made in this series of experiments.

The slightly lower friction observed in the mild wear experiments run at high temperatures was due to the less rough oxidised surfaces. A similar relation was found when comparing the air experiments run at 100°C (severe wear) and 300°C (mild wear).

5.4 Unidirectional mild wear at high temperatures

Several oxidational wear theories have been proposed (62, 76); those originating from this laboratory have been primarily concerned with the prediction of the wear rate from studies of the wear surface and debris using good estimates of the asperity radius, the number of contacts, the oxide thickness and the oxidation temperature (78). The theoretical modifications to an earlier theory (77, 129) described in section 4.1, used the experimentally determined wear rate and other measurable parameters in an attempt to calculate the above four quantities. These variables were more difficult to calculate from the slow speed experimental data due to the heat conduction from the disc to the pin and the high ambient temperature.

The modified computer program produced ten sets of solutions, presented in table 4.2. An expression for the asperity radius was derived in terms of the oxide thickness, which was assumed to be 3 μm from scanning electron microscopy observations, and the heat conduction across the gap between the areas of the pin and disc not in contact, estimated to be 1.01 Js^{-1} in air and 1.29 Js^{-1} in carbon dioxide experiments. The number of contacts was calculated knowing the contact radius, load and hardness; finally, the oxidation temperature was determined using all the above values. This was always less than the maximum possible contact temperature, as calculated from the Archard 'one-spot' flash temperature (89) in the above ten sets of solutions.

In the majority of experiments, the computer program yielded either a negative contact radius or an excessively high oxidation temperature. The former error was probably due to the use of an incorrect estimate of the conduction from disc to pin, Q_C. Of the thirty-eight mild wear experiments, all but eight produced a valid set of answers at one particular value of Q_C. It was

quite likely that Q_C varied considerably from one experiment to another; there was, however, no way of measuring it. A higher rate of rotation of the disc (i.e. a higher sliding speed) would cause more air movement and thus more conduction; whether the non-contacting surfaces were metallic or oxidised would also affect the conduction; vibrations set up by the rotating machinery would change the distance between pin and disc. The amount of heat conduction seemed to have no systemic variation with the sliding conditions and it was, therefore, chosen to have just two values, one for the air and one for the carbon dioxide experiments. This, unfortunately, reduced the number of valid solutions to just ten.

The disc loses heat from all surfaces to the atmosphere and other parts of the wear apparatus as well as the pin. More heat will be lost to the atmosphere when the gas is disturbed and replaced by cooler gas; a more rapidly rotating disc would, therefore, lose more heat to the environment by convection, and thus comparatively less to the pin. However, heat loss to the pin is largest when the temperature difference between the pin and disc is greatest; this will occur at high sliding speeds when the part of the disc in contact with the pin has less time (during contact) for its temperature to fall towards that of the pin. This argument suggests that the disc loses more heat to both the atmosphere and the pin at high speeds; this was not the case because the quantity of energy input to the disc, in order to maintain its constant elevated temperature, did not have to be increased at such speeds.

It is also likely that the heat conduction increased with increasing ambient temperature because of the higher thermal conductivity of the gas between pin and disc. Unfortunately, the gradually changing nature of the wear surfaces and the sliding speed meant that no relation between disc temperature and Q_C could be derived.

The estimate of the heat conduction across the air gap was not the only source of error; the environmental conditions were not rigorously measured. An increase in the ambient temperature had the effect of reducing the heat transfer coefficient which, in turn, reduced the heat flow into the pin and the bulk surface temperature. Further errors were introduced since the properties of the environment, the steel and the oxide at elevated temperatures were not known and had to be estimated from room temperature data.

Only one oxide was encountered in this work, unlike some previous high speed sliding experiments at elevated temperatures (90) in which transitions within the mild wear regime were observed as the oxide changed from α-Fe_2O_3 to Fe_3O_4 and, at still higher oxidation temperatures, to FeO. In this work, $(Fe,Cr)_2O_3$ was the oxide produced by both normal mild wear or oxidation-assisted severe wear. A rate just less than that associated with severe wear was found under conditions in which in-contact or tribo-oxidation did not occur; the static or out-of-contact oxidation which gave rise to this type of mild wear was found most often at very slow sliding speeds. It is possible that, at these speeds, significant oxidation can occur in the 17 seconds during which the disc makes one complete revolution; insufficient oxidation takes place in this time to support mild wear; it would also take time for sufficient surface disruption to occur to be able to support a protective oxide film. All the oxide together with some metal is removed during contact in the running-in period resulting in a high wear rate and mixed debris.

The more usual form of mild wear is found at high temperatures and high sliding speeds. Under these circumstances, sufficient tribo-oxidation takes place to support mild wear; such oxidation occurs on the load-bearing asperities rather than the bulk surface and so

is more efficient at initiating mild wear. The debris is almost completely oxidised.

The effect of reducing the partial pressure of oxygen, by using a carbon dioxide environment, prevented mild wear in the temperature range, 100°C to about 260°C. The general behaviour, however, was very similar. The vast majority of the oxygen in the carbon dioxide environment came from impurities inevitably allowed into the specimen chamber due to its crude assembly. It would have been interesting to discover how the transition temperature would have varied had the sole source of oxygen been the dissociation of carbon dioxide. From the variation of dissociation constant with temperature (equilibrium 1) (171), calculations show that one molecule in 10^{15} would dissociate at the ambient temperature and one in 10^{11} at the oxidation temperature. One outcome of this would be a slightly higher oxygen concentration at the asperities, with the result that in-contact oxidation would become relatively more important compared to static oxidation; it would be possible that the latter form of oxidation may reduce to the extent that the severe form of mild wear may no longer occur.

5.5 Reciprocating wear

The overall behaviour of the reciprocating experiments was very similar to that of the unidirectional wear tests. Equilibrium severe wear was obtained below 275°C; equilibrium mild wear, the onset of which was dependent upon load and sliding speed, occurred at 290°C and above.

The T_1 and T_2 transitions that have been discussed in the preceding sections referred to changes in the equilibrium wear regime at a particular load or speed while other variables including ambient temperature were all held constant; varying the temperature while maintaining a constant load and speed would have been an equally valid alternative approach to studying the overall

wear behaviour of a steel. The time at which the transition from running-in severe wear to equilibrium mild wear was, however, of most interest in the reciprocating experiments. The ambient temperature at which equilibrium wear became mild is similar to a T_2 transition; just less than the transition temperature, equilibrium severe wear was observed and no running-in times could be recorded; at higher temperatures, equilibrium wear was mild and the times of wear transitions were recorded. A T_2-type transition was observed between 275°C and 290°C with a sliding speed of 37 mms^{-1}; mild wear was only observed at the higher temperature.

Experiments at 275°C were carried out at sliding speeds of 18 mms^{-1} (twice), 37 mms^{-1} and 148 mms^{-1}; transitions from severe to mild wear occurred after 34.7 kcycles and 37.8 kcycles at the slowest speed. The other experiments were run for 710 kcycles (99 hours) and 806 kcycles (28 hours) respectively; long tests were carried out to ensure that no transition occurred, however much delayed (the longest running-in time in this work was later found to be 36 hours (850 kcycles)). Hence a T_1 transition similar to that observed at 100°C in the unidirectional experiments run in air was observed at 275°C with reciprocating sliding in carbon dioxide; the transition speed was between 18 mms^{-1} and 37 mms^{-1} for a load of 22 N. Hurricks (72), in his study of fretting wear between room temperature and 200°C in air, made no mention of a change in equilibrium wear mode. The difference in wear behaviour may be due to the difference between reciprocating and fretting wear. In the latter form of wear, with a much smaller amplitude (typically 100 μm), it is very likely that debris will be trapped at the sliding interface, and may be oxidised in situ; the larger stroke of reciprocating wear is better at moving debris away from the wear scar, thus presenting new metal to the surface. Taylor (145) investigating

wear of an 18Cr8Ni steel in carbon dioxide has reported finding accumulations of debris at the edge of the contact area.

Mild wear occurred where the rate of oxide formation due to both out-of-contact and tribo-oxidation was equal to the rate of removal due to wear. This was not always easily confirmed by a superficial study of the wear rates. Section 3.4.4 described the decrease in the instantaneous severe wear rate during running-in. It was, therefore, not possible to compare the average wear rates as determined by the weight losses. For example, the four experiments described above had the following average specific wear rates: 3.83×10^{-13} $m^3N^{-1}m^{-1}$ and 4.11×10^{-13} $m^3N^{-1}m^{-1}$ at 18 mms^{-1}, 1.76×10^{-13} $m^3N^{-1}m^{-1}$ at 37 mms^{-1} and 9.17×10^{-13} $m^3N^{-1}m^{-1}$ at 148 mms^{-1}. These data give the impression that wear decreased significantly with increasing speed; the last two wear rates, however, referred to equilibrium severe wear and not the mean severe wear during running-in. Equilibrium severe wear is defined at the rate of wear established after the friction has achieved its steady state value; for long tests, this is approximately equal to the average wear rate as determined by the overall weight loss during the experiment. Running-in severe wear is the wear occurring before equilibrium is achieved and has a much higher wear rate than either form of equilibrium wear. The variation of wear with sliding speed will be discussed later.

The variation in running-in period with increasing sliding speed was studied in four series of experiments. At 450°C, the running-in distance was proportional to speed with the consequence that the running-in time was independent of sliding speed; the mean time, averaged over six experiments, in which the sliding speed varied by a factor of eight, was 32 minutes with a standard

deviation of about 3 minutes.

It can be seen that, at these ambient temperatures, the duration of sliding only, and not the speed of sliding, is important for the initiation of mild wear. Although oxidation is occurring both at the asperities and on the general wear surface, it is concluded that out-of-contact oxidation is taking place at such a rate that any tribo-oxidation present on the asperities is not essential to the onset of mild wear. The amount of surface disturbance and tribo-oxidation increase per unit time as the sliding speed increases. It will be shown that, under different sliding conditions, these parameters can be important in initiating mild wear.

Experiments were also carried out with a sliding speed of 37 mms^{-1} at 550°C. The running-in times were not significantly different from the time recorded in experiments run at 450°C. As the rate of out-of-contact oxidation will be greater at the higher temperature, some other surface parameter or property must be prohibiting mild wear from starting after a shorter running-in time; this is likely to be the presence or not of the subsurface work-hardened layer. The rate of work-hardening will be related to the number of cycles per unit time, or the sliding speed. Although, at 550°C, sufficient oxidation occurs in less than 30 minutes, it may still take about 30 minutes for a hardened layer of sufficient depth, necessary to support the oxide, to be produced. It is likely that shorter running-in times would be measured in high speed tests at 550°C; unfortunately, all three experiments carried out at this temperature had a sliding speed of 37 mms^{-1}.

Tribo-oxidation is never important in determining the onset of mild wear at these high temperatures. Skinner (67) has carried out a similar series of experiments and concluded that the start of mild wear could be explained by a change from plastic to elastic contact

mechanisms; this, however, may have been due to the lower ambient temperatures in his tests. Several workers including Kayaba (68), Taylor (145) and Stott (146) in their studies of high temperature fretting, have referred to a reduction in friction and a change in wear mechanism at one particular temperature; it is probable that true fretting experiments, with small strokes, high frequencies and easily trapped debris, more readily identify the temperature above which out-of-contact oxidation is sufficient to initiate mild wear.

Hardness measurements made on specimens exhibiting mild wear revealed the presence of a surface layer much harder than the bulk material. Two series of experiments were carried out at 290°C to determine how this layer varied in hardness during running-in. The results, shown in figure 3.18, indicate that, under a 22 N load, the hardened layer is formed almost immediately during the first minutes of the experiment; the transition to mild wear, however, occurred after about 6 hours. It is possible that sliding producing thin surface layers with a higher shear strength; these layers are disturbed due to the reciprocating motion and rapidly form into a hardened subsurface layer. It is likely that it then takes time for this subsurface layer to coalesce to form the uniform work-hardened layer capable of supporting the oxide; Waterhouse (147), in one of his studies of mild wear fretting at high temperature, proposed that a creep-resistant subsurface layer was necessary to support the oxide.

Figure 3.19 shows that, under a load of 41 N, it takes several hours for a hardened layer to grow to the thickness found on specimens exhibiting equilibrium wear; no mild wear was observed in this set of experiments. The different behaviour during the early stages of running-in was probably due to the wear being proportional to the load, but that the depth in the specimen disturbed

by the sliding motion did not increase linearly with load. It is, therefore, likely that the greater disturbance at this load caused the removal of some of the hardened material.

One 4 hour dwell test was carried out at 450°C; no reduction in sliding distance to transition was observed. This shows that a minimum sliding distance is necessary for the establishment of a stable oxide film. It is concluded that both a hardened subsurface layer and an oxide film are essential for equilibrium mild wear; the hardened layer may be produced from the work-hardening caused by the reciprocating motion, while the oxide may be formed by exposing the metal to an oxidising environment for a minimum period of time. It would seem from the results of the tests at 450°C, 550°C and the one dwell test that 3600 cycles of sliding and 30 minutes of oxidation at 450°C (which may be concurrent with the sliding) give the shortest running-in distance encountered in this work. High sliding speeds and ambient temperatures above 450°C would probably give shorter running-in times. Longer periods of oxidation are necessary at lower ambient temperatures. As the frequency and amplitude of the motion are held constant during each experiment, the distance prior to mild wear is proportional to the number of cycles to transition, N_T.

Very different running-in behaviour was observed in the other three series of tests, run under the following sets of conditions: 300°C/22 N, 290°C/22 N and 300°C/ 41 N. In the first of these series, the running-in distance increased until the,sliding speed was about 110 mms^{-1} at which point there was a slight decrease at still higher speeds; the running-in times were approximately constant at the lower speeds, but decreased at the higher speeds; This shows that out-of-contact oxidation cannot be solely responsible for the onset of mild wear. The rate of tribo-oxidation should increase with increasing sliding

speed; this would have the effect of increasing the total rate of oxidation so that the running-in period would shorten.

Similar trends in running-in were found in the remaining two series of experiments. The magnitude of the variation was, however, so much greater that both running-in times and distances increased at low frequencies, but decreased as the frequency was further increased. This indicates, under conditions in which the rate of out-of-contact oxidation is relatively much less than the rate of wear, that the rate of tribo-oxidation becomes more important in determining the onset of mild wear.

It is assumed that the combined rates of oxidation are only just greater than the rate of material removal under conditions that necessitate long running-in periods. This is only so during running-in; the oxidation rate will equal the wear rate under conditions of equilibrium mild wear irrespective of the sliding parameters. Scanning electron microscopy revealed that the oxide layer reached an equilibrium thickness during mild wear; this equilibrium was used in deriving the equation describing wear during running-in, described in Chapter 4. At very low sliding speeds, there are short running-in distances, approximately proportional to the speed, with the outcome that, at equilibrium, out-of-contact oxidation occurs at a rate equal to that of wear, and tribo-oxidation is negligible. At medium sliding speeds, the rate of material loss is greater, but the rate of static oxidation is unaffected by the increase in speed; much longer running-in periods, therefore, are the result. At high sliding speeds, the rate of wear increases still further in comparison to the rate of static oxidation, but, as tribo-oxidation now occurs at a rapid rate on the asperities, then the running-in period or distance decreases.

The change in mechanism of oxide production is confirmed when the results of the dwell tests are considered, together with the absence of any change in oxide. Out-of-contact oxidation must be the mechanism in each of the dwell tests during the period of dwell; it is likely, therefore, that it is also the primary mechanism of oxidation during the slow speed experiments. The running-in distance is approximately proportional to the speed at these speeds; this is indicated by a linear relationship between the number of cycles during running-in and sliding speed. The rate of material removal is likely to increase with speed due to the increasing disturbance at the surface; the surface must, therefore, be subject to another mechanism of oxidation, tribo-oxidation, or work-harden to form a more wear-resistant surface at high speeds, if the running-in distances decrease. No evidence for extra work-hardening was found from any of the microhardness measurements. Tribo-oxidation would be expected to occur more quickly at high speeds for two reasons; the contact temperature at the asperities would increase with the sliding speed, and there would also be more contacts per unit time. This explains why there is a large reduction in running-in time or distance as the sliding speed increases from about 110 mms^{-1} to 140 mms^{-1}.

The above discussion has centred upon how the running-in time or distance is dependent on the mechanisms of oxidation. The changes occurring at or near the metal surface will now be considered in more detail.

Scanning electron micrographs of worn surfaces have shown that the transition to mild wear occurred only after the majority of each wear scar was covered with a stable oxide film, the thickness of which was approximately 6 μm. Krause (135) also reported finding layers as thick as 7 μm; these were not homogeneous and therefore may have been an agglomeration as seen in this work. The

measured hardness values of the oxide were as high as 1320 VPN (14.1 GPa) compared to a bulk steel hardness of 280 VPN (2.9 GPa). Microhardness measurements on taper sections revealed that the oxide was supported by a hardened metallic layer (maximum value 450 VPN or 4.8 GPa) extending to a depth of 30 μm into the sample. Specimens worn for just a few hundred cycles showed that this metallic layer was formed almost immediately at the start of each experiment.

These observations are similar but not identical to those made by Hsu et al. (85) and Skinner (67). Hsu suggests that two layers are necessary to support a stable surface film; in this work, however, the hardness of the steel decreased gradually with increasing depth. Skinner (67) also carried out short experiments that were stopped before any transition could occur, similar to those described in section 3.4.4. He reported finding subsurface hardnesses as high as 750 VPN (7.9 GPa) on specimens worn for just 50 seconds; this is attributed to oxide formation and subsequent incorporation into a highly disrupted surface layer. No such early oxidation was observed in the experiments described in this thesis, and it is suggested that a hardened metallic layer only is produced almost immediately upon commencing sliding, which then provides a stable base on which the oxide film may form. A reduced wear rate, an outcome of the hardened layer, leads to increasing surface oxidation until the oxide coverage is of sufficient area and thickness to permit mild wear.

Scanning electron microscopy gave further evidence confirming the mechanism of plateau formation. Figure 3.22(b) shows that the edge of a plateau is made up of an agglomeration of small particles of wear debris. X-ray diffraction analyses show that the oxide in the debris is the rhombohedral mixed oxide, $(Fe,Cr)_2O_3$, in which the oxygen concentration is 60%. This percentage

is in agreement with the value obtained by using auger spectroscopy. Figure 3.31 shows the decrease in oxygen concentration as the surface was progressively etched; the total depth analysed during the 2265 minutes of argon ion bombardment was about 5 μm and approximately equal to the total oxide thickness. The results show that the oxygen concentration decreases from 55%±10% at the surface to 20%±10% close to the plateau-metal interface; the gradual decrease in concentration is very different from the more sudden fall on oxygen concentration at a particular depth from the surface, observed in the unidirectional sliding experiments in this work (figure 3.32) and also by Sullivan and Athwal (90). Toth (137) considered that the surface layer was a solid solution of oxygen in metal as well as oxide; in principle, auger spectroscopy is able to characterise the chemical environments of each of the elements present (172, 173). No atomic oxygen was identified in this work.

All of the above results give an indication of the surface changes during the running-in period. Wear debris formed during the initial stages will consist primarily of metal, and will, being formed first, be more likely to be found at the bottom of each plateau; as the experiment progresses, increasing amounts of oxide will be produced and incorporated into the plateau until, at the surface of the plateau, the debris will comprise of oxide only at the onset of mild wear.

Chapter 4 developed a surface model which described how the wear varies during running-in, and calculates the cumulative wear to transition. The change from primarily metal-metal contact in the early cycles to primarily oxide-oxide contact during equilibrium mild wear formed the basis of the model. Figure 4.4 shows that the theory gives good agreement between the predicted material removal during an experiment and empirically determined values.

The measured total weight losses during each of the experiments for which calculations were made, were close to the weight losses predicted by the surface model. It is, therefore, likely that correct assumptions were made about the oxidation temperature, the rate constant for oxidation and the degree of oxide coverage necessary to support mild wear. Although it is probable that the oxidation temperature is the same, under similar sliding conditions, for both reciprocating and unidirectional sliding, the rate of oxidation was estimated from equilibrium mild wear when less agglomeration was occurring. Another approximation which has not produced significant error was considering the wear constant for metal-metal contact only during running-in; metal-oxide wear and oxide-oxide wear may not have been negligible during the later stages of running-in.

It is observed and predicted by the surface model that, in general, the wear rate decreases with increasing speed; this is because, as the running-in distance lengthens, the reduced severe wear rate caused by the presence of a work-hardened and partially oxidised surface occurs for a greater proportion of the total running-in period.

Another outcome of the varying running-in wear is the increase in mean wear rate occurring with an increase in ambient temperature. The greater oxidation rate at the higher temperature results in increased protection of the specimen surfaces; this parameter, however, does not reduce the mean wear rate due to the reason described in the preceding paragraph.

In summary, equilibrium severe wear occurs below 275°C, and equilibrium mild wear above 275°C. At 450°C and above, out-of-contact oxidation is the primary oxidation mechanism for all sliding speeds. At temperatures around 300°C, however, the running-in distance is dependent upon the balance between oxidation and wear;

at slow speeds, oxidation is mainly out-of-contact, and at high speed when disturbance caused by sliding is much greater, tribo-oxidation is essential for mild wear. At the intermediate sliding speeds of about 110 mms^{-1}, running-in times are much longer than in other experiments because the combined rates of out-of-contact oxidation and tribo-oxidation are only just greater than the rate of material removal during running-in.

CHAPTER 6
CONCLUSIONS

Experiments have been carried out using both unidirectional and reciprocating wear test apparatus to investigate factors affecting the transition from severe to mild wear during the running-in of a 9% chromium steel in atmospheres of air and carbon dioxide. The load applied was usually either 22 N or 41 N; the ambient temperature ranged from room temperature to 550°C with the majority of experiments being carried out in the range 250°C to 300°C; the mean sliding speed varied from 18 mms^{-1} to 160 mms^{-1}.

Unidirectional sliding experiments have been carried out by several other workers, but under conditions in which the rate of static or out-of-contact oxidation was much less than that of tribo-oxidation. A computer program has been written which takes into account the properties of the environment at elevated temperatures.

The program showed that some estimate of the heat conduction, Q_C, from the disc to the pin across the air gap had to be made if a self-consistent set of surface parameters (asperity radius, number of asperities, oxidation temperature and oxide thickness) was to be calculated. Many estimates of the value of Q_C were made; it was usually possible to select at least one value such that the oxidation temperature was consistent with the presence of the rhombohedral oxide found in the debris, and which was also less than the maximum temperature as predicted by Archard's approach (89).

It was not possible to relate the best value of Q_C with the sliding conditions (load, sliding speed, ambient temperature and environment), and so, rather than to postulate a different arbitrary value for each experiment,

just two values were chosen, one being applicable to each environment.

It was possible to form ten valid sets of solutions, four in air and six in carbon dioxide. More solutions were obtained at higher sliding speeds due to the error introduced in estimating the heat flow due to conduction being greater when it formed a large proportion of the total heat flow down the pin.

Mild wear was found in carbon dioxide environments with temperatures above 260°C. At 300°C, running-in periods were approximately ten times longer for those experiments run in carbon dioxide than those run in air. As the oxygen concentration in the carbon dioxide atmosphere was much less than one tenth of its concentration in air, it was concluded that the onset of mild wear occurred after the specimen surfaces had reached a certain condition, rather than having reacted with a particular volume of oxygen; mild wear was found on surfaces upon which an oxide layer covered the majority of the wear scar. This layer had to be supported by a work-hardened metallic layer approximately 30 μm deep in order to withstand the rigours of wear; the oxide was produced by out-of-contact or static oxidation on the general wear surface, or in-contact or tribo-oxidation at the asperities. A balance between material removal and out-of-contact oxidation was necessary to allow equilibrium mild wear, with tribo-oxidation being essential at high sliding speeds only.

Reciprocating sliding experiments were carried out in a slightly purer carbon dioxide environment. This had the effect of raising to 275°C the temperature at which mild wear became the equilibrium wear regime. The general wear behaviour, however, was similar; at temperatures just above 275°C, it was postulated that the primary mechanism of oxidation was out-of-contact oxidation at low speeds, and tribo-oxidation at high

speeds (above 110 mms^{-1}). At ambient temperatures above 450°C, out-of-contact oxidation only was found; tribo-oxidation was not significant at these temperatures with the sliding speeds maintained in this work.

Major differences were found in the ways in which the oxide plateaux, necessary for mild wear, were formed under unidirectional or reciprocating sliding. It was likely that the differences were due both to the mode of sliding and the angle of the sliding interface with respect to the vertical. The reciprocating sliding interface was horizontal whereas the unidirectional sliding interface was vertical; it was, therefore, much more likely that reciprocating sliding debris remained on the flat specimen and then agglomerated and compacted to form plateaux. It was also more difficult for the loose debris to move away from the middle of the wear scar as the reciprocating motion would tend to make such particles roll to and fro. Loose debris would be able to fall off the disc in the unidirectional sliding experiments, and would more easily get moved to the edge of the wear track. Diffusion-produced oxide plateaux were then grown in the absence of surface debris.

It was found, under reciprocating sliding, that a transition occurred when the majority of the surface was covered with stable plateaux, comprising mainly of oxide. The average thickness was about 6 μm, and the metal content increased with increasing depth into the specimen; the plateaux were supported by a work-hardened layer with an approximate thickness of 30 μm. It could be seen that the plateaux consisted of an agglomeration of smaller wear particles, compacted together. The surfaces of plateaux generated by either unidirectional or reciprocating sliding appeared very similar; the mode of sliding, however, could be deduced from the edge of the plateaux. Reciprocating sliding plateaux had edges comprising of small compacted particles; diffusion-produced

plateaux found on unidirectional pins had smoother edges.

A surface model was developed in order to explain the relative rates of material removal and oxide formation during a reciprocating experiment, leading to a transition from severe to mild wear. Good agreement was achieved between the predicted volumes of running-in debris and empirically determined values.

The oxidational wear equation for unidirectional wear, originally derived by Quinn (76) and many others (77, 78) was modified to take into account high ambient temperatures, heat flow from a hot disc and much slower sliding speeds. Only limited success was forthcoming due to the very approximate estimates of the environment temperatures around the pin, and in the gap between pin and disc, and of the heat conduction from disc to pin; nevertheless, ten sets of self-consistent surface parameters were calculated.

It would be very advisable to measure the environment temperature, and to maintain a purer and more constant carbon dioxide atmosphere around the pin and disc should this work be continued.

During the course of this research, a C.E.G.B. research group based at Leatherhead devised a method by which samples of steel may be cut from a steam-header in a turbine, and then subjected to accelerated testing (172). At present, this method is only applied to conventionally-fueled power stations. It is now possible, therefore, to compare materials subject to normal operating conditions for ten or more years with the test specimens worn in the experiments described in this thesis. It is important to discover whether the results from accelerated tests wholly in the laboratory reflect the real wear of the materials in use.

The effect of impurities in the atmosphere should also be further studied; there was always some oxygen in the carbon dioxide-based environments in this work. In

addition, the C.E.G.B. uses a coolant gas of carbon dioxide with some carbon dioxide plus traces of methane, hydrogen and water vapour. It is desirable that the effect of these gases on wear also be investigated.

APPENDIX 1

Table A1 presents the results of all the reciprocating experiments in chronological order, and includes reference to any unusual features in any of the tests. The accuracy with which each measurement was made is described below.

The frequency was first measured using damaged pin and disc specimens before the start of each experiment. It was checked using the correct test specimens at the start of each run, and rechecked during the longer tests. It was found to vary by less than one cycle per minute at low frequencies (less than 2 Hz), and by about one cycle in two hundred cycles at frequencies above 4 Hz.

The mean speed was calculated from the frequency and the stroke. The latter was set to 9.20 mm for the first 55 experiments, after which a worn crank had to be replaced. The stroke was 9.26 mm for all the later tests.

The load was applied by weights hung under the wear test apparatus. The weights were calibrated by measuring the upward force of the flat on the pin using a Newtons gauge. The load calibration was accurate to within 2%.

The temperature was controlled by a thermocouple immediately above the pin. It was unlikely that the temperature variation was more than $1^{o}C$ due to the metal test apparatus acting as a very large heat sink. The thermocouple reading was accurate to within $2^{o}C$.

The number of cycles in each test was the product of the frequency and the test time; the latter quantity was measured, for all tests except the very long test and the dwell tests, by a stop clock accurate to within 1%.

The accuracy with which N_T was determined was dependent upon the friction variation in each experiment. For this reason, each value has its own error in the table below.

The weight loss was determined using a balance sensitive to 0.01 mg. Each specimen was weighed a minimum of three times before and after the test; the mean reading was calculated. The weight loss, therefore, has an error of 0.02 mg.

The remaining columns in the table below may be calculated from preceding data.

Test number	Frequency /Hz	Sliding speed /mms^{-1}	Load /N	Temperature /°C	Test duration, N /kcycles	N_T /kcycles	Specimen weight loss, pin /mg	Specimen weight loss, flat /mg	Total sliding distance /m	Mean wear rate, K /m^{3}N^{-1}m^{-1}	Mean wear rate to transition, K_T /m^{3}N^{-1}m^{-1}
1	2	36.8	22	450	201.6	3.6±0.25	0.99	8.01	3709	7.21×10^{-15}	3.63×10^{-13}
2	2	36.8	22	450	9.0	4.0±0.25	5.63	18.88	165.6	4.40×10^{-13}	9.89×10^{-13}
3	2	36.8	22	300	50.4	26.7±1	50[a]	110[a]	927.4	5.12×10^{-13}	9.67×10^{-13}
4	2	36.8	22	550	7.2	5.0±0.25	8.81	10.04	132.5	4.29×10^{-13}	6.04×10^{-13}
5[b]	2	36.8	22	450	37.6	0.013	-0.26	0.13	691.1		
6	2	36.8	41	450	43.2	5.5±0.25	22.73	40.83	794.9	1.26×10^{-13}	9.89×10^{-13}
7	2	36.8	11	450	43.2	3.3±0.25	3.19	8.22	794.9	8.54×10^{-14}	1.12×10^{-12}
8	2	36.8	11	450	343.8	3.0±0.6	-2.18	-1.73	6326		
9	2	36.8	11	550	4.9	2.7±0.3	1.36	3.30	90.16	3.07×10^{-13}	5.57×10^{-13}
10[b]	2	36.8	22	450	195.8	0.011	-0.50	-0.02	3603		
11	2	36.8	22	300	64.2	41.7±2	30.01	143.10	1181	4.35×10^{-13}	6.70×10^{-13}
12	2	36.8	22	550	36.0	2.8±0.25	5.74	3.67	662.4	4.22×10^{-14}	5.43×10^{-13}
13	6	110.4	22	450	21.6	12.0±0.5	24.38	33.81	397.4	4.35×10^{-13}	7.83×10^{-13}
14	4	73.6	22	450	14.4	6.9±0.5	5.29	19.21	265.0	2.75×10^{-13}	5.73×10^{-13}
15	1	18.4	22	450	3.6	1.7±0.1	7.30	13.61	66.24	9.37×10^{-13}	2.11×10^{-12}
16	1	18.4	22	300	31.9	26.3±2.5	103.65	117.52	587.0	1.12×10^{-12}	1.36×10^{-12}
17[c]				300			-0.03	-0.23			
18	4	73.6	22	300	36.0	34.7±1.5	67.36	84.22	662.4	6.80×10^{-13}	7.05×10^{-13}
19	1	18.4	22	200	90.2		165.66	206.77	1660	6.66×10^{-13}	

Table A1 The conditions and measured wear parameters of the reciprocating sliding experiments

Test number	Frequency /Hz	Sliding speed /mms^{-1}	Load /N	Temperature /°C	Test duration, N /kcycles	N_T /kcycles	Specimen weight loss, pin /mg	Specimen weight loss, flat /mg	Total sliding distance /m	Mean wear rate, K /m^{3}N^{-1}m^{-1}	Mean wear rate to transition, K_T /m^{3}N^{-1}m^{-1}
20	2	36.8	22	200	179.4		173.74	216.69	3301	3.51×10^{-13}	
21	6	110.4	22	300	118.1	70.2±2	161.67	173.21	2173	4.58×10^{-13}	7.70×10^{-13}
22	4	73.6	22	300	63.4	39.1±0.25	83.65	95.21	1167	4.55×10^{-13}	7.39×10^{-13}
23	6	110.4	22	200	520.9		327.98	368.87	9585	2.16×10^{-13}	
24	4	73.6	22	200	360.0		235.92	243.74	6624	2.15×10^{-13}	
25	6	110.4	22	300	156.2	108.0±1	101.36	116.67	2874	2.25×10^{-13}	3.26×10^{-13}
26	2	36.8	22	300	65.2	43.9±1	123.74	136.00	1200	6.43×10^{-13}	9.55×10^{-13}
27	6	110.4	41	300	578.9	350 ±100[d]	1140.67	1119.31	10652	3.34×10^{-13}	5.53×10^{-13}
28	6	110.4	11	300	54.0	40.7±1	34.93	45.27	993.6	4.80×10^{-13}	6.36×10^{-13}
29	2	36.8	41	300	83.3	66.1±3	316.14	317.13	1532	6.51×10^{-13}	8.20×10^{-13}
30	1	18.4	41	300	95.4	62.5±2.5[e]	355.89	361.89	1755	6.44×10^{-13}	9.83×10^{-13}
31	4	73.6	41	300	327.4	166.0±10	658.83	637.15	6024	3.39×10^{-13}	6.68×10^{-13}
32[f]	6	110.4	41	300	498.6	95 ±15	362.12	319.88	9174	1.17×10^{-13}	6.14×10^{-13}
33	6	110.4	41	300	583.2	330 ±5[e]	934.12	878.60	10731	2.66×10^{-13}	4.70×10^{-13}
34	3	55.2	41	300	135.9	115 ±5[e]	423.09	447.05	2501	5.48×10^{-13}	6.48×10^{-13}
35	2	36.8	22	300	2764.8	47 ±1[e]	122.57	134.24	50872	1.50×10^{-14}	8.82×10^{-13}
36	1	18.4	22	250	259.2		237.92	262.92	4769	3.12×10^{-13}	
37	1	18.4	22	275	84.6	34.7±1	97.91	103.05	1557	3.83×10^{-13}	9.35×10^{-13}
38	2	36.8	22	275	709.8		369.74	404.55	13060	1.76×10^{-13}	

Table A1 (continued)

Test number	Frequency /Hz	Sliding speed /mms^{-1}	Load	Temperature /°C	Test duration, N /kcycles	N_T /kcycles	Specimen weight loss, pin /mg	Specimen weight loss, flat /mg	Total sliding distance /m	Mean wear rate, K /m^{3}N^{-1}m^{-1}	Mean wear rate to transition, K_T /m^{3}N^{-1}m^{-1}
39	1	18.4	22	275	86.0	37.8±1	103.38	115.29	1582	4.11×10^{-13}	9.34×10^{-13}
40	2	36.8	22	290	75.6	46 ±2	119.62	135.92	1391	5.46×10^{-13}	8.97×10^{-13}
41	6	110.4	22	290	605.2	400 ±100[d]	245.31	239.39	11136	1.29×10^{-13}	1.96×10^{-13}
42	4	73.6	22	290	81.6	68 ±3[e]	76.38	88.85	1501	3.27×10^{-13}	3.92×10^{-13}
43	1	18.4	22	290	33.8	31.0±1	78.76	92.00	621.9	8.16×10^{-13}	8.89×10^{-13}
44	5	92.0	22	290	139.2	125 ±10	94.46	98.59	2561	2.24×10^{-13}	2.49×10^{-13}
45	2	36.8	22	290	15.0		47.43	54.04	276.0	1.09×10^{-12}	
46	4.5	82.8	22	290	106.7	103.7±0.5	100.73	100.32	1963	3.04×10^{-13}	3.13×10^{-13}
47	5.5	101.2	22	290	189.8	120 ±10	90.74	96.57	3492	1.59×10^{-13}	2.52×10^{-13}
48	6.5	119.6	22	290	146.3	100 ±5	106.73	126.30	2692	2.57×10^{-13}	3.76×10^{-13}
49	6.5	119.6	22	300	140.4	108.8±0.5	149.91	163.78	2583	3.61×10^{-13}	4.65×10^{-13}
50	6	110.4	22	290	565.2	540.0±1	199.44	201.60	10400	1.15×10^{-13}	1.20×10^{-13}
51	6.5	119.6	22	290	561.6	285 ±10	129.88	117.09	10333	7.09×10^{-13}	1.40×10^{-13}
52	6.5	119.6	22	290	214.9	180 ±2	65.72	59.73	3954	9.43×10^{-14}	1.13×10^{-13}
53	2	36.8	22	290	30.0		63.11	60.47	552.0	6.65×10^{-13}	
54[f]	6.5	119.6	22	300	117.0	38.0±2	46.10	49.34	2153	1.32×10^{-13}	4.05×10^{-13}
55[f]	6.5	119.6	41	300	3210.1	71 ±2[e]	201.11	171.86	59066	9.94×10^{-15}	4.50×10^{-13}
56	5	92.6	41	300	432.0	302 ±2[e]	745 75	848.25	8001	3.14×10^{-13}	4.49×10^{-13}
57	7	129.6	22	300	126.0	80 ±10	112.61	102.32	2334	2.71×10^{-13}	4.27×10^{-13}

Table A1 (continued)

Test number	Frequency /Hz	Sliding speed /mms^{-1}	Load /N	Temperature /°C	Test duration, N /kcycles	N_T /kcycles	Specimen weight loss, pin /mg	Specimen weight loss, flat /mg	Total sliding distance /m	Mean wear rate, K /m^{3}N^{-1}m^{-1}	Mean wear rate to transition, K_T /m^{3}N^{-1}m^{-1}
58	7	129.6	22	290	100.8	70 ±2[e]	86.83	95.74	1867	2.90×10^{-13}	4.18×10^{-13}
59	7	129.6	41	300	1806.0	430 ±10[e]	947.96	956.54	33447	8.97×10^{-14}	3.77×10^{-13}
60	7.5	138.9	22	290	121.5	103 ±1	112.41	127.65	2250	3.17×10^{-13}	3.74×10^{-13}
61	2	37.04	22	290	5.0		17.17	24.55	92.6	1.34×10^{-12}	
62	7.5	138.9	22	300	54.0	49 ±1	63.59	73.25	1000	4.06×10^{-13}	4.48×10^{-13}
63	7.5	138.9	41	300	648.0	315 ±10[e]	761.76	674.52	12001	1.88×10^{-13}	3.88×10^{-13}
64	6.5	120.4	41	300	1667.3	525 ±70[e]	995.15	1019.89	30878	1.03×10^{-13}	3.26×10^{-13}
65	2	37.04	22	290	45.0		138.51	159.75	833.4	1.06×10^{-12}	
66[g]	2	37.04	22	290	4800.0[h]	52.7±1	214.43[i]	153.55[i]	86118[i]	1.27×10^{-14}[i]	
67	8	148.16	41	300	691.2	210 ±10	530.68	514.25	12801	1.29×10^{-13}	4.23×10^{-13}
68	8	148.16	41	300	242.9	190 ±2	711.51	620.26	4499	4.66×10^{-13}	5.96×10^{-13}
69	6.5	120.4	41	300	2129.4	850 ±50	1707.01	1773.97	39436	1.39×10^{-13}	3.48×10^{-13}
70	8	148.16	22	450	28.8	18.2±0.5	15.72	27.13	533.4	2.39×10^{-13}	3.78×10^{-13}
71	2	37.04	22	290	1.0		7.14	7.80	18.52	2.40×10^{-12}	
72	2	37.04	22	290	30.0		83.42	99.75	555.6	9.79×10^{-13}	
73	8	148.16	22	275	806.4		236.64	224.34	14935	9.17×10^{-14}	
74	6.5	120.4	41	300	200.0		147.37	160.71	3704	1.31×10^{-13}	
75	6.5	120.4	41	300	300.0		162.71	142.37	5556	8.65×10^{-14}	
76	6.5	120.4	41	300	400.0		185.61	174.65	7408	7.66×10^{-14}	

Table A1 (continued)

Test number	Frequency /Hz	Sliding speed /mms^{-1}	Load /N	Temperature /°C	Test duration, N /kcycles	N_T /kcycles	Specimen weight loss, pin /mg	Specimen weight loss, flat /mg	Total sliding distance /m	Mean wear rate, K /m^{3}N^{-1}m^{-1}	Mean wear rate to transition, K_T /m^{3}N^{-1}m^{-1}
77[j]	6.5	120.4	41	300	500.0		308.27	315.05	9260	1.06×10^{-13}	
78[j]	6.5	120.4	41	300	100.0		436.14	460.57	1852	7.62×10^{-13}	
79[j]	2	37.04	22	290	0.1		0.84	2.91	1.85	6.03×10^{-12}	
80[j]	6.5	120.4	41	300	100.0		294.55	312.92	1852	5.16×10^{-13}	
81[j]	2	37.04	22	290	100.0		50.93	66.92	1852	1.89×10^{-13}	
82[j]	2	37.04	22	290	100.0	14 ±2[e]	59.98	74.72	1852	2.16×10^{-13}	1.54×10^{-12}
83[j]	2	37.04	22	290	200.0	14 ±2[e]	64.33	74.39	3704	1.11×10^{-13}	1.59×10^{-12}
84[k]	6	111.1	22	290	80.0		73.19	84.49	1482	3.16×10^{-13}	
85	6.5	120.4	41	300	100.0		216.18	199.21	1852	3.53×10^{-13}	
86	2	37.04	22	290	200.0	[l]	202.51	215.97	3704	3.36×10^{-13}	
87	6.5	120.4	41	300	500.0		332.32	320.68	9260	1.11×10^{-13}	
88	6	111.1	22	290	100.0	[l]	152.85	167.15	1852	5.13×10^{-13}	
89	2	37.04	22	290	100.0	30.0±2[e]	119.08	138.67	1852	4.13×10^{-13}	1.38×10^{-12}
90[m]	6.5	120.4	41	300	70.0	50.0±0.25	139.47	143.39	1296	3.44×10^{-13}	4.81×10^{-13}
91[n]	6.5	120.4	41	300	10.0		54.76	57.47	185.2	9.54×10^{-13}	
92[o]	6	111.1	22	290	60.0	31.0±1	32.88	40.22	1111	1.95×10^{-13}	3.78×10^{-13}
93	9	166.7	41	300	162.0	151 ±10	452.26	383.94	3000	4.39×10^{-13}	4.71×10^{-13}
94[p]	6	111.1	22	290	400.0	300 ±50[e]	196.19	200.53	7408	1.59×10^{-13}	2.12×10^{-13}
95[n]	6	111.1	22	450	16.4	12.5±0.25	18.91	27.66	303.7	4.55×10^{-13}	5.97×10^{-13}

Table A1 (continued)

Notes

a) Weight loss approximate due to faulty balance

b) Experiment carried out in air at atmospheric pressure

c) Short static oxidation test; the specimens were heat to 300°C for 5 hours in carbon dioxide

d) Transition occurred overnight

e) Wear transition indicated by L.V.D.T. and not by decrease in friction

f) Some air admitted to the specimen chamber accidentally

g) The experiment was stopped soon after the wear transition in order to weigh the specimens, and empty the debris collector

h) 1st run 150 kcycles; 2nd run 4650 kcycles

i) Refers to 2nd run only

j) CO_2 cylinder had impurity of 0.7% O_2

k) Dwell test; 19 dwells

l) No wear transition identified

m) Dwell test; 6 dwells

n) Dwell test; 1 dwell

o) Dwell test; 5 dwells

p) 750 hours pre-heat before the wear test

Table A1 (conclusion)

APPENDIX 2

The program below uses an iterative technique to calculate the asperity radius (R1), the oxide thickness (TH), the number of asperities (N) and the oxidation temperature (TF) given the experimental conditions.

The program is written in BASIC for a Commodore PET. The ample REM statements within the program explain its operation.

```
1000 REM   OXIDATIONAL WEAR  PROGRAM  TO
1010 REM   SOLVE  THE  OXIDATIONAL  WEAR
1020 REM   EQUATION BY A FULL  ITERATIVE
1030 REM   TECHNIQUE.
1040 REM
1050 REM   N.W. GRANVILLE
1060 REM   FEBRUARY  1984
1070 REM
1080 REM
1090 REM   DIMENSION STATEMENTS FOLLOWED
1100 REM   BY DATA  FOR THE  CALCULATION
1110 REM   OF THE ENVIRONMENT PROPERTIES
1120 REM   AT DIFFERENT TEMPERATURES.
1130 REM
1140 REM   NG/VC    DYNAMIC    VISCOSITY
1150 REM     VC(I) AT TEMPERATURE  NG(I)
1160 REM   NH/CP    SPECIFIC  HEAT CP(I)
1170 REM     AT TEMPERATURE NH(I)
1180 REM   NI/KA    THERMAL CONDUCTIVITY
1190 REM     OF THE ENVIRONMENT KA(I) AT
1200 REM     TEMPERATURE NI(I)
1210 REM   MT/NT    THERMAL CONDUCTIVITY
1220 REM     OF  THE  9% CHROMIUM  STEEL
1230 REM     NT(I) AT TEMPERATURE  MT(I)
1240 REM
1250 DIM U(30),  W(30),  FF(30), TA(30), TB(30), TC(30)
1260 DIM HT(30), DE(30), TS(30), WR(30), H1(30), TD(30)
1270 DIM TE(30), NI(30), L1(30), L3(30), KA(20)
1280 NG(1)=18:  VC(1)=1.827E-5: NG(2)=40: VC(2)=1.904E-5
1290 NG(3)=54:  VC(3)=1.958E-5: NG(4)=74: VC(4)=2.102E-5
1300 NG(5)=229: VC(5)=2.638E-5
1310 NH(1)=37.78:  CP(1)=1004.8321
1320 NH(2)=93.33:  CP(2)=1009.0189
1330 NH(3)=148.89: CP(3)=1017.3925
1340 NI(1)=2:   KA(1)=2.428E-2: NI(2)=27:   KA(2)=2.624E-2
1350 NI(3)=52:  KA(3)=2.816E-2: NI(4)=77:   KA(4)=3.003E-2
1360 NI(5)=102: KA(5)=3.186E-2: NI(6)=127:  KA(6)=3.365E-2
1370 NI(7)=177: KA(7)=3.710E-2: NI(8)=227:  KA(8)=4.041E-2
1380 NI(9)=277: KA(9)=4.357E-2: NI(10)=327: KA(10)=4.661E-2
1390 MT(1)=20:  NT(1)=26.0: MT(2)=100: NT(2)=26.4
1400 MT(3)=200: NT(3)=26.8: MT(4)=400: NT(4)=27.6
1410 MT(5)=600: NT(5)=26.8: MT(6)=700: NT(6)=26.8
1420 PI=3.1415926:   KI=0.1045:  KS=26.7
1430 R=8.314: P=2E9: RA=0.00795: RT=0.003175
1440 M=SQR(2*KI/((KS*(RT*RT))*LOG(RA/RT)))
1450 C=0.00001174
1460 A$="SPEED (M/S)="
1470 B$="  LOAD (N)="
1480 C$="  F.FORCE (N)="
1490 D$="TA (C)="
```

```
1500 E$="          TB (C)="
1510 F$="    TC (C)="
1520 G$="    RADIUS    THICKNESS"
1530 H$="    NUMBER    TEMPERATURE"
1540 J$="    Q(CON)     DELTA"
1550 K$="    "
1560 L$="TDISC (C)="
1570 M$="       T AMB (C)="
1580 N$="H1 (W)="
1590 O$="       HTOT (W)="
1600 P$="  DELTA="
1610 Q$="     "
1620 R$="      "
1630 OPEN 1,4
1640 REM
1650 REM    INPUTTING THE DATA
1660 REM    FOR ONE EXPERIMENT
1670 REM
1680 PRINT "FOR ONE EXPERIMENT, WHAT WAS THE :-"
1690 PRINT " "
1700 INPUT "NUMBER"; I
1710 INPUT "SPEED IN M/S"; U(I)
1720 INPUT "LOAD IN N."; W(I)
1730 INPUT "FRICTION FORCE IN N."; FF(I)
1740 INPUT "TA IN DEGREES C"; TA(I)
1750 INPUT "TB IN DEGREES C"; TB(I)
1760 INPUT "TC IN DEGREES C"; TC(I)
1770 INPUT "TD IN DEGREES C"; TE(I)
1780 INPUT "TAMB IN DEGREES C"; TD(I)
1790 INPUT "WEAR RATE IN M↑3/M IN FORM OF 1.111E-11"; WR(I)
1800 INPUT "L1 IN MM"; L1(I)
1810 INPUT "L3 IN MM"; L3(I)
1820 L1=L1(I): L3=L3(I)
1830 REM
1840 REM    CALCULATING THE THERMAL
1850 REM    CONDUCTIVITY  OF  STEEL
1860 REM
1870 TT=TD(I): GOSUB 3100
1880 REM
1890 REM    CALCULATING THE DENSITY
1900 REM    OF    THE    ENVIRONMENT
1910 REM
1920 DN=1.293/(1+0.00367*TD(I))
1930 REM
1940 REM    CALCULATING    THE
1950 REM    DYNAMIC VISCOSITY
1960 REM
1970 IF TD(I)<40 THEN VV=1: GOTO 2010
1980 IF TD(I)<54 THEN VV=2: GOTO 2010
1990 IF TD(I)<74 THEN VV=3: GOTO 2010
```

```
2000 VV=4
2010 CZ=NG(VV+1)-NG(VV)
2020 VI=VC(VV)+(VC(VV+1)-VC(VV))*(TD(I)-NG(VV))/CZ
2030 REM
2040 REM   CALCULATING THE
2050 REM   SPECIFIC   HEAT
2060 REM
2070 IF TD(I)<37.78 THEN CP=CP(1): GOTO 2170
2080 IF TD(I)<93.33 THEN CC=1:     GOTO 2100
2090 CC=2
2100 CY=NH(CC+1)-NH(CC)
2110 CP=CP(CC)+(CP(CC+1)-CP(CC))*(TD(I)-NH(CC))/CY
2120 REM
2130 REM   CALCULATING THE THERMAL
2140 REM   CONDUCTIVITY   OF   THE
2150 REM   ENVIRONMENT
2160 REM
2170 IF TD(I)<27  THEN KK=1: GOTO 2230
2180 IF TD(I)<52  THEN KK=2: GOTO 2230
2190 IF TD(I)<77  THEN KK=3: GOTO 2230
2200 IF TD(I)<102 THEN KK=4: GOTO 2230
2210 IF TD(I)<127 THEN KK=5: GOTO 2230
2220 KK=6
2230 CX=NI(KK+1)-NI(KK)
2240 KA=KA(KK)+(KA(KK+1)-KA(KK))*(TD(I)-NI(KK))/CX
2250 REM
2260 REM   CALCULATING THE  NUSSELT
2270 REM   NUMBER, NU, AND THE HEAT
2280 REM   TRANSFER  COEFFICIENT, H
2290 REM
2300 CV=(78.48*RT↑3*(TA(I)-TD(I))*CP*DN*DN)/(VI*TD(I)*KA)
2310 NU=0.554*(CV↑0.25)
2320 H=NU*KA/(2*RT)
2330 REM
2340 REM   CALCULATING THE HEAT
2350 REM   FLOW  DOWN  THE PIN,
2360 REM   THE DIVISION OF HEAT
2370 REM   AND THE BULK SURFACE
2380 REM   TEMPERATURE
2390 REM
2400 Z=SQR(KS/(2*RT*H)): A=L1/(Z*RT)
2410 B=TA(I)-TB(I):      D=TB(I)-TC(I): E=TA(I)-TC(I)
2420 CH=0.5*(EXP(M*L3)+EXP(-M*L3))
2430 SH=0.5*(EXP(M*L3)-EXP(-M*L3))
2440 H3=KS*PI*(RT*RT)*M*((E*CH)-D)/SH
2450 H2=((C*E)/(RA-RT))+H3
2460 CH=0.5*(EXP(A)+EXP(-A))
2470 SH=0.5*(EXP(A)-EXP(-A))
2480 H1(I)=(PI*RT*(KS/Z)*(E*SH))+(H2*CH)
2490 HT(I)=FF(I)*U(I)
```

```
2500 DE(I)=H1(I)/HT(I)
2510 TS(I)=(E*CH)+((Z*H2/(KS*PI*RT))*SH)+TC(I)
2520 K=I
2530 REM
2540 REM   OUTPUTTING THE INPUT
2550 REM   DATA  AND  THE  HEAT
2560 REM   FLOW RESULTS
2570 REM
2580 H5=INT(H1(K)*1E4+0.5)/1E4: H6=INT(HT(K)*1E4+0.5)/1E4
2590 X=INT(DE(K)*1E4+0.5)/1E4:  T1=INT(TS(K)*1E4+0.5)/1E4
2600 PRINT#1, " "
2610 PRINT#1, " "
2620 PRINT#1, " "
2630 PRINT#1, "EXP NO";  K:  PRINT#1,   " "
2640 PRINT#1, A$; U(K);  B$; W(K);  C$; FF(K)
2650 PRINT#1, D$; TA(K); E$; TB(K); F$; TC(K)
2660 PRINT#1, L$; TE(K); M$; TD(K)
2670 PRINT#1, "WEAR RATE (M↑3/M)="; WR(K)
2680 PRINT#1, "L1 (MM)="; L1(K);  "   L3 (MM)="; L3(K)
2690 PRINT#1, N$; H5; O$; H6; P$; X
2700 PRINT#1, "BULK SURFACE TEMP TS (C)=";       TS(K)
2710 PRINT#1, "NUSSELT NUMBER=";  NU; "  H =";   H
2720 PRINT#1, "HARDNESS (N/M↑2) =";   P
2730 PRINT#1, " "
2740 PRINT#1, G$; H$; J$
2750 PRINT#1, " "
2760 REM
2770 REM   CALCULATING THE SURFACE
2780 REM   PARAMETERS   USING   AN
2790 REM   ITERATIVE TECHNIQUE
2800 REM
2810 TT=TS(I)+150: GOSUB 3100
2820 TH=3E-6
2830 J=1.29
2840 TG=TS(I)
2850 KO=8.39-6.63E-3*(TG+273)
2860 AB=4*KS/(PI*P)
2870 AC=4*KS/(PI*KO)
2880 R1=AB*(TE(I)-TS(I))*W(I)/(2*H1(I)-J)-HT(I) - AC*TH
2890 N=W(K)/(PI*P*R1*R1)
2900 CW=4*KS*KO*W(K)
2910 TF=TS(K)+(H1(K)-J)*P*(PI*R1*KO+4*TH*KS)/CW
2920 IF TG<0                    THEN 2960
2930 IF TG>1000                 THEN 2960
2940 IF ABS(TF-TG)<=(TF/1000)   THEN 2960
2950 TG=TF: PRINT TG: GOTO 2850
2960 DE=(H1(I)-J)/HT(I)
2970 TF=INT(TF*10+0.5)/10
2980 TH=INT(TH*1E10+0.5)/1E10
2990 R1=INT(R1*1E8+0.5)/1E8
```

```
3000 N=INT(N*10+0.5)/10
3010 J1=INT(J*1E4+0.5)/1E4
3020 DE=INT(DE*1E4+0.5)/1E4
3030 REM
3040 REM   OUTPUTTING THE
3050 REM   FINAL  RESULTS
3060 REM
3070 PRINT    R1; TH;  N; TF; J1
3080 PRINT#1, R1; K$; TH; Q$; N; R$; TF; K$; J1; K$; DE
3090 GOTO 1680
3100 REM
3110 REM   SUBROUTINE FOR CALCULATING
3120 REM   THE  THERMAL  CONDUCTIVITY
3130 REM   OF 9CR STEEL AT  THE  BULK
3140 REM   SURFACE   AND    OXIDATION
3150 REM   TEMPERATURES
3160 REM
3170 IF TT<100 THEN TU=1: GOTO 3220
3180 IF TT<200 THEN TU=2: GOTO 3220
3190 IF TT<400 THEN TU=3: GOTO 3220
3200 IF TT<600 THEN TU=4: GOTO 3220
3210 TT=5
3220 CT=MT(TU+1)-MT(TU)
3230 KS=NT(TU)+(NT(TU+1)-NT(TU))*(TT-MT(TU))/CT
3240 RETURN
```

Reciprocating sliding wear of 9% Cr steel in carbon dioxide at elevated temperatures

J. L. Sullivan and N.W. Granville*

Experiments were conducted on the initial stages of reciprocating sliding wear of a 9% chromium steel in an environment of carbon dioxide at temperatures in the range 200 to 550°C. At ambient temperatures of 290°C and above, an initial severe wear mode was followed by a transition to mild oxidational wear. At any given ambient temperature above 290°C, the distance of sliding required to reach such a transition was found to depend on load and mean sliding speed, although the dependency on speed was not simple. When a transition occurred, most of the surfaces were covered with a stable oxide film which consisted of an agglomerate layer of wear debris being mainly of oxide at the surface and mainly metallic at the metal boundary. This film was supported by a work hardened layer extending for about 30 μm into the bulk of the metal. A surface model is proposed to explain the mechanism of formation of the supportive oxide layer; predictions of volume of material removed and final oxide coverage at the transition are in close agreement with experimental values

Keywords: *wear, steels + chromium, high temperatures, carbon dioxide, sliding, oxides*

In order to minimize material loss, if the system is to wear, for long periods of time, perhaps in hostile environments and high temperatures, with the minimum of maintenance. Examples of such components are the boiler tubes and their supports in Advanced Gas Cooled Reactors which are subject to pressurized continually circulating gas, consisting mainly of carbon dioxide at high operating temperature, which is used to transfer heat from the reactor core to water within the tubes. Due to the generally high levels of noise within such a reactor system, the tubes are also subject to vibration and this can lead to component wear where contact occurs.

In order to minimize material loss, if the system is to wear, it must be designed so that components settle into stable mild oxidational wear conditions as rapidly as possible. Mild oxidational wear will not be established immediately, however, in any sliding system, but initial severe wear will occur and then after a period of sliding the system will either settle into an equilibrium severe wear mode or a transition to mild wear will occur. Whether such a transition occurs depends on a number of factors which include surface and contact temperatures, load, speed, environment and materials used. If such a transition does occur then initial severe wear rates are typically about three orders of magnitude greater than the final equilibrium mild oxidational wear rates. Hence, the majority of material removal in the life of a component could occur during these initial stages of reciprocating sliding. It is therefore of great practical importance to study these initial stages of reciprocating sliding and the factors leading to the appearance or non-appearance of a transition to mild oxidational wear.

*University of Aston, Gosta Green, Birmingham, UK, B4 7ET

There has been some recent work on the reciprocating wear of austenitic stainless steels[1-4], but relatively little on 9% Cr steels[5,6] similar to the materials used in this investigation. Further, most of this work has been carried out in an atmosphere of air, where in order to simulate practical conditions more closely, we have used environments of pure carbon dioxide. In this study, the 9% Cr steel was chosen not only for its possible practical applications in the nuclear power industry where it has been used in boiler components[7], but also since its oxidational behaviour is thought to be less complex than other materials of interest in the important temperature range from 200 to 550°C.

The broad objective of this study, then, is to examine the mechanisms leading to the formation of stable supportive oxide films during the early stages of reciprocating sliding in an atmosphere of carbon dioxide at elevated temperatures. This was achieved through continuous mechanical measurements of friction and wear together with extensive surface and subsurface examinations. It is hoped that the results of the investigation will not only provide information to estimate better component lifetimes, but also to give an insight into the processes leading to the establishment of mild oxidational wear conditions.

Experimental details

All the wear tests described in this study were carried out on a reciprocating wear test rig (Fig 1). In this rig, a flat specimen, 32 mm x 13 mm x 3 mm, was mounted on the lower driven beam and was subject to reciprocating sliding against a specimen with a domed end of 12 mm diameter and 13 mm length mounted on the upper loading beam. Loads of either 22 or 41 N were then applied to this upper beam by means of a pulley with dead weight loading. The

TRIBOLOGY international 0301–679X/84/020063–09 $03.00 © 1984 Butterworth & Co (Publishers) Ltd

lower reciprocating beam was driven by a variable speed motor through a crank. For this series of experiments, the crank was adjusted to give a constant value of stroke length of 9.2 mm and the reciprocating frequency was varied from 1 to 9 Hz by means of the variable speed motor. The mean sliding speed was then equal to the product of twice the stroke length and the reciprocating frequency.

The specimens were enclosed in an airtight chamber, of which the temperature inside could be maintained at values up to 600°C by means of ten 300 W heater elements. The temperature could be held constant at ± 1°C over the temperature range. The atmosphere within the specimen chamber was of pure carbon dioxide held at a pressure of 1.5 bar and admitted at a constant rate of 8×10^{-5} m^3 min^{-1} in order to ensure that oxidation did not alter the gas composition and that no back diffusion of air into the chamber occurred.

The specimens were produced from a 9% Cr steel, the composition of which is given in Table 1.

Friction was measured using a strain gauge dynamometer located at the end of the loading beam and due to the length of many of the experiments was recorded intermittently on an ultra violet recorder. Overall wear rates for the experiments were determined by specimen weight loss, but this, if an experiment was run to its conclusion, gave no indication of the proportions of the material removed in the various wear modes encountered. A linear voltage differential transducer was employed to remedy this situation, but since wear rates were low and the transducer necessarily had to be located remote from the wearing surfaces and was subject to vibration, the results from this source proved unreliable. The transducer did, however, prove useful in determining when a transition from severe to mild wear had occurred.

Wear test runs were conducted at 275°C, 290°C, 300°C and 450°C with a load of 22 N and at 300°C with a load of 41 N. Mean reciprocating sliding speeds were varied from 18 mm s^{-1} to 144 mm s^{-1} and the number of cycles required for the system to reach the severe/mild wear transition (N_T) was noted. From the value of N_T, the total sliding distance to reach such a transition, D_T, was calculated. In addition to these wear tests, experiments were conducted at a sliding speed of 36 mm s^{-1} and a load of 22 N for temperatures between 200°C and 550°C in order to establish a relationship between D_T and temperature, and a further series conducted to investigate the effects of static oxidation on the establishment of stable oxidational wear conditions. In the first of this latter series, specimens were mounted on the apparatus in the usual way and pre-heated to a temperature of 290°C for 750 h. After this period, the wear test was continued as previously described until a severe/mild wear transition occurred when the value of D_T was noted and compared with values obtained from similar experiments conducted without the extended period of pre-heating. Three tests were then carried out under various conditions where the specimens were worn for several thousand reciprocating cycles and then the motion

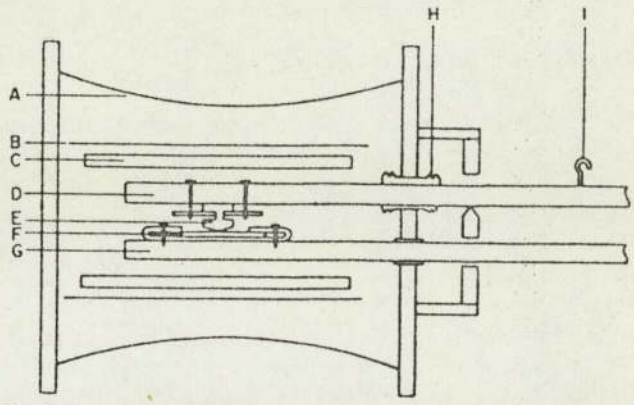

Fig 1 The reciprocating wear test machine. A Air-tight specimen chamber; B Metal heat shield; C One of the ten 300 W heaters; D Upper, or loading, beam; E Pin specimen; F Flat specimen; G Lower, or sliding, beam; H Bellows allowing vertical movement of the loading beam; I Point at which the load was applied

stopped when the specimens were left at the operating temperature for a 'dwell period' where static oxidation took place. The dwell period was then followed by a further period of sliding, the whole process being repeated several times until a transition occurred, when the value of D_T was noted. Two of these dwell tests were carried out at 290°C and 300°C with dwell periods of 96 h and loads of 22 N and 41 N and one at 450°C with a 4 h dwell period and a load of 22 N.

Debris was collected where possible after each test run and analysed using powder X-ray photography. Taper sections of selected specimens were produced in order that microhardness versus depth measurements might be made. Scanning electron microscopy was employed to study surface topography and subsurface features and a limited number of Auger depth profiles were recorded on oxide plateaux in order to study the oxygen concentration with depth into the protective oxide film.

Experimental results

Due to the difficulties mentioned in the previous section, it was not possible to determine accurately wear rates for the various wear modes experienced during these experiments. It was obvious, however, from extensive surface examinations and from careful monitoring of friction traces that three types of wear were occurring:

- running-in severe wear
- equilibrium severe wear
- equilibrium mild (oxidational) wear.

In all the experiments described here, running-in severe wear was encountered initially, before the system settled into one of the other two modes. For the conditions of our experiments, the type of equilibrium wear mode was determined by the ambient temperature. For temperatures of 290°C and above, a transition from severe to mild wear occurred for all the sliding speeds after a prolonged period of sliding. For temperatures below this value, no such transition occurred and the system settled into an equili-

Table 1 Composition of the 9% Cr steel used for the specimens

Element	C	Mn	Si	S	P	Cr	Mo	Ni	Fe
Concentration, %	0.1	0.4	0.6	> 0.01	> 0.005	9	1	0.25	Remainder

brium severe wear mode. Severe/mild wear transitions were indicated by the friction trace, an example of which is shown in Fig 2. This trace shows a gradual fall in friction coefficient from an initial value of 1.5 to a value of 0.7 over a sliding distance of more than 1000 m followed by a rapid fall to a value of 0.3 over a further sliding distance of 1.8 m. The data were recorded for an experiment conducted at 290°C with a load of 22 N and at a mean sliding speed of 36 mm s^{-1}. Experiments conducted at 275°C gave friction traces very similar to that shown in Fig 2, but these levelled out at a value of about 0.7 and showed no transition. Wilson *et al*[6] have observed similar long term behaviour for experiments on a 9.2% Cr steel run in air at elevated temperatures.

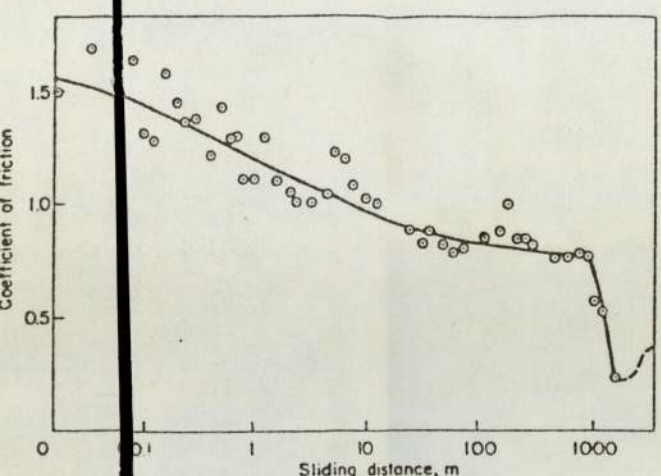

Fig 2 The variation of coefficient of friction with sliding distance. Mean sliding speed: 36 mm s^{-1}; load: 22 N; temperature: 290°C; D_T: 970 m

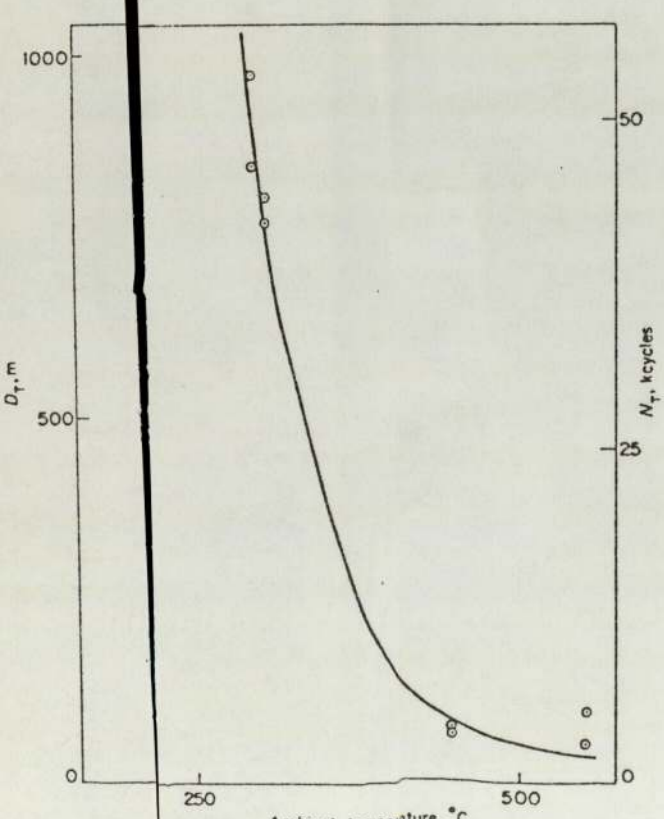

Fig 3 The variation of D_T with ambient temperature under a standard set of sliding conditions. There was no transition to the mild oxidational wear mode at 200°C or 275°C

In the majority of experiments conducted at 290°C and above during this investigation, the run was terminated soon after the severe/mild wear transition occurred and the sliding distance required to produce that transition, D_T, noted. (A small number of experiments were run on after the transition in order to estimate mild wear rates.) Fig 3 shows the variation of D_T with ambient temperature recorded at a sliding speed of 36 mm s^{-1}. The decrease in D_T was due to the increasing rate of production of oxide with increasing temperature. At temperatures below 290°C, the rate of oxide growth was clearly always less than its rate of removal and hence no transition occurred.

Fig 4 shows the variation in D_T with mean sliding speed at 290, 300 and 450°C with 22 N load and at 300°C with 41 N load. The lower temperature curves show the same general pattern; an increase in D_T to a maximum at a mean speed of about 110 mm s^{-1} followed by a fall with further increase in speed. The results at 450°C show a linear variation with speed indicating that the time taken to reach a transition was constant. The possibility that the peak in the D_T versus speed curves was due to machine resonance was discounted due to the fact that no such peak was observed at 450°C nor was there any increase in wear rates at that speed.

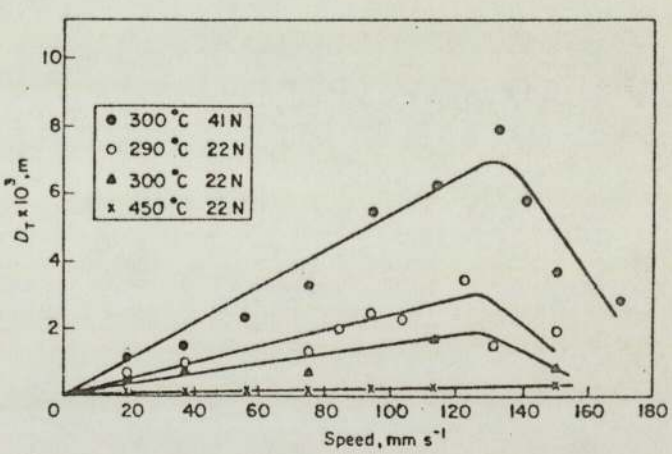

Fig 4 The variation of D_T with sliding speed at different ambient temperatures

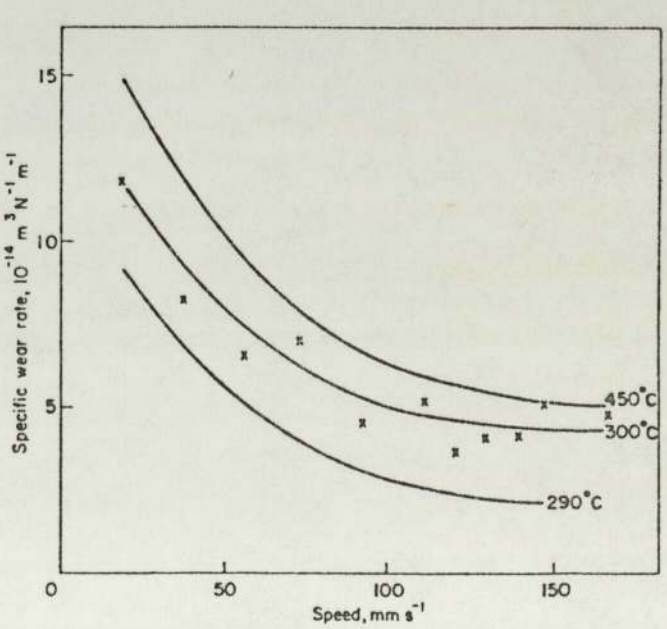

Fig 5 The variation of specific wear rate with sliding speed at different ambient temperatures

The mean specific wear rates for these experiments calculated from total weight loss are shown in Fig 5 as a function of speed. The individual points are plotted for the 300°C experiments to indicate the scatter, but in the interest of clarity best fit curves only are plotted for the other two series of experiments. All the curves show the same general trend, that is a decrease in mean specific wear rate with speed. The two curves also show an increase in specific wear rate with temperature at any given speed. It should be recognized that most of the wear will have occurred in the early stages of sliding and Fig 6, showing the cumulative volume removed with time of sliding, illustrates this point. In the series of experiments represented in this figure test runs were stopped after 100, 1000, 5000, 15 000, 30 000, 45 000, 75 000 and 100 000 reciprocating cycles and the weight loss for both pin and flat recorded, a new set of specimens being used for each run. The curves in Fig 6 show a continuously falling wear rate with time (or distance) for both pin and flat. The running-in severe wear on the flat was the greater of the two, but mild wear rates taken from the slope of the curve after the transition were about the same. Also included in this figure is a theoretically derived curve from the surface model proposed in the next section.

Taper sections of all the specimens produced from the above series of tests were prepared and microhardness measurements were made at various depths into the specimen. Fig 7 shows a typical hardness versus depth curve. In all cases there was a hardened layer near to the surface, the depth being fairly constant at about 30 μm for all specimens run between 1000 and 100 000 reciprocating cycles. The wear scar produced on the specimen run for 100 cycles was too small for any meaningful data to be obtained. Maximum hardness of the subsurface region for specimens taken from the severe wear region varied between 400 and 450 HV. Hardnesses as high as 1500 HV were recorded for some samples measured after the mild wear transition very close to the surface, but these were almost certainly due to the surface oxide film.

The results of 'dwell tests' conducted to investigate the effects of static oxidation are summarized in Table 2.

Measurements of weight gains during dwell periods show them to be always much less than weight losses due to wear in the shorter intervening sliding periods. For example, for a test carried out at 290°C, 22 N load and a mean sliding speed of 110 mm s^{-1}, the weight gain over the 96 h dwell periods averaged 0.1 mg, indicating an increase in oxide mass of a little over 0.3 mg. For this experiment, weight losses due to wear varied from 57 mg in the severe wear dominated first 180 m sliding period to 0.8 mg in the mild wear dominated last period of sliding.

Selected surfaces from all series of tests were studied using scanning electron microscopy. On surfaces after mild wear had been established, large oxide plateaux were observed to cover over half the area of the wearing surface. The thickness of the plateaux was about 6 μm. A typical surface photomicrograph taken from a mild wear experiment is shown in Fig 8(a). Examination of the edge of one of these plateaux (Fig 8(b)), suggests that they are formed by a different mechanism to plateaux formed in unidirectional sliding experiments[8] and consist largely of compacted debris. Granular debris was often seen on the surface surrounding such plateaux, as shown in Fig 8(b). No such

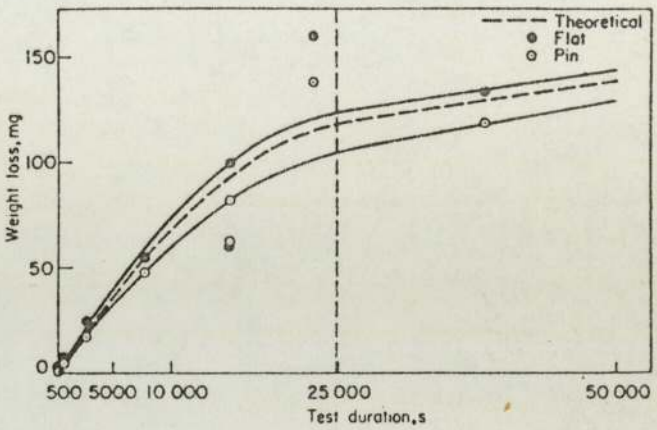

Fig 6 The increase in weight loss from each specimen, as an experiment progressed, with the theoretical mean weight loss

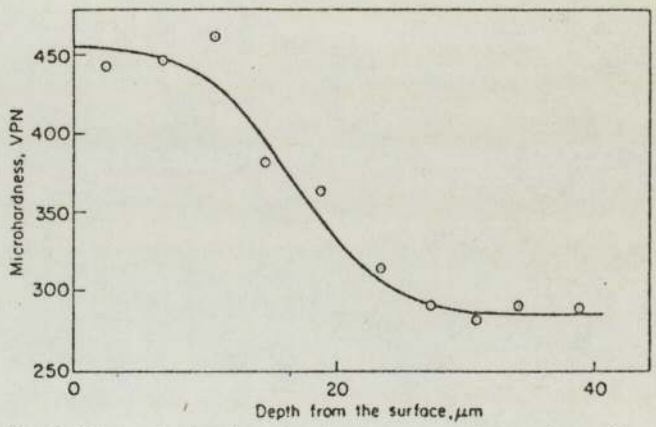

Fig 7. The variation in microhardness near the surface of a worn flat specimen. Mean sliding speed: 37 mm s^{-1}; load: 22 N; temperature: 290°C; test duration: 30 kcycles (660 m)

Table 2 Results of dwell tests conducted to investigate the effects of static oxidation

Sliding speed, mm s^{-1}	Load, N	Temperature, °C	Initial sliding distance, m	Dwell period, h	Transition distance, m
110	22	290	0	750*	5400 (6100)
	22	290	180	96	585 (6100)
	41	300	180	96	960 (9000)
	22	450	36	4**	225 (216)

**In this experiment, specimens were heated for 750 h prior to sliding, which was then continuous until a transition occurred*

***In this experiment, the initial sliding distance was followed by one 4 h dwell period. The test was then run continuously to the transition. Transition distances for experiments conducted under the same conditions but with no dwell periods are shown in brackets in the last column*

plateaux were seen on specimens from the initial severe wear mode regions although there is evidence to show that the plateau area increases with increased time of sliding. Fig 8(c) shows a typical severe wear surface examined soon after the start of a wear test.

Auger electron spectroscopic examination of some plateaux was carried out in order to show that they consisted of oxide and not simply raised areas of metal. The plateaux were gradually etched away by bombardment with 2 keV argon ions with the Auger spectra for oxygen, iron and chromium being recorded at specific time intervals. The relative atomic abundances for these three elements were then determined from peak-to-peak heights of the major Auger peaks and the application of corresponding inverse sensitivity factors[9]. Typical resultant concentration versus depth profiles are shown in Fig 9. Unlike the curves reported by one of the authors[8] for unidirectional sliding experiments, Fig 9 clearly shows a decreasing oxygen to iron ratio with depth into the sample. Calculations indicate that 20×10^3 μA is equivalent to a depth of about 5 μm.

Since most of the wear occurred in the initial severe wear mode, examination of debris by powder X-ray photography after the completion of a test run revealed only metal, Fe(Cr). This was not unexpected since the detection limit of the technique is only about 4% by volume. In order to identify the surface oxides produced, some experiments were run on for long periods after the severe/mild wear transition. Even here, Fe(Cr) lines dominated the diffraction photographs (as might be expected since initial severe wear rates were two orders of magnitude higher than mild wear rates), but oxides were detected. In all cases, the predominant oxide was the rhombohedral oxide (α - Fe_2O_3, Cr_2O_3) with just detectable amounts of the spinel ($Fe.Fe_{(2-x)}Cr_xO_4$). Specific wear rates measured in the mild wear region were about 10^{-14} m^3 N^{-1} m^{-1} compared with initial severe specific wear rates of 600×10^{-14} m^3 N^{-1} m^{-1}.

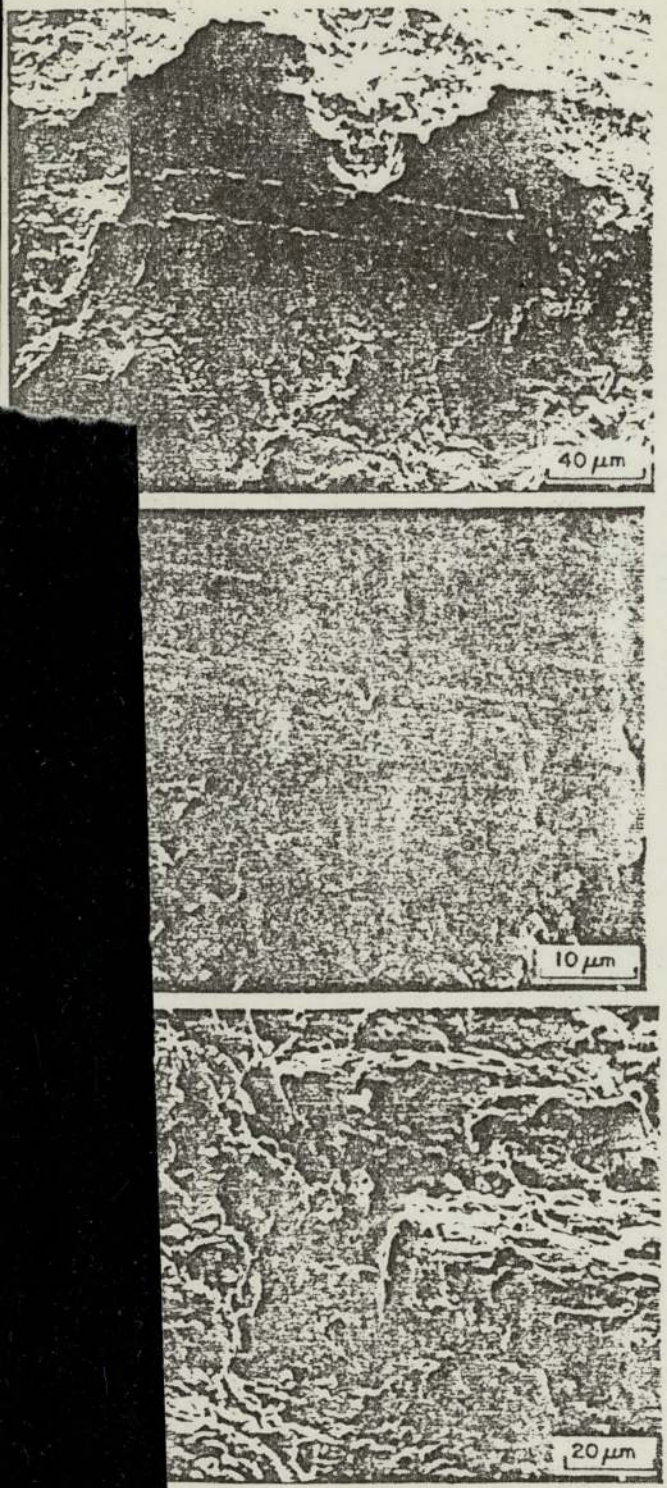

...cal mild wear surface. (b) Detail of a plateau ...e plateau to consist of compacted debris. ...vere wear surface

A surface model – Transition from severe to mild wear

During sliding at elevated temperatures, oxidation of the whole of the two contacting surfaces will occur out of contact at the ambient temperature T_A and at the real areas of contact at or near to the hot-spot temperature T_C. If the ambient temperature or the speed of sliding (or both) are too low, the rate of formation of protective oxide film will always be less than the rate of material removal and the system will operate in a continual severe wear mode. No severe/mild wear transition will occur. If the rate of oxide growth is sufficiently high, then oxide plateaux begin to form and the area of these plateaux increases with sliding until full support and hence oxidational wear occurs. This is probably equivalent to coverage of the majority of the two contacting surfaces by a stable oxide film of critical thickness ξ. In a reciprocating system where debris cannot easily escape, it is proposed that the following film formation mechanism applies.

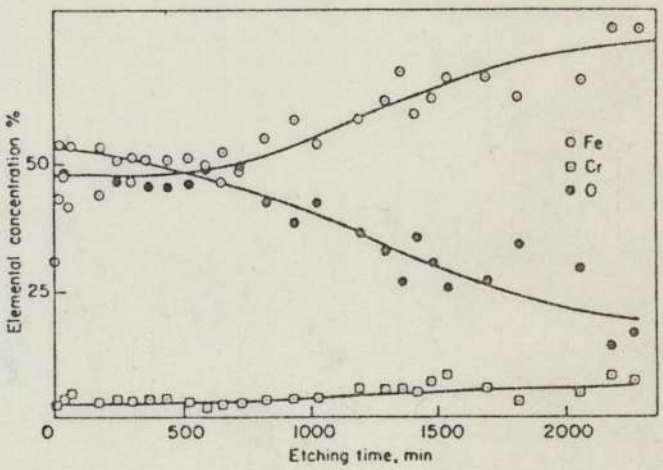

Fig 9 The variation in Fe, Cr and O concentration with depth on a flat specimen

Oxidation occurs over the whole surface at the ambient temprature T_A but particularly initially around nucleation sites, probably at the contact temperature T_C. Most of this oxide is then removed with some metal by the reciprocating sliding motion. When all the debris is not allowed to escape, some oxide (and metal) particles become entrapped and form agglomerate plateaux around some of the initial nucleation sites. These then become major load bearing areas where further oxidation takes place together with further particle agglomeration, resulting in a growth of area of the plateaux. Much experimental work in this and many other studies suggests that the thickness of the plateaux stabilizes at a critical value. The area of the plateaux continues to increase, however, until contacts are mainly oxide-oxide and mild wear ensues.

Let us consider the system at some time t after the start of a run. Let ΔV be the volume of material removed from the surface in time t to $t + \Delta t$.

Then,

$$\Delta V = \Delta V_{m-m} + \Delta V_{m-o} + \Delta V_{o-o} - \Delta V_{ox} \quad (1)$$

where

ΔV_{m-m} = volume removed due to metal-metal contact
ΔV_{m-o} = volume removed due to metal-oxide contact
ΔV_{o-o} = volume removed due to oxide-oxide contact
ΔV_{o} = volume of oxide produced.

If α is the fraction of the apparent contact area covered by oxide at time t, then[6]:

probability of a metal-metal contact, $P_{m-m} = (1 - \alpha)^2$

probability of a metal-oxide contact, $P_{m-o} = 2\alpha(1 - \alpha)$, and

probability of an oxide-oxide contact, $P_{o-o} = \alpha^2$

Further if we assume a linear growth relationship between the area of coverage of oxide film and time, then $\alpha = at/t_T$ where a is the fraction of the apparent contact area covered for equilibrium mild wear conditions and t_T is the time taken to reach the severe/mild wear transition.

The volume of material removed due to metal-metal contacts in time Δt may be written[10]:

$$\Delta V_{m-m} = K_{m-m} P_{m-m} A_r \Delta d$$

or

$$\Delta V_{m-m} = K_{m-m}(1 - \frac{at}{t_T})^2 \frac{W}{p_m} U \Delta t \quad (2)$$

where

K_{m-m} = wear constant for metal-metal contacts
A_r = real area of contact
Δd = total distance of sliding in time Δt
W = load
p_m = hardness
U = mean sliding velocity.

Similarly for metal-oxide and oxide-oxide contacts in the same time one can write:

$$\Delta V_{m-o} = K_{m-o} \frac{2at}{t_T} (1 - \frac{at}{t_T}) \frac{W}{p_m} U \Delta t \quad (3)$$

and

$$\Delta V_{o-o} = K_{o-o} (\frac{at}{t_T})^2 \frac{W}{p_m} U \Delta t \quad (4)$$

where K_{m-o} and K_{o-o} are wear constants for the metal-oxide and oxide-oxide contacts respectively.

If we assume a continual process of oxide attrition and subsequent agglomeration to form load bearing plateaux, the development of thick diffusion controlled oxide films is unlikely. The oxide growth rate may then be described by the linear relationship $\Delta m = k \Delta t$, where Δm is the mass uptake of oxygen per unit area and k is the linear oxidational rate constant.

The total oxide produced in time Δt is due to the sum of that produced out of contact at temperature T_A and that due to tribo-oxidation in the contact region at temperature T_c. Thus:

$$\Delta m_{total} = \Delta m_{out\ of\ contact} + \Delta m_{tribo\text{-}oxidation}$$

Written in terms of volume of oxide, this becomes

$$\Delta V_{ox} = k_{T_A} (\frac{A}{\rho f}) \Delta t + k_{T_c} (\frac{A_r}{\rho f}) \Delta t \quad (5)$$

where

k_{T_A} = oxidational rate constant for out-of-contact oxidation at T_A
k_{T_c} = oxidational rate constant for tribo-oxidation at T_c
ρ = density of the oxide
f = mass fraction of the oxide which is oxygen
A = apparent area of contact.

Substituting for Eqs (2), (3), (4) and (5) in Eq (1):

$$\Delta V = (P (\frac{at}{t_T})^2 - Q \frac{at}{t_T} + R) \Delta t$$

where

$$P = (K_{m-m} + K_{o-o} - 2K_{m-o}) \frac{WU}{p_m}$$

$$Q = 2(k_{m-m} - K_{m-o}) \frac{WU}{p_m}$$

and

$$R = K_{m-m} \frac{WU}{p_m} - \{k_{T_A} \frac{A}{\rho f} + k_{T_c} \frac{W}{p_m \rho f}\}$$

In the limit when $\Delta t \to 0$, the total volume removed in time t is given by

$$V = \int_0^t (P (\frac{at}{t_T})^2 - Q \frac{at}{t_T} + R)\, dt$$

or

$$V = \{\frac{P}{3} (\frac{at}{t_T})^2 - \frac{Q}{2} \frac{at}{t_T} + R\} t \quad (6)$$

and the instantaneous wear rate ω (in $m^3\ m^{-1}$) is given by:

$$\omega = \frac{1}{U} (P (\frac{at}{t_T})^2 - Q \frac{at}{t_T} + R) \quad (7)$$

Let us consider one series of wear tests conducted at 290°C, 22 N load and a speed of 36.8 mm s^{-1}, for which the experimental values of cumulative volume removed versus time are given in Fig 6. Then if we apply our surface model for these conditions, the values of P and Q in Eq (6) reduce to

$$P = K_{m-m} \frac{WU}{p_m}$$

$$Q = 2K_{m-m} \frac{WU}{p_m}$$

since the measured value of K_{m-m} for initial severe wear is 600 times greater than the value of K_{o-o} estimated from the mild wear region. Although there is no way of determining the value of K_{m-o}, it is thought that this will be close to that of K_{o-o}. The measured value of K_{m-m} for this series of experiments was 5.56×10^{-3}, the hardness was 2.8×10^9 N m^{-2} and $t_T = 2.5 \times 10^4$ s.

During mild oxidational wear, the volume of oxide produced per unit time (both out of contact and tribo-oxide) may be determined directly from the wear rate since in this wear mode the rate of production of the oxide must be equal to its rate of removal. Hence the volume of oxide produced per unit time, $V_{ox} = \omega U$, where ω is the mild wear rate in units of m^3 m^{-1}. If we assume further that the processes of oxide production are similar in the period of sliding wear leading up to the transition to mild oxidational wear, then this value of V_{ox} can replace the term $k_{T_A} A/\rho J + k_{T_c} W/p_m \rho f$ in Eq (6).

For the conditions of the experiments described in Fig 6, the mild specific wear rate was 5×10^{-15} m^3 N^{-1} m^{-1}. Thus $V_{ox} = 4.04 \times 10^{-15}$ m^3 s^{-1}.

Inserting the values of the various parameters into Eq (6) gives

$$V = 8.1 \times 10^{-22} a^2 t^3 - 6.52 \times 10^{-17} a t^2 + 1.61 \times 10^{-12} t - 4.04 \times 10^{-15} t$$

Different values of a were tried in the above equation to give a best fit to the experimentally derived curves in Fig 6. The theoretical curve plotted for a value of $a = 0.5$ on that figure gives very good agreement between experiment and theory. This theoretical result suggests that one half of the surface must be covered with a stable supportive oxide film for a transition from severe to equilibrium mild oxidational wear to occur. Visual observations of the surfaces just after mild wear has been established show that a little over half of the surface is covered by oxide plateaux. These results strongly suggest that the model is a good representation of the processes occurring during the initial stages of sliding of the surfaces.

Discussion

Scanning electron micrographs of worn surfaces show that for a transition from severe to mild wear to occur, most of each surface must be covered by a stable oxide film which, for the conditions in our experiments, averages about 6 μm in thickness. The maximum oxide hardness is about 1500 HV compared with bulk steel hardness of 280 HV. Microhardness measurements have shown that the oxide layer is supported by a hardened metallic layer of maximum hardness 450 HV extending to a depth of 30 μm into the sample. It was further found that this layer was formed very early during sliding. Hsu *et al*[2] suggested that, for surface stability, a two layer structure is necessary, but our measurements show a progressive reduction in hardness with depth into the bulk. Skinner[3], using a similar experimental arrangement, but austenitic stainless steel specimens, has also stopped wear test runs before any transition could take place and found that after just 100 cycles (a 50 s test) subsurface hardnesses reached 750 HV. He attributed this to oxide formation and incorporation into a highly disrupted surface layer. In our experiments, however, there is no evidence of any substantial amounts of oxide being formed at this early stage and we must conclude that the layer is a work hardened subsurface region which provides a stable base on which oxide films may grow. Once the hard layer has been established, wear rates are reduced and surface oxidation takes place. This leads to the growth of oxide plateaux, in both thickness and area, until mild wear conditions are established.

Evidence of the composition and mechanisms of growth of plateaux was gained from further surface examination. Scanning electron micrographs of the edges of plateaux, an example of which is shown in Fig 8(b), strongly suggests that they consist of agglomerate layers of sub-micron particles of wear debris. Auger electron spectroscopy depth profiles, showing relative concentration of oxygen, iron and chromium as a function of the product of ion current and time, reinforce this view. It is impossible to assign accurately a depth scale to the horizontal axis of Fig 9 for such a complex surface, but calculations indicate that the maximum depth removed from the plateau was approximately 5 μm, almost equal to the total thickness. In this region, oxygen concentration fell from 55% ± 10% at the surface to 20% ± 10% close to the plateau-metal interface. X-ray powder diffraction analyses indicate that oxide in the wear debris consists mainly of the rhombohedral (α - Fe_2O_3, Cr_2O_3) in which one would expect an oxygen concentration of 60%. Clearly the amount of oxide in the plateaux increases with thickness, with the surface regions consisting almost entirely of oxide. The Auger depth profile thus provides a history of the build-up of the plateau and it appears likely that the layer is formed by the sintering of wear particles which would consist initially mainly of metal debris with the amount of oxide increasing with distance of sliding. The depth profiles recorded during this investigation are quite different to those reported by Sullivan and Athwal[8] for experiments conducted on a pin-on-disc wear test rig for unidirectional sliding conditions. For those experiments, oxygen concentrations were relatively constant with depth into the layer, indicating a homogeneous wholly oxide film with a different mechanism of formation.

The results of average specific wear rates (m^3 N^{-1} m^{-1}) measured over the whole of the pre-transition period (Fig 5) show them to vary approximately as the reciprocal of the sliding speed. One might expect attrition rates to be independent of speed, but this would only be true if there were one dominant wear mode. In this region, modes are changing from initial severe wear to final oxidational mild wear with subsequent changes in surface hardness, topography and composition. Under these circumstances, it is likely that the proportion of the total wear attributed to oxidational wear will be greater in the case of the longer distance, higher speed runs and this will be reflected in the lower averages for higher speeds. The results also

show that these mean specific wear rates increase with increase in temperature.

At the lower speeds of sliding and high ambient temperatures used in these experiments, it is not unreasonable to assume that out-of-contact oxidation is primarily responsible for oxide production and subsequent plateau growth. If we consider the volume of static out-of-contact oxide produced per unit distance of sliding, then assuming a linear growth rate, the volume produced per unit time will be constant and hence the volume per unit distance of sliding will be inversely proportional to sliding speed. From the previous paragraph, we have seen that the mean rate of removal of material ($m^3\ m^{-1}$) up to the transition is similarly inversely proportional to sliding speed. Thus, if the speed is increased one would expect the transition distance, D_T, to grow and the volume of oxide required on the surface for equilibrium mild wear to occur, to increase by a similar factor. Hence there should be an (approximately) linear relationship between D_T and U. The curves in Fig 6 show such a relationship for temperatures of 450°C and for 290°C and 300°C up to speeds of about 110 mm s^{-1}. As one would expect, the curve corresponding to experiments conducted at 300°C and a load of 41 N exhibit longer transition distances due to the increased attrition rates at the higher load, the rate of production of oxide being not particularly affected by load.

At speeds greater than 110 mm s^{-1} (290°C and 300°C), there is a marked fall in values of D_T with increase in speed. No evidence of oxide type changes was found, hence this fall must be due to an increase in the amount of oxide formed due to tribo-oxidation, this being a consequence of increase in contact temperature and surface disruption with increase in speed. Calculations based on the work of Archard[11] would indicate maximum excess contact temperatures to be about 300°C at 160 mm s^{-1}, although in practice, considering multiple contacts, the temperature would be somewhat lower than this.

At temperatures below 290°C, the rate of material removal is clearly always greater than the rate of production in the speed range considered and transitions to mild wear will never occur.

The dwell tests further support the view that static out-of-contact oxidation has an important role to play in the formation of oxide plateaux. It should be noted, however, that static pre-oxidation alone has no significant effect. The experiment conducted at 290°C with a load of 22 N with a 70 h pre-sliding dwell period showed no statistically significant reduction in the time of sliding required to reach a transition. There could be a number of reasons for this, but it appears that a tribologically disturbed surface is necessary for the formation of an oxide layer capable of giving protective regenerative properties. The fact that prior to sliding no hard sub-surface layer had been formed to support the oxide would undoubtedly also have affected its protective properties. The experiments conducted at 290°C and 300°C, where sliding periods were interspersed by dwell periods, showed a significant effect of static oxidation. Here transition sliding distances were reduced by an order of magnitude. Oxidation over these long periods of dwell would probably have followed a parabolic rate law and the amounts of oxide produced during these 96 h dwells could not alone account for the observed reductions in transition sliding distances. Hence there must have been a substantial effect due to oxidation and consolidation of partially formed plateaux. It is not clear why dwell did not have a similar effect at 450°C. We may only assume that consolidation by further oxidation of plateaux was not necessary in the formation process at this high temperature.

It is not expected that the form of the results would be very different if the experiments were conducted in air, other than that the values of D_T would be greatly reduced due to the greater availability of oxygen at the surface. Experiments are in progress to study differences in performance in carbon dioxide, air and oxygen.

Conclusions

Using a reciprocating wear test rig, experiments were conducted on factors affecting the transition from severe to mild wear during running in of a 9% Cr steel in an atmosphere of carbon dioxide. Loads of 22 N and 41 N were used and temperatures were varied from 200°C to 550°C. It is hoped that the results gained will aid in the prediction of lifetimes of components which must be operated for long periods at high temperature.

It was found that when a transition occurred, most of the surfaces were covered by stable, mainly oxide, plateaux of average thickness 6 μm for the conditions of our experiments. Sub-surface examination showed that beneath the plateaux was a work hardened layer extending 30 μm into the bulk. The plateaux consisted of a sintered agglomerate of wear debris, the composition of which varied from mainly metallic particles at the boundary between plateau and substrate to mainly oxide at the plateau surface. Out-of-contact oxidation at the general surface temperature was probably responsible for most of the oxide growth during the running-in period, but in-contact tribo-oxidation became important as speed, and hence contact temperature and surface disruption, increased. Whether plateaux formed and subsequent transition occurred depended on the relative rates of attrition and oxide growth. For ambient temperatures of 275°C and below, the rate of wear was always greater than the growth of oxide and the system settled into an equilibrium severe wear mode. For temperatures of 290°C and above, the system eventually settled into an equilibrium mild oxidational wear mode.

A surface model was developed to explain the processes of material removal and oxide growth leading to a severe/mild wear transition and good agreement was found between volumes of material removed in the running-in period predicted on the basis of the model and experimentally determined values.

Acknowledgements

The authors would like to thank Dr T.C. Chivers and Dr J. Skinner of the Central Electricity Generating Board, Berkeley Nuclear Laboratories, for their helpful discussions, provision of specimens and for loan of apparatus during this study.

N.W. Granville would like further to thank the Central Electricity Generating Board and Science and Engineering Research Council for financial assistance.

References

1. Wilace L.R. Tribological studies of austenitic stainless steel under carbon dioxide. *PhD Thesis, University of Aston in Birmingham, UK, 1980*
2. Ha K.L., Ahn J.M. and Rigney D.A. Friction, wear and mirostructure of unlubricated austenitic stainless steels. *Wear, 1980, 60(1), 13–37*
3. Skmer J. Friction and wear transitions of an austenitic stahless steel in high temperature carbon dioxide. *CEGB Report RD/B/5220 N 81, 1981*
4. Taor D.E., Hardisty F.B., Waterhouse R.B. and Nehru R. Thfretting wear of an austenitic stainless steel in air and caron dioxide at elevated temperatures. *Wear, 1979, 56(1), 9–18*
5. Bares D.J., Stott F.H. and Wood G.C. The frictional behaviour of ion-chromium alloys at elevated temperatures. *Wear, 1977, 45(2), 199–209*
6. Wilson J.E., Stott F.H. and Wood G.C. The development of wear protective oxides and their influence on sliding friction. *Proc. Roy. Soc., 1980, A369, 557–574*
7. Newell J.E. Corrosion of 9% Cr steels in AGR boilers. *Nuc. Eng. Int., 1972, 17, 637–639*
8. Sullivan J.L. and Athwal S.S. Mild wear of low alloy steel at temperatures up to 500°C. *Tribology International, 1983, 16(3), 123–133*
9. Davis L.E., MacDonald N.C., Palmberg P.W., Riach G.E. and Weber R.E. *Handbook of Electron Spectroscopy, Physical Electronics Industries, Minnesota, (1976)*
10. Archard J.F. Single contacts and multiple encounters. *J. App. Phys., 1961, 32, 1420–1425*
11. Archard J.F. The temperature of rubbing surfaces. *Wear, 1959, 2, 438–445*

REFERENCES

1) W.E. Berry, "Corrosion in nuclear applications," Wiley, London.

2) J. Edwards, "Lessons from Three Mile Island," New Scientist, 97, (1983), 79-84.

3) L.I. Tsuprun and M.I. Tarytina, "Behaviour of the stainless steel 1X18H9T in contact with liquid lead and their eutectic alloy at temperatures of 500°C to 600°C," Proceedings of the International Conference on the Peaceful Uses of Atomic Energy; Volume 9, Reactor technology and chemical processing, (1955), 364-367, United Nations.

4) R. Hurst and J. Wright, "Chemical problems of power reactors," Proceedings of the International Conference on the Peaceful Uses of Atomic Energy; Volume 9, Reactor technology and chemical processing, (1955), 373-376, United Nations.

5) A.F. Smith, "The oxidation of 18/8 type stainless steels in high pressure CO_2/2%CO," (1980), RD/B/N4753, C.E.G.B..

6) B.A. Irving and C.D.J. Armitage, "Role of carbide stabilising elements on the corrosion of mild steels by CO_2," Brit. Corros. J., 2, (1967), 230.

7) R. Darras, D. Leclercq and C. Bunard, "Oxidation of ordinary steel heated in carbon dioxide under pressure," Proceedings of the second International Conference on the Peaceful Uses of Atomic Energy; Volume 5, Properties of reactor materials, (1958), 261-265, United Nations.

8) D.D. Kalafati, "Thermodynamic cycles of nuclear power stations," (1965), 160-161, Israel Program for Scientific Translations, Jerusalem.

9) J.E. Newell, "Corrosion of 9% chromium in A.G.R. boilers," Nucl. Eng. Int., 17, (1972), 637-639.

10) R.A. Brierley, "Studies of the oxidation of 9 and 12 Cr steels in high temperature, high pressure CO_2," (1974), Corrosion of steels in CO_2, B.N.E.S. conference, Reading.

11) L.R. Wallace, "Oxidational and tribological studies of austenitic stainless steels under CO_2 based environments," (1980), PhD thesis, University of Aston in Birmingham.

12) C.A.S.E. Award Abstract, S3007, (1980), S.E.R.C., Swindon.

13) C. Wagner, "Diffusion and high temperature oxidation of metals," Atom Movements, (1951), 153-173, American Society for Metals, Cleveland, Ohio.

14) E.A. Gulbransen, "General concept of gas-metal reactions," Corrosion, 21, (1965), 76-83.

15) O. Kubaschewski, A. Cibula and D.C. Moore, "Gases and metals," (1970), 1-21, Iliffe Books, London.

16) J.K. Stanley, J. von Hoene and R.T. Huntoon, "The oxidation of pure iron," Trans. A.S.M., 43, (1951), 426-453.

17) A. Fick, "Uber diffusion," Pogg. Ann., 94, (1855), 59.

18) J. Paidassi, "Sur la cinetique de l'oxydation du fer dans l'air dans l'intervalle 700-1250°C," Acta Met., 6, (1958), 184-194.

19) P.C. Rowlands and W.H. Whitlow, private communication.

20) A.U. Seybolt, "Observations on the Fe-Cr-O system," J. Electrochem. Soc., 107, (1960), 147-156.

21) R.L. Rickett and W.P. Wood, "The action of oxygen and hydrogen sulphide upon iron-chromium alloys at high temperatures," Trans. A.S.M., 22, (1934), 347-384.

22) H.M. McCullough, M.G. Fontana and F.H. Beck, "Formation of oxides on some stainless steels at high temperatures," Trans. A.S.M., 43, (1951). 404-425.

23) D. Caplan and M. Cohen, "High temperature oxidation of some iron-chromium alloys," Trans. A.I.M.E., 194, (1952), 1057-1065.

24) P.E. Wretblad, "Rontgenographische Untersuchung der Systeme Fe_2O_3-Cr_2O_3 und Fe_2O_3-Mn_2O_3," Z. anorg. Chem., 189, (1930), 329-336.

25) H.J. Yearian, J.M. Kortright and R.H. Langenheim, "Lattice parameters of the $FeFe_{(2-x)}Cr_xO_4$ spinel system," J. Chem. Phys., 22, (1954), 1196-1198.

26) R.E. Carter and F.D. Richardson, "An examination of the decrease of surface-activity method of measuring self-diffusion coefficients in wustite and cobaltous oxide," J. Metals, 6, (1954), 1244-1257.

27) C. Wagner, "Theoretical analysis of the diffusion process determining the oxidation rate of alloys," J. Electrochem. Soc., 99, (1952), 369-380.

28) C. Wagner, "The distribution of cations in metal oxide and metal sulphide solutions formed during the oxidation of alloys," Cor. Sci., 9, (1969), 91-109.

29) G.L. Wulf, M.B. McGirr and G.R. Wallwork, "Theoretical analysis of alloy oxidation with reference to Fe-Cr alloys," Cor. Sci., 9, (1969), 739-754.

30) M.G.C. Cox, B. McEnaney and V.D. Scott, "A chemical diffusion model for partitioning of transition elements in oxide scales on alloys," Phil. Mag., 26, (1972), 839-851.

31) P.K. Footner, D.R. Holmes and D. Mortimer, "Oxidation of iron-chromium binary alloys," Nature, 216, (1967), 54-56.

32) L.V. Azaroff, "Role of crystal structure in diffusion. I. Diffusion paths in closest-packed crystals," J. Appl. Phys., 32, (1961), 1658-1662.

33) J.E. Antill, C.S.Campbell, D. Goodison, W.B. Jepson and C.G. Stevens, "Corrosion behaviour of steels in CO_2/CO atmospheres," Proceedings of the third United Nations International Conference on the Peaceful Uses of Atomic Energy; Volume 9, Reactor materials, (1964), 523-528, United Nations.

34) H. Loriers, D. Leclercq and R. Darras, "Corrosion of low alloy steels in CO_2," Brit. Corros. J., 2, (1967), 230.

35) R.J. Harris and J.A. Menzies, "Variability in CO_2 oxidation resistance of 2¼Cr1Mo and 1Cr½Mo steels," Brit. Corros. J., 3, (1968), 34-36.

36) D. Goodison, R.T. Harris and P. Goldenbaum, "The influence of gas pressure on the long term oxidation behaviour of mild and low alloy steels in CO_2 atmospheres at 350°C to 450°C," Brit. Corros. J., 2, (1967), 229.

37) C.G. Stevens and J. Board, "The effect of moisture on the oxidation of mild and low alloy steels in CO_2," Brit. Corros. J., 2, (1967), 229-230.

38) B.A. Irving and C.D.J. Armitage, "Role of carbide stabilising elements on the corrosion of mild steels by CO_2," Brit. Corros. J., 2, (1967), 230.

39) W.R. Price and I. Whittle, "Breakaway phenomenon during oxidation of mild steel," J. Iron Steel Inst., 205, (1967), 668-670.

40) R.J.P. Cribb, R. Sumerling and E. Dobing, "Corrosion of a vented stainless-steel tube exposed to CO_2 containing 1%CO in a nuclear reactor," Brit. Corros. J., 3, (1968), 176-181.

41) N. Birks, "Note on transport in porous oxides and the simultaneous oxidation and carburisation of stabilised steels in carbon dioxide," Brit. Corros. J., 3, (1968), 56.

42) P.C. Rowlands, R.A. Brierley, J.C.P. Garrett, D.R. Holmes and A. Whittaker, "The oxidation behaviour of Fe9Cr1Mo steels," (1982), Gas-cooled reactors today, B.N.E.S. conference, Reading.

43) J. Hampton, P.C. Rowlands and P.W. Teare, "The morphology of oxide scales formed on 9Cr steels in high pressure CO_2 atmospheres," (1978), RD/L/N49/78, C.E.R.L..

44) D. Mortimer, H. Sen and P.C. Rowlands, private communication.

45) R. Darras and H. Loriers, "Compatibility of cladding materials with carbon dioxide at high temperatures," Proceedings of the third United Nations International Conference on the Peaceful Uses of Atomic Energy; Volume 9, Reactor materials, (1964), 515-520, United Nations.

46) J.D. Noden, C.J. Knights and M.W. Thomas, "Growth of austenitic stainless steels oxidised in carbon and oxygen bearing gases," Brit. Corros. J., 3, (1968), 47-55.

47) J.M. Francis, "Structure of surface oxides formed on a 20%Cr/25%Ni/Nb stabilised steel in carbon dioxide at high temperatures," Brit. Corros. J., 3, (1968), 113-119.

48) H.E. McCoy, "Type 304 stainless steel vs flowing CO_2 at atmospheric pressure and 1100-1800F," Corrosion, 21, (1965), 84-94.

49) J.F. Archard and W. Hirst, "The wear of metals under unlubricated conditions," Proc. Roy. Soc., 236A, (1956), 397-410.

50) N.C. Welsh, "The dry wear of steels. I. The general pattern of behaviour," Phil. Trans. Roy. Soc., 257A, (1964), 31-50.

51) N.C. Welsh, "The dry wear of steels. II. Interpretation and special features," Phil. Trans. Roy. Soc., 257A, (1964), 51-70.

52) I.V. Kragelskii, "Friction and wear," (1965), Butterworths, London.

53) J.T. Burwell and C.D. Strang, "Metallic wear," Proc. Roy. Soc., A212, (1952), 470-477.

54) J.T. Burwell, "Survey of possible wear mechanisms," Wear, 1, (1957), 119-141.

55) E. Rabinowicz, Friction and wear of materials," (1965), Wiley, New York.

56) E. Rabinowicz and D. Tabor, "Metallic transfer between sliding metals: an autoradiographic study," Proc. Roy. Soc., A208, (1951), 455-475.

57) F.B. Bowden and D. Tabor, "The friction and lubrication of solids. Part I," (1950), O.U.P., Oxford.

58) B.W.E. Avient, J. Goddard and H. Wilman, "An experimental study of friction and wear during abrasion of metals," Proc. Roy. Soc., A258, (1960), 159-180.

59) E. Rabinowicz, L.A. Dunn and P.G. Russell. "A study of abrasive wear under three-body conditions," Wear, 4, (1961), 345-355.

60) E.E. Klaus and H.E. Bieber, "Effect of some physical and chemical properties of lubricants on boundary lubrication," A.S.L.E. Trans., 7, (1964), 1-10.

61) T.F.J. Quinn, "Role of oxidation in the mild wear of steel," Brit. J. Appl. Phys., 13, (1962), 33-37.

62) F.F. Tao, "A study of oxidation phenomena in corrosive wear," A.S.L.E. Trans., 12, (1969), 97-105.

63) T.F.J. Quinn, "The effect of "hot spot" temperature on the unlubricated wear of steel," A.S.L.E. Trans., 10, (1967), 158-168.

64) H. Miki and S. Kobayashi, "Pitting failure of annealed carbon steel under rolling contact," Wear, 67, (1981), 1-13.

65) C.S. Ram and A.R. Rao, "The effect of tufftriding on the rolling contact fatigue behaviour of low alloy steel cylindrical specimens," Wear, 70, (1981), 53-62.

66) H. Sundquist, "Rolling contact fatigue of case-hardened chromium steel," Wear, 66, (1981), 111-123.

67) J. Skinner, "Friction and wear transitions of an austenitic stainless steel in high temperature carbon dioxide," (1981), RD/B/5220/N81, C.E.G.B..

68) T. Kayaba and A. Iwabuchi, "The fretting wear of a 0.45%C steel and austenitic stainless steel from 20 to 650°C in air," Wear, 74, (1981-1982), 229-245.

69) J.S. Halliday and W. Hirst, "The fretting corrosion of mild steel," Proc. Roy. Soc., A256, (1956), 411-425.

70) D. Godfrey and J.M. Bailey, "Early stages of fretting of copper, iron and steel," Lub. Eng., 10, (1954), 155-159.

71) K.H.R. Wright, "An investigation of fretting corrosion," Proc. Inst. Mech. Eng., 1B, (1952-53), 556-574.

72) P.L. Hurricks, "The fretting wear of mild steel from room temperature to 200°C," Wear, 19, (1972), 207-229.

73) P.L. Hurricks, "The fretting wear of mild steel from 200°C to 500°C," Wear, 30, (1974), 189-212.

74) T.H.C. Childs, "The sliding wear mechanisms of metals, mainly steels," Trib. Int., 13, (1980), 285-293.

75) J.F. Archard, "Contact and rubbing of flat surfaces," J. Appl. Phys., 24, (1953), 981-988.

76) T.F.J. Quinn, "Oxidational wear," Wear, 18, (1971), 413-419.

77) T.F.J. Quinn, D.M. Rowson and J.L. Sullivan, "Application of the oxidational theory of mild wear to the sliding wear of low alloy steels," Wear, 65, (1980), 1-20.

78) J.L. Sullivan, T.F.J. Quinn and D.M. Rowson, "Developments in the oxidational theory of mild wear," Trib. Int., 13, (1980), 153-158.

79) N.P. Suh, "The delamination theory of wear," Wear, 25, (1973), 111-124.

80) N.P. Suh, S. Jahanmir, E.P. Abrahamson and P.L. Turner, "Further investigation of the delamination theory of wear," Trans. ASME, Series F, 96, (1974), 631-637.

81) M. Kerridge and J.K. Lancaster, "The stages in a process of severe metallic wear," Proc. Roy. Soc., A236, (1956), 250-264.

82) J.K. Lancaster, "The formation of surface films at the transition between mild and severe metallic wear," Proc. Roy. Soc., A273, (1963), 466-483.

83) J.P. Hirth and D.A. Rigney, "Crystal plasticity and the delamination theory of wear," Wear, 39, (1976), 133-141.

84) D.A. Rigney and W.A.Glaeser, "The significance of near surface microstructure in the wear process," Wear, 46, (1978), 241-250.

85) K-L. Hsu, T.M. Ahn and D.A. Rigney, "Friction, wear and microstructure of unlubricated austenitic stainless steels," Wear, 60, (1980),13-37.

86) D. Hull, "Introduction to dislocations," 2nd edition, (1975), Pergamon Press, Oxford.

87) G. Yoshimoto and T. Tsukizoe, "On the mechanism of wear between metal surfaces," Wear, 1, (1957), 472-497.

88) N. Tenwick and S.W.E. Earles, "A simplified theory for the oxidative wear of steels," Wear, 18, (1971), 381-391.

89) J.F. Archard, "The temperature of rubbing surfaces," Wear, 2, (1959), 438-455.

90) J.L. Sullivan and S.S. Athwal, "Mild wear of a low alloy steel at temperatures up to 500°C," Trib. Int., 16, (1983), 123-131.

91) J.F. Archard, "Single contacts and multiple encounters," J. Appl. Phys., 32, (1961), 1420-1425.

92) T.F.J. Quinn, "Dry wear of steel as revealed by electron microscopy and X-ray diffraction," Proc. I. Mech. E., 182(3N), (1967-68), 201-213.

93) T.F.J. Quinn, "An experimental study of the thermal aspects of sliding contacts and their relation to the unlubricated wear of steel," Proc. I. Mech. E., 183(3P), (1968-69), 129-137.

94) N. Saka, A.M. Eleiche and N.P.Suh, "Wear of metals at high sliding speeds," Wear, 44, (1977), 109-125.

95) M.M. Khruschov, "Principles of abrasive wear," Wear, 28, (1974), 69-88.

96) R.T. Spurr, " The abrasive wear of metals," Wear, 65, (1980), 315-324.

97) D. Dowson, "The history of tribology," (1978), Longmans, London.

98) J.E. Williams, "An asperity interaction machining theory of friction," Wear, 56, (1979), 363-375.

99) M.M. Koura, "The effect of surface texture on friction mechanisms," Wear, 63, (1980), 1-12.

100) P.B. Madakson, "The frictional behaviour of materials," Wear, 87, (1983), 191-206.

101) F.B. Bowden and D. Tabor, "The friction and lubrication of solids. Part II," (1964), O.U.P., Oxford.

102) E. Rabinowicz, "Influence of surface energy on friction and wear phenomena," J. Appl. Phys., 32, (1961), 1440-1444.

103) D.A Rigney and J.P. Hirth, "Plastic deformation and sliding friction of metals," Wear, 53, (1979), 345-370.

104) D. Walton, "Mechanism of friction," Wear, 6, (1963), 257-261.

105) D. Walton, "Mechanism of friction," J. Appl. Phys., 33, (1962), 519-526.

106) C. Rubenstein, "A general theory of the surface friction of solids," Proc. Roy. Soc., B69, (1956), 921-933.

107) N.P. Suh and H-C. Sin, "The genesis of friction," Wear, 69, (1981), 91-114.

108) J.T. Burwell and E. Rabinowicz, "The nature of the coefficient of friction," J. Appl. Phys., 24, (1953), 136-139.

109) F.J. Carignan and E. Rabinowicz, "Friction and wear at high sliding speeds," ASLE Trans., 23, (1980), 451-459.

110) J.R. Whitehead, "Surface deformation and friction of metals at light loads," Proc. Roy. Soc., A201, (1950), 109-124.

111) J.F. Archard, "Elastic deformation and the laws of friction," Proc. Roy. Soc., A243, (1957), 190-205.

112) P.J. Blau, "Interpretations of the friction and wear break-in behaviour of metals in sliding contact," Wear, 71, (1981), 29-43.

113) M. Cocks, "Role of atmospheric oxidation in high speed sliding phenomena," J. Appl. Phys., 28, (1957), 835-843.

114) O. Ruggeri, G. Sambogna, C.P. Balboni and G.A. Volpato, "Dry lubrication with soft metals: the tribological behaviour of a thin film of cadmium rubbing on carbon steel," Wear, 59, (1980), 433-446.

115) K-H. Habig, E. Broszeit and A.W.J. de Gee, "Friction and wear tests on metallic bearing materials for oil-lubricated bearings," Wear, 69, (1981), 43-54.

116) D.J. Barnes, F.H. Stott and G.C. Wood, "The frictional behaviour of iron and iron-chromium alloys at elevated temperatures," Wear, 45, (1977), 199-209.

117) A. Iwabuchi, T. Kayaba and K. Kato, "Effect of atmospheric pressure on friction and wear of 0.45%C steel in fretting," Wear, 91, (1983), 289-305.

118) D. Tabor, "Junction growth in metallic friction: the role of combined stresses and surface contamination," Proc. Roy. Soc., A251, (1959), 378-393.

119) F.P. Bowden and J.E. Young, "Friction of clean metals and the influence of adsorbed films," Proc. Roy. Soc., A208, (1951), 311-325.

120) D.J. Barnes, J.E. Wilson, F.H. Stott and G.C. Wood, "The influence of specimen geometry and sliding mode on the friction and wear of iron-chromium alloys in controlled environments," Wear, 45, (1977), 97-111.

121) R. Ward, "A comparison of reciprocating and continuous sliding wear," Wear, 15, (1970), 423-434.

122) T.S. Eyre, "Wear characteristics of metals," Trib. Int., 9, (1976), 203-212.

123) R.M. Farrell and T.S. Eyre, "The relationship between load and sliding distance in the initiation of mild wear in steels," Wear, 15, (1970), 359-372.

124) T.S. Eyre and A. Baxter, "The formation of white layers at rubbing surfaces," Metals and materials, 6, (1972), 435-439.

125) E.M. Trent, "The formation and properties of martensite on the surface of rope wire," J. Iron Steel Inst., 143, (1941), 401-412.

126) K. Nakajima and Y. Mizutani, "Structural change of the surface layer of low carbon steels due to abrading," Wear, 13, (1969), 283-292.

127) C.B. Allen, "The oxidational wear of diesel engine materials," (1982), PhD thesis, University of Aston in Birmingham.

128) M.B. Peterson and R.E. Lee, "Sliding characteristics of the metal-ceramic couple," Wear, 7, (1964), 334-343.

129) S.S. Athwal, "Wear of low alloy steels at elevated temperatures," (1983), PhD thesis, University of Aston in Birmingham.

130) J. Skinner, "Friction fluctuations and the effects of stroke and speed," (1982), RD/B/0110/N82, C.E.G.B..

131) P.L. Hurricks, "The mechanism of fretting - a review," Wear, 15, (1970), 389-409.

132) P.L. Hurricks, "The mechanism of fretting and the influence of temperature," Ind. Lub. Trib., 27, (1975), 209-214.

133) P.L. Hurricks, "The mechanism of fretting and the influence of temperature," Ind. Lub. Trib., 28, (1976), 1-17.

134) R.B. Waterhouse and M.H. Wharton, "Titanium and tribology," Ind. Lub. Trib., 26, (1974), 20-23.

135) H. Krause, "Metallographic investigations of tribochemical reaction layers," Prak. Metall., 6, (1969), 167-171.

136) B.I. Kostetskii and I.K. Filipchuck, "Surface wear due to oxidising in rolling friction conditions," Russ. Eng. J., 42(6), (1962), 23-25.

137) L. Toth, "The investigation of the steady stage of steel fretting," Wear, 20, (1972), 277-286.

138) I.F. Stowers and E. Rabinowicz, "The mechanism of fretting wear," Trans. A.S.M.E., Series F, 95, (1973), 65-70.

139) R.B. Waterhouse and D.E. Taylor, "Fretting debris and the delamination theory of wear," Wear, 29, (1974), 337-344.

140) P.M. Dunckley, "The effect of elevated temperatures and speed upon the wear of mild steel," PhD thesis, University of Aston in Birmingham.

141) D.M. Rowson and T.F.J. Quinn, "Frictional heating and the oxidational theory of wear," J. Phys. D: Appl. Phys., 13, (1980), 209-219.

142) B.J. Isherwood and T.F.J. Quinn, "The application of a glancing-angle X-ray diffraction film technique to the study of the low-temperature oxidation of iron-chromium alloys," Brit. J. Appl. Phys., 18, (1967), 717-725.

143) R.B. Waterhouse and M.K. Dutta, "The fretting fatigue of titanium and some titanium alloys in a corrosive environment," Wear, 25, (1973), 171-175.

144) I.M. Feng and H.H. Uhlig, "Fretting corrosion of mild steel in air and nitrogen," J. Appl. Mech., 21, (1954), 395-400.

145) D.E. Taylor, F.B. Hardisty, R.B. Waterhouse and A.Y. Nehru, "The fretting wear of an austenitic stainless steel in air and in carbon dioxide at elevated temperatures," Wear, 56, (1979), 9-18.

146) F.H. Stott, D.S. Lin and G.C. Wood, "The structure and mechanism of formation of the 'glaze' oxide produced on nickel-based alloys during wear at high temperatures," Cor. Sci., 13, (1973), 449-469.

147) R.B. Waterhouse, "Fretting at high temperatures," Trib. Int., 14, (1981), 203-207.

148) T. Kayaba and A. Iwabuchi, "Effect of the hardness of hardened steels and the action of oxides on fretting wear," Wear, 66, (1981), 27-41.

149) N. Ohmae and T. Tsukizoe, "The effect of slip amplitude on fretting," Wear, 27, (1974), 281-294.

150) J.C. Killeen, A.F. Smith and R.K. Wild, "Chromium depletion profiles after preferential removal of chromium from alloys," Cor. Sci., 16, (1976), 551-559.

151) A.S.T.M. index to the powder diffraction file, (1963).

152) A.S.T.M. powder diffraction file.

153) J.G. Brown, "X-rays and their applications," (1966), Iliffe Books, London.

154) T.S. Eyre and D. Maynard, "Surface aspects of unlubricated metal-to-metal wear," Wear, 18, (1971), 301-310.

155) T.F.J. Quinn, "The division of heat and surface temperatures at sliding steel interfaces and their relation to oxidation wear," A.S.L.E. Trans., 21, (1978), 78-86.

156) L.E. Davis, N.C. MacDonald, P.W. Palmberg, G.E. Riach and R.E Weber, "Handbook of electron microscopy," Physical Electronics Industries, Minnesota, (1976).

157) R.C. Weast (Ed.), "Handbook of chemistry and physics," 54th ed., (1975-1976), CRC Press, Ohio.

158) S.T. Hsu, "Engineering heat transfer," (1963), D. Van Nostrand Company Inc., New Jersey, U.S.A..

159) G.F.C. Rogers and Y.R. Mayhew, "Thermodynamic and transport properties of fluids," 3rd ed., (1980), Blackwell, Oxford.

160) E.A. Brandes (Ed.), "Smithells metal reference book," 6th ed., (1983), Butterworths, London.

161) R.H. Greaves, "Chromium steels," (1935), H.M.S.O., London.

162) J.E. Wilson, F.H. Stott and G.C. Wood, "The development of wear protective oxides and their influence on sliding friction," Proc. Roy. Sos., A369, (1980), 557-574.

163) T.F.J. Quinn, A.R. Baig, C.A. Howarth and H. Muller, "Transitions in the friction coefficients, the wear rates and the compositions of the wear debris produced in the unlubricated sliding of chromium steels," A.S.L.E. Trans., 16, (1973), 239-244.

164) S.J. Rosenberg and L. Jorden, "The influence of oxide films on the wear of steels," Trans. A.S.M., 23, (1935), 577-613.

165) N.C. Welsh, "Frictional heating and its influence on the wear of steel," J. Appl. Phys., 28, (1957), 960-968.

166) T.F.J. Quinn, J.L.Sullivan and D.M. Rowson, "New developments in the oxidational theory of the mild wear of steel," Proc. A.S.M.E. Conference on Wear, (1979), Dearborn, Michigan, A.S.M.E., New York.

167) J.A. Greenwood and J.B.P. Williamson, "Contact of nominally flat surfaces," Proc.Roy. Soc., A295, (1966), 300-319.

168) M. Kawamoto and K. Okabayashi, "Study of dry sliding wear of cast iron as a function of surface temperature," Wear, 58,(1980), 59-95.

169) T.F.J. Quinn, J.L. Sullivan and D.M. Rowson, "Origins and development of oxidational wear at low ambient temperatures," Wear, 94, (1984), 175-191.

170) D.S. Lin, F.H. Stott and G.C. Wood, "The effects of elevated ambient temperatures on the friction and wear behaviour of some commercial nickel base alloys," A.S.L.E. Trans., 17, (1974), 251-262.

171) G.J. Van Wylen and R.E. Sonntag, "Fundamentals of classical thermodynamics," 2nd ed., S.I. version, (1976), John Wiley and Sons, Inc., New York.

172) C.D. Wagner, "Auger lines in X-ray photoelectron spectrometry," Anal. Chem., 44, (1972), 967-973.

173) B.P. Straughan and S. Walker (Eds.), "Spectroscopy," Volume 3, (1976), Chapman and Hall, London.